DISSERTATION

‘CLONEABLE’ NANOPARTICLES: IDENTIFICATION AND UTILIZATION OF METAL REDUCING ENZYMES AS BIOLOGICAL ELECTRON MICROSCOPY TAGS

Submitted By

Zachary J. Butz

Department of Chemistry

In partial fulfillment of the requirements

For the Degree of Doctor of Philosophy

Colorado State University

Fort Collins, Colorado

Fall 2019

Doctoral Committee:

Advisor: Christopher J. Ackerson

James R. Neilson
Christopher D. Snow
Thomas J. Santangelo

ABSTRACT

‘CLONEABLE’ NANOPARTICLES: IDENTIFICATION AND UTILIZATION OF METAL REDUCING ENZYMES FOR BIOLOGICAL ELECTRON MICROSCOPY TAGS

The ability to image individual proteins in biological systems has yet to be realized. The identification and utilization of ‘cloneable’ nanoparticles (cNP), *i.e.* genetically encoded tags capable of forming *in situ* inorganic nanoparticles from soluble inorganic precursors is the focus of this dissertation. The long-term goal of this project is to produce GFP analogues that can then be used in electron microscopy, light microscopy, and correlative light/electron microscopy.

The first chapter of this dissertation explores a metal reducing enzyme capable for converting soluble inorganic materials to insoluble (nano)particulates. Glutathione reductase-like metalloid reductase, GRLMR, was first isolated from *Pseudomonas moraviensis* stanleyae and characterized. GRLMR was identified as not only being able to reduce the precursor seleno-diglutathione to produce Se^0 nanoparticles but was also capable of increasing a host cells resistance to 10-fold that of the cell sans GRLMR. The structure of the enzyme was then predicted using Phyre^2 and related to other glutathione reductases to determine possible residues important for its inherent activity.

In the second chapter a dodecapeptide was identified using phage display for its ability to bind to Se^0 nanoparticles produced by GRLMR. Fusing this peptide to the C-terminus of GRLMR resulted in unexpected enzymes characteristics. Only when concatenated to GRLMR, the Se^0 binding peptide conveyed increased size control of nanoparticle product over a wide range of substrate not seen with GRLMR alone. The peptide facilitated greater affinity between the enzyme and the nanoparticle product as well. Finally, presence of the peptide on GRLMR was also able

to increase the enzyme's kinetics for precursor reduction. Raman spectroscopy was used to characterize which residues on the peptide were responsible for the interaction between the peptide and the nanoparticle surface.

The third chapter explores the application of GRLMR as a cNP. A cNP tag containing two concatenated copies of GRLMR and two Se^0 binding peptides was constructed and fused to the polymerizing protein FtsZ for expression and studies in native activity. Variants of the tagged FtsZ were isolated and studied *in vitro* or observed *in vivo*. *In vitro* studies resulted in filaments decorated with Se^0 nanoparticles that could be observed with and without formal staining with uranyl acetate. Images resulting from *in vivo* studies indicated that both the tag and FtsZ were able to function to produce filaments within cells of high contrast.

The fourth chapter isolates and characterizes a Te-reducing enzyme identified from screening environmental isolates collected throughout the Colorado Mineral Belt. A specific isolate, *R. erythropolis* PR4 possessed resistance to a broad range of metal and metalloid species. Specifically, *R. erythropolis* grew exceptionally well in up to 4.5 mM of TeO_3^{2-} determined by broth microdilution. The lysate from the bacteria was also incubated in different metals and metalloids to identify any proteins with metal reductase activity. Mycothione reductase, a glutathione reductase analogue was characterized with Te-reductase activity. Mycothione reductase was then isolated and characterized and could form Te^0 nanoparticles and bundled fibers. Although mycothione reductase was able to reduce SeO_3^{2-}, when the enzyme was incubated with TeO_3^{2-} and an excess of SeO_3^{2-} the resulting particulate had a mole ratio in favor of Te.

ACKNOWLEDGEMENTS

First and foremost, I need to thank Dr. Chris Ackerson. When I was at my lowest 3 years ago, ready to leave grad school, you were willing to take me on as a research assistant. You didn't know what I was capable of or what my skills were (I was also still figuring that out myself) you were willing to support me financially and intellectually. You made me want to work harder to prove to you that you could depend on me. I hope that over these years, I have at least started to repay you for the unbelievable support you have given me. Truly I cannot thank you enough.

To all the members of the Ackerson squad, both past and present, it has been one heck of an experience. Being able to work, goof around, and explore with all of you will be something I will cherish forever. Going to festivals, outdoor adventures, the lab reunions have been some of the best memories of my time here in Colorado. Specifically, Ricky Nemeth, I must thank you. You vouched for me when I was looking to jump into the Ackerson lab. You bet on me and I hope you saw a payout. Dr. Ryan Riskowski, being able to discuss and bounce ideas off you has been more help than you know. Kanda Borgognoni, it has been awesome to see your development as a researcher. Thank you so much for the help and input in all our projects. The progress, especially with the cNP tag would not have happened if you had not developed your expert skills in microscopy.

To everyone that has befriended me: I don't get why but man has it been entertaining to explore Colorado and beyond with you. I honestly couldn't be luckier with the number of people that I feel incredibly close to. The love I get from the tribe is overpowering and I hope that I have reciprocated even a fraction of it back to those who have given so much to me. Leaving Colorado will be difficult largely because of you Colorado Adventurers.

To Jennifer Bjerke (who I am sure will shed a tear while reading this) we have experienced all of grad school together. We were in lab together for the first three years. You convinced me to at least ask Ackerson about joining his lab. We have lived together, 4 out of the 6 years. We have

experienced a lot together and I can say that you are an incredibly strong person who has fought through some extremely difficult times. I will cherish our friendship long past the point of us departing each other.

To Nicholas Deweerd: I am glad I have been able to always be able to get along with you. We have lived together for 6 years and I have never found it hard to do so. Being able to rely on you as a great friend has been such a relief. I still think the best times were our dinner dates and a movie thanks to the Moviepass (which ended up costing us more money, awkwardly enough).

To my parents: how did you guys do it? You provided our home with so much love and comfort. You bolstered all our interests and unique personalities. You taught us to care for each other and others with humility and kindness. You two are truly the most inspiring people. I thank you from the bottom of my heart and hope that I make you proud throughout my life.

To my siblings: it has been a joy to grow up with all of you. One of the greatest joys of my life is being able to go home and hangout with any and all of you. Jake, you are an amazing older brother. Because you were willing to take on the older brother role I was permitted to be silly and explore. I knew you always had my back and I hope you know I will always have yours. Daniel, I hope that I was to you what Jake was to me. Frankly, I don't know what else to say because I don't think it can be nor needs to be said. Sarah, watching you discover yourself has been awe inspiring. You have had to learn many life lessons without Jake or I around but know that we are always there for you. To Rachel, I am stunned every time I see you. You have grown so much. It is impossible for me not to see you as the baby you were for most of my life at home. I continue to be impressed by your maturity and can't wait to see what you do in life.

Finally, to Harika: you mean everything to me. We have been through much over the last 7 years. You have made me a better person and loved me to unfathomable depths. Your drive has been an inspiration. I hope that I can return everything you have given to me because you deserve nothing less. I love you and cannot wait to spend the rest of my life doing so.

TABLE OF CONTENTS

LIST OF TABLES

LIST OF FIGURES

LIST OF COMMONLY USED SYMBOLS

Abbrev. /Symbol	Full Name
GFP	green fluorescent protein
DAB	3,3'-diaminobenizidine
cNP	cloneable nanoparticle
GRLMR	glutathione reductase-like metalloid reductase
SeBP	Se^0 binding peptide
GSHR	glutathione reductase
Mtr	mycothione reductase
FtsZ	filamenting temperature sensitive protein Z
SeNP	Se^0 nanoparticle
GSSG	oxidized glutathione
GSSeSG	seleno-diglutathione
NADPH	nicotinamide adenine dinucleotide phosphate
NADH	nicotinamide adenine dinulceotide
IPTG	isopropyl β-D-1-thiogalactopyranoside
GTP	guanosine triphosphate
K	Hill affinity constant
K_M	Michaelis constant
k_{cat}	turnover number
DLS	dynamic light scattering
SEM	scanning electron microscopy
TEM	transmission electron microscopy
EDS	energy dispersive spectroscopy
PAGE	polyacrylamide gel electrophoresis

INTRODUCTION

Background and Motivation

The ability to observe biology has led to incredible advancements in understanding of molecular and cellular biology. Being able to view the inner workings of cells has not been an easy development and largely goes under appreciated. Behind the images of distinct cellular structures stained with organic fluorophores or expressed fluorescent proteins is centuries of development and experimentation. From the initial staining using carmine by Joseph Von Gerlach in 1858 which showed a selectivity of staining nuclei and nuclear granules a push to further develop stains for selective imaging has been underway.[1,2] Light microscopy does have one major drawback in that it is a diffraction limited system which inhibits resolutions proportionately smaller than the wavelength of light being used. The Abbe diffraction limit (equation 1) shows the relationship between the wavelength, λ, and the resolvable distance, d.[3]

$$d = \frac{\lambda}{2nsin} \qquad (\mathbf{1})$$

The denominator, $nsin\theta$ is the numerical aperture (NA) and in modern optics reaches 1.4 – 1.6. For example, using green light emitting at 500 nm the diffraction limit is 250 nm which is sufficient for a cell (>1 μm) however incapable of resolving virions (100 nm), protein (10 nm), or molecules (1 nm). Therefore, green light can resolve a cell but would not be able to resolve individual virions or proteins. Eventually techniques utilizing localized fluorescing probes were developed using molecules like ReAsH or proteins such as green fluorescing protein (GFP).[4,5] The further manipulation of these probes has led to a wide array of fluorophores with different excitation/emission profiles permitting multiple fluorescing tags to be used within a single cell image. The 2014 Nobel prize in Chemistry was then awarded to Eric Betzig, Stefan Hell, and WE Moerner for their development of high-resolution light microscopy capable of overcoming the diffraction limit of light. This technique, however is extremely arduous and costly requiring very specific instrumentation and computational power.[6–13]

A new approach of visualizing images using an electron beam was developed by Max Knoll and Ernst Ruska at the Berlin Technische Hochschule in 1931.[14] The wavelength of an electron is calculated using DeBroglie's equation (equation 2) where λ is the wavelength, h is Planck's constant, m is the mass of the particle, and v is the velocity of the particle.

$$\lambda = \frac{h}{m*v} \qquad (\mathbf{2})$$

After making assumptions about the velocity and mass of an electron the wavelength value from **Equation 2** can be substituted into **Equation 1** the final resolution for electron microscopy becomes:

$$d = \frac{1.23\ \text{nm}}{\alpha\sqrt{\text{V}}} \qquad (\mathbf{3})$$

where d is the resolution in nm, α is the half aperture angle, and V is the acceleration velocity of the particle. The above equation would then indicate that with higher voltage used for imaging, the greater the resolution. Eventually due to aberrations in the lenses used in an electron microscopy a limiting resolution will be reached however the resolutions still permit 1 – 5 Å resolution.

The first successful electron micrograph image of a cell was realized by Porter, Claude, and Fullam in 1945.[15] The cultured chick embryo fibroblasts were fixed with formaldehyde and/or osmium tetroxide which doubles as a fixative and contrasting agent. The use of electron dense osmium tetroxide is required for contrast in biological systems since the major constituents are "electronically light" elements. Osmium tetroxide is still widely used today for fixation and contrast, but the limitations identified in this original paper are still present in approaches used today. Specifically, osmium tetroxide is a general stain causing high background and will sometimes form reduced aggregates within the sample. Osmium tetroxide is also extremely toxic hindering its wide use in many laboratories. As such, great importance has been put on identifying protocols that would allow for specific staining of structures and proteins above the background of the proteinaceous cytoplasm.

Currently, the leading approaches utilize an osmiophilic molecule, 3,3'-diaminobenzidine (DAB). Controlled polymerization of DAB is generally initiated by photooxidation or peroxidases

that can be expressed fused to a protein of interest akin to GFP.[16–21] The final step of the protocol is to then stain with osmium tetroxide which is reduced and aggregated within the vicinity of plaques of DAB polymer. This technique still runs into the same limitations identified by the original 1945 paper in which osmium has preferential affinity for various cellular structures and will aggregate away from the DAB polymer. The DAB molecule itself adds another layer of complexity as polymerization will occur in other areas as peroxidases are naturally occurring

Figure 1. Graphical representation of GFP fused proteins (left) and the expectation for the cNP (right).

enzymes in any biological system. Polymerizing DAB will also diffuse away from the spot of initiation leading to high background. In this document a new approach for specific labeling of proteins utilizing a tag termed here as a 'clonable nanoparticle' (cNP) is developed and utilized for EM imaging of biological specimens.

Considered here as a GFP-analogue, there are several characteristics attributed to a cNP. (i) there needs to be a genetic component that provides the ability to fuse the cNP to a protein target, hence its clonability. (ii) The genetic component must be able to generate insoluble (nano)particulate from soluble precursor. Currently the identification and usage of oxidoreductases is the basis for cNPs as this class of enzyme has been implicated in bioremediation of inorganic materials.[22–25] Another expectation is the diversification of the cNP enzymes available resulting in nanoparticles of different elemental make-up within a system.

3 main criteria must be met by an enzyme to be used in this application. (i) The enzyme needs to be capable of forming an inorganic precipitate from soluble precursor. This can be done through reduction, oxidation, or other catalytic means. (ii) The enzyme must be able to retain the nanoparticle formed reducing background or unbound tags. (iii) The enzyme tag must be capable

of size control and stabilization of the product. The aggregation of inorganic tags would disrupt the native function of a protein of interest and lead to artifacts during imaging.

The first two chapters in this document will be exploring the activity of a glutathione reductase like metalloid reductase (GRLMR) isolated from *Pseudomonas moraviensis* stanleyae. GRLMR can form Se^0 nanoparticles from soluble Se-containing precursors both *in vitro* and *in vivo*. Specifically, GRLMR has shown high activity in the reduction of seleno-diglutathione, a common Se metabolite after cellular Se uptake.[26,27] GRLMR is capable of size control and product retention although not at the desired proficicency.[23] Regardless this enzyme provides a springboard for the development of a cNP tag. First, GRLMR is explored in its portability into other species, specifically *E. coli*. Confirming portability of the enzyme's activity into other species would indicate its potential for common use as an EM tag.

The second chapter looks at modifying GRLMR activity to better meet the 3 required criteria through fusion of a selenium binding peptide (SeBP) to the enzyme. Refinement of the enzymes product retention and size control pushes the enzyme closer to being utilized as a tag in EM. The identification of SeBP was through screening of a phage library against GRLMR produced SeNPs.

The third chapter will discuss the use of GRLMR as an EM tag *in vitro* and *in vivo*. FtsZ will be the target protein on which a concatenated GRLMR dimer will be fused. FtsZ, a polymerizing protein, has been extensively studied both *in vivo* and *in vitro*. Capable of polymerizing into various filaments and coils, the presence of selenium nanoparticles along these structures would confirm the native function of a target protein while fused to the cNP.

The final chapter then discusses the expansion of possible tag constructs by identifying an enzyme, mycothione reductase, capable of reducing TeO_3^{2-} preferentially to SeO_3^{2-}. The overall expectation cNPs is that several nanoparticle producing tags can be used in a single sample analogous to the fluorescing protein variants. Although EM itself does not offer much contrast when comparing heavy metals, elemental analysis which is coupled to many electron microscopes could be used to make these distinctions.

REFERENCES

1. Gerlach, J. von. *Mikroskopische Studien aus dem Gebeite der menschlichen Morphologie*. (Ferdinand Enke, 1858).
2. Titford, M. Progress in the Development of Microscopical Techniques for Diagnostic Pathology. *Journal of Histotechnology* **32**, 9–19 (2009).
3. Abbe, E. Beiträge zur Theorie des Mikroskops und der mikroskopischen Wahrnehmung. *Archiv f. mikrosk. Anatomie* **9**, 413–418 (1873).
4. Adams, S. R. *et al.* New Biarsenical Ligands and Tetracysteine Motifs for Protein Labeling in Vitro and in Vivo: Synthesis and Biological Applications. *J. Am. Chem. Soc.* **124**, 6063–6076 (2002).
5. Chalfie, M., Tu, Y., Euskirchen, G., Ward, W. W. & Prasher, D. C. Green fluorescent protein as a marker for gene expression. *Science* **263**, 802–805 (1994).
6. Moerner, W. E. & Ambrose, W. P. Finding a single molecule in a haystack: laser spectroscopy of solids from (square root of)N to N=1. in *Optical Methods for Ultrasensitive Detection and Analysis: Techniques and Applications* **1435**, 244–251 (International Society for Optics and Photonics, 1991).
7. Dickson, R. M. *et al.* Single Molecules Solvated in Pores of Polyacrylamide Gels. *Molecular Crystals and Liquid Crystals Science and Technology. Section A. Molecular Crystals and Liquid Crystals* **291**, 31–39 (1996).
8. Dickson, R. M., Norris, D. J., Tzeng, Y.-L. & Moerner, W. E. Three-Dimensional Imaging of Single Molecules Solvated in Pores of Poly(acrylamide) Gels. *Science* **274**, 966–968 (1996).
9. Hänninen, P. E., Lehtelä, L. & Hell, S. W. Two- and multiphoton excitation of conjugate-dyes using a continuous wave laser. *Optics Communications* **130**, 29–33 (1996).
10. Hell, S. & Wijnaendts-van-Resandt, R. W. The Application Of Polarized Confocal Microscopy For The Size Measurement Of Resist Structures. in *Optical Storage and Scanning Technology* **1139**, 92–98 (International Society for Optics and Photonics, 1989).
11. Harootunian, A., Betzig, E., Isaacson, M. & Lewis, A. Super-resolution fluorescence near-field scanning optical microscopy. *Appl. Phys. Lett.* **49**, 674–676 (1986).
12. Betzig, E., Lewis, A., Harootunian, A., Isaacson, M. & Kratschmer, E. Near Field Scanning Optical Microscopy (NSOM): Development and Biophysical Applications. *Biophysical Journal* **49**, 269–279 (1986).
13. Betzig, E., Harootunian, A., Lewis, A. & Isaacson, M. Near-field diffraction by a slit: implications for superresolution microscopy. *Appl. Opt., AO* **25**, 1890–1900 (1986).
14. Freundlich, M. M. Origin of the Electron Microscope. *Science* **142**, 185–188 (1963).
15. Porter, K. R., Claude, A. & Fullam, E. F. A Study of Tissue Culture Cells by Electron Microscopy: Methods and Preliminary Observations. *Journal of Experimental Medicine* **81**, 233–246 (1945).
16. Lysova, I. *et al.* ReAsH/tetracystein-based correlative light-electron microscopy for HIV-1 imaging during the early stages of infection. *Methods Appl. Fluoresc.* **6**, 045001 (2018).
17. Novikoff, P. M. & Novikoff, A. B. Peroxisomes in Absorptive Cells of Mammalian Small Intestine. *The Journal of Cell Biology* **53**, 532–560 (1972).

18. Beard, M. E. Distribution of Peroxisomes (Microbodies) in the Nephron of the Rat: A Cytochemical Study. *The Journal of Cell Biology* **42**, 501–518 (1969).
19. Antoine, J.-C. Plasma Membrane and Internalized Immunoglobulins of Lymph Node Cells Studied with Conjugates of Antibody or its FAB Fragments with Horseradish Peroxidase. *The Journal of Cell Biology* **63**, 12–23 (1974).
20. Shu, X. *et al.* A Genetically Encoded Tag for Correlated Light and Electron Microscopy of Intact Cells, Tissues, and Organisms. *PLOS Biology* **9**, e1001041 (2011).
21. Martell, J. D. *et al.* Engineered ascorbate peroxidase as a genetically-encoded reporter for electron microscopy. *Nat Biotechnol* **30**, 1143–1148 (2012).
22. Fox, B. & Walsh, C. T. Mercuric reductase. Purification and characterization of a transposon-encoded flavoprotein containing an oxidation-reduction-active disulfide. *J. Biol. Chem.* **257**, 2498–2503 (1982).
23. Ni, T. W. *et al.* Progress toward clonable inorganic nanoparticles. *Nanoscale* **7**, 17320–17327 (2015).
24. Avazéri, C. *et al.* Tellurite reductase activity of nitrate reductase is responsible for the basal resistance of Escherichia coli to tellurite. *Microbiology* **143**, 1181–1189 (1997).
25. Yamamura, S. & Amachi, S. Microbiology of inorganic arsenic: From metabolism to bioremediation. *Journal of Bioscience and Bioengineering* **118**, 1–9 (2014).
26. Tapiero, H., Townsend, D. M. & Tew, K. D. The antioxidant role of selenium and seleno-compounds. *Biomed Pharmacother* **57**, 134–144 (2003).
27. Turner, R. J., Weiner, J. H. & Taylor, D. E. Selenium metabolism in Escherichia coli. *Biometals* **11**, 223–227 (1998).

CHAPTER 1: GLUTATHIONE REDUCTASE LIKE METALLOID REDUCTASE IMPARTS SELENITE RESISTANCE

1.1 Introduction

The enzymatic conversion of soluble inorganic ions into insoluble forms is carried out by enzymatic centers such as those present in ferritin, magnetosomes and silicateins facilitating the synthesis of biogenic inorganic materials.[28–30] Natural catalysts, as well as accessory proteins, can control the composition, the oxidation state, the morphology and the structure of the material. This suggests that the engineering of biological molecules underlies the diversity of inorganic materials synthesized biogenically. Inorganic materials - made from biomolecules (peptides, proteins and nucleic acids) developed or modified in the laboratory, attract attention for catalysis, self-assembly and bio-contrast (labeling) applications.[31–34]

Many biological systems for inorganic precipitation require oxidoreductase activity, allowing the conversion of soluble inorganic ions to insoluble oxidation states. Ferritins and DPS proteins accomplish this with ferroxidase enzyme centers.[35,36] Mercuric reductases which share a striking resemblance to lipoamide dehydrogenases, remove Hg^{2+} by reduction to Hg^0 and subsequent volatilization using an active dithiol.[22,37]

Glutathione reductase (GSHR) is capable of enzymatically reducing selenite (SeO_3^{2-}) to red Se^0 in the presence of the cofactor NADPH.[23] Diminished activity was also observed for the same enzyme in reducing tellurite (TeO_3^{2-}) to Te^0. *Pseudomonas moraviensis* stanleyae has been previously characterized with selenite reductase activity.[38] This microbe was identified as an endophyte in the selenium tolerant plant, *Stanleya pinnata*. Upon isolation and culture of *P. moraviensis* stanleyae was tolerant in media supplemented with SeO_3^{2-} up to 120 mM. This is much higher than most other reported SeO_3^{2-} tolerance values.[39–43] The selenite reduction activity of *P. moraviensis* was attributed to a GSHR-like enzyme based on proteomic mass spectrometry of an in-gel in situ selenium reduction.[23]

GSHRs generally belong to the family of pyridine nucleoside dependent oxidoreductases which also contains the well characterized mercuric reductase.[44] Within this enzyme family, active sites are highly conserved. Typical active site peptide sequences are CXXXXC for type I and CXXC for type II enzymes.[45] This class of enzyme has demonstrated reductase activity for a variety of metal ions including Se, Hg, Te, Fe, Cr, and U.[46–49] GSHR is also reported to reduce Au(III) to Au^0.[50] Thus, the class of pyridine nucleoside dependent oxidoreductases may represent an evolutionarily adaptable platform of inorganic ion reductases.

In the present study, a metalloid reductase was characterized from the seleno-specialist *P. moraviensis* stanleyae. It was determined that the metalloid reductase showed a higher k_{cat} and similar affinities for both the native substrate, oxidized glutathione (GSSG) and selenium containing seleno-diglutathione (GSSeSG) determined by the Hill equation. These enzymatic properties can be partially rationalized in terms of sequence and corresponding homology-modeled structure of the enzyme. In addition, expression of the metalloid reductase in laboratory strains of *E. coli* (BL21, SS320) resulted in increased tolerance to SeO_3^{2-} through the production of Se^0 nanoparticles (SeNPs). Overall, the data suggests that the enzyme may be best described as a glutathione reductase-like-metalloid reductase (GRLMR).

1.2 Results and Discussion

1.2.1 *GRLMR from P. moraviensis* stanleyae

Altered substrate specificity of GRLMR enzymes, favoring GSSeSG over GSSG as a substrate could underlie the remarkable SeO_3^{2-} tolerance of *P. moraviensis* stanleyae. The previously identified GRLMR enzyme was characterized from *P. moraviensis* stanleyae. The DNA sequence of the enzyme was acquired through a full-genome sequencing (ACGT Inc,Wheeling, IL). Sequencing was conducted using de novo paired end sequencing.[51] This revealed a genome where 70.3% of the nucleobases have, at the most, a 1:1000 probability of mis-assignment.

A BLAST search of the genomic sequence, using the *Pseudomonas* R-28S GSHR as a reference, identified one GSHR-like sequence, with 93% sequence homology. Sequence alignment of this GRLMR DNA using Serial Cloner showed high similarity (98.00%) to

Pseudomonas fluorescens GSHR and modest similarity (67 – 71%) to *E. coli*, *S. cerevisiae*, and *Homo sapiens* GSHR DNA. The sequence similarities are summarized in **Table 1.1**. Resulting DNA and structural homology studies indicated that all of the domains associated with Type I oxidoreductases were present in GRLMR including dimerization, cofactor, and substrate domains.[45,52,53] Such homology would suggest the GRLMR enzyme would conduct substrate reduction for GSSG, and related molecules, in a similar fashion to previously reported GSHR reduction pathways via an active site dithiol.[54,55] GRLMR however only showed 19% DNA sequence homology to mercuric reductase from *Pseudomonas Aeruginosa*.

Table 1.1 Genomic similarity (left values) and structural homology (right values) of GRLMR

	PM MTLR	**PF GSHR**	**EC GSHR**	**SC GSHR**	**HS GSHR**
PM MTLR		93.10%/ 1.56	74.14%/ 1.23	60.78%*/ 1.27	64.71%/ 1.31
PF GSHR	98.00%/ 1.71		77.59%/ 1.05	75.47%*/ 1.12	68.00%*/ 1.07
EC GSHR	67.42%/ 1.44	68.31%/ 1.42		81.48%*/ .87	79.63%*/ .85
SC GHSR	70.92%/ 1.56	73.48%/ 1.33	74.61%/ 1.17		84.91%/ .56
HS GSHR	70.34%/ 1.44	70.63%/ 1.24	78.97%/ 1.07	75.77%/ .92	

PF- *P. fluorescens*, EC- *E. Coli*, SC- *S. cerevisiae*, HS- *H. sapiens*.

Homology modeling using intensive parameters on the Phyre[2] server suggests that the structure of the *P. fluorescens* derived GSHR and GRLMR enzymes are homologous to other GSHR enzymes, despite modest DNA sequence divergence (**Appendix A, A.1, Table A.1**).[56] **Table 1.1** shows the root mean squared deviation of atomic positions (RMSD) values for a set of GSHR homology models and/or crystal structures against GRLMR. Overall, the RMSD values for these structures are similar, suggesting an overall structural homology between GRLMR, and GSHR from *P. fluorescens*, *E. coli*, *H. sapiens*, and *S. cerevisiae*. A full amino acid sequence alignment of the 5 enzymes in **Table 1.1** can be found in **Appendix A, A.2**.

1.2.2 *Kinetics of GRLMR*

Under the hypothesis that the GRLMR enzyme has altered selectivity relative to other characterized GSHRs, the enzyme kinetics of both GRLMR and *S. cerevisiae* GSHR were characterized. GRLMR was expressed recombinantly in *E. coli* BL21 cells. Following a Ni-affinity purification, affinity constants (K) were determined using the Hill equation for both

GRLMR and commercially sourced *S. cerevisiae* GSHR. The K of GRLMR and *S. cerevisea* GSHR was determined for GSSG and GSSeSG. It has been previously reported that GSHR enzymes can reduce these two substrates, with proposed mechanisms for the GSH based substrates.[23,54,55] While GSSG is commercially available, GSSeSG was synthesized according to previous published methods.[55]

A

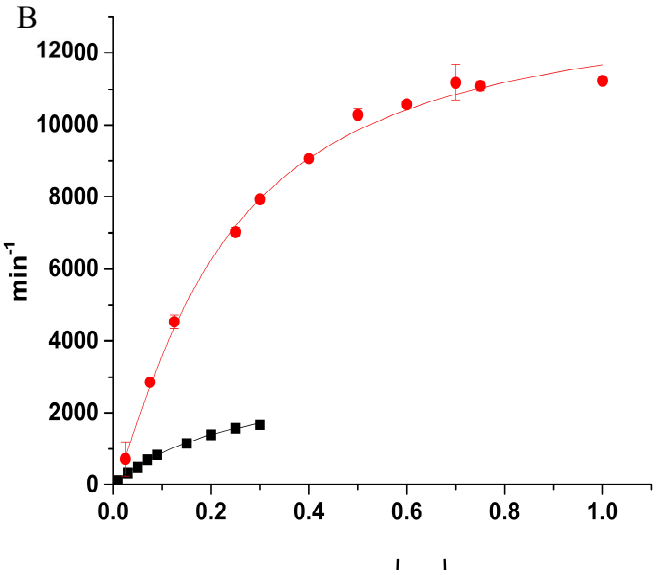

Figure 1.1 Kinetics assays for GRLMR (•) and GSHR (▪) against GSSeSG (**A**) and GSSG (**B**).

The enzymatic rates for both enzymes with both GSSG and GSSeSG substrates are plotted in **Figure 1.1**. Data is plotted as NADPH cofactor consumption, observed experimentally as depletion of a spectroscopic peak characteristic of NADPH at 340nm. The decay rate as measured

at 340 nm was converted to a normalized reaction rate and fitted with the Hill function. Analogous to the Michaelis-Menten constant, K defined by the Hill equation correlates to the substrate affinity. Vmax can also be calculated from the Hill equation providing comparative values between *S. cerevisiae* GSHR and *P. moraviensis* stanleyae GRLMR. Values for K and k_{cat} are listed in **Table 1.2**.

Table 1.2. kinetic values for GSHR and GRLMR

	GSSG		GSSeSG	
	GSHR	GRLMR	GSHR	GRLMR
K (μM)	274.9±27.8	223.5±11.8	28.0±3.3	101.6±5.9
k_{cat} (min^{-1})	3285±167	13433±457	1277±85	4684±205
k_{cat}/K	11.95	60.10	45.61	46.38

The values in **Table 1.2** represent the affinity of the enzyme for the substrate (K), the rate of substrate to product conversion (k_{cat}), and the catalytic efficiency (k_{cat}/K).[57–59] Unexpectedly, a large difference was found between the two enzymes' ability to reduce the native substrate, GSSG. Although K was close to being within error and agreed well with literature values, the k_{cat} was vastly different with GSHR at 3285±167 min^{-1} and GRLMR at 13433±457 min^{-1}.[60] Reported k_{cat} values for *S. cerevisiae* specifically have been much closer to the value collected for GRLMR when reducing GSSG. However, all kinetic reactions were run identically so comparison can be made for the kinetic values calculated here. Not surprisingly, when GSSeSG was the substrate the k_{cat} dropped considerably however the calculated K seemed to decrease for both enzymes signifying an increase in substrate affinity. When comparing the k_{cat}/K ratio, GSHR and GRLMR appear to be within error of each other. The k_{cat} of GRLMR for GSSeSG is slightly skewed. At higher [S] a plateau was not observed. GSSeSG reduces the pH of the reduction solution. At [S] > 0.4 mM, PBS was not able to buffer the solution, arresting the activity of GRLMR. The plateau in **Figure 1.1** is a false plateau making the k_{cat} far higher than what is shown here. What can be gathered from the graphs in **Figure 1.1, panel A** is that at concentrations above 50 μM the velocity

of GRLMR for GSSeSG overtakes GSHR. The concentration of glutathione in the cytoplasm has been reported up to 10 mM. The chemical equation is presented below.[61] When this is considered with the concentration of Se cells are supplemented with (1 – 2 mM) it stands to reason that the concentration of GSSeSG would be more than 50 μM.[62]

$$4GSH + H_2SeO_3 \rightarrow GSSeSG + GSSG + 3H_2O \quad (1)$$

Overall, the kinetic values indicate greater activity by GRLMR for the reduction of both GSSG and GSSeSG under physiological conditions. Especially interesting is the propensity GRLMR has for the reduction of GSSeSG. This high activity makes the GRLMR enzyme a prime candidate for a cNP contrast inducing EM tag.

1.2.3 *Portability of Se-resistance*

It was hypothesized that if the GRLMR conveys SeO_3^{2-} tolerance to *P. moraviensis* stanleyae than expressing GRLMR in a non-native host species could convey an increase in Se-resistance. To evaluate this hypothesis, lab expression strains of *E. coli*, specifically BL21 (DE3) (Cat#: C2527I) and SS320 (Cat#: 60512-1) were transformed with expression vectors containing GRLMR. For GRLMR expressing *E. coli*, selenite tolerance was determined as the concentration of SeO_3^{2-} that kills 90% of the cells (IC_{90}). As a control BL21 (DE3) cells containing a plasmid encoding GFP were also used. Cells were also observed in EM to determine whether SeNPs were present in the cytosol.

For IC_{90} determination, identical volumes of cells were plated on LB agar with varying concentrations of SeO_3^{2-}, each in triplicate, and grown overnight at 37°C. The following day, colony forming units (*cfu*) were counted. IC_{90} was calculated as the percentage of *cfu* present relative to an identical control supplemented with 1 μM SeO_3^{2-}. This concentration did not seem to affect the number of colonies observed when GRLMR was not expressed; concurrently 1 μM SeO_3^{2-} did provide enough selenium for cells expressing the Se-scavenging GRLMR. It became clear when starting IC_{90} studies that if the cells expressing GRLMR did not receive supplemental selenium, fewer *cfu* were observed on control plates. This observation alone lends credence to the

hypothesis that GRLMR is capable of increasing Se-resistance through the formation of bio-inert Se-species.[63]

Figure 1.2 shows relative growth inhibition as a function of selenite concentration. The $\log_{10}[SeO_3^{2-}]$ gives a linear concentration dependence for SeO_3^{2-} growth inhibition. An IC_{90} of

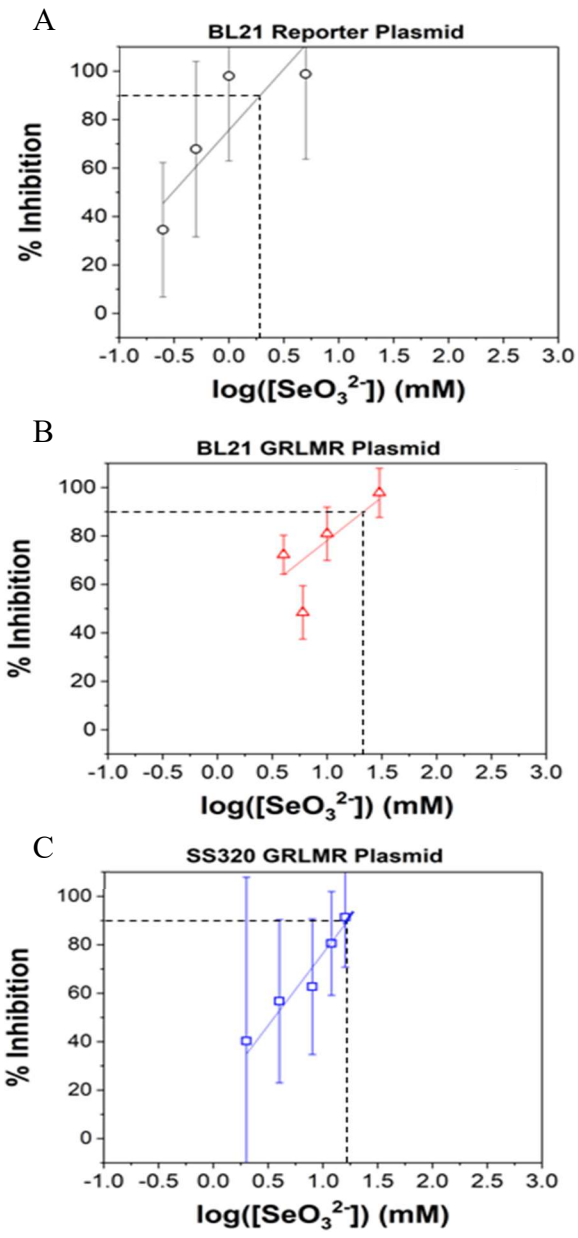

Figure 1.2. IC_{90} assays reported in percent inhibition vs. selenite concentration for BL21 (DE3) cells expressing (**A**) GFP and (**B**) GRLMR. (**C**) SS320 cells expressing GRLMR are also plotted.

21.3±9.8 mM was observed under conditions of GRLMR overexpression, whereas an IC_{90} of 1.89±0.46 mM is observed in a corresponding control experiment. When GRLMR is recombinantly overexpressed in SS320 cells, an IC_{90} of 18.3±19.5 mM was observed. The large deviations in *cfu* present in experimental replicates could be due to the heterogenous expression of GRLMR throughout the culture population after induction by IPTG. Even with the large error bars a statistically significant increase in SeO_3^{2-} tolerance is induced by the presence of the GRLMR plasmid. The error resulting in the IC_{90} could be due to heterologous expression in the culture population.

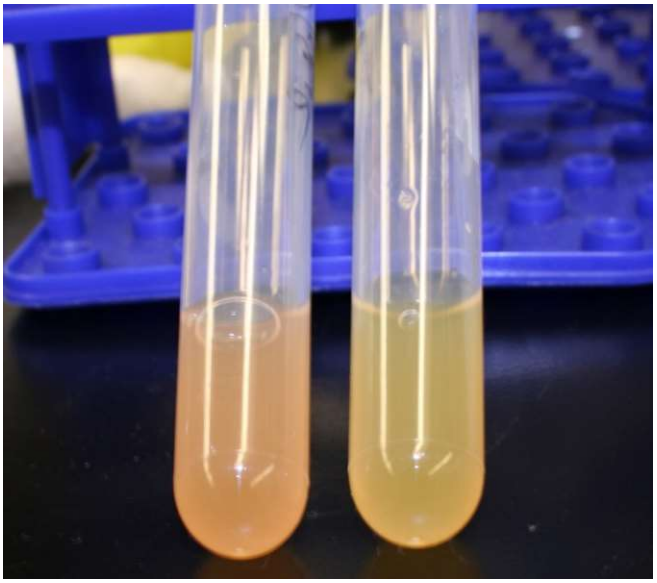

Figure 1.3. Cultured BL21 (DE3) cells expressing GRLMR (left) and GFP (right) in the presence of 5 mM SeO_3^{2-} for 3 hours.

Of note is the color change cultures undergo when expressing GRLMR in media supplemented with SeO_3^{2-}. The red color observed in these cultures is indicative of Se^0 nanoparticulate. Cultures grown without GRLMR expression do not develop a red color. To illustrate this, **Figure 1.3** shows cell cultures expressing GRLMR (left) or GFP (right) in the presence of 5 mM SeO_3^{2-} after 3 hours of exposure. This 'bulk color' change suggests that the cells expressing the recombinant enzyme may also be forming SeNPs observed previously in *P. moraviensis* stanleyae.[38]

Examination of cells by SEM revealed the presence of selenium nanoparticles in cells expressing the recombinant enzyme and grown in Se supplemented media. **Figure 1.4** shows scanning transmission electron micrographs of glutaraldehyde fixed dry-mounted BL21 (DE3) cells expressing GFP or GRLMR after growth in SeO_3^{2-} supplemented media. Both GFP-expressing and GRLMR-expressing cells show dark inclusions (**Figure 1.4, panel A & B**), with more inclusions observed in the GRLMR-expressing cell line. The dark inclusions seen in both cell lines near the cell walls are most likely the bacterial nucleoid. Electron dispersive

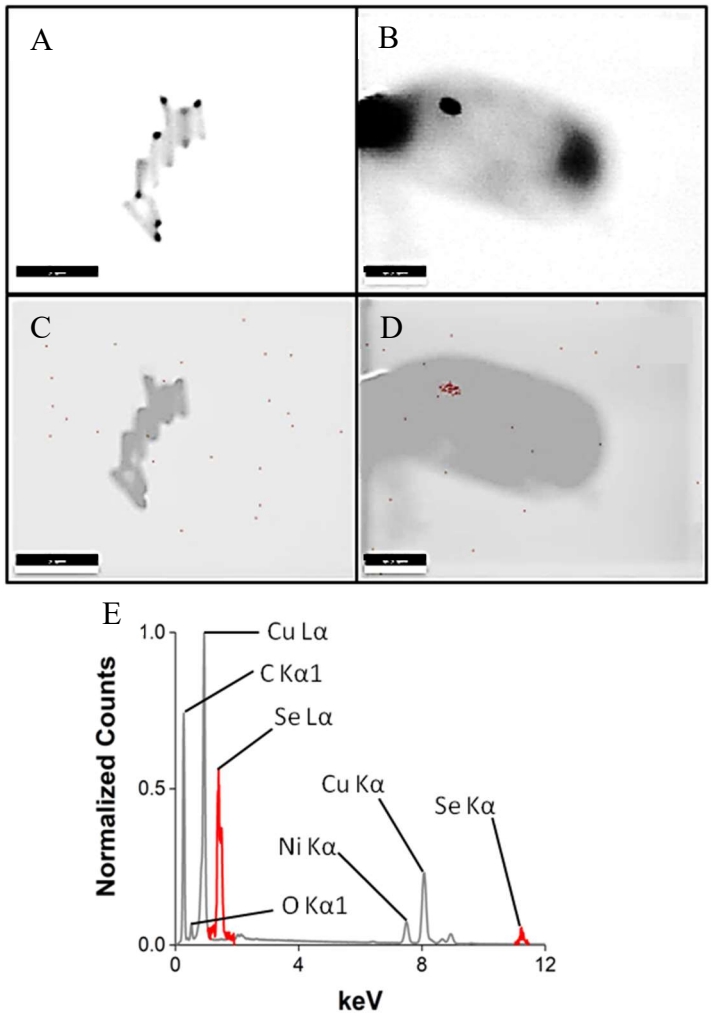

Figure 1.4. SEM images of fixed (**A**) GFP-expressing and (**B**) GRLMR-expressing cells after 3 hours of SeO_3^{2-} incubation. EDS overlays for (**A**) and (**B**) are shown in (**C**) and (**D**) respectively with red indicating Se. (**E**) The corresponding EDS spectra with gray peaks indicating peaks of GFP-expressing cells and red peaks indicating GRLMR-expressing cells. The presence of Cu stems from the Cu-coated grid used during imaging.

spectroscopy (EDS) mapping confirms that the dark inclusions are Se rich for the GRLMR-expressing cells (**Figure 1.4, panel D**), whereas any inclusions observed in GFP-expressing cells show no evidence of Se presence (**Figure 1.4, panel C**). The corresponding EDS spectra further confirms these conclusions by the presence of signature selenium peaks being present for the GRLMR-expressing cells, and the absence of these peak for the GFP-expressing cells (**Figure 1.4, panel E**). Further EDS analysis can be found in **Appendix A, A.3, Figure A.1 – A.4**. The intracellular Se rich NPs have an amorphous surface similar to previously reported results, suggesting a partially cytosol exposed surface.[23] This appears to be unique to GRLMR synthesized particles since inorganic/bio-inorganic methods tend to make smooth surfaced particles and require capping agents for stabilization.[64,65] Transportability of enzymatic function to foreign cell lines further demonstrates the ability for this enzyme's potential application as a cNP contrast generator.

1.2.4 ***Structural Analysis of GRLMR***

Differences in the product/substrate binding pocket of this family of enzymes may underlie any observed differences in substrate specificity and enzyme activity. Pymol graphics of the product binding pocket of GSHR from *H. sapiens*, *E. coli, S. cerevisiae, P. fluorescens,* and GRLMR are depicted in **Figure 1.5**. Structural alignment between GRLMR and *P. fluorescens* GSHR reveals an RMSD of 1.71 Å for the full enzyme and 1.56 Å for the product/substrate binding pocket. These values show the largest deviation between any of the enzymes considered here, but to date no crystal structure of a *Pseudomonas* glutathione reductase has been obtained which would affect the generated structure models.

The product/substrate binding pocket for GSHR contains a set of evolutionarily conserved residues, most notably including a cysteine that is implicated in glutathionylation regulatory mechanisms. There are three residues that dominate the binding interaction, one on an α-helix, and two on parallel β-strands. Comparing GRLMR to other GSHR enzymes it is observed that they contain the same key residues Ser, Lys, Glu (**Figure 1.5, panels D & E**).[60]

This absence of a sulfur-containing residue in the *P. moraviensis* GRLMR, suggests that the enzyme is not subject to the glutathionylation regulatory mechanism well established for canonical

glutathione reductase enzymes such as *S. cerevisiae* glutathione reductase. Glutathionylation of enzymes is a common post translation modification for proteins in signaling pathways and survival gene modification.[66–69] This reversible post-translation modification is the binding of glutathione to an unpaired cysteine residue.[70] Such modification alters enzyme activity, presumably as a regulation mechanism.[71,72] In the case of *S. cerevisiae* GSHR, glutathionylation at C239 (**Figure 1.5, panel C**) inhibits the enzyme. Chemically blocking the glutathionylation pathway is shown to increase GSHR activity by a factor of 2.1.[73] Overall, the absence of the possibility of a glutathionylation regulation mechanism for the GRLMR enzyme suggests that it might not fall under the same regulation ass other proteins.

The selenium metabolism literature highlights several examples of species within the Pseudomonas genus with remarkable tolerance to Se. In many cases GSHR enzymes are implicated in the tolerance. GSHR was responsible for reducing selenite and tellurite to insoluble NP's using *Pseudomonas maltophilia* strain O-2.[74] GSHR and thioredoxin reductase are

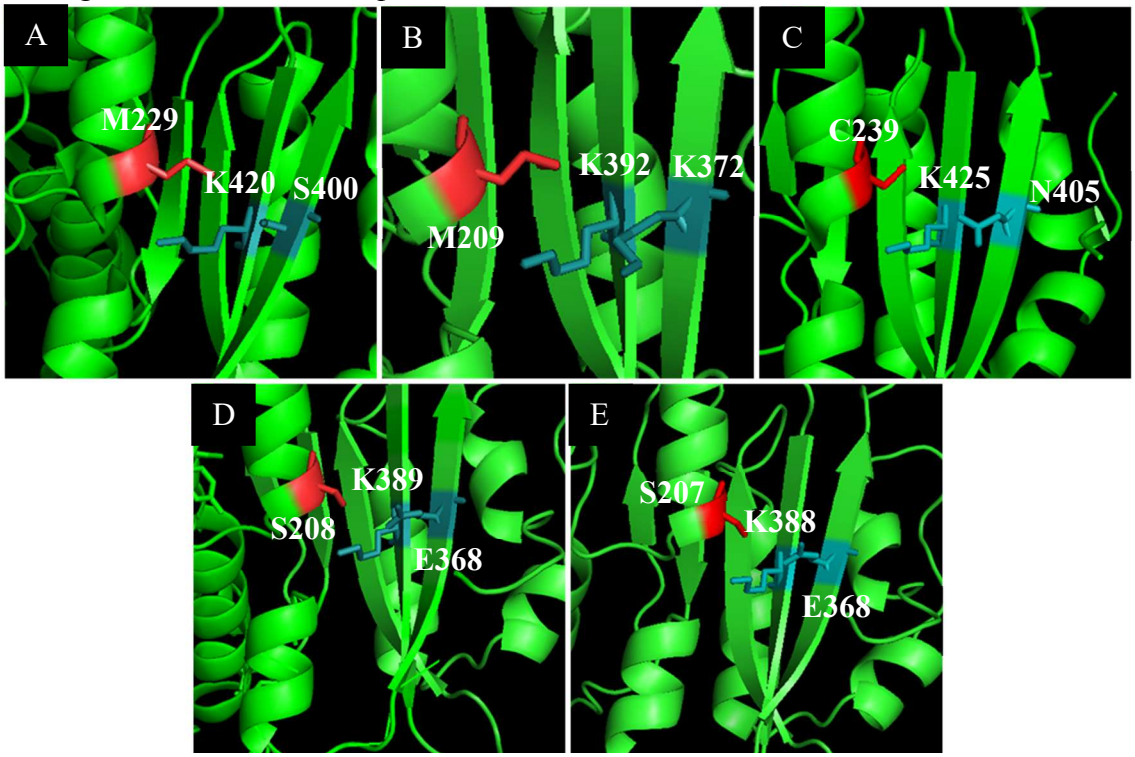

Figure 1.5. Product binding pockets of various GSHR enzymes from (**A**) *H. sapiens*, (**B**) *E. coli,* (**C**) *S. cerevisiae,* (**D**) *P. fluorescens,* and (**E**) GRLMR. The red residue lies on the α-helix while the teal residues reside on the β-sheet. Single letter coding identifies the residue.

responsible for selenite and selenate reduction in *Pseudomonas seleniipraecipitan*.[75–77] The highly conserved sequence across species within the *Pseudomonas* genus, including conservation in the product/substrate binding pocket, is suggestive that the ability to handle normally toxic amounts of SeO_3^{2-} may be a general feature of the Pseudomonas genus and Se tolerance may arise from the nature of GSHRs in this genus.

1.3 Summary and Conclusions

In summary, a glutathione reductase-like metalloid reductase (GRLMR) from the bacterium Pseudomonas moraviensis stanleyae has been characterized. Kinetic studies showed an overall increase in enzyme activity by GRLMR for both GSSeSG and GSSG when compared to *S. cerevisiae* GSHR. The k_{cat} of GRLMR was greater for both substrates than either substrate was for GSHR. Transportability of the gene was tested by transforming lab strain *E. coli* with GRLMR. Selenite tolerance increased ten-fold compared to cells without the gene, and the formation of elemental red selenium when GRLMR was present. SEM/EDS further confirmed this by showing selenium particles associated with cells containing the gene.

All these characteristics instills further confidence that GRLMR can be applicable as a cNP tag for biological EM imaging. The enzyme has shown itself to at least meagerly meet the criteria required for cNP tags, namely reduction of the inorganic products. The next steps will be to try to boost the desired characteristics of the enzyme to better suit the criteria laid out for a cNP.

1.4 Experimental Details

1.4.1 *GRLMR Identification/Isolation*

An LB agar plate with colonies of the original *P. moraviensis* cell line was submitted for full genome sequencing. The DNA sequence from the most closely related enzyme identified by MALDI-TOF was used to identify the sequence of the enzyme of interest. This sequence was cloned into a pD441-CH *E. coli* vector and a standard heat-shock protocol was used to transform BL21 (DE3) cells. The full plasmid sequence with the GRLMR insertion can be found at **Appendix A, A4.**

Standard protein purification was conducted by growing cells in 1 L of LB to an optical density at 600 nm (OD_{600}) of 0.6 and inducing protein expression with 1 mM IPTG for 2 hours. Cells were collected and re-suspended in 25 ml of lysis buffer and homogenized on ice by sonication. The soluble cell lysate was collected, and a Ni-NTA column was used to isolate GRLMR. SDS-PAGE indicated high purity of the resulting protein. GSHR from *S. cerevisiae* was purchased from Sigma.

1.4.2 *GSSeSG Synthesis*

Protocol from Ganther was followed for the synthesis of the selenodiglutathione.[55] 400 µmoles of $HNaSeO_3$ was added to 24 ml of 0.1 M HCl and cooled to 4°C. Another solution of 0.1 M GSH was cooled to 4°C and added quickly to the selenite solution. The mixture reacted at 4°C for 20 minutes. 2.5 mL of 2 M sodium acetate was added to obtain a final pH of 4.5. A C-18 column was used to separate the products using pH 2.0 HCl. TLC was used to check the contents of lyophilized fractions. Isolated GSSeSG was identified and the amount quantified using the UV-Vis absorption at 263 nm. An example spectrum can be found in **Appendix A, A.5, Figure A.5**.

1.4.3 *Kinetics Studies*

Reactions of 1 mL total volume were conducted in PBS, pH 7.4 with 0.2 mM NADPH, and 3 µg (GSHR) or 1.5 µg (GRLMR) of enzyme. Concentrations from 0.01 – 1.0 mM of either GSSG or GSSeSG were used. The depletion of the NADPH peak at 340 nm was monitored every 2 seconds after the contents were mixed.

1.4.4 *Determining IC_{90} Values*

IC_{90}s were determined by standard plating experiments. In short, a culture of BL21 (DE3) cells containing either a plasmid encoding GRLMR or GFP were grown overnight in LB at 37°C. The following morning 100 µl of this starter culture were added to 2.5 mL of fresh LB and grown for roughly 2.5 hours to reach an $OD_{600} = 0.6$. Various amounts of selenite were added to each culture and exposure was continued for 24 hours. After exposure the cells were diluted 10^6-fold and 20 µL of each dilution was plated in triplicate on LB agar plates. Plates were grown at 37°C and colonies were counted the following day.

1.4.5 *STEM*

3 mL cultures of BL21 (DE3) cells containing either a GRLMR gene or GFP reporter gene were grown separately in 10 mL culture tubes overnight in LB. The following morning the culture was added to a 125 mL Erlenmeyer flask containing 50 mL LB medium. The cells were grown for 2.5 hours and 100 mM Na_2SeO_3 was added to reach a final concentration of 5 mM. The cells were collected by centrifugation for 20 minutes at 4000 RPM and 4°C after 3 hours of growth with selenite. Cells were washed with 20 mM Tris, pH 7.4 three times followed by resuspension in 1 mL of fixing solution (2% glutaraldehyde/2.5% formaldehyde); the fixing solution could react for 12 hours at 4°C. Fixed cells were centrifuged, and the pellet was washed five times in 20 mM Tris, pH 7.4. The cells were resuspended in 1 mL 20 mM Tris, pH 7.4. Aliquots (4 uL) were mounted on 400 mesh Cu grids with 50 nm C-coating and washed two times with H_2O. Dry-mounted cells on TEM grids were loaded onto a STEM holder. STEM images were taken on a JEOL JSM-6500-F Scanning Electron Microscope at an accelerating voltage of 15 kV.

1.4.6 *EDS*

EDS was performed on *P. moraviensis* stanleyae cells in the SEM as described above. EDS was collected on a Noran System 7 X-ray Microanalysis detector with a time interval of 1 sec.

REFERENCES

22. Fox, B. & Walsh, C. T. Mercuric reductase. Purification and characterization of a transposon-encoded flavoprotein containing an oxidation-reduction-active disulfide. *J. Biol. Chem.* **257**, 2498–2503 (1982).
23. Ni, T. W. *et al.* Progress toward clonable inorganic nanoparticles. *Nanoscale* **7**, 17320–17327 (2015).
28. Harrison, P. M. The structure and function of ferritin. *Biochemical Education* **14**, 154–162 (1986).
29. Kolinko, I. *et al.* Biosynthesis of magnetic nanostructures in a foreign organism by transfer of bacterial magnetosome gene clusters. *Nature Nanotechnology* **9**, 193–197 (2014).
30. Müller, W. E. G. *et al.* Silicateins, the major biosilica forming enzymes present in demosponges: Protein analysis and phylogenetic relationship. *Gene* **395**, 62–71 (2007).
31. Carter, C. J. *et al.* In vitro selection of RNA sequences capable of mediating the formation of iron oxide nanoparticles. *J. Mater. Chem.* **19**, 8320–8326 (2009).
32. Slocik, J. M., Kuang, Z., Knecht, M. R. & Naik, R. R. Optical Modulation of Azobenzene-Modified Peptide for Gold Surface Binding. *ChemPhysChem* **17**, 3252–3259 (2016).
33. Yeh, H.-C., Sharma, J., Han, J. J., Martinez, J. S. & Werner, J. H. A DNA−Silver Nanocluster Probe That Fluoresces upon Hybridization. *Nano Lett.* **10**, 3106–3110 (2010).
34. Klug, M. T. *et al.* Mediated Growth of Zinc Chalcogen Shells on Gold Nanoparticles by Free-Base Amino Acids. *Chem. Mater.* **29**, 6993–7001 (2017).
35. Wang, Q., Mercogliano, C. P. & Löwe, J. A Ferritin-Based Label for Cellular Electron Cryotomography. *Structure* **19**, 147–154 (2011).
36. Castruita, M. *et al.* Overexpression and Characterization of an Iron Storage and DNA-Binding Dps Protein from Trichodesmium erythraeum. *Appl. Environ. Microbiol.* **72**, 2918–2924 (2006).
37. Reed, J. K. Studies on the kinetic mechanism of lipoamide dehydrogenase from rat liver mitochondria. *J. Biol. Chem.* **248**, 4834–4839 (1973).
38. Staicu, L. C. *et al.* Pseudomonas moraviensis subsp. stanleyae, a bacterial endophyte of hyperaccumulator Stanleya pinnata, is capable of efficient selenite reduction to elemental selenium under aerobic conditions. *J. Appl. Microbiol.* **119**, 400–410 (2015).
39. Fernández-Llamosas, H., Castro, L., Blázquez, M. L., Díaz, E. & Carmona, M. Speeding up bioproduction of selenium nanoparticles by using Vibrio natriegens as microbial factory. *Sci Rep* **7**, 16046 (2017).
40. Fernández-Llamosas, H., Castro, L., Blázquez, M. L., Díaz, E. & Carmona, M. Biosynthesis of selenium nanoparticles by Azoarcus sp. CIB. *Microb. Cell Fact.* **15**, 109 (2016).
41. Wang, Y. *et al.* Selenite Reduction and the Biogenesis of Selenium Nanoparticles by Alcaligenes faecalis Se03 Isolated from the Gut of Monochamus alternatus (Coleoptera: Cerambycidae). *Int J Mol Sci* **19**, (2018).
42. Bebien, M., Chauvin, J.-P., Adriano, J.-M., Grosse, S. & Verméglio, A. Effect of Selenite on Growth and Protein Synthesis in the Phototrophic Bacterium Rhodobacter sphaeroides. *Appl. Environ. Microbiol.* **67**, 4440–4447 (2001).
43. Weiss, K. F., Ayres, J. C. & Kraft, A. A. Inhibitory Action of Selenite on Escherichia coli, Proteus vulgaris, and Salmonella thompson. *Journal of Bacteriology* **90**, 857–862 (1965).

44. Lian, P. *et al.* X-ray Structure of a Hg2+ Complex of Mercuric Reductase (MerA) and Quantum Mechanical/Molecular Mechanical Study of Hg2+ Transfer between the C-Terminal and Buried Catalytic Site Cysteine Pairs. *Biochemistry* **53**, 7211–7222 (2014).
45. Fox, B. S. & Walsh, C. T. Mercuric reductase: homology to glutathione reductase and lipoamide dehydrogenase. Iodoacetamide alkylation and sequence of the active site peptide. *Biochemistry* **22**, 4082–4088 (1983).
46. Li, X. & Krumholz, L. R. Thioredoxin Is Involved in U(VI) and Cr(VI) Reduction in Desulfovibrio desulfuricans G20. *Journal of Bacteriology* **191**, 4924–4933 (2009).
47. Freedman, Z., Zhu, C. & Barkay, T. Mercury Resistance and Mercuric Reductase Activities and Expression among Chemotrophic Thermophilic Aquificae. *Appl Environ Microbiol* **78**, 6568–6575 (2012).
48. Pugin, B. *et al.* Glutathione Reductase-Mediated Synthesis of Tellurium-Containing Nanostructures Exhibiting Antibacterial Properties. *Appl Environ Microbiol* **80**, 7061–7070 (2014).
49. Otwell, A. E. *et al.* Identification of proteins capable of metal reduction from the proteome of the Gram-positive bacterium Desulfotomaculum reducens MI-1 using an NADH-based activity assay. *Environ. Microbiol.* **17**, 1977–1990 (2015).
50. Scott, D., Toney, M. & Muzikár, M. Harnessing the mechanism of glutathione reductase for synthesis of active site bound metallic nanoparticles and electrical connection to electrodes. *J. Am. Chem. Soc.* **130**, 865–874 (2008).
51. Wang, Z. *et al.* De novo assembly and characterization of root transcriptome using Illumina paired-end sequencing and development of cSSR markers in sweet potato (Ipomoea batatas). *BMC Genomics* **11**, 726 (2010).
52. Arscott, L. D., Gromer, S., Schirmer, R. H., Becker, K. & Williams, C. H. The mechanism of thioredoxin reductase from human placenta is similar to the mechanisms of lipoamide dehydrogenase and glutathione reductase and is distinct from the mechanism of thioredoxin reductase from Escherichia coli. *Proc. Natl. Acad. Sci. U.S.A.* **94**, 3621–3626 (1997).
53. Mittl, P. R. & Schulz, G. E. Structure of glutathione reductase from Escherichia coli at 1.86 A resolution: comparison with the enzyme from human erythrocytes. *Protein Sci* **3**, 799–809 (1994).
54. Pai, E. F. & Schulz, G. E. The catalytic mechanism of glutathione reductase as derived from x-ray diffraction analyses of reaction intermediates. *J. Biol. Chem.* **258**, 1752–1757 (1983).
55. Ganther, H. E. Reduction of the selenotrisulfide derivative of glutathione to a persulfide analog by gluthathione reductase. *Biochemistry* **10**, 4089–4098 (1971).
56. Kelley, L. A., Mezulis, S., Yates, C. M., Wass, M. N. & Sternberg, M. J. E. The Phyre2 web portal for protein modeling, prediction and analysis. *Nat Protoc* **10**, 845–858 (2015).
57. Dowd, J. E. & Riggs, D. S. A Comparison of Estimates of Michaelis-Menten Kinetic Constants from Various Linear Transformations. *J. Biol. Chem.* **240**, 863–869 (1965).
58. Choi, B., Rempala, G. A. & Kim, J. K. Beyond the Michaelis-Menten equation: Accurate and efficient estimation of enzyme kinetic parameters. *Sci Rep* **7**, (2017).
59. Carrillo, N., Ceccarelli, E. & Roveri, O. Usefulness of kinetic enzyme parameters in biotechnological practice. *Biotechnol. Genet. Eng. Rev.* **27**, 367–382 (2010).
60. Yu, J. & Zhou, C.-Z. Crystal structure of glutathione reductase Glr1 from the yeast Saccharomyces cerevisiae. *Proteins* **68**, 972–979 (2007).
61. Kice, J. L., Lee, T. W. S. & Pan, S.-T. Mechanism of the reaction of thiols with selenite. *J. Am. Chem. Soc.* **102**, 4448–4455 (1980).

62. Forman, H. J., Zhang, H. & Rinna, A. Glutathione: Overview of its protective roles, measurement, and biosynthesis. *Mol Aspects Med* **30**, 1–12 (2009).
63. Hunter, P. A toxic brew we cannot live without. Micronutrients give insights into the interplay between geochemistry and evolutionary biology. *EMBO Rep.* **9**, 15–18 (2008).
64. Ramamurthy, C. *et al.* Green synthesis and characterization of selenium nanoparticles and its augmented cytotoxicity with doxorubicin on cancer cells. *Bioprocess Biosyst Eng* **36**, 1131–1139 (2013).
65. Nath, S., Ghosh, S. K., Panigahi, S., Thundat, T. & Pal, T. Synthesis of selenium nanoparticle and its photocatalytic application for decolorization of methylene blue under UV irradiation. *Langmuir* **20**, 7880–7883 (2004).
66. Grek, C. L., Zhang, J., Manevich, Y., Townsend, D. M. & Tew, K. D. Causes and consequences of cysteine S-glutathionylation. *J. Biol. Chem.* **288**, 26497–26504 (2013).
67. Sullivan, D. M., Wehr, N. B., Fergusson, M. M., Levine, R. L. & Finkel, T. Identification of oxidant-sensitive proteins: TNF-alpha induces protein glutathiolation. *Biochemistry* **39**, 11121–11128 (2000).
68. Townsend, D. M. *et al.* A glutathione S-transferase pi-activated prodrug causes kinase activation concurrent with S-glutathionylation of proteins. *Mol. Pharmacol.* **69**, 501–508 (2006).
69. Fiaschi, T. *et al.* Redox regulation of beta-actin during integrin-mediated cell adhesion. *J. Biol. Chem.* **281**, 22983–22991 (2006).
70. Hill, B. G. & Bhatnagar, A. Protein S-glutathiolation: redox-sensitive regulation of protein function. *J. Mol. Cell. Cardiol.* **52**, 559–567 (2012).
71. Humphries, K. M., Juliano, C. & Taylor, S. S. Regulation of cAMP-dependent protein kinase activity by glutathionylation. *J. Biol. Chem.* **277**, 43505–43511 (2002).
72. Townsend, D. M. *et al.* Nitrosative stress-induced s-glutathionylation of protein disulfide isomerase leads to activation of the unfolded protein response. *Cancer Res.* **69**, 7626–7634 (2009).
73. Stepovaya, E. A. *et al.* The role of oxidative protein modification and the glutathione system in modulation of the redox status of breast epithelial cells. *Biochem. Moscow Suppl. Ser. B* **10**, 235–239 (2016).
74. Blake, R. C. *et al.* Chemical transformation of toxic metals by a Pseudomonas strain from a toxic waste site. *Environmental Toxicology and Chemistry* **12**, 1365–1376 (1993).
75. Hunter, W. J. & Manter, D. K. Reduction of Selenite to Elemental Red Selenium by Pseudomonas sp. Strain CA5. *Curr Microbiol* **58**, 493–498 (2009).
76. Lortie, L., Gould, W. D., Rajan, S., McCready, R. G. L. & Cheng, K.-J. Reduction of Selenate and Selenite to Elemental Selenium by a Pseudomonas stutzeri Isolate. *Appl. Environ. Microbiol.* **58**, 4042–4044 (1992).
77. Avendaño, R. *et al.* Production of selenium nanoparticles in *Pseudomonas putida* KT2440. *Scientific Reports* **6**, 37155 (2016).

CHAPTER 2: ALTERATION IN METALLOID REDUCTASE ACTIVITY BY A SE^0 BINDING PEPTIDE

2.1 Introduction

Metal and metalloid reducing and/or oxidizing enzymes represent a key component in cellular metal homeostasis. They can be involved in metal storage, for instance the ferroxidase centers in ferritin.[78] They can also be involved in handling metal/metalloid toxicity, for instance by reducing species from soluble to an insoluble form, as exemplified by mercuric reductase.[22,47,79] Extremophile bacteria species have also been identified capable of sequestering toxic metal ions through formation of bio-inert species. The formation of varied morphological nanoparticles consisting of cadmium sulfide, palladium, selenium, chromium, cobalt, tellurium and others have been formed by environmental bacterial isolates.[38,80–86] Various fungal species have also undertaken the reduction of metal ions by way of quinones and intra- and extracellular enzymes.[87,88]

From many of the species that form inorganic nanoparticles, enzymes are identified in that reduce inorganic ions including as silica, chromate, cerium, selenite, selenate, tellurite, and tellurate.[89–94] For most of the enzymes identified, reduction occurs through an electron transfer utilizing the cofactors NADH or NADPH. In the case of bioremediase identified by Chowdury *et al.* the formation of SiO_2 from tetraethyl orthosilicate was catalyzed through a Zn^{2+} ion bound by the enzyme resulting in 25 ± 5 nm diameter nanoparticles.[95] An extracellular cystathione γ-lyase from *S. maltophilia*, capable of removing a sulfide from cysteine was isolated and used to make CdS quantum dots. This same enzyme was then used to produce numerous core-shell quantum dots by utilizing cysteine and/or selenocysteine.[96–99] A glutathione reductase like-metalloid reductase (GRLMR) was identified capable of reducing seleno-diglutathione, selenite, and selenate to amorphous Se nanoparticles (SeNP).[23,100] GRLMR, which will be used in this present work is also capable of forming CdSe quantum dots of varying size when the enzyme is

incubated with seleno-diglutathione, Cd^{2+}, and NADPH (submitted to *J. Phys. Chem. C*, June 2019). The majority of resulting inorganic materials are dependent on the *in vitro* reaction parameters, *e.g.* pH, precursor concentration, buffer components; conditions that would otherwise not result in a desired product over a wide range of environments and reaction conditions.

Whereas natural evolutionary processes result in inorganic ion reducing enzymes, *in vitro* selections have identified peptides that can bind to and sometimes exert control over the synthesis of inorganic materials such as CdS, FePt, ZnS, GeO_2, TiO_2, CoPt, and $CaCo_3$.[101–106] The pioneering work of Angela Belcher at MIT revealed the use of M13 phage for the ordering of quantum dots through the identification and fusion of inorganic interacting peptides to M13's major coat protein, p8.[107] Subsequently, Belcher used this approach to produce highly structured hybrid materials.[108–110] A peptide was isolated by Ahmad *et al.* exhibiting an ability to form $BaTiO_3$ precipitates although without any major size controlling effects.[111] Two other sequence-unique peptides were identified by Bassindale *et al.* capable of interacting with AgNPs. Ag-22 formed triangular, quadrangular, and spherical shapes while Ag-28 formed uniformly spherical NPs.[112] Feldheim showed that a peptide originally isolated for binding to germanium could exert profound effects on the formation of Ag nanostructures.[113]

The motivation for this current work is the production of genetically encoded tags analogous to green fluorescent protein (GFP), however, these tags can form insoluble inorganic particulate which can then be detected by electrons or X-rays. Our approach hopes to remedy what we have termed the 'contrast problem' in biological microscopy.[23] So far, labeling of biological samples for electron microscopy requires either immuno-labeling or two step deposition of diaminobenzidine followed by osmium tetroxide in order to get desired contrasts and resolutions.[20,21,114] These approaches while revealing, present their own drawbacks including rigorous sample preparation, material cost and toxicity, and high background. The use of a metal reducing enzyme to produce insoluble particulate from soluble metal salt precursors in concurrence with a peptide capable of binding to the produced particulate forms a construct that would solve the 'contrast problem' without the use of expensive or toxic materials.

So-far, the investigations of metal binding peptides and metal reducing enzymes represent separate fields of inquiry. For the first time, herein the effect of a selected SeNP binding peptide on enzymatic production of SeNPs is investigated for the eventual application as a GFP analogue for biological electron microscopy. It was determined that the peptide changes the SeNP sizes and distributions – an expected result. However, this is only observed when the peptide is genetically concatenated to the enzyme, not when the peptide is freely available in solution. More unexpectedly, a change in the enzyme's kinetic properties is observed. Based on Raman spectroscopy, the interaction between the peptide and the SeNP was characterized.

2.2 Results and Discussion

2.2.1 *Identification of Se^0 Binding Peptide*

Isolation of SeNP binding peptides was accomplished using a New England Biolabs PhD phage display library (Catalog # E8110S). This kit contains a library of 10^9 unique dodecapeptides expressed on the pIII protein of M13 bacteriophage. Selection was against GRLMR produced SeNPs of 8.4 ± 2.7 nm in diameter, confirmed by TEM (**Figure 2.1**). These SeNPs were adhered nonspecifically to a polystyrene 96-well plate. Following standard blocking and washing steps, the immobilized SeNPs were exposed to the phage library. To isolate phage that display peptide sequences that bind to SeNPs, the phage solution was first diluted to 10^9 plaque forming units (pfu) for all binding steps. Phage binding to SeNPs proceeded for 1 hour in selection rounds 1 and 2 but was reduced to 10 minutes in round 3. After the allotted binding time, supernatant was removed, and the SeNP coated 96-well plate washed to remove any remaining unbound phage. In selection rounds 2 and 3, detergent concentrations in the wash step were increased, to remove less favorably bound peptides. After each selection round, bound phage were acid-eluted with a Glycine-HCl (pH 2.2) based elution buffer for 20 minutes.

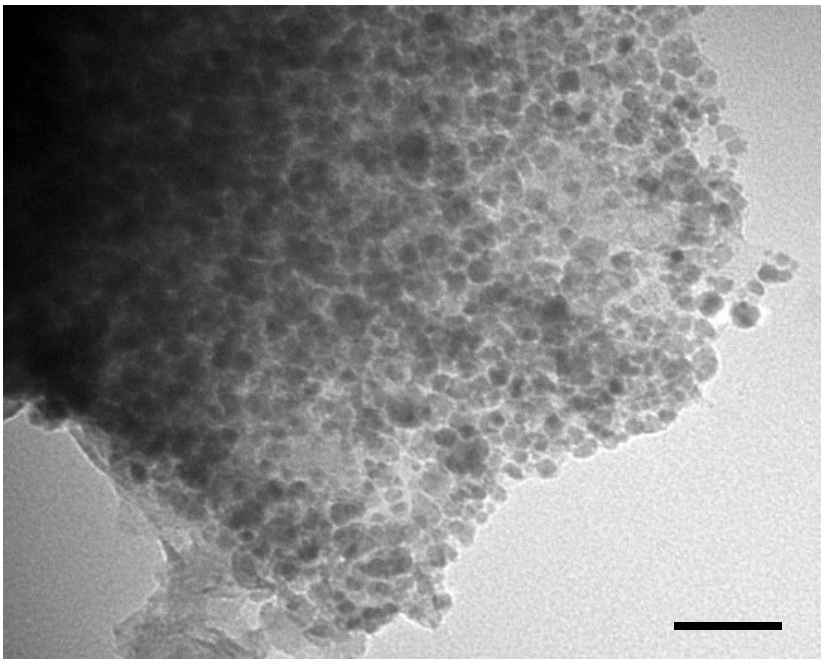

Figure 2.1. GRLMR produced SeNPs for peptide selection. Scale bar = 50 nm

DNA sequencing of the 3rd round eluted phage revealed an evolved library dominated by two sequences, LTPHKHHKHLHA (SeBP) and GPHHMHHHRTHH (SeBP2). Seven other sequences were also found. **Figure 2.2** illustrates relative residue identity frequency at each position in the peptide.

To control for the possibility of non-specific binding to either polystyrene or to non-selenium inorganic particles, negative selections were attempted using 20 nm Silica nanoparticles, GRLMR,

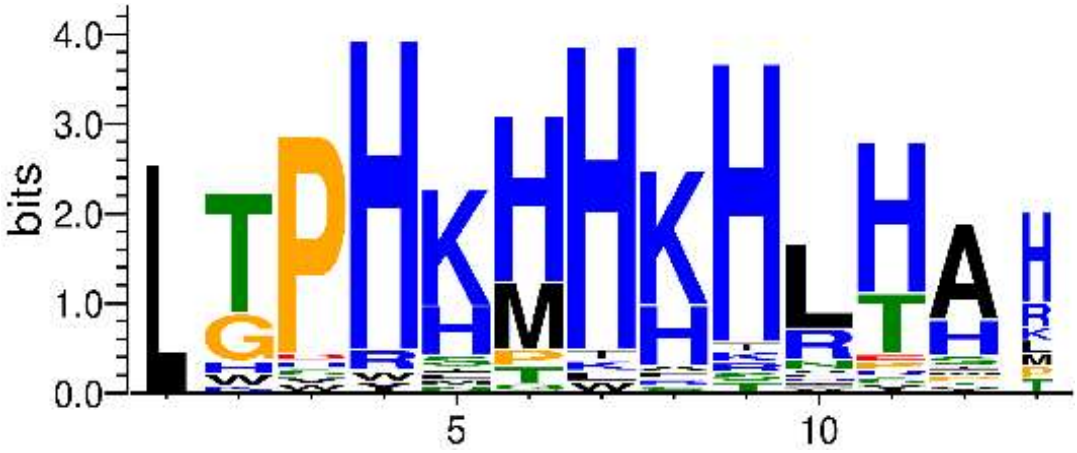

Figure 2.2. Frequency plot produced after sequencing 33 individually infected colonies. Letter width indicates the number of residues at the peptide position upon alignment. Height correlates to the frequency of a specific residue at a specific position.

and a polystyrene surface. Negative binding assays were performed in triplicate and eluted phage were immediately titered using a beta-galactosidase based assay indicating *E. coli* infection. The peptides chosen for the negative binding assays are highlighted in yellow and were of interest because of their sequencing frequency or picked randomly for comparison. **Table 2.1** shows the phage titer resulting eluted from each negative binding target. For reference, each titer began with an initial phage titer of 10^{10} pfu.

Based on this titer, SeBP, SeBP4, and SeBP5 show comparable binding to all the negative targets as phage that display no peptide (wild type, wt). In comparison SeBP2 and SeBP3 show notable binding to polystyrene, GRLMR, and SiNPs, indicating that these are relatively nonspecific binders. Therefore, we eliminate SeBP2 and SeBP3 from further investigation. Since SeBP1 represented most of the evolved pool and didn't incorporate substantial nonspecific binding, this peptide was further investigated.

Table 2.1. Sequences identified after peptide selection

				Negative Target Screen*		
Sample	Pep. Seq.	Frequency	p*I*	Polystyrene	GRLMR	SiNP
	Wild Type	N/A	N/A	$3.9x10^4$	$1.5x10^5$	$1.8x10^4$
SeBP	LTPHKHHKHLHA	19/33	9.37	$3.7x10^4$	$2.6x10^5$	$3.0x10^5$
SeBP2	GPHHMHHHRTHH	7/33	10.47	$1.1x10^9$	$2.1x10^9$	$7.9x10^9$
SeBP3	WPRHHWHTNYMR	1/33	11.15	$2.3x10^8$	$3.9x10^8$	$1.3x10^8$
SeBP4	GWHSPHAHWRVK	1/33	10.61	$4.3x10^4$	$3.3x10^5$	$3.7x10^5$
SeBP5	THYNPLRINPIT	1/33	9.95	$9.8x10^3$	$6.8x10^5$	$1.8x10^4$
SeBP6	KVHTMHFHHHSL	1/33	9.08	N/A	N/A	N/A
SeBP7	HSWSTIKRIETM	1/33	9.07	N/A	N/A	N/A
SeBP8	WPHLQHHKATSR	1/33	10.61	N/A	N/A	N/A
SeBP9	HDRMTKSSFSPP	1/33	9.07	N/A	N/A	N/A

*Values are in *pfu*

2.2.2 *Fusion of SeBP onto GRLMR*

Primers were designed for outward PCR, one of which containing the sequence encoding the identified SeBP and BspQI restriction sites to allow for eventual digestion and circularization of the linear PCR product. Circularized plasmids were transformed into BL21 (DE3) cells and desired products were identified through sequencing. To confirm the presence of the SeBP and the

function of GRLMR upon SeBP fusion GRLMR-SeBP was isolated as previously described.[100] It is important to reiterate the importance of supplementing induced cultures with 1 μM $HNaSeO_3$. GRLMR is capable of scavenging Se, an essential element, impeding growth of host cells and subsequent GRLMR expression. A Ni-affinity column was used to isolate enzyme, which was dialyzed into filter sterilized PBS, pH 7.4 and stored at -80°C in aliquots for further study. Yields of GRLMR-SeBP were >100 mg/L of culture.

Native-PAGE was run on GRLMR and GRLMR-SeBP to test for the presence of SeBP on GRLMR. Identically ran gels were either soaked in Coomassie for the presence of protein or soaked in a solution of 5 mM SeO_3^{2-}/1 mM NADPH in an inert atmosphere. **Figure 2.3** shows the results of the native-PAGE gels. The difference in migration between the two enzymes, GRLMR in Lane 1 and GRLMR-SeBP in Lane 3 is attributed to the presence of the positively charged SeBP. After soaking in SeO_3^{2-}, a red band develops corresponding to the location of the enzyme indicated by Coomassie stain.

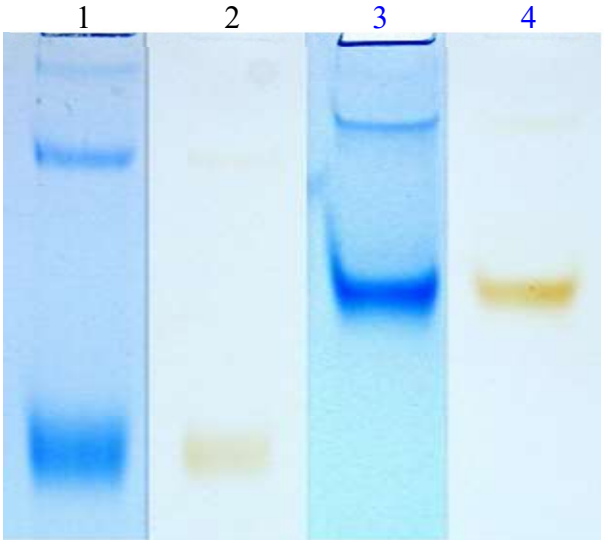

Figure 2.3. Native PAGE of GRLMR stained with Coomassie (Lane 1) or SeO_3^{2-}/NADPH (Lane 2) and GRLMR-SeBP stained with Coomassie (Lane 3) or SeO_3^{2-}/NADPH (Lane 4).

2.2.3 *Characterization GRLMR-SeBP*

From previous work, in the presence of sufficient concentrations of SeO_3^{2-} and NADPH, the enzymatic activity will result in the precipitation of red-selenium.[23] This known activity is

depicted in **Figure 2.4**, as the black dynamic light scattering (DLS) signal trace in **panel A** and as the top cartoon and cuvette photo in **panel B**. Briefly, the ultimate enzymatic product in conditions of excess reactant are micron sized particles that collect at the bottom of the reaction vessel.

Remarkably, when SeBP is concatenated to GRLMR, the product size and distribution changes dramatically. The blue trace in **Figure 2.4, panel A** shows that the Se^0 product size is dramatically restricted to a size of ~85 nm, several orders of magnitude smaller than the micron sized particles that result in the absence of concatenated SeBP. Consistent with SeNPs growth-arrest at a sub-

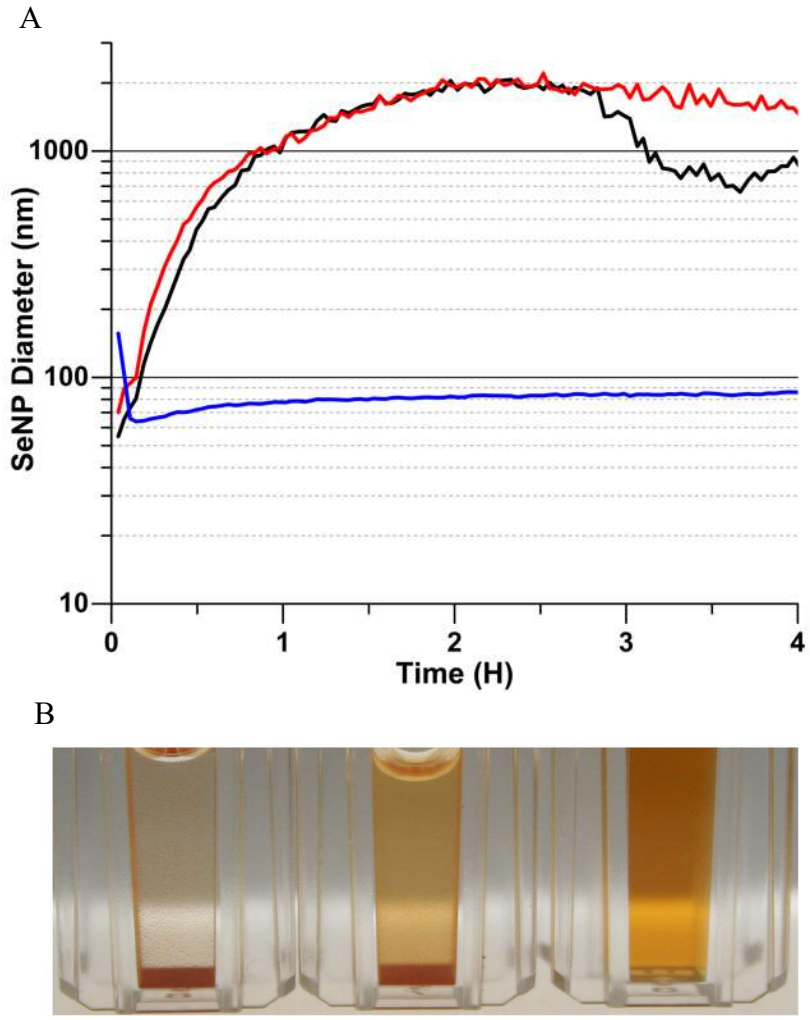

Figure 2.4. Intensity based DLS data (**A**) comparing SeNPs produced by GRLMR (black), GRLMR with exogenous SeBP (red), and GRLMR with fused SeBP (blue). (**B**) Resulting particulate from SeO_3^{2-} reduction with wild type GRLMR (left), wild type GRLMR and 1.4 µM exogenous SeBP (middle), and GRLMR-SeBP (right).

100 nm diameter, the reaction solution is red in color, with no precipitate forming at the bottom of the reaction vessel.

Interestingly, for the size-control effect to be observed, it is compulsory that the peptide is concatenated to the enzyme. If the peptide is simply added exogenously to the solution, no such limitation to Se^0 product size is observed, as shown in the red trace of **Figure 2.4, panel A** and the middle cartoon of **panel B**. Intensity data from DLS skews to show larger objects. Upon conversion to population number data, the diameter of the SeNPs were arrested at ~35 nm (**Appendix B, B.1, Figure B.1**).

The dramatically smaller hydrodynamic radius of SeNPs produced by GRLMR-SeBP implies a stable non-covalent binding interaction between the SeNP reaction product and the peptide-modified enzyme. To determine if GRLMR-SeBP is stably associated with SeNPs, a pull-down assay was executed as depicted in **Figure 2.5**. The basis of the pull-down assay is that the density of SeNPs allows them to be centrifugally removed from suspension, accompanied by any associated enzyme. This assay shows 83.1 ± 1.0% and 14.4 ± 2.6% of GRLMR-SeBP and GRLMR, respectively, associated with the SeNP fraction, as shown in **Figure 2.5, panel A**. It is possible that this assay under-estimates the amount of enzyme associated with particles, as

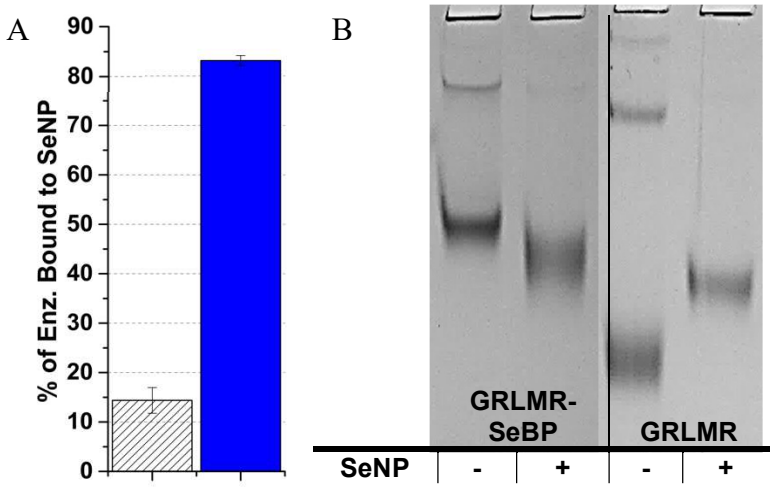

Figure 2.5 (**A**) Soluble GRLMR (diagonal stripe) and GRLMR-SeBP (blue), determined by Bradford assay, present after removal of enzyme coated SeNPs through centrifugation. (**B**) Native PAGE gel of unreacted GRLMR-SeBP (Lane 1) and GRLMR (Lane 3) and soluble GRLMR-SeBP (Lane 2) and GRLMR (Lane 4) post-SeNP synthesis.

sufficiently small SeNPs may not be centrifugally removed at the speeds used here, yet remain enzyme-associated, as depicted in **Figure 2.5, panel 5** and supported by the data in **Figure 2.5, panel B** (*vide infra*).

A native/nondenaturing Polyacrylamide Gel Electrophoresis (native-PAGE) experiment (**Figure 2.5, panel B**) suggests qualitatively that indeed a larger fraction than 83.1±1.0% of GRLMR-SeBP is bound to SeNPs. The gel mobility in this pH 8.3 matrix of GRLMR-SeBP and GRLMR are shown in lanes 1 and 3, respectively. The addition of 5 His and 2 Lys residues in the SeBP concatenation that produces GRLMR-SeBP provokes a notable gel-shift relative to native GRLMR, which was attribute to a substantial change in net-charge to a more positive value. The presence of the SeBP on GRLMR increases the calculated pI from 6.06 to 6.37. To further accentuate the charge difference between GRLMR and GRLMR-SeBP, a pH 6.6 native-PAGE gel was run following the buffer solution described by McLellan.[115] GRLMR-SeBP only slightly migrates into the gel indicating a pI closer to 6.6 (**Appendix B, B.2, Figure B.2**).

Lanes 2 and 4 in **Figure 2.5** show GRLMR-SeBP and GRLMR, respectively, present in the supernatant post-SeNP synthesis and centrifugation and dialyzed into milliQ water to remove excess salts from the reaction. For each reaction, a gel-shift relative to unreacted enzyme was observed, which is attributed to the enzyme-SeNP complexation. In other words, SeNPs are bound to the enzyme, which alters its electrophoretic mobility. In the case of reacted GRLMR-SeBP/SeNP complexes, observed is an electrophoretic mobility shift toward a *lower* mass-to-charge product. Here the shift is attributed to the SeNP binding specifically to the SeBP component, thereby neutralizing the charge added to the GRLMR-SeBP by the SeBP concatenation. In the case of reacted GRLMR, the electrophoretic mobility shift is toward a *higher* mass-to-charge product, which is attributed to the increased mass of a GRLMR/SeNP complex relative to GRLMR. The change in migration was not credited to the enzyme binding to NADPH or SeO_3^{2-}. This provides strong evidence that the SeNPs are binding to the SeBP. Charge neutralization of the SeBP fragment coupled with the mass change of SeNP binding to GRLMR gives both enzyme-SeNP products a similar gel-mobility.

2.2.4 *SEM of SeNPs Produced by GRLMR-SeBP*

The DLS data (*vide supra*) implies substantial difference in Se^0 product size which depends upon the presence or absence of concatenated SeBP. The enzymatic Se^0 products were examined by Scanning electron microscopy (SEM). As previously noted, the SeO_3^{2-} precursor concentrations had a strong influence on resultant SeNP size, the enzymatic products with SeO_3^{2-} concentrations ranging from 40 μM to 10 mM were examined. NADPH was present in excess except for samples containing 10 mM SeO_3^{2-}. GRLMR-SeBP produced SeNPs of diameter 37.38 ± 5.75 nm (n = 533), 32.60 ± 6.29 nm (n = 546), 37.34 ± 7.12 nm (n = 1288), and 45.89 ± 6.98 nm (n = 694) when the reactions contained 40 μM, 1 mM, 5 mM, and 10 mM $HNaSeO_3$, respectively (**Figure 2.6, left column**). Thus, at the lower three 'physiological-like' concentrations of SeO_3^{2-}, the particles were indistinguishable within measurement error. In contrast, GRLMR sans SeBP produces SeNPs that are larger, more polydisperse, and more prone to aggregation. GRLMR produced SeNPs of diameter 48.48 ± 17.63 nm (n = 1078), 61.59 ± 24.99 nm (n = 846), and 59.92 ± 21.19 nm (n = 1172) at $HNaSeO_3$ concentrations of 1 mM, 5 mM, and 10 mM, respectively (**Figure 2.6, right column**). Diameters of particles produced by GRLMR at 40 μM could not be satisfactorily measured, so values were not reported; although a representative micrograph is shown implying that the resultant particles are quite smaller than at higher concentrations.

Overall, the SEM images show that GRLMR-SeBP produces spherical, well-dispersed products of a narrow size range independent of SeO_3^{2-} concentration. This contrasts with GRLMR, wherein the SeNPs are of a much wider size range, not as apparently spherical, and prone to aggregation (consistent with the DLS measurements). Notably, when GRLMR was used to make SeNP products for these SEM experiments, precipitates were visible in the reaction vessels. Precipitation of larger particles and/or aggregates may have excluded larger materials from the SEM analysis, biasing the results toward measuring smaller Se^0 products.

2.2.5 *Kinetics of GRLMR-SeBP*

Because of the dramatic difference in SeBP size, morphology and aggregation state that depends on SeBP concatenation to GRLMR, we were curious if this concatenation also alters the

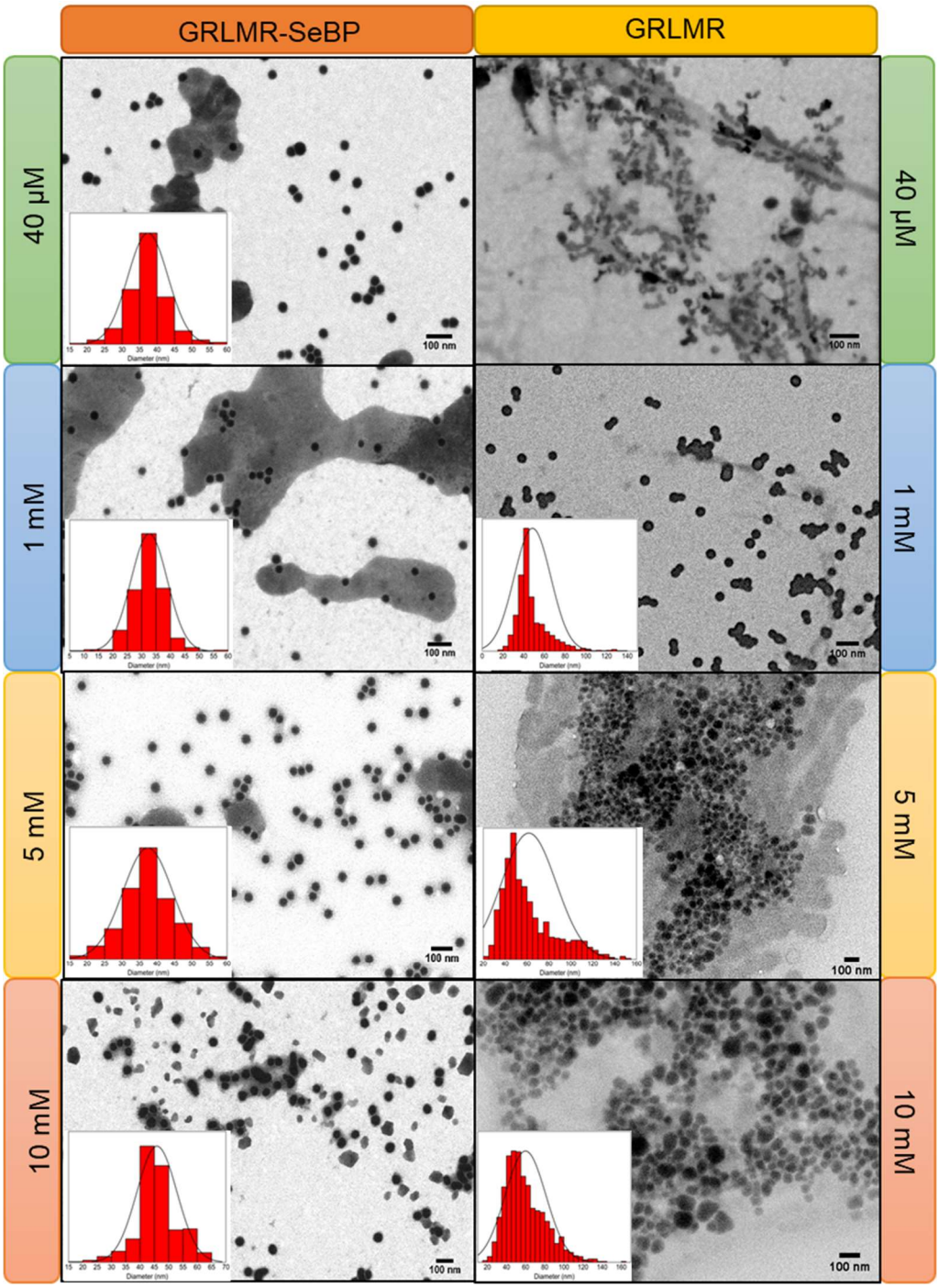

Figure 2.6. SEM images of SeNPs produced by either GRLMR-SeBP (**left column**) or GRLMR (**right column**). Rows correspond to the concentrations of SeO_3^{2-} used in the reactions.

kinetic properties of the enzyme. To explore this possibility, NADPH concentrations were monitored spectroscopically during GRLMR enzymatic reactions to establish fundamental

enzymatic kinetics in the presence and absence of the peptide. **Figure 2.7** depicts the plots of V_0s attained by the GRLMR with and without SeBP over a range of substrate concentrations.

The activities of GRLMR and GRLMR-SeBP, as judged by K_M and k_{cat} values, are markedly different when $HNaSeO_3$ is used as the substrate (**Figure 2.7, panel A**). K_M and k_{cat} for both GRLMR-SeBP and GRLMR are shown in **Table 2.2** against the different substrates $HNaSeO_3$ and GSSG. The K_M of GRLMR-SeBP (0.217 ± 0.057 mM) decreased compared to GRLMR (1.921 ± 1.279 mM), indicating a more favorable enzyme-substrate complex. k_{cat}s were measured at 40.316 ± 2.486 min^{-1} and 22.823 ± 8.839 min^{-1} for GRLMR-SeBP and GRLMR, respectively, indicating the peptide modification results in a faster enzyme for the reduction of SeO_3^{2-}.

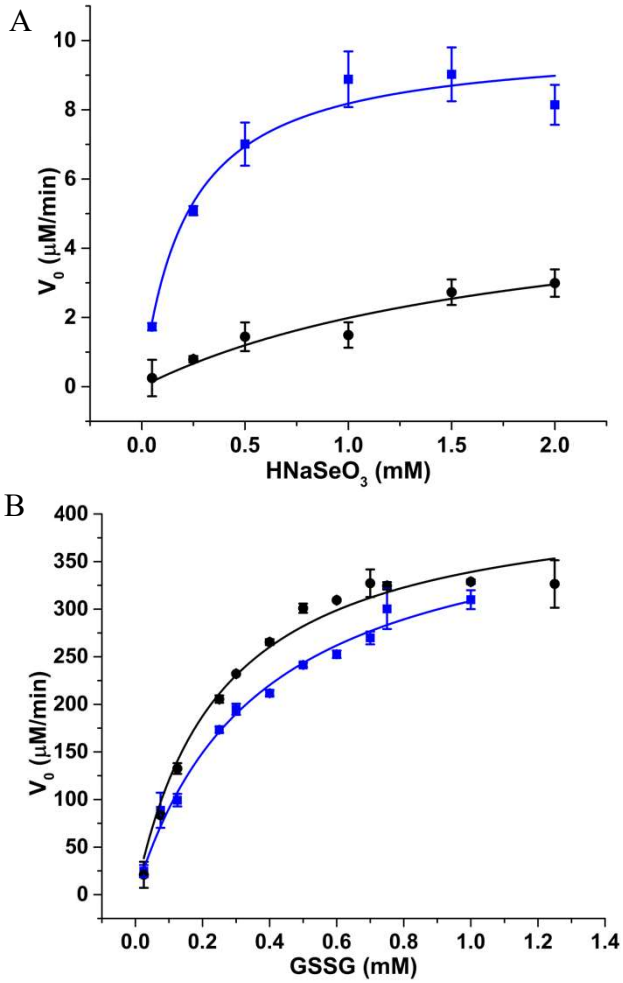

Figure 2.7. V_0 plotted against substrate concentration of GRLMR-SeBP (▪) and GRLMR (•) comparing (**A**) $HNaSeO_3$ and (**B**) GSSG.

The differences in activity indicated by these kinetic experiments, notably, are also reflected in the SEM examination of enzymatic product (**Figure 2.6,** *vide supra*). Specifically, at the lowest concentrations of SeO_3^{2-} (40 μM) no enzymatic product for GRLMR was observed but do observe it for GRLMR-SeBP. At higher concentrations of $HNaSeO_3$ (10 – 40 mM) both GRLMR-SeBP and GRLMR had the same overall activity within error (data not shown), and both enzymes produce abundant nanoparticle product.

Table 2.2. Kinetic values for GRLMR-SeBP and GRLMR

	$HNaSeO_3$		GSSG	
	GRLMR-SeBP	GRLMR	GRLMR-SeBP	GRLMR
K_M (mM)	0.217±0.057	1.921±1.279	0.365±0.043	0.253±0.033
k_{cat} (min^{-1})	40.316±2.486	22.823±8.839	14784±720	14498±624

In the reduction of GSSG, the k_{cat} for the two enzymes was unaffected by the presence of the SeBP as both values were within error of each other. These results indicate that the presence of SeBP on GRLMR does not hinder native function of the enzyme but does increase the enzymes ability to reduce a secondary substrate, SeO_3^{2-}. It was hypothesized that some of the increased activity of GRLMR-SeBP arises from the peptide introducing 5 positively charged residues proximal (34 Å) to the enzyme active site. The introduction of these residues results in a favorable charge-charge interaction with the negatively charged SeO_3^{2-} anions and may allow for a higher effective concentration of the substrate near the active site.

2.2.6 *Raman Spectroscopy of SeBP*

Attempts to calculate a binding isotherm for SeBP to SeNPs proved unsuccessful and can be found in **Appendix B.3**, however evidence was strong in supporting the interaction between the two. Raman Spectroscopy allows structural insight into the nature of the interaction between SeBP and the SeNP surface. **Figure 2.8** shows an overlay of the Raman spectra of the peptide in the

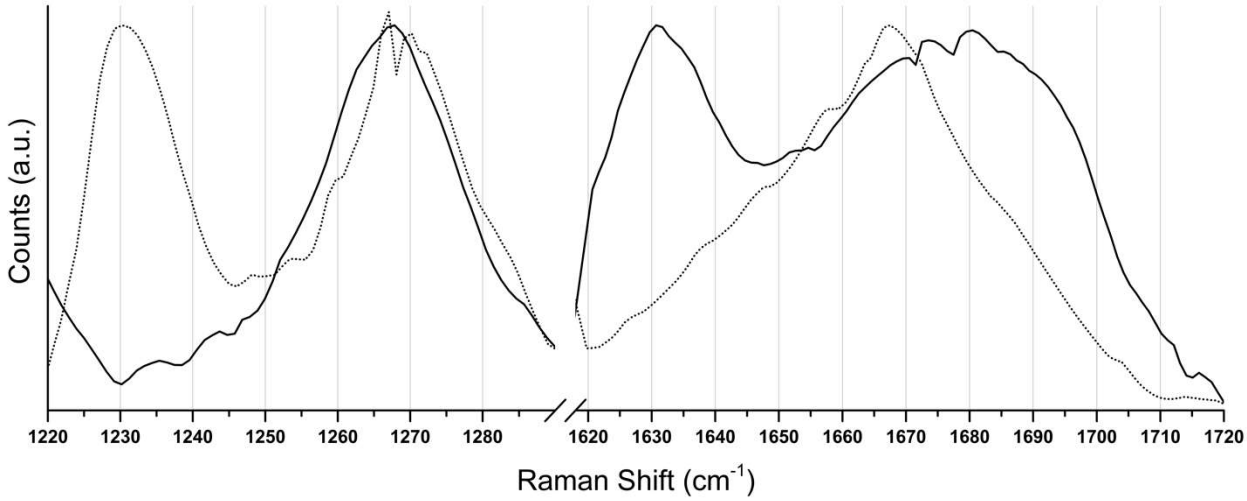

Figure 2.8. Raman spectra of bound (**dotted**) and unbound (**solid**) SeBP. The peak at ~1230 cm^{-1} represents an approximate assignment depicting the shift of the amide III mode to a β-sheet like structure when bound to the surface of the particle. The broad peak seen at 1680 cm^{-1} indicates a random or α-helical structure of the SeBP backbone when SeNP is omitted from the sample.

presence and absence of SeNPs, where the large differences in the spectra suggest a substantial interaction between peptide and nanoparticle.

It was interpreted that these spectral changes in the presence of SeNPs were arising from two changes in the peptide: First, a change in the peptide backbone conformation. Second, multiple changes to the ligation environment of the imidazole rings of the histidine residues in the peptide.

Changes in peptide backbone conformation are ascertained in Raman spectra from the so-called Amide I, Amide II and Amide III vibrational modes. This corresponds to complex amide related vibrational modes in the peptide backbone. The amide I backbone mode is located in the 1600 – 1700 cm^{-1} region.[116] This mode is considerably influenced by transition dipole coupling, which describes the conformational dependence of the dipole interaction energy on spatial separation and orientation.[116,117] The amide III mode is located in the 1200 – 1320 cm^{-1} region and is also sensitive to structural rearrangement.[116–118]

The amide I mode is in the 1650 – 1710 cm^{-1} region as shown in **Figure 2.8**. The broadness and location of peak corresponding to the amide I mode in the absence of SeNPs is suggestive of a disordered backbone structure (**Figure 2.8, solid trace**). In the presence of SeNPs, the peak

corresponding to the amide I mode narrows and downshifts to 1667 cm^{-1}, suggestive of a β-sheet type backbone structure (**Figure 2.8, dashed trace**). This assignment of a change in backbone structure from disordered to β-sheet-like after SeNP binding interaction is also suggested in the amide III mode.

The amide III mode is in the 1200 – 1320 cm^{-1} region as shown in **Figure 2.8** and when unbound the mode may be hidden behind the His modes centered at 1268 cm^{-1} (**Figure 2.8, solid trace**). An amide III mode centered about 1260 cm^{-1} suggests an unordered structure, and one that is centered at 1265 cm^{-1} is suggestive of either an α-helix or a polyproline II (PPII) type structure. The presence of PPII structure is likely, since the peptide contains a Pro residue, which is the cause of this structure type.[116] Furthermore, the presence of a proline makes helical structure unlikely in a dodecapeptide. Upon binding to a NP, it is proposed that the amide III mode downshifts to 1230 cm^{-1} which also corresponds with a β-sheet structure.[118,119]

In addition to the evidence for an ordering in backbone structure that is induced by the presence of SeNPs, evidence was also observed that binding of the SeNP to the peptide is driven by interactions with the imidazole rings of the 5 His residues in the peptide. Imidazole is well-known to coordinate with metal ions. In the context of Raman spectra, tautomer markers in the 900 – 1630 cm^{-1} region are used to identify His-metal binding.[120]

By convention, each atom within the imidazole ring of His is labeled as shown in the Lewis diagram of Histidine shown as an inset in **Figure 2.9**. Vibrations arising from bonds between nitrogen and carbon atoms (and bonded hydrogen atoms) that are labeled C^2, C^4, C^5, N^τ and N^π are of special interest in examining His-metal binding.[120–123] Tautomer markers used to assign His – SeNP binding are listed in **Appendix B, B.4, Table B.**1.

The **Figure 2.9** peak spanning 1631 – 1636 cm^{-1} correlates with the histidine C^4-C^5 stretch mode, consistent with a specific N^τ-H/N^π-H protonation state ($HisH^{2+}$). This assignment is supported by the presence of the peak at 1268 cm^{-1} (**Appendix B, B.5, Figure B.3**), which also corresponds to a $HisH^{2+}$ imidazolium ion. In the SeNP bound SeBP trace, the C^4-C^5 stretching mode downshifts to a broad peak centered at 1571 cm^{-1}. The features of this peak are shown in

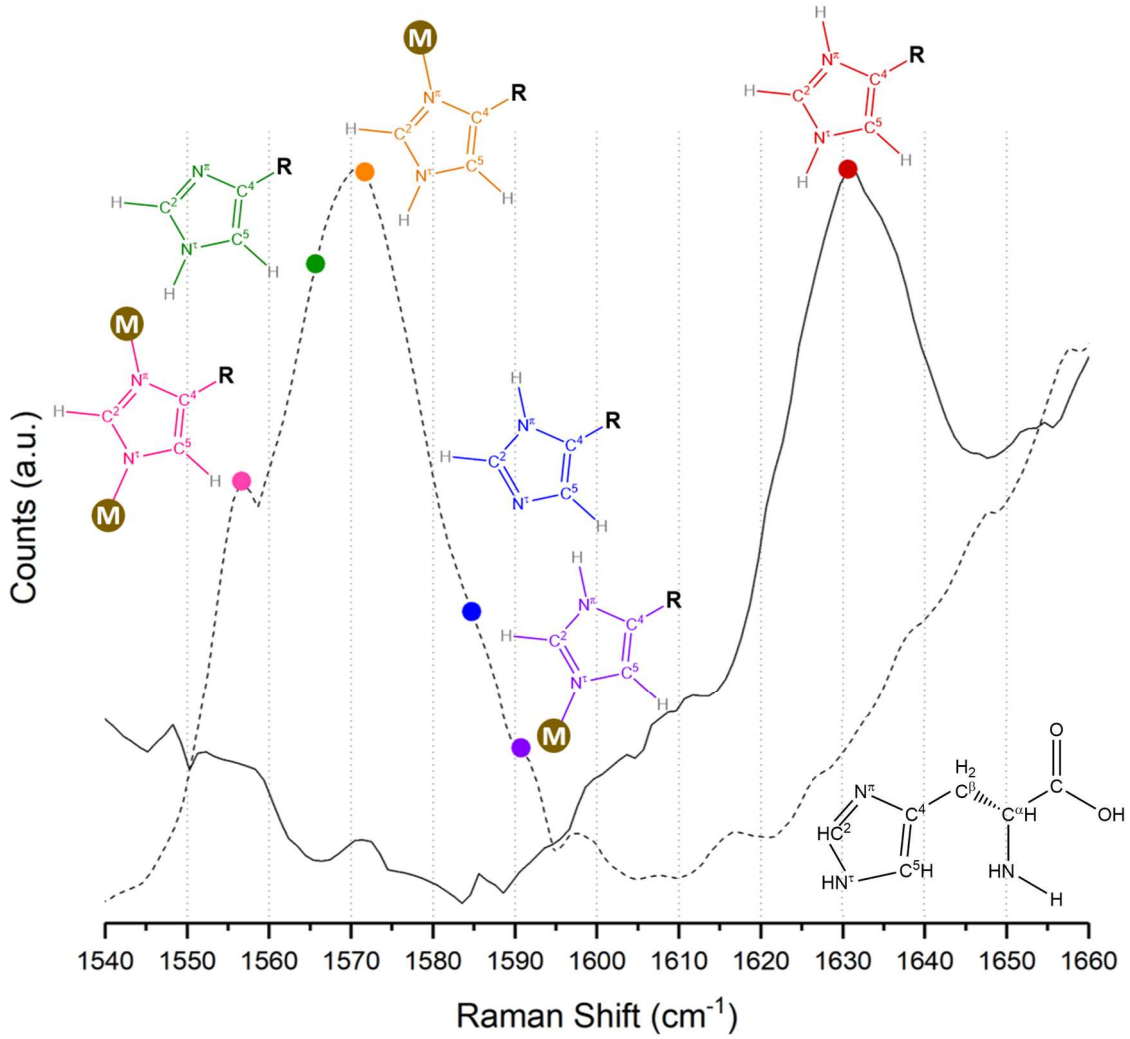

Figure 2.9. Traces of SeBP (solid) and SeBP/SeNP (dashed) from **Figure 5**, expanded to the 1540 – 1660 cm^{-1} region to show the relevant His modes described. The marks are color coded to the structure that represents each shift shown. Histidine is represented in the lower right corner.

Figure 2.9 and are color-coded with the respective vibration depicted. The region of the peak from 1565 – 1573 cm^{-1} likely corresponds to a neutral imidazole form (HisH) that is unbound with the N^{τ} tautomer protonated and the N^{π} unprotonated. The portion of the peak above 1573 cm^{-1} likely corresponds with a metal bound His in the form N^{τ}-H/N^{π}-M.

This assignment is supported by the shift in the band at 1268 cm^{-1} (**Figure S6**).[120] Upon metal binding to SeNP with the tautomer form N^{τ}-H/N^{π}-M, the band splits into a doublet with peaks at 1267 cm^{-1} and 1271 cm^{-1}. The 1267 cm^{-1} band is attributed to HisH in the form Nτ-H and unbound

Nπ whereas the 1271 cm^{-1} band correlates with a Nτ-H/Nπ-M form, which agrees with the findings by Takeuchi.[120] The peak at 1556 cm^{-1} is likely due to a metal bridging form of His (N^{τ}-M/N^{π}-M) with the corresponding shoulder arising at 1282 cm^{-1} (**Appendix B, B.5, Figure B.3**).

Overall, the Raman spectra of the peptide in the presence and absence of SeNPs support a specific interaction between SeBP and SeNPs. Here, SeNP binding is mediated primarily by previously described His-metal ligation interactions, and the aggregate of these interactions appears to drive a change in peptide backbone conformation that is consistent with a change from random coil to beta-sheet-like.

2.3 Summary and Conclusions

This work demonstrates the ability to manipulate the enzymatic activity and product outcome of a SeNP producing GRLMR isolated from *P. moraviensis* stanleyae by fusion of a SeBP to the enzyme. SeBP, selected from a phage display library against GRLMR produced SeNPs of ~8nm, when studied exogenously did not show any propensity for size control or particularly strong SeNP binding. However, once fused to the C-terminal of GRLMR, improvements in resulting SeNP stability, size control, SeNP retention, and improved reduction rates of selenite were all observed. The outcome of this work proves exciting for the future identification of metal reducing enzymes which already can make inorganic nanostructures. In combination with substrate binding peptides that can also be expressed fused to the metal reducing enzyme, inorganic materials with defined characteristics can be produced in a completely green approach with everything but the inorganic salt being produced within a cell.

2.4 Experimental Details

2.4.1 *Materials*

The Ph.D.™ Phage Display Kit, BSA, BspQI, T4 Ligase, Q5 High Fidelity polymerase, dNTPs, and BL21(DE3) *E. coli* were purchased from New England Biolabs. Antibiotics were purchased from GoldBio. Na_2SeO_3 and $HNaSeO_3$ were purchased from Alfa Aesar. NADPH was purchased from BioVision and Coomassie Plus Bradford Reagent from Thermo Scientific. GeneJet Plasmid

Miniprep Kit (Cat# K0503) and PCR Cleanup Kit (Cat# K0702) were purchased from ThermoFisher Scientific.

2.4.2 *Phage Binding Assays*

Initial preparation of the plate for SeNP binding assays were prepared as follows: in a 96-well polystyrene plate a mixture of GRLMR, selenite and NADPH at concentrations previously found to produce ~5 nm SeNPs was added to 3 x 23 wells in 100 µL aliquots.[23] The wells then incubated overnight at RT with agitation and then spun for 2 hr at 4000 RPM and 4°C. Supernatant was then dumped and a 100 µL of a solution of filter sterilized 5 mg/mL BSA and 0.1 M $NaHCO_3$ pH 8.6 was then added to each well and allowed to incubate for at least 1 hour under agitation at 4°C. This solution was then dumped, and the wells were then washed 6 times with TBS supplemented with 0.1% [v/v] Tween-20. 100 µL of a phage solution diluted to 10^{11} pfu in TBS supplemented with 0.1% [v/v] Tween-20 was added to the first 23 wells. Phage was permitted to bind for 60 minutes after which time the excess solution was dumped from the wells. Wells were then rapidly washed 10 times with a TBS buffer supplemented with 0.25% [v/v] Tween-20 to remove weak binding phage. These steps were repeated 2 times for a total of 3 rounds of selection with progressively more stringent binding and washing steps to ensure stronger binders would be collected. In round 2 the wash step was performed using TBS supplemented with 0.5% [v/v] Tween-20. In round 3 the binding step was reduced to 10 minutes and washing was done using TBS supplemented with 0.5% [v/v] Tween-20. Bound phage was eluted after each wash step using 100 µL of a 0.2 M glycine-HCl pH 2.2, BSA 1 mg/mL solution in each well for 15 minutes. This solution was then immediately neutralized using 1 M Tris-HCl pH 9.1. Negative binding assays were run similarly with the targets polystyrene, unreacted GRLMR, or SiNPs in a 0.1 M $NaHCO_3$ pH 8.6.

2.4.3 *Phage Titers*

Phage titers were performed using *E. coli* ER2738 from the NEB Ph.D.™ Phage Display Kit. Initially, ER2738 cells were plated on a clean LB Agar plate supplemented with tetracycline and grown overnight. A small volume of LB with tetracycline was inoculated with a colony of ER2738

and grown overnight at 37°C and 225 RPM. A volume of LB required for the titers was then inoculated the next day and grown to an $OD_{600} \approx 0.4$. A phage solution was then diluted in the ranges of $10^1 - 10^8$ *pfu*. In a 96-well plate, 180 µL of the cells was added to several wells that corresponds to the number of dilutions to be titered. 20 µL of the diluted phage solutions were added to the corresponding wells and infection was allowed for 30 minutes. After infection, 3 x 10 µL of infected cells were deposited on a LB plate containing Xgal and IPTG in a β-galactosidase based identification of infected cells. The plate was then grown overnight at 37°C and the next day blue spots, correlating to the number of infected colonies were counted. The number of infected colonies could then be multiplied by the dilution factor to give an estimate on the concentration of phage in the phage solutions.

2.4.4 *Protein Isolation/Characterization*

SeBP was fused to GRLMR through way of outward PCR with one of the primers used containing the SeBP insert. The PCR product was then digested and circularized before transformation into BL21 (DE3) cells. The plasmids used are shown in **Appendix B, B.6**. For expression and isolation of GRLMR-SeBP 7 mL cultures of BL21(DE3) cells containing the GRLMR-SeBP or GRLMR were started and grown O/N in a shaker at 37°C and 225 RPM. The dense cultures were diluted into 1 L of LB Kan/Cam and allowed to grow until an OD_{600} ~0.5 – 0.6. Induction was started using a 1 mM final concentration of IPTG and was supplemented with 1 µM of $HNaSeO_3$. Growth was O/N at 37°C. Cells were then spun down at 14000 RPM for 20 minutes and resuspended into B-PER and sonicated to lyse the cells. The insoluble cell debris was removed by centrifugation and the soluble cell lysate was collected for Ni-NTA purification. Nickel columns were prepared using Ni-NTA agarose beads. Beads were washed as follows: 3x3 column volumes of H_2O, 3x3 column volumes of binding buffer (50 mM Tris-HCl pH 8, 5 mM imidazole, 100 mM NaCl). The lysate was then run through the column 3x before 4 cycles of washing the column using washing buffer (50 mM Tris-HCl pH 8, 20 mM imidazole, 300 mM NaCl). Finally, the column was incubated with column volume of elution buffer (50 mM Tris-HCl pH 8, 300 mM imidazole, 50 mM NaCl) for at least 5 minutes before the elution buffer was

collected. The isolated protein solution was dialyzed into PBS before the concentration was collected using UV-Vis and stored at -80°C in aliquots for further study. A native PAGE gel was then run to ensure the positively charged SeBP was present on the isolated GRLMR.

2.4.5 *Enzymatic SeNP formation*

100 µg of enzyme and aliquots of a 100 mM $HNaSeO_3$ solution were added to PBS, pH 7.4. The reaction was then started by the introduction of NADPH and allowed to react for several hours. After a several hours, the SeNPs were spun down and separated from the supernatant for further study.

2.4.6 *Bradford Assay*

Stocks of enzyme in PBS, pH 7.4 at various concentrations were prepared of which 100 µL were diluted by 900 µL of Bradford reagent. Standard curves were collected for both the GRLMR and GRLMR-SeBP by monitoring the absorbance at 595 nm. Samples were then prepared for measurement in the same fashion by taking 100 µL of the target solution and diluting it up with 900 µL Bradford reagent. The concentration was then calculated by monitoring the absorbance at 595 nm.

2.4.7 *PAGE Electrophoresis*

Native gels were prepared as follows: 1.25 mL of 40% polyacrylamide, 1.25mL of Tris buffer (pH 8.8), and 50 µL of a 10% ammonium persulfate (w/v) were diluted into 2.45mL of milli-Q water with or without 50 µL of a 10% SDS solution for denaturing or native gels. Polymerization was initiated by adding 7µL of TEMED before pouring the PAGE solution into a cast and allowing to solidify. PAGE gels were run in tris/glycine, pH 8.3 buffer with or without SDS at 150 V for 2.5 h at 4°C. For pH 6.6 PAGE gels, the gel buffer and running buffer was replaced with buffer containing 25 mM histidine and 30 mM MOPS giving a buffer of similar ionic strength and pH of 6.6.[39] Gels were then submerged in Coomassie blue and microwaved for 30 sec and incubated for an addition 5 min at RT. Coomassie stain was then replaced by milliQ water and microwaved for 5 min, then washed again in the same way before imaging. Native gels would also be run and later

soaked in 5 mM $HNaSeO_3$ and 1 mM NADPH inside of a plastic bag under nitrogen. These gels would result in red bands of reduced selenium that could then be visualized the next day.

2.4.8 *Dynamic Light Scattering*

Reactions for DLS monitoring were prepared in disposable plastic cuvettes as described above. SeNP formation was monitored using a refractive index of 2.6 and an absorbance of 0.5 for α-Se and a refractive index and viscosity of PBS of 1.332 and 0.8898 cP, respectively. Reactions ran for at least 4 hours at RT.

2.4.9 *Kinetics Studies*

Initial velocities (V_0) of the GRLMR-SeBP were performed in various concentrations of $HNaSeO_3$ or GSSG while monitoring 340 nm correlating to NADPH absorbance. The reactions were run in PBS, pH 7.4 and with 13 µg of enzyme with substrate SeO_3^{2-} (1.5 µg of enzyme with substrate GSSG) and 200 µM of NADPH with 0.05 mM – 2 mM of substrate. Enzymatic V_0s were plotted against substrate concentration in OriginPro from which K_M and k_{cat} could then be calculated.

2.4.10 *Synthesis of SeBP capped SeNPs*

Peptide-capped SeNPs were synthesized based on the method from Nath *et al*. For the SeNPs, 50 – 100 µL of acidic 10 mM SeO_3^{2-} and 0.5 – 1.0 mL of 10 mM $NaBH_4$ (aq) were added to a 15 mL conical tube and diluted to a final volume of 1.5 – 3.0 mL with milliQ water. The solution was mixed and placed on a rocker for 90 – 300 seconds, after which 50 – 100 µL of 10 mM of the SeBP was added and thoroughly mixed into the solution and placed back on the rocker. Within 10 minutes the tube was placed in an ice bag and allowed to conjugate for 4 hours on the rocker. After this, the solution was dialyzed using a 3,500 MWCO cassette on ice in 2.0 L milliQ water for at least 2 hours. The resulting mixture was lyophilized and stored in a refrigerator until future analysis. The sample was diluted into 50 µL PBS, pH 7.4.

2.4.11 *Raman Spectroscopy*

Raman spectra were collected using an inverted Raman microscope with an Olympus IX73 frame and objectives with a Horiba iHR 550 Spectrometer with a neural synapse thermoelectrically

cooled charge-coupled device (CCD) detector attached to a Horiba ONDAX T-Hz Raman 532 nm laser. This setup was accompanied with a LabSpec software package. The specimen was prepared by drop-casting 3-7 μL of sample onto a glass cover slip and allowed to dry in air at room temperature. Double-sided tape was used to seal the sample and to adhere the coverslip to a glass slide. Spectra were collected using an incident laser power of 83 mW. A 60x water objective was used with a 1200 blazes/mm grating, which has a resolution of approximately 2 cm^{-1} per pixel. The laser was manually focused on the sample using the optical setup. If signal was insufficient, the laser was refocused until signal was obtained. The software's denoiser program was used, which is essentially a smoothing algorithm, to obtain a smoother curve. Backscatter collection ranged from 30 – 300 seconds per acquisition, and a total of 1 – 15 spectra were accumulated and averaged, depending on the level of noise. Any spikes caused by cosmic rays were removed using the software's spike removal function.

REFERENCES

20. Shu, X. *et al.* A Genetically Encoded Tag for Correlated Light and Electron Microscopy of Intact Cells, Tissues, and Organisms. *PLOS Biology* **9**, e1001041 (2011).
21. Martell, J. D. *et al.* Engineered ascorbate peroxidase as a genetically-encoded reporter for electron microscopy. *Nat Biotechnol* **30**, 1143–1148 (2012).
22. Fox, B. & Walsh, C. T. Mercuric reductase. Purification and characterization of a transposon-encoded flavoprotein containing an oxidation-reduction-active disulfide. *J. Biol. Chem.* **257**, 2498–2503 (1982).
23. Ni, T. W. *et al.* Progress toward clonable inorganic nanoparticles. *Nanoscale* **7**, 17320–17327 (2015).
38. Staicu, L. C. *et al.* Pseudomonas moraviensis subsp. stanleyae, a bacterial endophyte of hyperaccumulator Stanleya pinnata, is capable of efficient selenite reduction to elemental selenium under aerobic conditions. *J. Appl. Microbiol.* **119**, 400–410 (2015).
39. Fernández-Llamosas, H., Castro, L., Blázquez, M. L., Díaz, E. & Carmona, M. Speeding up bioproduction of selenium nanoparticles by using Vibrio natriegens as microbial factory. *Sci Rep* **7**, 16046 (2017).
47. Freedman, Z., Zhu, C. & Barkay, T. Mercury Resistance and Mercuric Reductase Activities and Expression among Chemotrophic Thermophilic Aquificae. *Appl Environ Microbiol* **78**, 6568–6575 (2012).
78. Mackenzie, E. L., Iwasaki, K. & Tsuji, Y. Intracellular Iron Transport and Storage: From Molecular Mechanisms to Health Implications. *Antioxid Redox Signal* **10**, 997–1030 (2008).
79. Engst, S. & Miller, S. M. Rapid Reduction of Hg(II) by Mercuric Ion Reductase Does Not Require the Conserved C-Terminal Cysteine Pair Using HgBr2 as the Substrate. *Biochemistry* **37**, 11496–11507 (1998).
80. Holmes, J. D. *et al.* Energy-dispersive X-ray analysis of the extracellular cadmium sulfide crystallites of Klebsiella aerogenes. *Arch. Microbiol.* **163**, 143–147 (1995).
81. Cunningham, D. P. & Lundie, L. L. Precipitation of cadmium by Clostridium thermoaceticum. *Appl. Environ. Microbiol.* **59**, 7–14 (1993).
82. Klaus-Joerger, T., Joerger, R., Olsson, E. & Granqvist, C.-G. Bacteria as workers in the living factory: metal-accumulating bacteria and their potential for materials science. *Trends in Biotechnology* **19**, 15–20 (2001).
83. Reduction of Selenite and Detoxification of Elemental Selenium by the Phototrophic BacteriumRhodospirillum rubrum | Applied and Environmental Microbiology. Available at: https://aem.asm.org/content/65/11/4734.long. (Accessed: 14th December 2018)
84. Yong, P., Rowson, N. A., Farr, J. P. G., Harris, I. R. & Macaskie, L. E. Bioreduction and biocrystallization of palladium by Desulfovibrio desulfuricans NCIMB 8307. *Biotechnology and Bioengineering* **80**, 369–379 (2002).
85. Sweeney, R. Y. *et al.* Bacterial Biosynthesis of Cadmium Sulfide Nanocrystals. *Chemistry & Biology* **11**, 1553–1559 (2004).
86. Bai, H. J., Zhang, Z. M., Guo, Y. & Yang, G. E. Biosynthesis of cadmium sulfide nanoparticles by photosynthetic bacteria Rhodopseudomonas palustris. *Colloids and Surfaces B: Biointerfaces* **70**, 142–146 (2009).

87. Ovais, M. *et al.* Biosynthesis of Metal Nanoparticles via Microbial Enzymes: A Mechanistic Approach. *International Journal of Molecular Sciences* **19**, 4100 (2018).
88. Singh, P. *et al.* Biosynthesis, characterization, and antimicrobial applications of silver nanoparticles. *Int J Nanomedicine* **10**, 2567–2577 (2015).
89. Zhou, S. *et al.* Reducing capacity and enzyme activity of chromate reductase in a ChrT-engineered strain. *Exp Ther Med* **14**, 2361–2366 (2017).
90. Chasteen, T. G., Fuentes, D. E., Tantaleán, J. C. & Vásquez, C. C. Tellurite: history, oxidative stress, and molecular mechanisms of resistance. *FEMS Microbiol Rev* **33**, 820–832 (2009).
91. Castro, M. E., Molina, R., Díaz, W., Pichuantes, S. E. & Vásquez, C. C. The dihydrolipoamide dehydrogenase of Aeromonas caviae ST exhibits NADH-dependent tellurite reductase activity. *Biochemical and Biophysical Research Communications* **375**, 91–94 (2008).
92. Calderón, I. L. *et al.* Catalases Are NAD(P)H-Dependent Tellurite Reductases. *PLOS ONE* **1**, e70 (2006).
93. Sabaty, M., Avazeri, C., Pignol, D. & Vermeglio, A. Characterization of the Reduction of Selenate and Tellurite by Nitrate Reductases. *Appl. Environ. Microbiol.* **67**, 5122–5126 (2001).
94. Curran, C. D. *et al.* Direct Single-Enzyme Biomineralization of Catalytically Active Ceria and Ceria–Zirconia Nanocrystals. *ACS Nano* **11**, 3337–3346 (2017).
95. Chowdhury, T., Sarkar, M., Chaudhuri, B., Chattopadhyay, B. & Halder, U. C. Participatory role of zinc in structural and functional characterization of bioremediase: a unique thermostable microbial silica leaching protein. *J Biol Inorg Chem* **20**, 791–803 (2015).
96. Dunleavy, R., Lu, L., Kiely, C. J., McIntosh, S. & Berger, B. W. Single-enzyme biomineralization of cadmium sulfide nanocrystals with controlled optical properties. *PNAS* **113**, 5275–5280 (2016).
97. Spangler, L. C. *et al.* Enzymatic biomineralization of biocompatible CuInS2, (CuInZn)S2 and CuInS2/ZnS core/shell nanocrystals for bioimaging. *Nanoscale* **9**, 9340–9351 (2017).
98. Spangler, L. C., Lu, L., Kiely, C. J., Berger, B. W. & McIntosh, S. Biomineralization of PbS and PbS–CdS core–shell nanocrystals and their application in quantum dot sensitized solar cells. *J. Mater. Chem. A* **4**, 6107–6115 (2016).
99. Yang, Z., Lu, L., Kiely, C. J., Berger, B. W. & McIntosh, S. Single Enzyme Direct Biomineralization of CdSe and CdSe-CdS Core-Shell Quantum Dots. *ACS Appl. Mater. Interfaces* **9**, 13430–13439 (2017).
100. Nemeth, R., Neubert, M., Butz, Z. J., Ni, T. W. & Ackerson, C. J. Metalloid Reductase of Pseudomonas moravenis Stanleyae Conveys Nanoparticle Mediated Metalloid Tolerance. *ACS Omega* **3**, 14902–14909 (2018).
101. Flynn, C. E. *et al.* Synthesis and organization of nanoscale II–VI semiconductor materials using evolved peptide specificity and viral capsid assembly. *J. Mater. Chem.* **13**, 2414–2421 (2003).
102. Dickerson, M. B. *et al.* Identification and Design of Peptides for the Rapid, High-Yield Formation of Nanoparticulate TiO2 from Aqueous Solutions at Room Temperature. *Chem. Mater.* **20**, 1578–1584 (2008).
103. Dickerson, M. B., Naik, R. R., Stone, M. O., Cai, Y. & Sandhage, K. H. Identification of peptides that promote the rapid precipitation of germania nanoparticle networks via use of a peptide display library. *Chem. Commun.* **0**, 1776–1777 (2004).

104. Reiss, B. D. *et al.* Biological Routes to Metal Alloy Ferromagnetic Nanostructures. *Nano Lett.* **4**, 1127–1132 (2004).
105. Naik, R. R. *et al.* Peptide Templates for Nanoparticle Synthesis Derived from Polymerase Chain Reaction-Driven Phage Display. *Advanced Functional Materials* **14**, 25–30 (2004).
106. Li, C., Botsaris, G. D. & Kaplan, D. L. Selective in Vitro Effect of Peptides on Calcium Carbonate Crystallization. *Crystal Growth & Design* **2**, 387–393 (2002).
107. Lee, S.-W., Mao, C., Flynn, C. E. & Belcher, A. M. Ordering of Quantum Dots Using Genetically Engineered Viruses. *Science* **296**, 892–895 (2002).
108. Oh, D. *et al.* Biologically enhanced cathode design for improved capacity and cycle life for lithium-oxygen batteries. *Nature Communications* **4**, 2756 (2013).
109. Courchesne, N.-M. D. *et al.* Assembly of a bacteriophage-based template for the organization of materials into nanoporous networks. *Adv Mater* **26**, 3398–3404 (2014).
110. Oh, D. *et al.* M13 Virus-Directed Synthesis of Nanostructured Metal Oxides for Lithium–Oxygen Batteries. *Nano Lett.* **14**, 4837–4845 (2014).
111. Ahmad, G. *et al.* Rapid Bioenabled Formation of Ferroelectric BaTiO3 at Room Temperature from an Aqueous Salt Solution at Near Neutral pH. *J. Am. Chem. Soc.* **130**, 4–5 (2008).
112. Bassindale, A. R., Codina-Barrios, A., Frascione, N. & Taylor, P. G. An improved phage display methodology for inorganic nanoparticle fabrication. *Chem. Commun.* **0**, 2956–2958 (2007).
113. Carter, C. J., Ackerson, C. J. & Feldheim, D. L. Unusual Reactivity of a Silver Mineralizing Peptide. *ACS Nano* **4**, 3883–3888 (2010).
114. Birrell, G. B., Hedberg, K. K. & Griffith, O. H. Pitfalls of immunogold labeling: analysis by light microscopy, transmission electron microscopy, and photoelectron microscopy. *J Histochem Cytochem.* **35**, 843–853 (1987).
115. McLellan, T. Electrophoresis buffers for polyacrylamide gels at various pH. *Analytical Biochemistry* **126**, 94–99 (1982).
116. Singh, B. R. *Infrared analysis of peptides and proteins*. (American Chemical Society, 2000).
117. Barth, A. Infrared spectroscopy of proteins. *Biochimica et Biophysica Acta (BBA) - Bioenergetics* **1767**, 1073–1101 (2007).
118. Talari, A. C. S., Movasaghi, Z., Rehman, S. & Rehman, I. ur. Raman Spectroscopy of Biological Tissues. *Applied Spectroscopy Reviews* **50**, 46–111 (2015).
119. DiGuiseppi, D. & Schweitzer-Stenner, R. Probing conformational propensities of histidine in different protonation states of the unblocked glycyl-histidyl-glycine peptide by vibrational and NMR spectroscopy. *Journal of Raman Spectroscopy* **47**, 1063–1072 (2016).
120. Takeuchi, H. Raman structural markers of tryptophan and histidine side chains in proteins. *Biopolymers* **72**, 305–317 (2003).
121. Zhu, G., Zhu, X., Fan, Q. & Wan, X. Raman spectra of amino acids and their aqueous solutions. *Spectrochim Acta A Mol Biomol Spectrosc* **78**, 1187–1195 (2011).
122. Toyama, A., Ono, K., Hashimoto, S. & Takeuchi, H. Raman Spectra and Normal Coordinate Analysis of the N1−H and N3−H Tautomers of 4-Methylimidazole: Vibrational Modes of Histidine Tautomer Markers. *J. Phys. Chem. A* **106**, 3403–3412 (2002).
123. Hasegawa, K., Ono, T. & Noguchi, T. Vibrational Spectra and Ab Initio DFT Calculations of 4-Methylimidazole and Its Different Protonation Forms: Infrared and Raman Markers of the Protonation State of a Histidine Side Chain. *J. Phys. Chem. B* **104**, 4253–4265 (2000).

CHAPTER 3: CONSTRUCTION AND UTILIZATION OF A 'CLONEABLE' NANOPARTICLE TAG

3.1 Introduction

Biological imaging continues to be difficult and arduous to attain. At this point in cellular understanding, the ability to identify with precision the location of individual proteins in a cell has yet to be recognized. High resolution light microscopy is being continuously refined to mitigate its own limitations, yet these protocols are arduous and expensive. Current techniques rely on two main approaches, photoactivated localization microscopy (PALM), and stochastic optical reconstruction microscopy (STORM). These foundational techniques work by localizing emitted light by way of utilizing on/off states of the fluorescing probes. A fundamental difference between these two approaches is the way fluorescence is introduced to the sample and as a result the nature of the on/off states. Immunostaining with a fluorescent molecule is utilized in STORM. This fluorescent dye then undergoes photo blinking, a result of the competitive radiative and non-radiative relaxation from the dye's excited state.[124] PALM relies on genetically encoded fluorescing proteins which undergo activation, a lifetime of emission, and finally photobleaching rendering the fluorophores inactive.[125] The ability for individual fluorophores to be "on" in a backdrop of "off" states allows for the sharpening of the point spread function of the emitted photons. Images collected over a time frame can then be layered to elucidate cellular structures with resolution of 10s of nanometers.

These techniques although deserving of the 2014 Nobel prize in Chemistry, have several drawbacks that bottleneck their general application.[8,10,12] First, STORM utilizes immunostaining, a technique relying on the diffusion of large antibodies in a post-fixed cell. This limits the technique in two significant ways: (i) to develop an antibody for a unique target requires time and money not readily available to many labs. (ii) The processing of a sample provides many points at which the antibody is hindered in its target binding.[126–128] Second, PALM relies on

photobleaching for the localization of fluorescence signals. Photobleaching is a double-edged sword; while providing a way to isolate individual fluorescence signals the photobleaching limits the number of photons that can be collected by the detector thereby reducing point spread function sharpening.[129] Both techniques also require expensive instrumentation not readily available to institutions without a well-funded light microscopy division.

Approaches utilizing electron microscopy (EM) show great promise in meeting the resolutions desired in biological imaging by utilizing electrons instead of light. An electron beam is shot at a sample which are then scattered or absorbed. Transmission electron microscopy (TEM) detects electrons that have passed through a sample and hit the detector while scanning electron microscopy (SEM) detects the scattered electrons from a sample. TEM is capable of greater resolution than SEM due to a higher energy electron beam while SEM is generally less time intensive and damaging to the sample. One hinderance of using EM for biological imaging is the composition of the sample. Biology consists of electron "light" elements, *i.e.* carbon, oxygen, hydrogen, phosphorous, and nitrogen. These electronically "light" atoms interact less with the electron beam than heavier elements resulting in a lack of contrast within a sample.

Heavier elemental stains have been used to add contrast to biological samples. Uranyl acetate (UA), potassium permanganate ($KMnO_4$), and osmium tetroxide (OsO_4) have been widely used to give contrast to biological electrographs both *in vitro* and *in vivo* through interaction with biological molecules.[130–132] UA is generally used as a stain for *in vitro* samples. It is applied directly to a grid that contains a protein sample and interacts with functional groups present on the proteins. $KMnO_4$ and the acutely toxic OsO_4 are used for staining cell and tissue sections samples and can both be used as fixatives and contrasting agents. Care must be taken when using these strong oxidizers. OsO_4 sublimes at room temperature and even low doses can stain the cornea of the eye and cause strong irritation of the respiratory tract. OsO_4 is however reacts quickly and can fix proteins, lipids, and lipoproteins. OsO_4 is slow at penetrating however which limits the thickness the sample can be. $KMnO_4$ is far easier to handle and causes high contrast within cell membranes however much of the cellular material is lost during fixation and staining. Although

these various stains have provided contrast across a whole sample, they all still lack the specificity of contrast that is otherwise achieved in fluorescence microscopy. These stains also selectively bind certain biological molecules causing other structures or materials to be lost during the sample preparation.[133–136]

The state-of-the-art approach for specific biological contrast in EM uses a two-tier system. Initially, a protein-based tag is fused and expressed to a protein of interest. The first tier involves soaking the fixed sample in DAB which is stimulated to polymerize in the vicinity of the protein tag. The resulting DAB polymers are extremely osmiophilic and upon osmium staining (tier 2), increase the amount of deposition of osmium at the location of the DAB polymers. Ascorbic peroxidase (APEX) and mini-Single Oxygen Generator (mini-SOG) can be used as protein tags that can then stimulate the polymerization of DAB.[20,21,137]

Both APEX and min-SOG have been extensively studied since their discoveries in 2012 and 2011, respectively. Through circular permutation both enzymes can be used as split proteins that aid in studies of protein-protein interactions (PPi).[137–139] APEX can also be used in proteomic mapping through proximal biotinylation and later mass spectrometry analysis.[140] Mini-SOG has the advantage of being able to fluoresce as well as produce light-induced singlet oxygens that stimulate the polymerization of DAB although less effectively than APEX. Being able to combine fluorescence and EM contrast in a single tag is beneficial for correlative light-electron microscopy (CLEM), a technique that utilizes both light and electron imaging techniques. Biological samples are prone to beam damage over long viewing times or high voltages.[141] Being able to first identify locations of interest within a sample using fluorescence microscopy instead of scanning samples in EM could help reduce beam damage and prevent artifacts or sample destruction. As beneficial as these developed tags are, contrast is still a product of osmium localization through DAB polymerization which is prone to the issues previously discussed. First, DAB polymerization can occur away from the intended target as peroxidases are naturally occurring enzymes in any system. Secondly, the growing DAB polymers are susceptible to diffusion as the polymers grow. Thirdly,

OsO_4 staining has its own drawbacks of, slow penetration, cellular structure affinity, and acute toxicity.

The benefits to moving away from general metal stains or systems that attempt to localize them cannot be overstated. Incubation of a sample either pre- or post-fixation with soluble metal salts that diffuse readily through a sample overcomes the limitations of OsO_4. Utilizing a protein tag capable of forming inorganic particulate that can then be observed with EM also removes any of the drawbacks associated with DAB polymerization. An extended benefit of using protein-based tags is the expectation of identification of new enzymes or the mutational analysis of existing constructs to allow for the interactions with other metal salts not yet available. Much like GFP, cNPs could be used to add contrast to multiple target proteins using several different elemental nanoparticles.

The progress discussed in this chapter illustrates the work done to produce and confirm the function of cNPs. A glutathione reductase-like metalloid reductase, GRLMR isolated from *Pseudomonas moraviensis* stanleyea acts as the cNP enzyme for its Se-reductase activity.[23] An identified Se-binding peptide (SeBP) would also be fused to GRLMR conferring better activity, size control, and affinity to the Se-nanoparticle (SeNP) product. FtsZ, a tubulin homologue present in bacteria would act as the model system. FtsZ is a polymerizing protein responsible for forming the Z-ring in dividing bacterial cells.[142,143] The Z-ring is responsible for pinching off a bacterium into two daughter cells. FtsZ is of interest to this study as it has been explored extensively as a possible target for anti-bacterial medicines.[144–147] FtsZ structures have been observed *in vitro* and *in vivo* utilizing both EM and fluorescence microscopy. Overproduction of FtsZ, or the production of FtsZ in foreign hosts, often leads to longitudinal filaments formed in the cytoplasm. Structures observed by FtsZ tagged with GFP on the N- and C-term extended from formation of a proper Z-ring, periodic aggregates, and coils.[143,148–156] *In vitro,* FtsZ can form filaments, clumped filaments, coils, and rings depending on the polymerization environment, *i.e.* GTP/GDP, divalent cations, crowding molecules, interacting proteins, and pH.[149,151,157–167] Capable of being isolated in large

quantities and maintaining function in a wide range of environments makes FtsZ an excellent model system for purposes of cNP optimization.

GRLMR, like other glutathione reductases, is a homodimer and initial attempts were made to try to monomerize the enzyme through a sequence of truncations of the enzyme. Monomerization would serve two purposes: (i) preventing the protein tag from causing aggregation of the POI and (ii) minimizing the size of the tag which would otherwise inhibit native maturation and function of the POI. Attempts were also made by site specific mutagenesis in the dimerization interface as well as to concatenate a second, truncated binding domain of GRLMR to one of full length. These approaches are still undergoing various iterations.

In the meantime, two full length copies of GRLMR, both expressing SeBP at their C-terms were concatenated together and fused to either the C- or N-term of FtsZ (F-cSeNPHis and cSeNP-F, respectively). Experiments, both *in vitro* and *in vivo* result in structures with higher selenium density than surrounding areas when characterized using EM coupled with the elemental analysis technique, energy dispersive spectroscopy (EDS). SeNPs were also observed *in vitro* decorating F-cSeNPHis filaments that were seen in EM. Preparation and imaging of F-cSeNPHis *in vivo* proved difficult for several reasons but ultimately resulted in filaments of high contrast that could be observed in whole and sectioned cell samples.

3.2 Results and Discussion

3.2.1 *Attempts to Produce Monomeric GRLMR*

The GRLMR enzyme is a ~52 KDa homodimer and aligns well with glutathione reductase (GSHR) from *E. coli* shown in **Figure 3.1**. Like GSHR, GRLMR was assumed to be composed of 3 different domains: An FADH binding domain (AA 1 – 140, 265 – 336), an NADPH binding domain (AA 141 – 264), and a dimerization domain (337 – 450).[53] Dimerization poses a challenge when trying to utilize the enzyme as a cNP since it disrupts native function of target protein. To try to combat this, several attempts to monomerize GRLMR were attempted. Initially, truncations of the enzyme were produced trying to remove segments of the C-terminal binding domain. In another approach, point mutations were introduced in the dimer interface. Various mutations were

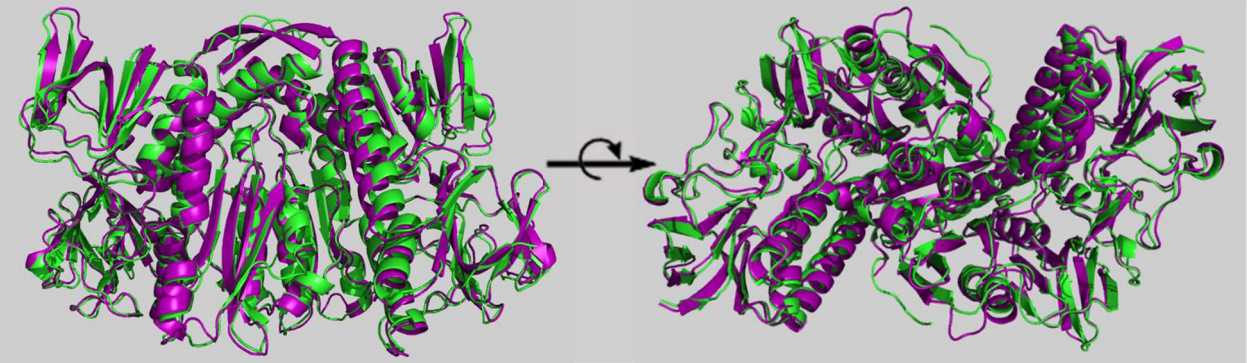

Figure 3.1. Alignment of the predicted structure for GRLMR (green) to GSHR (purple) from *E. coli*. The right image has been rotated 90° perpendicular to the plain of symmetry.

made however stable protein could not be isolated. The last attempt to be discussed in this chapter will be the fusion of a secondary binding domain to the C-terminus of GRLMR. Point mutations were made in the NADPH and FADH binding domains that had previously been described to improve stability of the dimerization domain.[168] None of these attempts were successful although all routes were not exhausted.

3.2.1.1 *GRLMR Truncation*

Protein truncation is a common tool in molecular biology used for expression of non-native proteins in host cells especially insoluble proteins, the identification of protein domains, or to identify crucial segments within a protein.[169–171] Truncation has also been used in order to produce split proteins that only act natively when the multiple segments of the same protein are brought into proximity as seen with GFP, APEX2, and mini-SOG.[137,172,173] It is was therefore hypothesized that truncation of the dimerization domain could lead to the production of a stable enzyme.

Three truncated variants were produced cutting 50 ($GRLMR_{400}$), 100 ($GRLMR_{350}$), and 150 ($GRLMR_{300}$) amino acids off the C-terminus. In order to produce these GRLMR variants, inverse PCR was used on the expression plasmid containing GRLMR. Construction of the variants were confirmed with sequencing. Plasmids were then transformed into *E. coli* cells and induction time screens were run to confirm expression of the truncate. Bands corresponding to the expected sizes of the GRLMR truncates were observed and grew in intensity throughout the induction screen (**Figure 3.2**). Next step was to try to isolate the enzymes and confirm the Se-reductase activity by

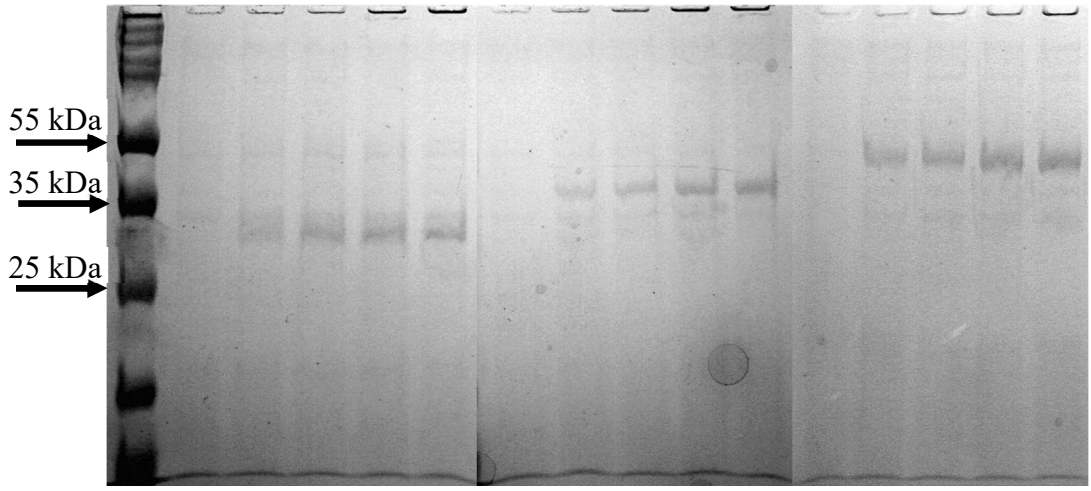

Figure 3.2. SDS-PAGE gel of an induction time assay of the three GRLMR truncates. The furthest left lane is a protein ladder. Times tested were 0, 1, 2, 3, and 4 hr induction times corresponding to the lanes. Lanes 2 – 6 are $GRLMR_{300}$ (35 kDa), lanes 7 – 11 are $GRLMR_{350}$ (41 kDa), and lanes 12 – 16 are $GRLMR_{400}$ (45 kDa).

the formation of red selenium particulate. With the lack of protein degradation, *E. coli* containing either the $GRLMR_{400}$, $GRLMR_{350}$, or the $GRLMR_{300}$ were induced for 8 hr. The next morning cells were homogenized, and soluble lysate was run on a Ni-NTA column. Wild type GRLMR possesses a bright yellow color when in solution making the presence of the protein easy to detect. A color change was not seen when the lysates containing the truncated variants was loaded onto the Ni-NTA column. Nevertheless, isolation proceeded and after several washes, the remaining bound protein was eluted using a high concentration of imidazole.

SDS-PAGE gel was then run to check on the presence of the truncated GRLMR variants but no bands were observed at corresponding molecular weights. Instead, when the insoluble cell debris was run in SDS-PAGE, a high concentration of protein could be seen at the expected molecular weights. Stable GRLMR truncates could not be isolated.

The stability of the GRLMR truncates was of concern. However, there are many examples of proteins being fused to an insoluble/unstable protein leading to its isolation and native function. Glutathione-S-transferase, thioredoxin, maltose-binding protein, calmodulin-binding protein, protein A, and DsbA have all been used to increase yields of foreign protein expression in host

cells.[174–179] $GRLMR_{300}$ was fused to the C-terminal of FtsZ in case the FtsZ imbued stability to $GRLMR_{300}$ (FG_{300}).

Growth and isolation of FG_{300} was similarly to GRLMR with an 8 hr induction and isolation using a Ni-NTA column. SDS-PAGE was run to check the purity of the isolated protein. Several bands, including a band that corresponded to FG_{300} at was found indicating the presence of degradation products or chaperone proteins (**Figure 3.3, Lane 2**). Further understanding of FtsZ expression and degradation pathways revealed that high levels of FtsZ are toxic to the cell and also prone to degradation by ClpXP after 3 hours of overproduction.[154,155,180,181] Induction times were then cut down to 3 hours resulting in a high purity FG_{300} that was then carried forward in polymerization studies (**Figure 3.3, Lane 3**).

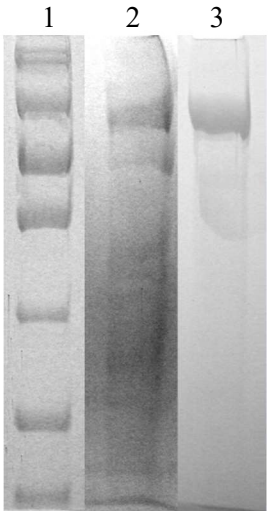

Figure 3.3. SDS-PAGE gel lanes of the eluted FG_{300} 8 hr induction (Lane 2) and 3 hr induction (Lane 3). Lane 1 is a protein ladder.

Polymerization reactions of FG_{300} were run with varying $[K^+]$, $[Mg^{2+}]$, $[FG_{300}]$, [Ficoll-70], [GTP], [GDP], and polymerization times in order to optimize polymerization. Sedimentation during centrifugation was used to gauge the ability of FG_{300} to polymerize. SDS-PAGE was used qualitatively to compare the soluble and insoluble fractions upon polymerization. Resulting PAGE gels however showed no difference between the various environments tested making it apparent that the utilization of a truncated GRLMR was infeasible and other routes would need to be taken.

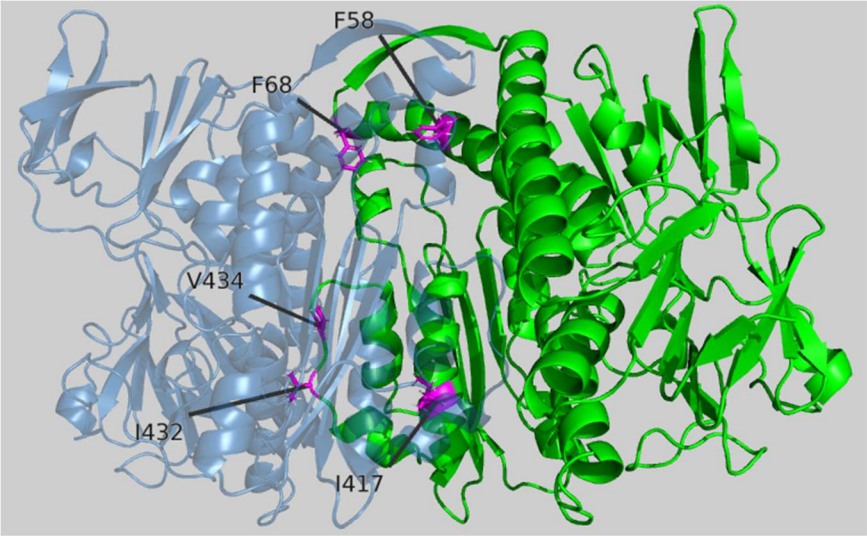

Figure 3.4. Graphical representation of the target residues (magenta) for dimerization impedance.

3.2.1.2 *Dimerization Domain Mutations*

Another common tactic to monomerize a protein is through the introduction of point mutations in order to make a protein interface more hydrophilic.[21,182,183] Mutations were performed that would change non-polar residues to the polar residue, Ser. Based off the GRLMR alignment to *E. coli* GSHR, 5 residues were chosen not currently identified as necessary for enzymatic function; F58, F68, I417, I432, and V434 highlighted in **Figure 3.4**. Mutations to these residues were confirmed with sequencing but did not result in any soluble monomeric GRLMR upon isolation.

3.2.1.3 *Fusion of Secondary Dimerization Domain*

The last approach attempted involved concatenating a secondary GRLMR dimerization (AA 334-452) domain with a short spacer to the C-terminus of the complete GRLMR sequence ($GRLMR_{dimdom}$). Mutations were made to the full length GRLMR (M374E, L376S, T377S, L378S, and T379S) and to the concatenated dimerization domain (I337E, V341S, and I347S) analogous to those identified by Leistler and Perham in solubilizing the extracted dimerization domain of *E. coli* GSHR.[168] The construct is illustrated in **Figure 3.5** sans linker between the truncated and full length GSHR. Upon construction of $GRLMR_{dimdom}$, several small batch isolations (from 50 mL cultures) using a Ni-NTA column were attempted to optimize protein

expression and isolation however none of the growth experiments performed resulted in stable enzyme.

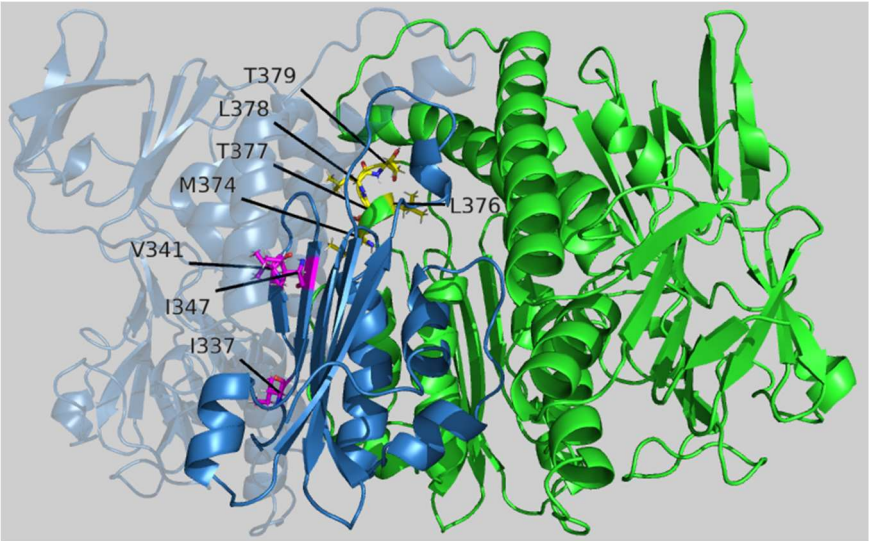

Figure 3.5. Graphical representation of the secondary dimerization domain (light blue) to be fused to a full length GRLMR (green). Residues to be mutated on the secondary dimerization domain are in magenta. Residues to be mutated on the full length GRLMR are in yellow.

3.2.2 *Construction and Isolation of F-cSeNPHis and cSeNP-F*

While it is still desirable to produce a monomer protein tag for EM imaging another approach that could be taken was to produce a fully concatenated GRLMR pair and fuse that to the model protein FtsZ. Although the tag would now be ~100 KDa in size, this would give an idea as to the possibility of using a metal reducing enzyme tag for EM. To create the concatenated GRLMR dimer, a gene containing two GRLMR copies ($GRLMR^1$ and $GRLMR^2$) on the C-term of FtsZ was designed similar to many fluorescence studies utilizing a GFP tag.[143,149–152,157] In order to test the effect of various linkers between $GRLMR^1$, $GRLMR^2$, and FtsZ, restriction enzyme sites were incorporated between the various protein sequences that would allow for golden gate assembly to insert different linker sequences. Linkers to be inserted between the FtsZ and concatenated GRLMR tags were flexible $(GGGGS)_n$ (n=1, 2, or 3) or rigid $(EAAAK)_n$ (n=1, 2, or 3) linker sequences.[184,185] Tags between the two GRLMR copies were $(GGGGS)_n$ (n=1, 2, or 3), or a combination of (GGGGS) and (EAAAK). Initially an $(EAAAK)_2$ linker was inserted between the FtsZ and GRLMR tag. Linkers that would then be used in-between GRLMR copies were inserted

and FtsZ tagged variants were expressed and. Further isolation of the tagged FtsZ variants was performed by precipitation using NH_4SO_4 and resuspended in a TKEM buffer (20 mM Tris, 50 mM KCl, 1 mM EDTA, 2.5 mM $MgCl_2$, pH 8.0).

All the tagged FtsZ variants were isolated except when only a single GGGGS was placed between the GRLMR copies. The length of this linker might have hindered the concatenated GRLMR copies from being able to dimerize within the tag possibly leading to protein aggregation. The 4 other variants (rigid-flexible-rigid, flexible-rigid-flexible, $(GGGGS)_2$, and $(GGGGS)_3$) were diluted to a concentration of 62.5 μM determined by UV-Vis. All the variants appeared to be able to produce Se^0 particulate upon incubation with NADPH and $HNaSeO_3$ in solution. Sedimentation experiments were conducted to identify the variant that also allowed native activity of the FtsZ. Ability for the FtsZ to polymerize was to be gauged qualitatively by comparing the amounts of pelleted tagged-FtsZ after polymerization and sedimentation. To ensure sedimentation was occurring due to the presence of GTP and not merely crashing out upon centrifugation, experiments were run in the presence and absence of GTP.

Results indicated that the most stable linker that had the least amount of tagged FtsZ pelleted omitting GTP and the most when incubated with GTP was the rigid-flexible-rigid linker present between the GRLMR copies. The rigid-flexible-rigid linker variant was then carried forward to test for the most stable linker between the FtsZ and $GRLMR^1$. Linkers between FtsZ and $GRLMR^1$ were inserted using golden gate assembly and confirmed with sequencing. Study of these linkers were performed as previously stated. Sedimentation experiments indicated all variants remained soluble when incubated without GTP. To further explore the stability of the variants, induction-time screens were run to identify variants that could be expressed at high levels without degradation within the cells. Of the linkers between FtsZ and $GRLMR^1$ the single copy of EAAAK and $(EAAAK)_2$ provided the highest levels of expression. To complete the construct, copies of a Se-binding peptide (SeBP) identified previously were then inserted at the C-termini of the GRLMR copies. The final constructs of the tagged FtsZ is shown in **Figure 3.6**, referred to as F-cSeNPHis (C-term) and cSeNP-F (N-term sans His-tag), to be used in further *in vitro* studies. The production

of the N-tagged FtsZ was to not hinder the C-terminal tail of FtsZ, a an essential sequence for the interaction between FtsZ and other essential cytokinesis proteins.[186]

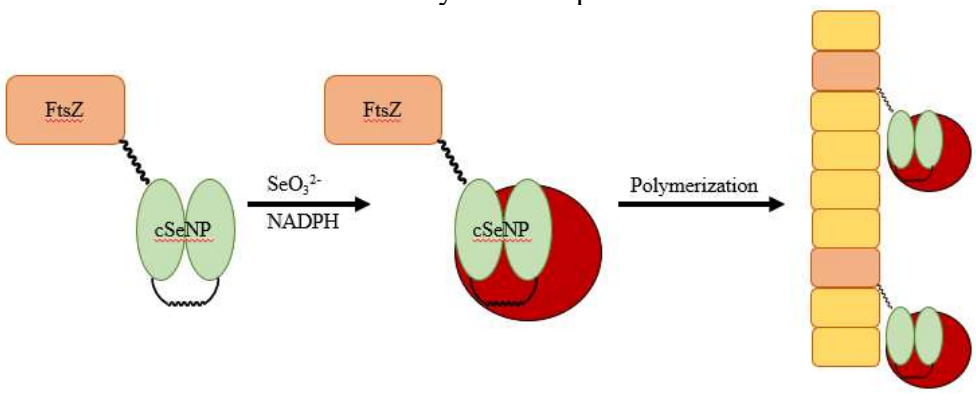

Figure 3.6. Illustration of F-cSeNPHis construct and functionality. The cSeNP tag, composed of two copies of GRLMR (green oval) produces a SeNP (red circle) in the presence of SeO_3^{2-} and NADPH. F-cSeNPHis can then be mixed within a population of wild type FtsZ (yellow rectangles) and be incorporated into the resulting filaments.

3.2.3 *In Vitro Studies of F-cSeNPHis and cSeNP-F*

FtsZ tagged variants were isolated using either a Ni-affinity column or precipitation with GTP and Ca^{2+} or NH_4SO_4 as described previously.[157,158,166,187] FtsZ GTPase activity was tested between the two variants. Inorganic phosphate (P_i) production from the dephosphorylation of GTP was measured using a malachite green assay. The dephosphorylation of GTP corresponds directly to the association of FtsZ subunits during polymerization. Polymerization reactions containing the

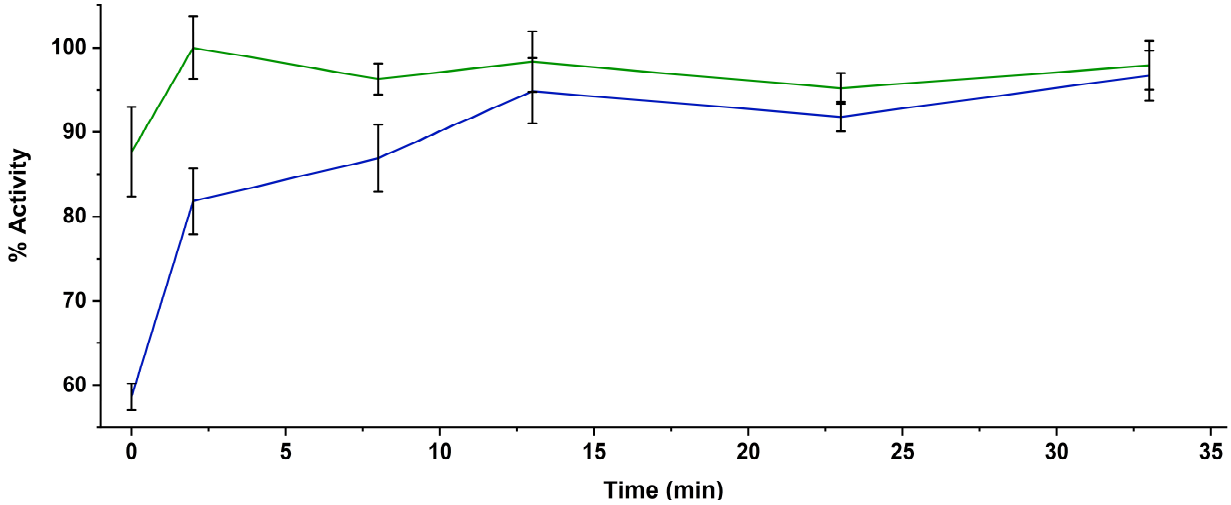

Figure 3.7. Malachite Assay of F-cSeNPHis (green) and cSeNP-F (blue) reported in % activity to wild type FtsZ.

two variants were initiated with 1 mM GTP at various time points and related back to the activity of wild type FtsZ P_i production. Resutls from the malachite assay are depicted in **Figure 3.7** and confirmed that the production of P_i was highest for F-cSeNPHis which was then carried forward for EM imaging experiments.

To confirm the functions of the cSeNP and FtsZ were conserved, F-cSeNPHis was incubated with SeO_3^{2-} and NADPH before polymerization was initiated by the addition of GTP. After 10 min at 37°C, an aliquot of the polymerization reaction was placed on an EM grid for imaging. Initially, these filaments were stained with an unbuffered 2% uranyl acetate stain however the electron density of the uranyl ion prevented observation of the expected contrast from the presence of SeNPs (**Figure 3.8, panel A**). Energy Dispersive Spectroscopy (EDS) was used to detect elemental makeup of the filaments. The Se map overlaid well with that of N indicating the presence of Se and protein present in the filament. To increase contrast of the SeNPs, the

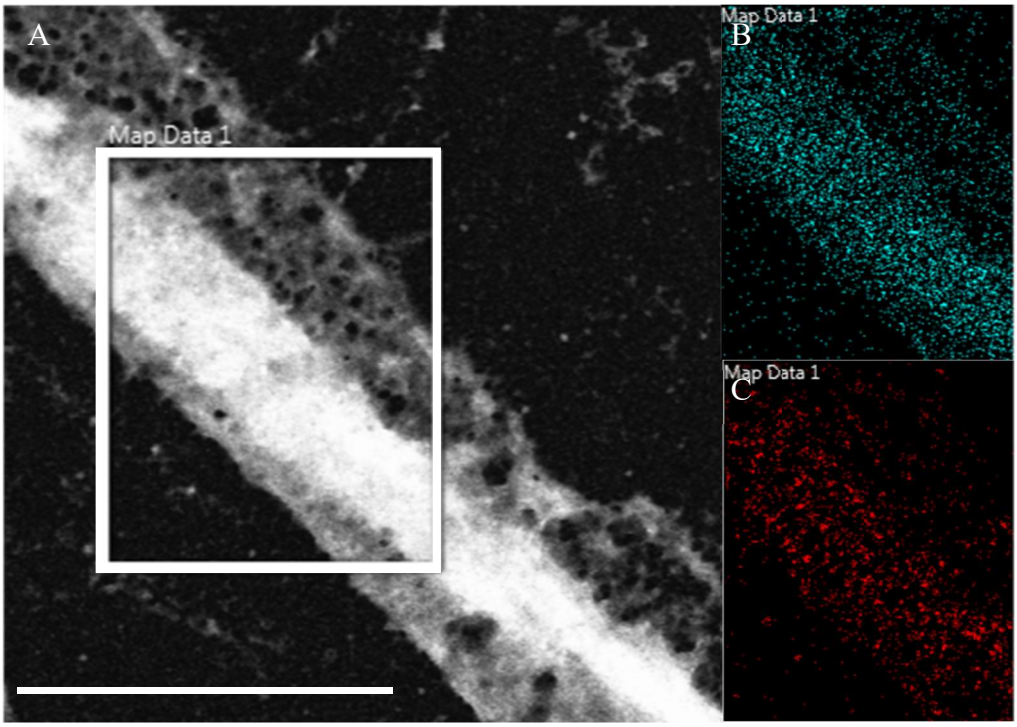

Figure 3.8. (**A**) An SEM electron micrograph of a filament formed by F-cSeNPHis after SeNP production and polymerization. Filaments were stained with 2% uranyl acetate. The square corresponds to the area that underwent elemental analysis. (**B**) EDS mapping the presence of N. (**C**) EDS mapping of Se in the filament. Scale bar = 1μm

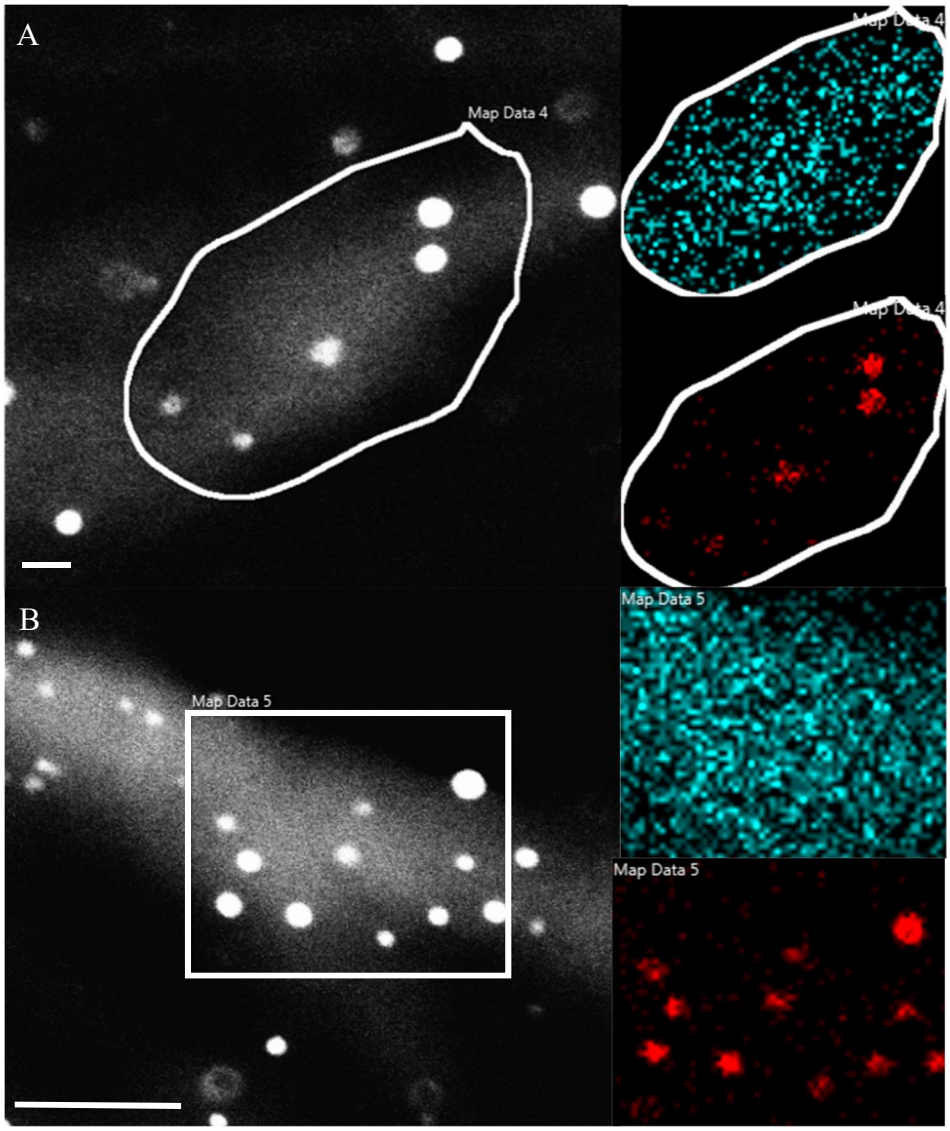

Figure 3.9. Filaments resulting from F-cSeNPHis, post-SeNP formation and omitting uranyl acetate staining. (**A**) and (**B**) are examples of filaments formed by F-cSeNPHis found decorated with SeNPs. The panels to the right of (**A**) and (**B**) are EDS maps of the outlined areas indicating the presence of N (cyan) and Se (red). Scale bar = 100 nm

concentration of uranyl acetate was decreased to 1%. Individual SeNPs did became more visible. Eventually, staining with uranyl acetate was completely omitted allowing for visualization of precise spherical particulate of high contrast on what would appear to be bundles of filaments (**Figure 3.9**). EDS maps confirmed the elemental make-up of the nanoparticles to be Se. This result indicated function of both the cSeNP tag and FtsZ. The next steps would include exploring the efficacy of the F-cSeNPHis within *E. coli.*

3.2.4 *In Vivo Electron Microscopy Imaging of F-cSeNPHis and cSeNP-F*

In vitro studies do not always represent the activity of a protein when in a complex environment like within a cell. *In* vitro, concentrations of precursors and monomeric F-cSeNPHis can be controlled to result in SeNP decorated filaments. In a cell, concentrations of Se, NADPH, FtsZ, and GTP are far more unpredictable. First, biology has natural pathways to utilize and store concentrations of Se which is usually converted to seleno-diglutathione rapidly upon entering a cell.[26,188] The cSeNP tag will need to be able to divert enough of the seleno-diglutathione as to permit SeNP formation. FtsZ polymerization and cSeNP activity also depend on NADPH and GTP, ubiquitous enzymatic cofactor, possibly depleting cellular stores upon overexpression. Control of FtsZ expression will also be important as too few copies of tagged FtsZ might make it difficult to identify filaments. Too high of a concentration of FtsZ could reach levels toxic to the host cell. There is also the degradation of FtsZ overtime possibly causing a high background of formed SeNPs.

Initial *in vivo* imaging experiments were first performed on whole *E. coli* cells containing an expression plasmid encoding F-cSeNPHis. Several screens involving SeO_3^{2-} and IPTG concentrations, and induction times were tested. Cells were fixed with a glutaraldehyde/formaldehyde solution prior to SEM imaging. All expression cultures were grown at room temperature to separate the division events of individual cells. In rich media, such as LB, growing at 37°C *E. coli* have a doubling time of about 20 minutes but the replication time, the time required to duplicate the chromosome, takes 60 – 90 minutes.[189] The separation of division events was hypothesized to aid in the identification of individual Z-rings within the cells preparing to divide. Room temperature growth would also increase the duration of the log-phase in which most cells are dividing and therefore forming Z-rings. The expectation in viewing these cells in EM after induction and incubation with SeO_3^{2-} was to observe areas of contrast mid-cell indicating a higher concentration of Se, analogous to the GFP tagged FtsZ studies.[143,152,153,156,162] Initial screens

for SeO_3^{2-} concentrations and induction times were run and resulted in a concentration of 2 mM $HNaSeO_3$ and 30 minutes of induction. The resulting whole cell EM images for the SeO_3^{2-} incubation concentration screen are shown in **Figure 3.10**. When induced with 1 mM IPTG, elongated cells were identified with aggregates every 1 – 2 μm and filaments existing longitudinally through the cell (**Figure 3.10, D**). These structures have been reported previously when FtsZ has been overexpressed or degradation of FtsZ was prevented.[143,151,154] The presence of these structures within the whole cell indicates two things: First, the cSeNP tag seems to be

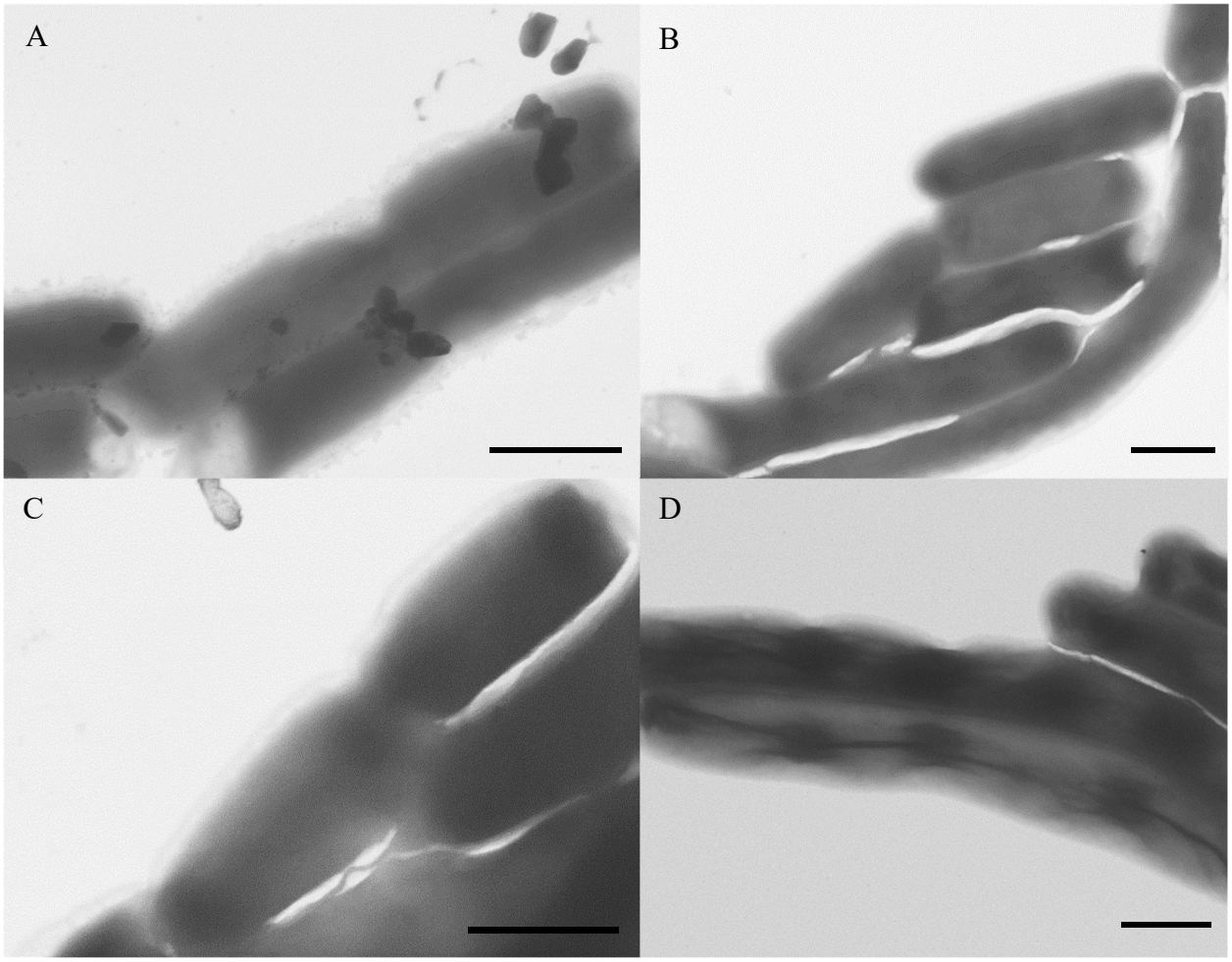

Figure 3.10. Resulting SEM images of the [Se] screen of *E. coli* expressing F-cSeNPHis. Expression of F-cSeNPHis was initiated with the addition of 1 mM IPTG in (**A**) 0 mM, (**B**) 250 μM, (**C**) 1 mM, and (**D**) 2 mM of $HNaSeO_3$. As [Se] increases, contrast within the cell increases until aggregates and filaments can be seen throughout the cell (**D**). Scale bar = 1μm

working as indicated by the high contrast structures in the cell; Second, FtsZ must also be operational as these structures have been seen when FtsZ is over produced.[143]

To reduce the overproduction of tagged FtsZ, IPTG concentration was reduced to 1, 10, and 100 μM. At the lowest concentration most cells on the grid seemed to have been destroyed possibly because of the high level of Se (2 mM) and lack of cSeNP to aid in processing it. At 10 μM IPTG more cells appeared to survive the incubation with 2 mM Se. At 100 μM IPTG, many of the cells were intact with points of division easily identified. **Figure 3.11** shows cells resulting from the various concentrations of IPTG used. Cells induced with 100μM IPTG had good cellular contrast and the presence of pinch points where two daughter cells would be separated. The optimized conditions of 100 μM IPTG for 30 minutes in the presence of 2 mM $HNaSeO_3$ was used for all remaining imaging experiments. Next, cells were grown in the optimized conditions and fixed for viewing in TEM/EDS to give better resolution. Dividing cells with clear pinch points, **Figure 3.12,** were shown to have a gradient of Se, highest at the point of division and decreasing moving towards the distal end of the cell.

Getting the elemental map of a whole cell expressing the cSeNP tag proved difficult and with high backgrounds. Cells were grown up in the optimized conditions but were instead prepared for sectioning in order to try to visualize filaments within the cytoplasm. For cell sectioning, a sample would be high pressure frozen (HPF) in water and freeze substituted (FS) using glutaraldehyde dissolved in acetone, and imbedded in a resin for sectioning.[190] Resulting cells lacked the presence of Se, however there did seem to be structures that were not confined to the resin but had the resemblance of cells and the appearance of aligned particles shown clearly in **Figure 3.13, panels A and B**. EDS was performed on one of these cells mapping of N, P, and Se. Maps for N and Se tracked the presence of the cell yet P did not seem to be present. These maps are insets of **Figure**

3.13, panel C. These cells had the size and shape expected from an *E. coli* cell but did not seem to possess a membrane, hence the inability to map P. Perhaps these cells somehow avoided fixation and resin imbedding. All other cells within the section did not show any increase of Se

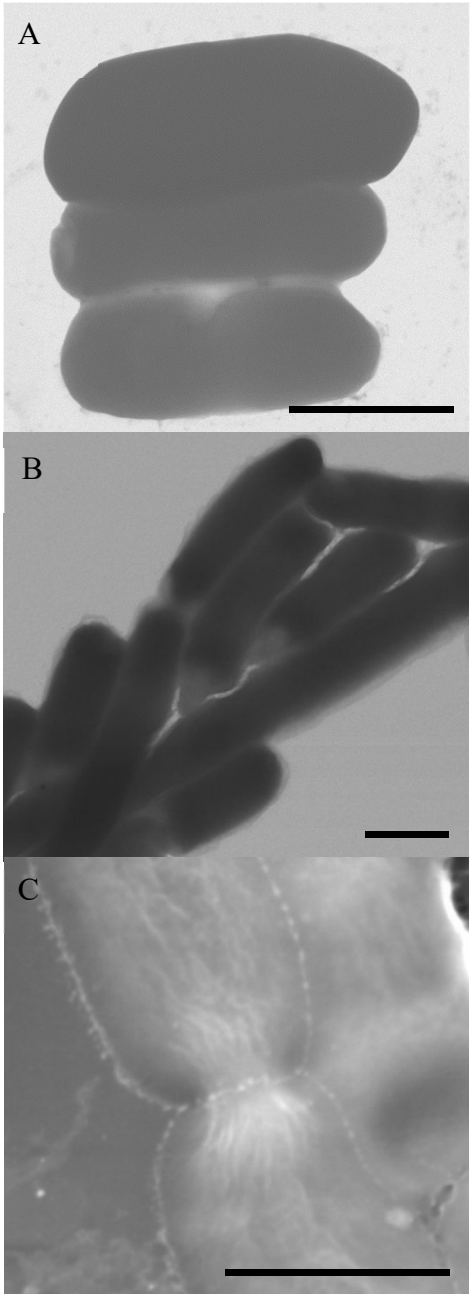

Figure 3.11. Whole cell SEM images of resulting cells after induction with either (**A**) 1 µM, (**B**) 10 µM, or (**C**) 100 µM of IPTG. Once induced, cells were incubated for 30 minutes with 2 mM SeO_3^{2-} before fixation. Scale bars = 1 µm.

leading to the hypothesis that something in the processing of these cells could be degrading SeNPs present in the cytosol.

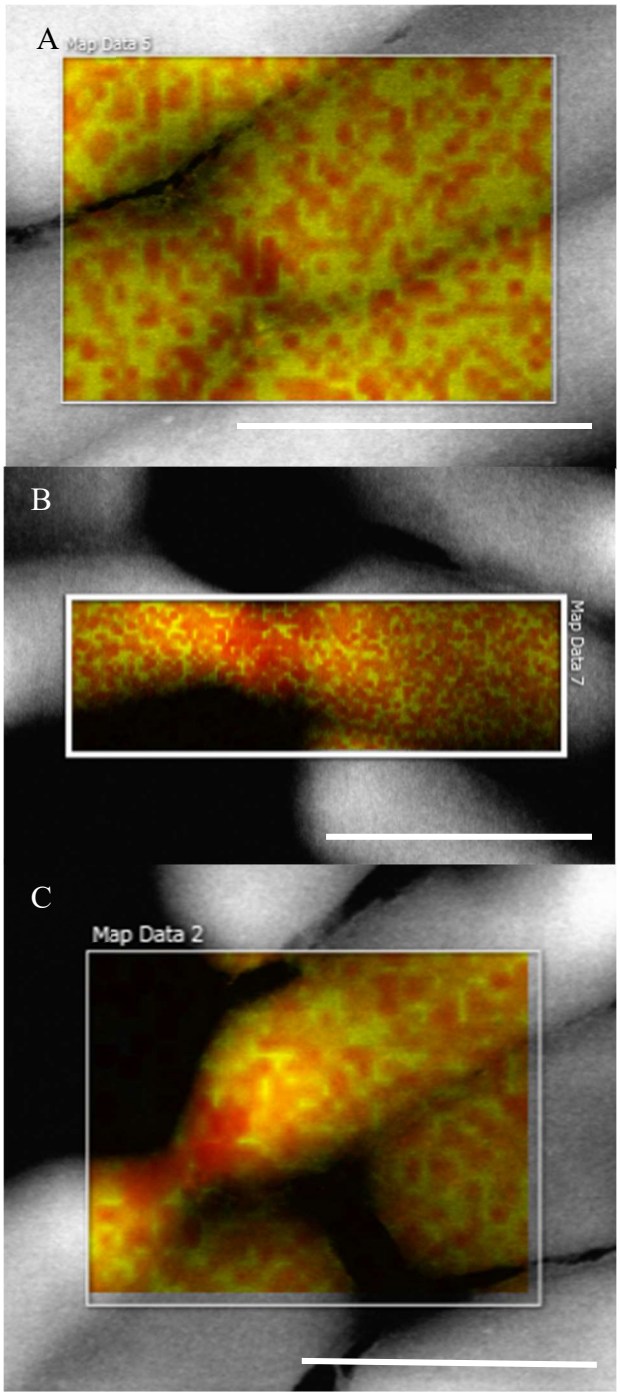

Figure 3.12. Whole cell TEM images with overlaying EDS maps. Yellow indicates P correlating with the membrane and red indicates Se. All images were taken from cells grown in the optimized conditions for F-cSeNPHis function. Scale bar = 1 µm

The protocol described by McDonald and Auer and used for these initial sectioned cells uses acetone for dehydration of the cells and the introduction of fixative. To ensure the stability of the cSeNP throughout the process, GRLMR-produced SeNPs were incubated with the various solvents and reagents used in the freezing and fixation protocol. It became apparent after testing that acetone was detrimental to the SeNPs formed by GRLMR. Upon incubation of GRLMR-produced

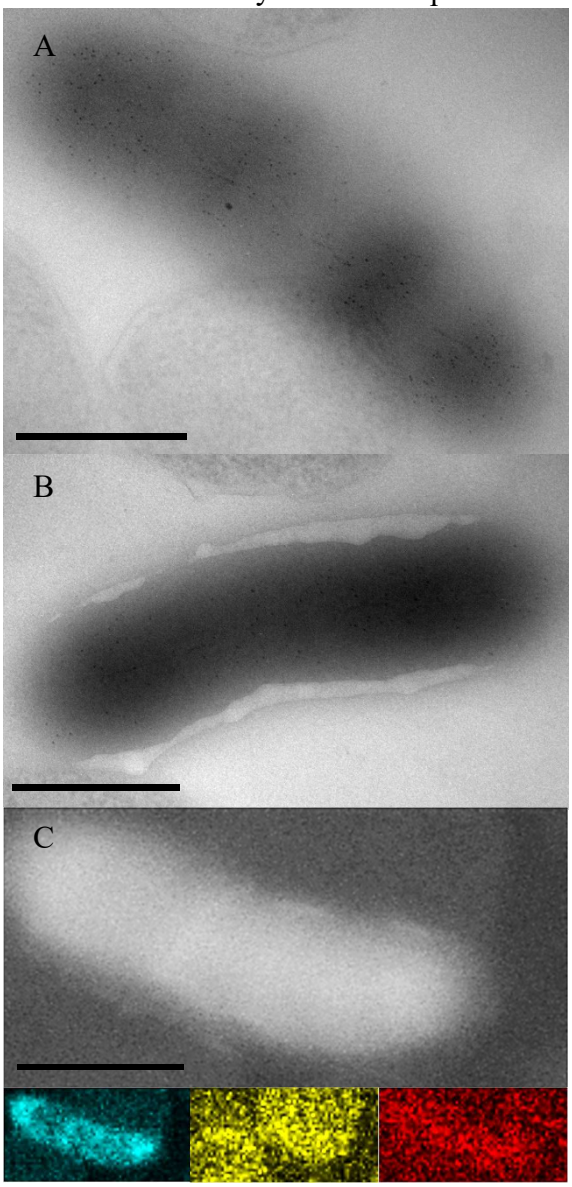

Figure 3.13. TEM images from the sectioned samples expressing F-cSeNPHis. (**A**) and (**B**) are bright field images showing examples of what appeared to be cells containing SeNPs in filamentous structure. Bands are also seen perpendicular to the cell indicating densities of Se. (**C**) A dark field TEM image of a cell like (**A**) and (**B**) with corresponding EDS maps below. Cyan indicates N, yellow indicates P, and red represents Se. Scale bar = 500 nm

SeNPs in acetone, the pellet originally observed before addition of the acetone was reduced in size and a color change of red to black was observed. It was apparent that SeNPs below a specific size would degrade in the presence of acetone. Ethanol was also tested and proved detrimental to the SeNPs however over several days, far beyond the scope of the fixation process.

Great lengths were taken to ensure the stability of the SeNPs during the HFP/FS process. It was imperative to reduce the use of acetone by changing the dehydrant used from acetone to ethanol.

Cells containing cSeNP-F were grown as described previously except dehydrated with ethanol, fixed, and either viewed whole cell in SEM or sectioned and viewed in TEM. Whole cell images revealed localized contrast at mid-cell or aggregations of contrast along the cell shown in **Figure 3.14, panels (A) – (C) & (E)**. Sectioned samples provided clearer presence of high contrast filamentous structures going longitudinally through the cell (**Figure 3.14, panels (D) & (F)**). Although still indicative of an overproduction of FtsZ these high contrast filaments demonstrate the functionality of both cSeNP and FtsZ.

3.3 Future Considerations

There is still much work to be done in the further refinement of the GRLMR tag, specifically the fixation method used. Like APEX and mini-SOG it would be beneficial if the enzyme was still functional after fixation since one limiting factor in this process is the abundance of Se inside of the cell at the time of induction. Being able to express, fix, and then soak samples in a solution of $HNaSeO_3$ and NADPH would mitigate any concerns present with trying to form nanoparticles during the lifetime of the native protein the tag is attached to. Preliminary data suggests that GRLMR can still function in 0.8% EDC and up to 0.175% glutaraldehyde. Such combinations of

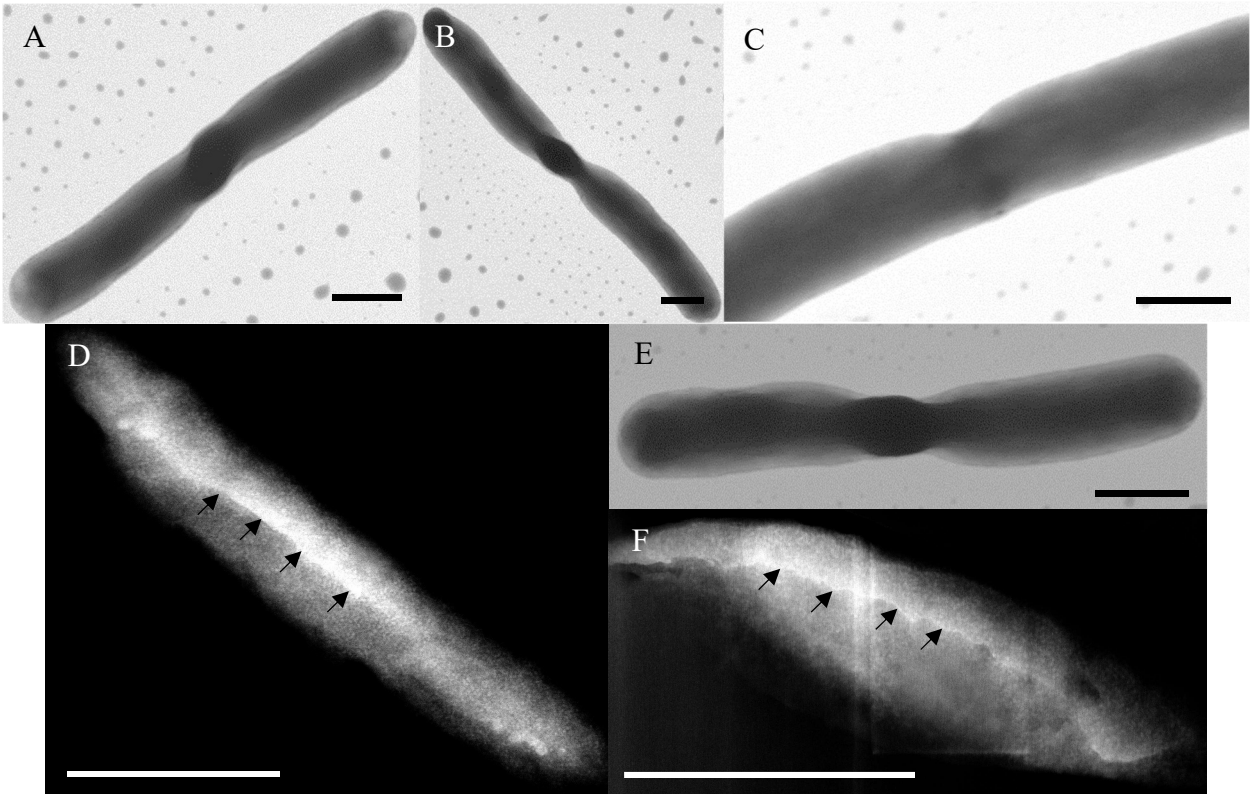

Figure 3.14. Whole cell and sectioned cells producing cSeNP-F in media supplemented with 1 mM SeO_3^{2-}. (**A**) – (**C**) & (**E**) show whole cell images of *E. coli* with densities seen at mid-cell. Images (**D**) & (**F**) are sectioned cells in which high contrast filaments can be seen longitudinally in the cell. Black arrows point to the high contrast filament. Bar scale = 1 µm

fixatives have been used in the past to fix cells for immunostaining and could provide an avenue for the post-fixation formation of SeNPs.[191]

More exploration into the production of a monomer must be conducted although it might be more beneficial to find monomeric proteins with oxidoreductase activity from literature or other sources. The fusion of this large concatenated tag to a POI is sure to have some effect on the POIs activity and as such lead to misrepresentations in EM. A monomeric oxidoreductase could also be used as a scaffold to insert active sites from other metal reductases that would otherwise be unsuitable as tags themselves.

The elongation of the cells indicates the overproduction FtsZ. In order to control the population of F-cSeNPHis or cSeNP-F more stringently, the expression vector or the cell strain will need to

be changed. IPTG uptake is a stochastic event within a population of cells with both passive diffusion and active transports involved.[192,193] Active transports are expressed at varying levels from cell to cell within a given population making IPTG uptake heterologous. Cell lines do exist that possess a mutation in the IPTG transporter lactose permease (LacY) inhibiting its function allowing only passive diffusion and therefore homologous dose-dependent induction.

3.4 Summary and Conclusion

In this chapter, it has been demonstrated that fusion of a concatenated GRLMR dimer onto the C-term of FtsZ provides a functioning protein construct that is able to undergo polymerization and form SeNPs *in situ*. Attempts to monomerize the GRLMR protein through truncation, point mutations within the dimer interface, and concatenation of a secondary GRLMR binding domain were attempted but did not result in a stable protein capable of isolation. However, efforts on this front have not been exhausted and work in this area is still on going. F-cSeNPHis was able to be constructed, optimized, and isolated. Upon SeNP formation and polymerization, filaments of F-cSeNPHis decorated with SeNP and high in Se content were observed in SEM. After optimization of growth and induction conditions, *in vivo* studies resembled previous images collected utilizing GFP-FtsZ by forming long longitudinal filaments and aggregates throughout cells that were themselves elongated. Optimization of the fixation and sectioning process and transposing the GRLMR tag to the N-terminus of FtsZ later resulted in high contrast filaments observed in TEM.

3.5 Experimental Details

3.5.1 *Materials*

PCR and ligation components, restriction enzymes, and T7 Expression *lysY/I*^{q} Competent *E. coli* cells (Cat # C3013I) were purchased from New England Biolabs, Inc. Primers were purchased from Integrated DNA Technologies. Original plasmids containing GRLMR and F-cSeNPHis were

designed and purchased from ATUM (Dna Twopointo Inc.) in their pD441-CH expression vector. Antibiotics were purchased from GoldBio. Na_2SeO_3 and $HNaSeO_3$ were purchased from Alfa Aesar. NADPH was purchased from BioVision and Coomassie Plus Bradford Reagent from Thermo Scientific. GTP was purchased from Chem-Impex Int'l Inc. GeneJet Plasmid Miniprep Kit (Cat# K0503) and PCR Cleanup Kit (Cat# K0702) were purchased from ThermoFisher Scientific. Araldite 502 Kit (Cat# 18050) was purchased from Ted Pella.

3.5.2 *Construction/Isolation of GRLMR Variants*

GRLMR truncates were achieved using outward PCR on the plasmid encoding GRLMR. PCR reactions were digested initially with DpnI, cleaned using the GeneJet Purification kit. PCR products were then digested with BspQI and circularized through ligation. Mutations for the inhibition of dimerization were performed using basic mutational techniques. $GRLMR_{DimDom}$ was constructed by initial mutations at the NADPH or FADH binding domains of two different GRLMR plasmids. The dimerization domain of one was amplified and inserted into the plasmid containing the full length GRLMR with a small linker introduced by the primers used to amplify the second dimerization domain.

The starting template for FcSeNP-His was designed and purchased. Oligonucleotides encoding the various linkers to be tested were designed with overhangs that would permit Golden Gate Assembly. The two restriction enzymes used for the assembly were BbsI-HF and BsmBI. Briefly, 4 µL of a 50 µM stock solution of mixed oligomers were added with 2 µL ligase buffer and diluted to a total volume of 20 µL with milliQ water. Reaction tubes were heated to 95°C for 5 minutes. The heat block was then turned off and allowed to cool to RT to ensure annealing of the single stranded oligos. For insertion of the linker into the template 25 ng of template, 1 µL of the annealed oligo solution, 2 µL of 10x restriction buffer, 1 µL of restriction enzyme and diluted up to 17 µL.

The reactions were heated at the temperature required by the restriction enzyme overnight. The next day 1 μL of T4 Ligase, 10 mM final concentration of DTT, 1 mM final concentration of ATP for a final volume of 20 μL and ligated at 22.5°C for 45 minutes. Copies of SeBP were then inserted at the C-term of each copy of GRLMR using outward PCR. The complete purchased plasmid and all primers used for linker and SeBP insertion can be found in **Appendix C, C.1 – C.3**.

All sequence confirmed plasmids were transformed into DH5α cells for storage. For the expression of cells, plasmids were transformed into BL21 (DE3) cells. A liquid culture was started and grown overnight. The next day, a larger volume of LB media was inoculated and grown to an OD_{600} of ~0.4 for the GRLMR variants and OD_{600} of ~1.2 for variants fused to FtsZ. Cultures were grown for 4 – 8 hours after being induced by 1 mM IPTG and supplemented with 1 μM $HNaSeO_3$. After the allotted time, cells were collected, resuspended into lysis buffer and sonicated on ice. Soluble and insoluble fractions were separated, and the soluble fraction was collected.

For variants that possess a His tag, soluble fractions were run through a 5 mL Histrap FF column with a gradient of 0 – 500 mM imidazole for 75 minutes at 3 mL/min with a fraction being collected every minute. 10 μL of each fraction was added to 190 μL of Bradford Reagent to identify fractions with protein. Fractions that turned blue were run on an SDS-PAGE gel to determine whether the desired protein was present. Fractions containing the desired protein were combined, concentrated on a spin column, and dialyzed into the desired buffer.

The variant cSeNP-F did not contain a His tag. In order to isolate cSeNP-F cells were grown as before but after the cells were lysed, the insoluble fraction was pelleted at 30000 RPM and 4°C for 2 hours. The soluble fraction was then incubated with 1 mM GTP and 20 mM $CaCl_2$ at 37°C for 10 minutes following the procedure from Monterroso *et al.*[187] The solution was then spun for

15 minutes at 4°C and 10000 RPM. The protein pellet was resuspended in buffer, spun to remove any aggregated protein and the soluble fraction was again incubated with GTP and $CaCl_2$. The incubation and centrifugation steps were repeated as before, and the final protein was concentrated and dialyzed into the desired buffer.

3.5.3 *Malachite Green Assay*

0.045% Malachite Green hydrochloride and 4.2% ammonium molybdate in 4M HCl were mixed in a 3:1 ratio for 20 minutes and filter sterilized for future use. Polymerization reactions (50 μL final volume) were prepared using 5 μM total of FtsZ. 4 μM of wildtype FtsZ and 1 μM of tagged FtsZ were combined and compared to 5 μM wild type FtsZ. Polymerization reactions were performed in 50 mM MES, 50 mM KCl, pH 6.5 with either 10 mM $MgCl_2$ or 10 mM EDTA, pH 8.0. Reactions were then initiated with the addition of 1 mM GTP at various time points and incubated under agitation at 37°C. After reaction times, 10 μL of the polymerization reactions were combined with 40 μL of the malachite solution and the absorbance at 630 nm was monitored. A linear concentration standard was obtained by mixing various concentrations of KH_2PO_4 with the malachite solution.

3.5.4 *Sedimentation Experiments*

Sedimentation experiments were conducted following Król and Scheffers.[194] Briefly, FtsZ variants were spun at 100000 *g* at 4°C for 30 minutes to remove inactive protein. Spun protein stock solution was then diluted to 12 μM in 50 mM MES pH 6.5, 50 mM KCl, and 10 mM $MgCl_2$. The solution was incubated at 37°C for 5 minutes before polymerization was initiated by the addition of 2 mM GTP. Reactions were gently shaken at 37°C for 10 minutes before being spun at 352900 *g* at RT for 10 minutes. Soluble fractions were collected. To the insoluble pellets, 25 μL of 4xSDS loading buffer and 25 μL of milliQ water was added and the spin tubes were heated

to 95°C until the pellets were solubilized. Soluble and insoluble fractions were then run on SDS-PAGE gels for a qualitative determination of efficient polymerization.

3.5.5 *In Vitro Polymerization and Staining*

In vitro polymerization was performed using the optimized reaction conditions determined in the sedimentation experiments but modified to allow for SeNP growth. Specifically, after the initial centrifugation to remove inactive protein, polymerization reactions were set up omitting the GTP initiation. 100 μM $HNaSeO_3$ and 100 μM NADPH were added to the reactions and allowed to incubate for 10 minutes. The polymerization was then initiated with 2 mM GTP and incubated at 37°C for 10 minutes. 3 μL of each reaction were then deposited onto an EM grid. Samples were stained with 0 – 2% unbuffered uranyl acetate for future imaging.

3.5.6 *In Vivo Sample Preparation*

BL21 (DE3) cells containing cSeNP tagged FtsZ were grown in 2 mL LB media overnight. The next day, 5 mL of LB media was inoculated with 50 μL dense culture and grown at room temperature for ~3 hours before being induced by 100 μM IPTG and supplemented with 2 mM $HNaSeO_3$. Cells were then grown for 2 hours and collected through gentle spinning at 3000 RPM in a microcentrifuge. Cells were then washed 6x 1 mL PBS, pH 7.4. Cells were then fixed with 2% formaldehyde/2.5% glutaraldehyde on ice for at least 1 hour. Cells were again collected and washed 3 times with PBS, pH 7.4.

For cell sectioning, after fixation cells were encapsulated in 2% agar by resuspending cells in 50 – 100 μl PBS. Cells were transferred to a 45°C water bath and ~100 μL of molten 4% agar was added and mixed thoroughly. The cell/agar solution was added to a glass slide to harden. A 0.5 mm^3 cube was cut and dehydrated. Agar was dehydrated using ethanol from 30% to 100% over the course of 1 hour. In the fume hood the cube was then immediately infiltrated using the Araldite 502 kit. 50% Araldite in ethanol was added to the sample for 30 minutes at RT with constant

agitation. This was followed by two 100% Araldite infiltrations at 30 minutes each and agitation while incubating at 60°C to ensure dryness for the polymerization. Molds were removed from the oven, labeled, and embedded. Sections were produced using a glass microtome.

3.5.7 *EM Imaging*

Aliquots (3 µL) were mounted on 400 mesh Cu grids with a 40 nm C coating. Cells were dry mounted on TEM grids were loaded onto a STEM holder. SEM images were taken on a JEOL JSM-6500-F Scanning Electron Microscope. TEM images were taken on a JEOL JEM-1400 Transmission Electron Microscope.

REFERENCES

8. Dickson, R. M., Norris, D. J., Tzeng, Y.-L. & Moerner, W. E. Three-Dimensional Imaging of Single Molecules Solvated in Pores of Poly(acrylamide) Gels. *Science* **274**, 966–968 (1996).
10. Hell, S. & Wijnaendts-van-Resandt, R. W. The Application Of Polarized Confocal Microscopy For The Size Measurement Of Resist Structures. in *Optical Storage and Scanning Technology* **1139**, 92–98 (International Society for Optics and Photonics, 1989).
12. Betzig, E., Lewis, A., Harootunian, A., Isaacson, M. & Kratschmer, E. Near Field Scanning Optical Microscopy (NSOM): Development and Biophysical Applications. *Biophysical Journal* **49**, 269–279 (1986).
20. Shu, X. *et al.* A Genetically Encoded Tag for Correlated Light and Electron Microscopy of Intact Cells, Tissues, and Organisms. *PLOS Biology* **9**, e1001041 (2011).
21. Martell, J. D. *et al.* Engineered ascorbate peroxidase as a genetically-encoded reporter for electron microscopy. *Nat Biotechnol* **30**, 1143–1148 (2012).
23. Ni, T. W. *et al.* Progress toward clonable inorganic nanoparticles. *Nanoscale* **7**, 17320–17327 (2015).
26. Tapiero, H., Townsend, D. M. & Tew, K. D. The antioxidant role of selenium and seleno-compounds. *Biomed Pharmacother* **57**, 134–144 (2003).
53. Mittl, P. R. & Schulz, G. E. Structure of glutathione reductase from Escherichia coli at 1.86 A resolution: comparison with the enzyme from human erythrocytes. *Protein Sci* **3**, 799–809 (1994).
124. Rust, M. J., Bates, M. & Zhuang, X. Sub-diffraction-limit imaging by stochastic optical reconstruction microscopy (STORM). *Nature Methods* **3**, 793–796 (2006).
125. Sengupta, P., Van Engelenburg, S. B. & Lippincott-Schwartz, J. Superresolution imaging of biological systems using photoactivated localization microscopy. *Chem Rev* **114**, 3189–3202 (2014).
126. de Matos, L. L., Trufelli, D. C., de Matos, M. G. L. & da Silva Pinhal, M. A. Immunohistochemistry as an Important Tool in Biomarkers Detection and Clinical Practice. *Biomark Insights* **5**, 9–20 (2010).
127. Bolognesi, M. M. *et al.* Multiplex Staining by Sequential Immunostaining and Antibody Removal on Routine Tissue Sections. *J Histochem Cytochem* **65**, 431–444 (2017).
128. Kim, S.-W., Roh, J. & Park, C.-S. Immunohistochemistry for Pathologists: Protocols, Pitfalls, and Tips. *J Pathol Transl Med* **50**, 411–418 (2016).
129. Gustafsson, M. G. L. Nonlinear structured-illumination microscopy: Wide-field fluorescence imaging with theoretically unlimited resolution. *PNAS* **102**, 13081–13086 (2005).
130. Litman, R. B. & Barrnett, R. J. The mechanism of the fixation of tissue components by osmium tetroxide via hydrogen bonding. *Journal of Ultrastructure Research* **38**, 63–86 (1972).
131. Scarff, C. A., Fuller, M. J. G., Thompson, R. F. & Iadaza, M. G. Variations on Negative Stain Electron Microscopy Methods: Tools for Tackling Challenging Systems. *J Vis Exp* (2018). doi:10.3791/57199
132. Booth, D. S., Avila-Sakar, A. & Cheng, Y. Visualizing Proteins and Macromolecular Complexes by Negative Stain EM: from Grid Preparation to Image Acquisition. *J Vis Exp* (2011). doi:10.3791/3227

133. Hopwood, D. Fixatives and fixation: a review. *Histochem J* **1**, 323–360 (1969).
134. Mundkur, B. Problems of fixation and staining in microbial cytology. *Trans N Y Acad Sci* **24**, 30–35 (1961).
135. Wolman, M. Problems of Fixation in Cytology, Histology, and Histochemistry. in *International Review of Cytology* (eds. Bourne, G. H. & Danielli, J. F.) **4**, 79–102 (Academic Press, 1955).
136. Bullock, G. R. The current status of fixation for electron microscopy: A review. *Journal of Microscopy* **133**, 1–15 (1984).
137. Boassa, D. *et al.* Split-miniSOG for detecting and localizing intracellular protein-protein interactions: application to correlated light and electron microscopy. *bioRxiv* 423566 (2018). doi:10.1101/423566
138. Han, Y. *et al.* Directed evolution of split APEX peroxidase. *bioRxiv* (2018). doi:10.1101/452888
139. Han, Y. *et al.* Directed Evolution of Split APEX2 Peroxidase. *ACS Chem. Biol.* **14**, 619–635 (2019).
140. Lam, S. S. *et al.* Directed evolution of APEX2 for electron microscopy and proteomics. *Nat Methods* **12**, 51–54 (2015).
141. Thach, R. E. & Thach, S. S. Damage to Biological Samples Caused by the Electron Beam during Electron Microscopy. *Biophysical Journal* **11**, 204–210 (1971).
142. Blaauwen, T. D., Buddelmeijer, N., Aarsman, M. E. G., Hameete, C. M. & Nanninga, N. Timing of FtsZ Assembly in Escherichia coli. *J. Bacteriol.* **181**, 5167–5175 (1999).
143. Ma, X., Ehrhardt, D. W. & Margolin, W. Colocalization of cell division proteins FtsZ and FtsA to cytoskeletal structures in living Escherichia coli cells by using green fluorescent protein. *PNAS* **93**, 12998–13003 (1996).
144. Haydon, D. J. *et al.* An Inhibitor of FtsZ with Potent and Selective Anti-Staphylococcal Activity. *Science* **321**, 1673–1675 (2008).
145. Mathew, B. *et al.* Screening and Development of New Inhibitors of FtsZ from M. Tuberculosis. *PLOS ONE* **11**, e0164100 (2016).
146. Stokes, N. R. *et al.* An Improved Small-Molecule Inhibitor of FtsZ with Superior In Vitro Potency, Drug-Like Properties, and In Vivo Efficacy. *Antimicrobial Agents and Chemotherapy* **57**, 317–325 (2013).
147. Domadia, P., Swarup, S., Bhunia, A., Sivaraman, J. & Dasgupta, D. Inhibition of bacterial cell division protein FtsZ by cinnamaldehyde. *Biochem. Pharmacol.* **74**, 831–840 (2007).
148. Pazos, M. *et al.* FtsZ Placement in Nucleoid-Free Bacteria. *PLOS ONE* **9**, e91984 (2014).
149. Chen, Y., Anderson, D. E., Rajagopalan, M. & Erickson, H. P. Assembly Dynamics of Mycobacterium tuberculosis FtsZ. *J. Biol. Chem.* **282**, 27736–27743 (2007).
150. Srinivasan, R. & Ajitkumar, P. Bacterial cell division protein FtsZ is stable against degradation by AAA family protease FtsH in Escherichia coli cells. *J. Basic Microbiol.* **47**, 251–259 (2007).
151. Moore, D. A., Whatley, Z. N., Joshi, C. P., Osawa, M. & Erickson, H. P. Probing for Binding Regions of the FtsZ Protein Surface through Site-Directed Insertions: Discovery of Fully Functional FtsZ-Fluorescent Proteins. *Journal of Bacteriology* **199**, e00553-16 (2017).
152. Anderson, D. E., Gueiros-Filho, F. J. & Erickson, H. P. Assembly Dynamics of FtsZ Rings in Bacillus subtilis and Escherichia coli and Effects of FtsZ-Regulating Proteins. *J Bacteriol* **186**, 5775–5781 (2004).

153. Sun, Q. & Margolin, W. FtsZ Dynamics during the Division Cycle of Live Escherichia coli Cells. *J Bacteriol* **180**, 2050–2056 (1998).
154. Camberg, J. L., Hoskins, J. R. & Wickner, S. The Interplay of ClpXP with the Cell Division Machinery in Escherichia coli. *Journal of Bacteriology* **193**, 1911–1918 (2011).
155. Camberg, J. L., Viola, M. G., Rea, L., Hoskins, J. R. & Wickner, S. Location of Dual Sites in E. coli FtsZ Important for Degradation by ClpXP; One at the C-Terminus and One in the Disordered Linker. *PLoS One* **9**, (2014).
156. Zupan, J. R., Cameron, T. A., Anderson-Furgeson, J. & Zambryski, P. C. Dynamic FtsA and FtsZ localization and outer membrane alterations during polar growth and cell division in Agrobacterium tumefaciens. *PNAS* **110**, 9060–9065 (2013).
157. Yu, X.-C. & Margolin, W. Ca2+-mediated GTP-dependent dynamic assembly of bacterial cell division protein FtsZ into asters and polymer networks in vitro. *The EMBO Journal* **16**, 5455–5463 (1997).
158. Popp, D., Iwasa, M., Narita, A., Erickson, H. P. & Maéda, Y. FtsZ Condensates: An In Vitro Electron Microscopy Study. *Biopolymers* **91**, 340–350 (2009).
159. Díaz-Espinoza, R. *et al.* Domain folding and flexibility of Escherichia coli FtsZ determined by tryptophan site-directed mutagenesis. *Protein Sci* **16**, 1543–1556 (2007).
160. Lu, C., Stricker, J. & Erickson, H. P. FtsZ from Escherichia coli, Azotobacter vinelandii, and Thermotoga maritima—quantitation, GTP hydrolysis, and assembly. *Cell Motility* **40**, 71–86 (1998).
161. Huecas, S. *et al.* Self-Organization of FtsZ Polymers in Solution Reveals Spacer Role of the Disordered C-Terminal Tail. *Biophys J* **113**, 1831–1844 (2017).
162. Galli, E. & Gerdes, K. FtsZ-ZapA-ZapB Interactome of Escherichia coli. *Journal of Bacteriology* **194**, 292–302 (2012).
163. Mukherjee, A. & Lutkenhaus, J. Analysis of FtsZ Assembly by Light Scattering and Determination of the Role of Divalent Metal Cations. *J. Bacteriol.* **181**, 823–832 (1999).
164. Lu, C. & Erickson, H. P. [25] Purificationa and assembly of FtsZ. in *Methods in Enzymology* **298**, 305–313 (Academic Press, 1998).
165. Mukherjee, A. & Lutkenhaus, J. Dynamic assembly of FtsZ regulated by GTP hydrolysis. *EMBO J* **17**, 462–469 (1998).
166. Pacheco-Gómez, R., Roper, D. I., Dafforn, T. R. & Rodger, A. The pH Dependence of Polymerization and Bundling by the Essential Bacterial Cytoskeltal Protein FtsZ. *PLOS ONE* **6**, e19369 (2011).
167. Monterroso, B., Reija, B., Jiménez, M., Zorrilla, S. & Rivas, G. Charged Molecules Modulate the Volume Exclusion Effects Exerted by Crowders on FtsZ Polymerization. *PLOS ONE* **11**, e0149060 (2016).
168. Leistler, B. & Perham, R. N. Solubilizing Buried Domains of Proteins: A Self-Assembling Interface Domain from Glutathione Reductase. *Biochemistry* **33**, 2773–2781 (1994).
169. Poussu, E., Jäntti, J. & Savilahti, H. A gene truncation strategy generating N- and C-terminal deletion variants of proteins for functional studies: mapping of the Sec1p binding domain in yeast Mso1p by a Mu in vitro transposition-based approach. *Nucleic Acids Res* **33**, e104 (2005).
170. Himanen, J.-P. *et al.* Crystal structure of an Eph receptor–ephrin complex. *Nature* **414**, 933 (2001).
171. Köker, T., Fernandez, A. & Pinaud, F. Characterization of Split Fluorescent Protein Variants and Quantitative Analyses of Their Self-Assembly Process. *Sci Rep* **8**, (2018).

172. Xue, M. *et al.* Optimizing the fragment complementation of APEX2 for detection of specific protein-protein interactions in live cells. *Scientific Reports* **7**, 12039 (2017).
173. Feng, S. *et al.* Improved split fluorescent proteins for endogenous protein labeling. *Nature Communications* **8**, 370 (2017).
174. Nygren, P.-Å., Stefan, S. & Uhlén, M. Engineering proteins to facilitate bioprocessing. *Trends in Biotechnology* **12**, 184–188 (1994).
175. LaVallie, E. R. *et al.* A Thioredoxin Gene Fusion Expression System That Circumvents Inclusion Body Formation in the E. coli Cytoplasm. *Bio/Technology* **11**, 187 (1993).
176. Pryor, K. D. & Leiting, B. High-Level Expression of Soluble Protein inEscherichia coliUsing a His6-Tag and Maltose-Binding-Protein Double-Affinity Fusion System. *Protein Expression and Purification* **10**, 309–319 (1997).
177. Zheng, C.-F., Simcox, T., Xu, L. & Vaillancourt, P. A new expression vector for high level protein production, one step purification and direct isotopic labeling of calmodulin-binding peptide fusion proteins. *Gene* **186**, 55–60 (1997).
178. Samuelsson, E., Moks, T., Uhlen, M. & Nilsson, B. Enhanced in vitro Refolding of Insulin-like Growth Factor I Using a Solubilizing Fusion Partner. *Biochemistry* **33**, 4207–4211 (1994).
179. Collins-Racie, L. A. *et al.* Production of Recombinant Bovine Enterokinase Catalytic Subunit in Escherichia coli Using the Novel Secretory Fusion Partner DsbA. *Bio/Technology* **13**, 982 (1995).
180. Dai, K. & Lutkenhaus, J. The proper ratio of FtsZ to FtsA is required for cell division to occur in Escherichia coli. *Journal of Bacteriology* **174**, 6145–6151 (1992).
181. Dewar, S. J., Begg, K. J. & Donachie, W. D. Inhibition of cell division initiation by an imbalance in the ratio of FtsA to FtsZ. *Journal of Bacteriology* **174**, 6314–6316 (1992).
182. von Stetten, D., Noirclerc-Savoye, M., Goedhart, J., Gadella, T. W. J. & Royant, A. Structure of a fluorescent protein from Aequorea victoria bearing the obligate-monomer mutation A206K. *Acta Crystallogr. Sect. F Struct. Biol. Cryst. Commun.* **68**, 878–882 (2012).
183. Roberts, G. A. *et al.* Mutations of the domain forming the dimeric interface of the ArdA protein affect dimerization and antimodification activity but not antirestriction activity. *FEBS J* **280**, 4903–4914 (2013).
184. Huston, J. S. *et al.* Protein engineering of antibody binding sites: recovery of specific activity in an anti-digoxin single-chain Fv analogue produced in Escherichia coli. *Proc Natl Acad Sci U S A* **85**, 5879–5883 (1988).
185. Arai, R., Ueda, H., Kitayama, A., Kamiya, N. & Nagamune, T. Design of the linkers which effectively separate domains of a bifunctional fusion protein. *Protein Eng Des Sel* **14**, 529–532 (2001).
186. Romberg, L. & Levin, P. A. Assembly Dynamics of the Bacterial Cell Division Protein FtsZ: Poised at the Edge of Stability. *Annu Rev Microbiol* **57**, 125–154 (2003).
187. Monterroso, B. *et al.* Mg2+-Linked Self-Assembly of FtsZ in the Presence of GTP or a GTP Analogue Involves the Concerted Formation of a Narrow Size Distribution of Oligomeric Species. *Biochemistry* **51**, 4541–4550 (2012).
188. Weekley, C. M. & Harris, H. H. Which form is that? The importance of selenium speciation and metabolism in the prevention and treatment of disease. *Chem. Soc. Rev.* **42**, 8870–8894 (2013).
189. Fossum, S., Crooke, E. & Skarstad, K. Organization of sister origins and replisomes during multifork DNA replication in Escherichia coli. *EMBO J* **26**, 4514–4522 (2007).

190. McDonald, K. L. & Auer, M. High-Pressure Freezing, Cellular Tomography, and Structural Cell Biology. *BioTechniques* **41**, 137–143 (2006).
191. Willingham, M. C. & Yamada, S. S. Development of a new primary fixative for electron microscopic immunocytochemical localization of intracellular antigens in cultured cells. *J Histochem Cytochem.* **27**, 947–960 (1979).
192. Rosano, G. L. & Ceccarelli, E. A. Recombinant protein expression in Escherichia coli: advances and challenges. *Front Microbiol* **5**, (2014).
193. Dvorak, P. *et al.* Exacerbation of substrate toxicity by IPTG in Escherichia coli BL21(DE3) carrying a synthetic metabolic pathway. *Microb Cell Fact* **14**, (2015).
194. Król, E. & Scheffers, D.-J. FtsZ Polymerization Assays: Simple Protocols and Considerations. *J Vis Exp* (2013). doi:10.3791/50844

CHAPTER 4: IDENTIFICATION OF TeO_3^{2-} REDUCER MYCOTHIONE REDUCTASE FROM *RHODOCOCCUS ERYTHROPOLIS* PR4

4.1 Introduction

The discovery and identification of organisms, enzymes, and peptides capable of interacting with inorganic materials has been an area of interest for decades. This interest stems from the added control in design and function that can be attributed to biology that is harder to achieve in inorganic synthetic approaches. The relationship between metals and organisms was first explored by Carl Wilhelm von Nägeli in 1893. Termed the Oligodynamic Effect, it was observed that many metals seemed to have anti-microbial properties.[195] This led to the use of various metals, *e.g.* mercury, copper, silver, arsenic, antimony, being used for medicinal purposes.[196] However, throughout the years as exposures to these metals has increased, bacterial resistances to these metals have been widely established. Many of the exposures to metals are anthropogenic, stemming from the First Industrial Revolution some 260 years ago. Poor regulation and poorer understanding as to the effects of heavy metal pollution led to widespread contamination of many water ways and soils to the detriment of native flora and fauna. Microorganisms however have evolved ways to adapt to these environs. Metal-resistant bacteria have been identified from urban sewage, mine seepage, and agricultural sources.[197–199] Although detrimental, these environs do provide greater opportunity for the isolation of unique biological processes capable of handling metal toxins.

Generally, the biologically active forms of metals exist as ions. Resistance to metal ions can take manifest through several approaches usually involving either ion sequestration, conversion of soluble species to insoluble materials, volatilization, or the control of ion transport pathways.[200–208] These pathways usually operate with a level of redundancy, *i.e.* multiple protein cascades responsible for step-wise removal of toxins, however single enzymes have been identified solely responsible for metal detoxification. Cysteine-rich metallothioneins have been identified for their

role in metal sequestration.[209–214] Cystathione γ-lyase is capable of extracting a sulfur group from cysteine which is capable of binding and precipitating Cd^{2+}.[99,215] Mercuric Reductase (MerR) has been identified in the reduction of Hg(II) to elemental Hg which rapidly volatilizes.[22,47,79] Numerous enzymes have been identified that are capable of forming inorganic particulate through the reduction of metal ionic species. Dihydrolipoamide dehydrogenase, nitrate reductase, catalase and have been identified that are capable of reducing selenite, selenite, tellurite and tellurate to form inorganic precipitate.[24,91–93] Although it doesn't form precipitate, chromate reductase is responsible for the reduction of Cr(VI), a labile and toxic form of chromium, to the far less promiscuous Cr(III).[89]

Of great interest in this section is the remediation of soluble metal ions by way of conversion to an insoluble bio-inert form for the application of a genetically encoded tag for biological EM imaging. Many of the enzymes that are expected to be found are will either be unstable or toxic in other microorganisms or for multimers that would hinder their applications as tags. With further expansion of the catalogue of metal reducing enzymes in any form, consensus of active sites that permit such reduction events can be built. This active site consensus would be used to direct the engineering of enzymes that could be a better candidate for a genetically encoded tag for biological EM imaging.

In this chapter, screening of lysates from heavy metal contaminated waters in the Colorado Mining Belt were performed for the identification of specific enzymes capable of reducing soluble metal precursors to form nanomaterials. Currently, the endeavor of creating 'clonable nanoparticles' (cNP) (*i.e.* a genetically encoded enzyme capable of forming nanomaterials upon incubation with precursor) is being realized using Glutathione Reductase-like Metalloid Reductase (GRLMR) from *Pseudomonas moraviensis* stanleyae. GRLMR has shown itself to be a great springboard for the development of cNPs as it conservatively meets three criteria defined as (i) reduction of soluble metal precursors to insoluble (nano)particulate (ii) retention of the (nano)particulate and (iii) an ability to control the growth of the (nano)particulate. But the end goal of the cNP is to have several tag constructs capable of reducing, with specificity, various

precursors to form NPs with different elemental make-ups. Analogous to the variety of fluorescing proteins available for fluorescence imaging, the development of a toolbox of different metal reducing constructs would be advantageous for widespread application for biological EM imaging.[5]

Specifically, selection of an environmental isolate identified as *Rhodococcus erythropolis* PR4 by LC-MS/MS was cultured from mine site seepage in the Colorado Mining Belt. *R. erythropolis* PR4 showed high resistance to several metals, of most interest, TeO_3^{2-}. Nanoparticulate was observed in SEM for both Se and Te as large aspect ratio elemental extrusions of Se or nanorods in the cytoplasm composed of Te. Lysate from *R. erythropolis* PR4 was run in a native PAGE-gel and a single dark band was observed after incubation with K_2TeO_3 and NADPH indicating an enzyme with Te-reductase activity. This enzyme was identified as mycothione reductase. After the enzyme was isolated, activity assays showed a selectivity for the reduction of Te over the reduction of Se, another chalcogen 1 row above Te.

4.2 Results and Discussion

4.2.1 *Environmental Bacterial Isolation and Metal Screening*

The collection of water and soil samples were collected from various locations within the Colorado Mining Belt. Water sources in the area have been contaminated with heavy metals since the early 1800s with unregulated mining. On a microbial level, the time scale of metal contamination provides a greater chance for finding bacteria that have evolved processes to handle high concentrations of metal. Water and soil samples were then diluted into PBS to collect bacteria and plated on various LB or minimal media agar plates of varying pH to provide different bacteria chances to grow. Plates were grown at room temperature (RT) and as colonies began to become visible, they were picked and grown up in corresponding liquid media. Once grown to density, freezer stocks were made and samples were diluted into media containing either Fe(II) (5 mM), Cu(II) (2 mM), AsO_3^{2-} (2 mM), SeO_3^{2-} (2 mM), TeO_3^{2-} (0.1 mM), Cd(II) (1 mM), or Zn(II) (2 mM) and allowed several days to grow. Bacterial samples were observed for both the ability to grow to density and if a color change was observed indicating a change in metal speciation. Of the ~200

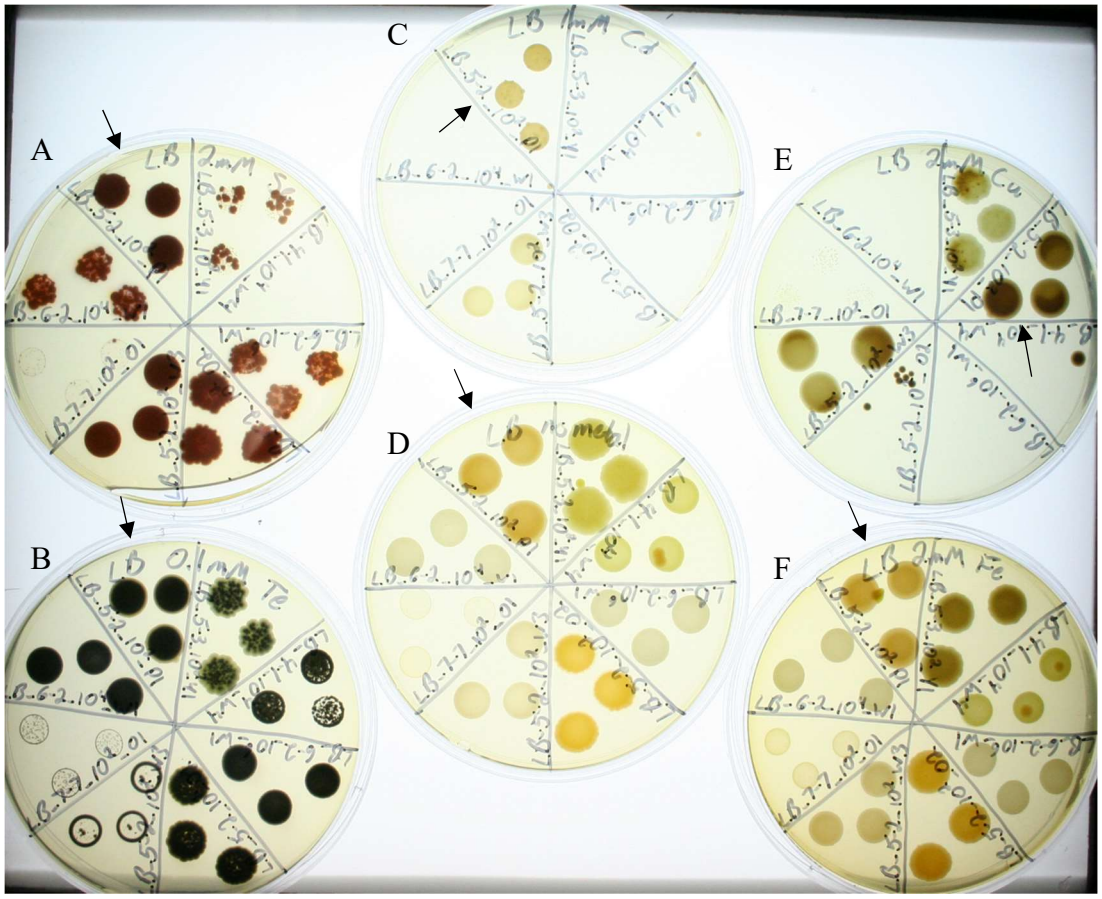

Figure 4.1. Various metal supplemented LB agar plates on which 8 different environmental isolates were plated. (**A**) 2 mM SeO_3^{2-}, (**B**) 0.1 mM TeO_3^{2-}, (**C**) 1 mM Cd(II), (**D**) no metal, (**E**) 2 mM Cu(II), (**F**) 2 mM Fe(II). The black arrows indicate the environmental isolate LB_5-2_10^2_P1.

bacterial colonies capable of growing in a lab setting, 16 isolated bacterial cultures showed growth and/or color change in all the metals tested. The sample LB_5-2_10^2_P1 (indicated by the arrow in **Figure 4.1**) was able to grow in liquid culture and agar plates supplemented with metals. Color changes were also observed when incubated with Fe(II), Cu(II), SeO_3^{2-}, and TeO_3^{2-}. LC-MS/MS was used to identify the species as *Rhodococcus erythropolis* PR4, a gram-positive nonmotile Actinomycete closely related to *Mycobacterium* and *Corynebacterium*.

R. erythropolis PR4 has been studied for its production of numerous siderophores and utilization of diesel oil and other hydrocarbons as carbon sources.[216–220] The genome of *R. erythopolis* PR4 has been sequenced along resulting in a circular genome of 6.5 Mb, two smaller circular plasmids of 104 kb and 3.6 kb, and a linear plasmid of 272 kb.[221] Encoded on the linear

plasmid were genes that were homologous to metal resistance genes, namely a cation-efflux-family transporter known to increase resistance to cadmium, zinc, and cobalt, and a possible membrane-associated cadmium-binding protein, and a predicted cadmium-transporting P-type ATPase.[222,223] A protein belonging to the CopC/PcoC family involved in copper sequestration was also identified in this region although some amino acid residues were not conserved possibly preventing functionality.[224]

4.2.2 *MIC of Rhodococcus erythropolis PR4*

The minimal inhibitory concentration (MIC) for *R. erythropolis* PR4 was found using broth microdilution.[225,226] Resulting MICs for *R. erythropolis* PR4 are in **Table 4.1**. The wide range of metal resistances of *R. erythropolis* PR4 was impressive, specifically the resistance identified against tellurium. There have been many species identified with Te-resistance with most falling between 1 – 2 mM MIC however bacteria isolated from hydrothermal vents in the Juan de Fuca Ridge were capable of growing in 10 mM concentrations.[205,206,227–229] Although not the highest resistance, growth up to 4.5 mM TeO_3^{2-} was an impressive outcome.

Table 4.1. MIC values for *R. erythropolis* PR4 determined by broth microdilution

Metal	TeO_3^{2-}	SeO_3^{2-}	Cd(II)	Cu(II)	Ni(II)	Co(II)	AsO_3^{2-}	Fe(II)	Zn(II)
Conc. (mM)	4.5	2.5	1.5	5.5	8	2.5	>10	5	5.5

In order to see if the color change observed in the cultures was due to formation of metal precipitate intra- or extracellularly, *R. erythropolis* PR4 was grown in LB supplemented with 2 mM of either SeO_3^{2-} or TeO_3^{2-}. After culture reached density, cells were collected and fixed for scanning electron microscopy (SEM) imaging. The resulting images showed a dramatic difference between cells incubated with SeO_3^{2-} and TeO_3^{2-} (**Figure 4.2**). When incubated with SeO_3^{2-} cells had large extrusions with high aspect ratios from the outer membranes composed of Se. When incubated with TeO_3^{2-} nanostructures were observed mostly at the distal ends of the cells. This

variance between the two metals was unexpected and poses the question of what mechanisms are provoking such differences.

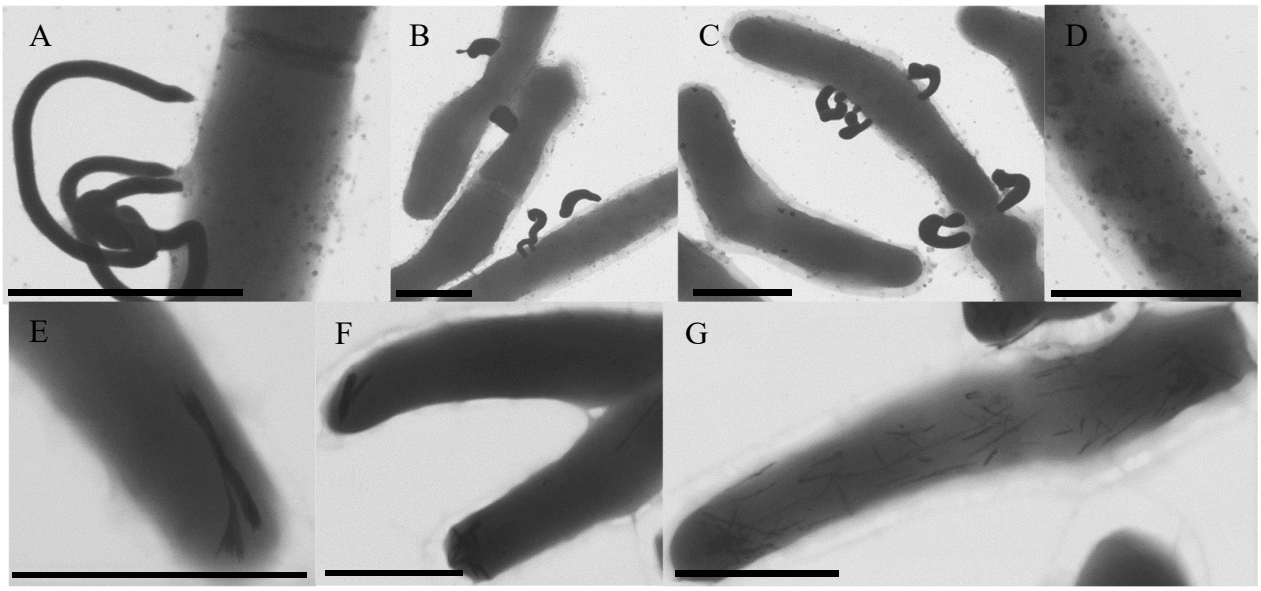

Figure 4.2. SEM images of *R. erythropolis* PR4. Panels (**A**) – (**D**) cells incubated in 2 mM SeO_3^{2-} with large nanostructures and/or nanoparticulate composed of Se on the cell surface. Panels (**E**) – (**G**) cells incubated with 2 mM TeO_3^{2-} with nanostructures present in the cytoplasm of the cell. Scale bar = 1 μm

4.2.3 *Mycothione Reductase Identification and Isolation*

To probe whether individual enzymes were responsible for the nanostructures observed in SEM, *R. erythropolis* PR4 was grown in culture, lysed, and the lysate was run in native PAGE gel as previously described.[23,205] Native PAGE gels were then sectioned vertically and the slices were incubated in 5 mM of either TeO_3^{2-}, SeO_3^{2-}, Cu(II), Fe(II), and Zn(II) with either NADPH or NADH as a cofactor. The expectation was if individual enzymes were responsible for the removal of soluble metal ions through precipitation a band would develop in the native PAGE slice corresponding to an enzyme with reductase activity. Upon running the lysate in native-PAGE a single band developed when incubated in TeO_3^{2-} and NADPH. **Figure 4.3** shows an example of a native PAGE gel after metal and cofactor soaking. Lane 3 in the native-PAGE corresponds to Cu(II) and was continuously observed as precipitating within the gel regardless of protein presence and therefore couldn't be used to identify Cu(II)-reductases. The same band was able to develop

when incubated with NADH although to a lesser extent indicating the enzyme was preferential to NADPH as the cofactor.

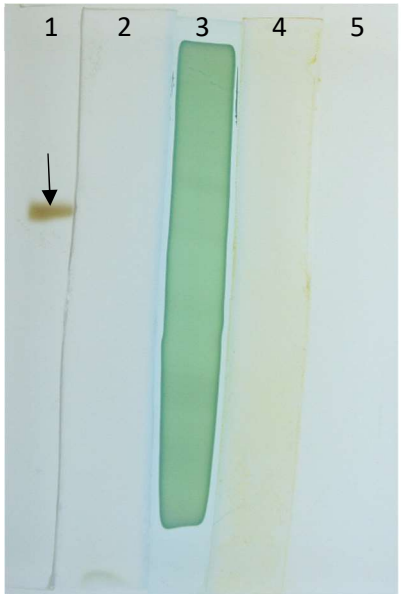

Figure 4.3. Native PAGE gel slices that were incubated in 5 mM of TeO_3^{2-} (Lane 1), SeO_3^{2-} (Lane 2), Cu(II) (Lane 3), Fe(II) (Lane 4), Zn(II) (Lane 5) from left to right. The band that developed in the TeO_3^{2-} incubated slice (Lane 1) is indicated by a black arrow.

In order to identify this enzyme with Te-reductase activity, lysate from *R. erythropolis* PR4 was run through a DEAE column for an initial separation. Aliquots (150 µL) of the fractions collected were deposited into a 96-well plate and 50 µL of a solution of 2 mM K_2TeO_3 and 1 mM of NADPH was added. The plate was incubated at RT until wells developed a darker color indicating the presence of elemental TeO_3^{2-}. Several fractions were observed as turning dark and these fractions were then run in 2 identical native PAGE gels for a final separation before LC-MS/MS. One resulting PAGE gel was stained with Coomassie dye for the visualization of individual protein bands. The other native gel was soaked in a TeO_3^{2-}/NADPH solution to identify which protein band would correspond to the Te-reductase activity. The corresponding band in the Coomassie stained gel was then excised to prevent any complications that might come from the presence of Te oxyanions or nanostructures.

LC-MS/MS resulted in the identification of 13 proteins, 5 of which were predicted to have NADPH binding motifs (**Table 4.2, Appendix D.1**). Putrescine oxidase (PUO), malate

dehydrogenase (MDH), thioredoxin (TrxR), 3-hydoxyisobutryrate dehydrogenase (HIBADH), and mycothione reductase (Mtr) were then amplified from *R. erythropolis* PR4, inserted into an expression vector containing a C-terminal His tag, and isolated after expression from *E. coli*. These 5 proteins were then run in a native PAGE gel and soaked in a TeO_3^{2-}/NADPH solution. Of the 5 enzymes tested, Mtr developed a dark band indicating Te-reductase activity. The flavo-dependent oxidoreductase Mtr is analogous to glutathione reductase, reducing the redox homeostasis molecule mycothione (MSSM) to mycothiol (MSH). *R. erythropolis* PR4 does not use glutathione and is in fact toxic to mycobacteria.[230,231] Mtr is therefore orthogonal to species

Table 4.2 LC-MS/MS Data of Possible Te-Reductase from *R. erythropolis* PR4

Protein	**Accession #**	**Molecular Weight**	**NAD(P)H Binding**	**Percent Coverage**
Putrescine Oxidase	C1A3D2	49 kDa	Y	59.8
β-ketoadipyl-CoA Thiolase	C1A2Z1	42 kDa		49.4
Mycothione Reductase	C0ZY75	49 kDa	Y	39.1
Malate Dehydrogenase	C1A2K5	41 kDa	Y	33.8
Aminopeptidase N	C1A007	91 kDa		10.9
Superoxide Dismutase	C0ZLP5	23 kDa		24.2
Enoyl-CoA Hydratase	COZXP4	27 kDa		19.7
Thioredoxin Reductase	Q3L9K9	35 kDa	Y	18.6
3-hydroxyisobutyrate Dehydrogenase	C1A225	30 kDa	Y	9.1
DNA-directed RNA Polymerase Subunit α	C0ZW54	38 kDa		6.8
Zinc-Dependent Metalloprotease	C0ZX51	50 kDa		12.4
Metallo-hydrolase	C0ZZY6	48 kDa		6.0
Phosphoenolpyruvate Carboxykinase	PCKG	67 kDa		9.9

that use glutathione, providing a unique enzyme for the production of cNPs. Orthogonality of a metal reducing enzyme could be a good candidate for the application as a cNP since it would not be interacting in the cellular metabolism.

4.2.4 *Substrate Selectivity of Mycothione Reductase*

Further study into the activity and selectivity of the enzyme was performed. Luckily, Mtr was not toxic to cells, another possibility with orthogonal proteins.[232] Surprisingly however, the presence of Mtr in *E. coli* did not lend to an increase in Te-resistance by the host strain. Crude purification was done using a Ni-NTA column however the protein was eluted from the column at low imidazole concentrations requiring further purification on a DEAE ion exchange column. The purification of the Mtr was able to be isolated in the 100s of mg from a 1 L culture. Reduction reactions of TeO_3^{2-} by Mtr were set up in order to see the resulting Te^0 structures formed. Concentrations of 1, 3, and 7 mM of K_2TeO_3 with excess of NADPH were reduced in the presence of 15 µg of Mtr. Reactions proceeded overnight and the Te^0 nanostructures were applied to a copper grid for SEM imaging. The product formed by the 1 mM TeO_3^{2-} were spherical or oblong and about 50 nm (**Figure 4.4, panel A**). As the TeO_3^{2-} concentrations were increased, the structures resembled bundled nanowires (**Figure 4.4, panel B**), and finally large aggregates of fused nanowire bundles (**Figure 4.4, panel C**).

Initial Mtr reduction experiments were performed in PBS, 20 mM TEA, and 50 mM HEPES with pHs 6 – 9 to test buffer and pH stability of the enzymatic reaction. Substrates tested were 2

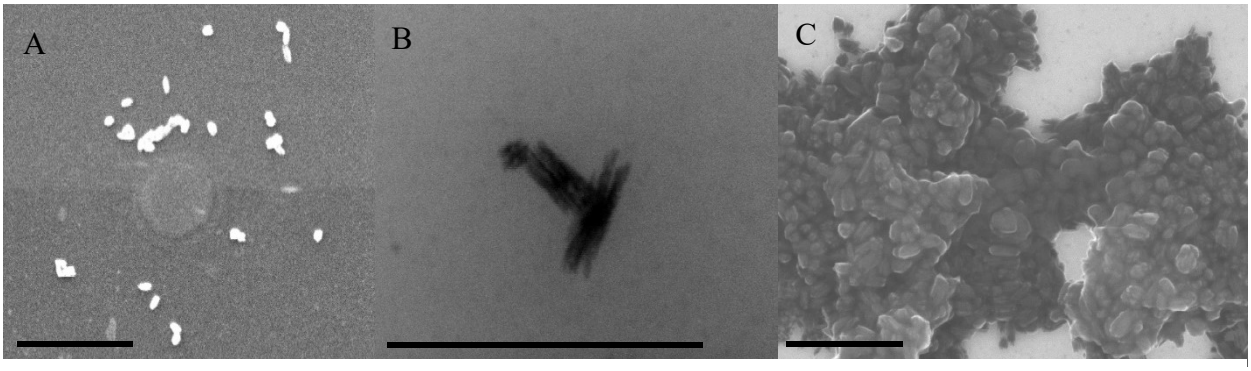

Figure 4.4 SEM of Te-nanostructures produced from Mtr incubated with (**A**) 1 mM, (**B**) 3 mM, and (**C**) 7 mM TeO_3^{2-}. Scale bar = 500 nm

mM starting concentrations of SeO_3^{2-}, TeO_3^{2-}, or oxidized glutathione (GSSG) and initial velocities were determined through monitoring the degradation of 200 μM NADPH at 340 nm. When the native PAGE gel was soaked in the various metals Se did not result in an observable red band (*vide supra*). The result of the pH/buffer screen (**Figure 4.5**) indicated further the selectivity of Mtr towards the reduction of TeO_3^{2-}. In every environ screened, the reduction of TeO_3^{2-} occurred at a faster rate that SeO_3^{2-}. At lower pH values, some amount of TeO_3^{2-} crashed out of solution yet Mtr still reduced TeO_3^{2-} at a faster rate. Physiological conditions are best represented by PBS pH 7.2 – 7.8 for *E. coli*.[233,234] The activity of Mtr overall drops dramatically between pH 7 – 8 in PBS possibly hindering the use of Mtr itself as a cNP.

In order to test the orthogonality of Mtr, GSSG was used as a substrate. In all the buffers tested, NADPH degradation was similar to NADPH degradation omitting the Mtr (data not shown). With the exception of TEA-HCl pH 6, which is below physiological pH, these results indicated that Mtr was not capable of reducing GSSG within a host cell. When Mtr was expressed in *E. coli*, resistance to Te did not increase. The lack of interaction with GSSG and the drop in activity at physiological pHs could explain why Te-resistance is not portable between species. GSH is a well-known metal chelator in the cytoplasm of cells.[27,235–237] Capable of being present at

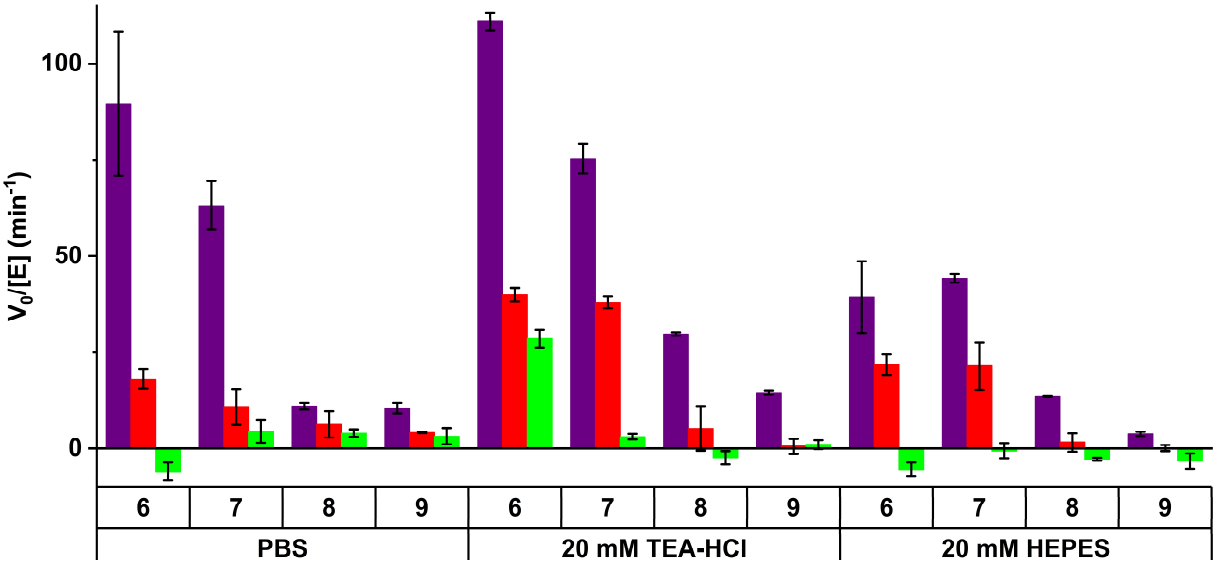

Figure 4.5 Buffer and pH screen for Mtr with substrates TeO_3^{2-} (purple), SeO_3^{2-} (red), and GSSG (green). Substrates were at a starting concentration of 2 mM.

concentrations of up to 10 mM in *E. coli*, GSH quickly chelates selenium once it enters the cell for future metabolism. *S. cerevisiae* under arsenic stress will release extracellular GSH for the chelation and reduction of arsenic. It has also been observed that 5 mM GSH can reduce tellurite to Te^0. Much like selenium, tellurium might be chelated by the high concentration of GSH or other sulfur containing compounds in the cytoplasm preventing tellurite from interacting with Mtr once in the cell.

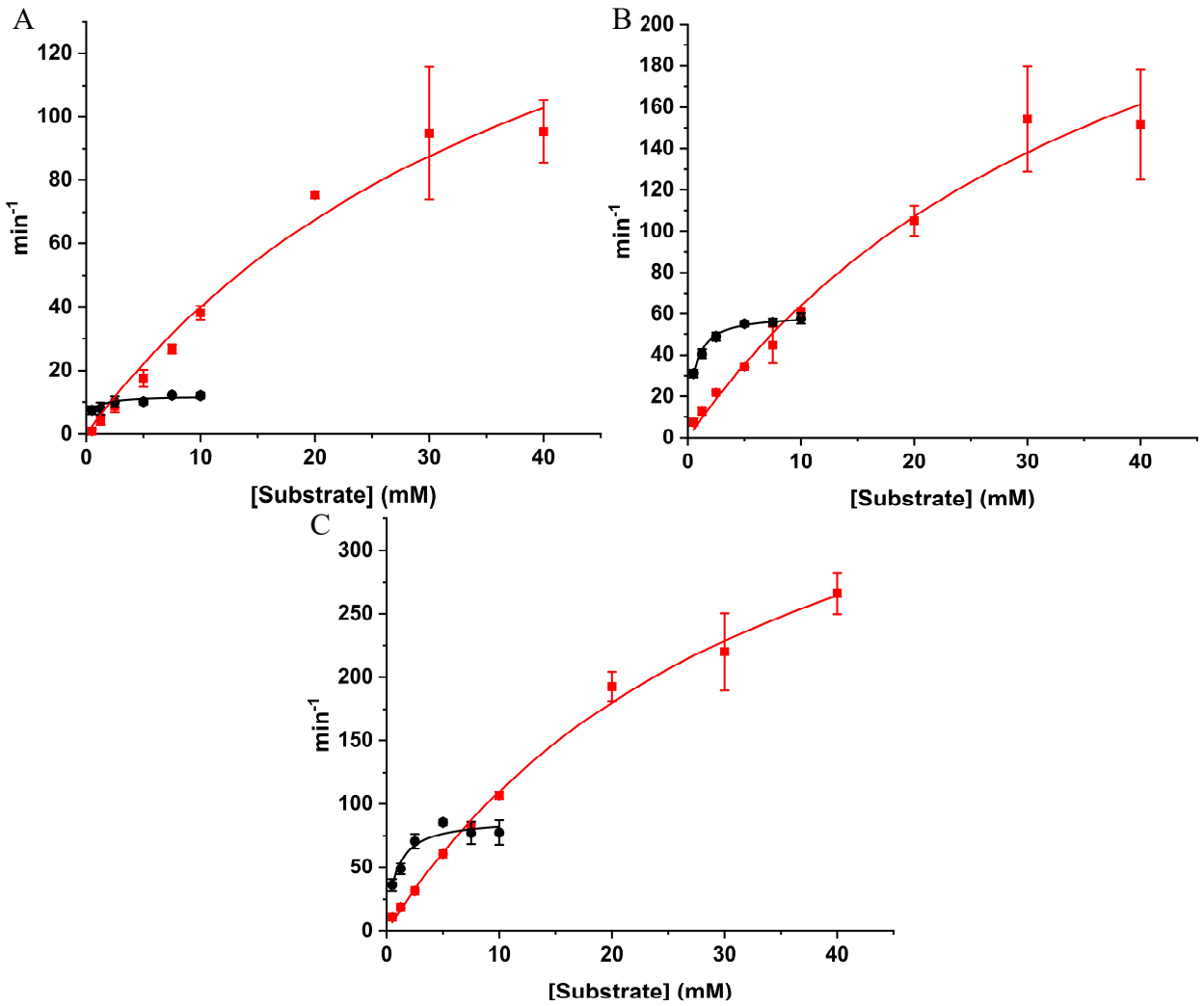

Figure 4.6 Plots of enzymatic rate (min^{-1}) v. substrate concentration (mM) of Mtr in either (**A**) PBS pH 7.4, (**B**) 20 mM HEPES pH 7, or (**C**) 20 mM TEA-HCl pH 7.6. Substrates were either TeO_3^{2-} (•) or SeO_3^{2-} (▪).

Table 4.3 Kinetics Data for Mtr

	20 mM HEPES, pH 7		20 mM TEA-HCl, pH 7.6		PBS, pH 7.4	
	TeO_3^{2-}	SeO_3^{2-}	TeO_3^{2-}	SeO_3^{2-}	TeO_3^{2-}	SeO_3^{2-}
K_M (mM)	0.517±0.050	41.14±11.69	0.779±0.050	35.23±4.51	0.413±0.141	43.9±14.7
k_{cat} (min^{-1})	59.85±1.07	327.4±56.7	88.60±5.40	497.1±36.9	11.92±0.68	215.8±44.9

In order to calculate the K_M of Mtr, a range of 0.5 – 10 mM of either TeO_3^{2-} or SeO_3^{2-} in PBS (pH 7.4), 20 mM TEA-HCl (pH 7.6), and 20 mM HEPES (pH 7.0). Being able to compare these values would indicate the selectivity of Mtr for the tested oxyanion substrates. Once again, NADPH degradation was tracked at 340 nm. Plots of the V_0 at varying substrate concentrations are shown in **Figure 4.6**. In all the buffers tested, Mtr possessed a greater affinity for TeO_3^{2-} when compared to SeO_3^{2-} indicated by a lower K_M. Of note is that the curves for SeO_3^{2-} do not have similar plateaus observed for TeO_3^{2-}. This difference is largely in part due to the limited solubility of TeO_3^{2-} at the pHs tested. Especially observed for PBS, at higher concentrations of TeO_3^{2-} the pH of the reaction also increased. As seen in the pH screen (*vide supra*) enzymatic activity drops dramatically with the increased basicity of the reaction. Both the insolubility of TeO_3^{2-} and the increased pH of the reactions leads to a rather difficult analysis of the kinetics studies in **Figure 4.6**.

In order to deconvolute the selectivity of Mtr reductions would need to be perform in the presence of both selenite and tellurite. For the final selectivity experiment, Mtr was exposed to a mixed solution of selenite and tellurite of varying ratios. A limiting concentration of NADPH was then added to the solution and the reduction was run overnight. Ratios of 1:1, 1:5, and 1:10 of Te to Se were used. The buffer was PBS, pH 7.4 since it is a common buffer for most systems and the Mtr seemed to have the worst activity for TeO_3^{2-} reduction in PBS. Inductively coupled plasma mass spectrometry (ICP-MS) is a useful technique for determining metal ion concentrations and was used to determine the ratios of Se and Te present in the insoluble products. The nanoparticles formed after the reaction collected through centrifugation and dissolved in 70% HNO_3. The solution was eventually diluted to concentrations within the range of the standard curve in 2%

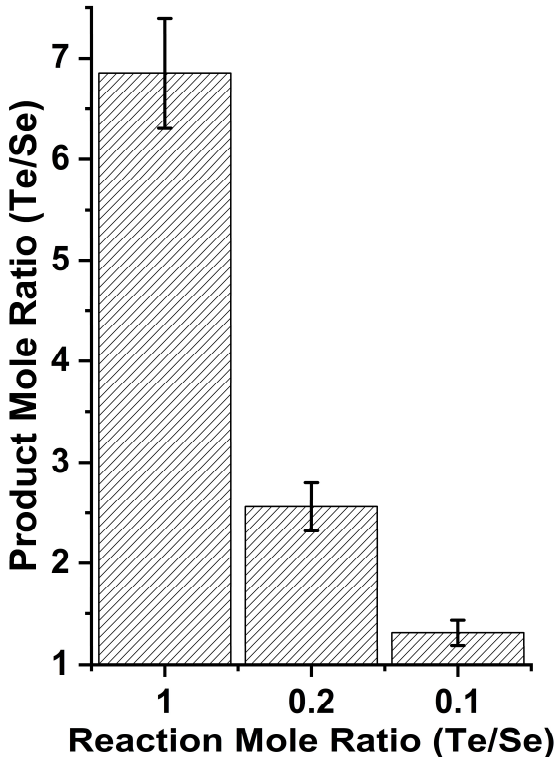

Figure 4.7 ICP-MS results of varying reaction ratios of TeO_3^{2-} and SeO_3^{2-} with Mtr. All reactions were performed with a limiting amount 500 μM NADPH

HNO_3. ICP-MS results are shown graphically in **Figure 4.7**. When the molar ratio of tellurite to selenite was 1:1 there was a molar ratio of 6.85 Te to Se in the particulate produced in the reaction. As the ratio was increased to 1:5 and 1:10 Te to Se, there was a decrease in the molar ratio of the resulting nanoparticle (2.56 and 1.31 Te to Se, respectively). It must be noted that even with 10 times the concentration of SeO_3^{2-}, Mtr still had a proclivity to reduce TeO_3^{2-}. It is also important to reiterate that this selectivity test was performed in the worst tested buffer system in relation to Mtr reductase activity (*vide supra*).

Mtr's selectivity for TeO_3^{2-} is interesting since the reduction potential of reducing Te(IV) to Te^0 is ~210 mV more negative than the reduction of Se(IV) to Se^0.[238] This affinity could be based on the difference in size of the substrate. The Te(IV) ion has a radius twice as large as Se(IV), 97 pm and 50 pm respectively.[239] Tellurium is also capable of undergoing stronger secondary bonding interactions than sulfur or selenium due to its easier polarisability.[240]

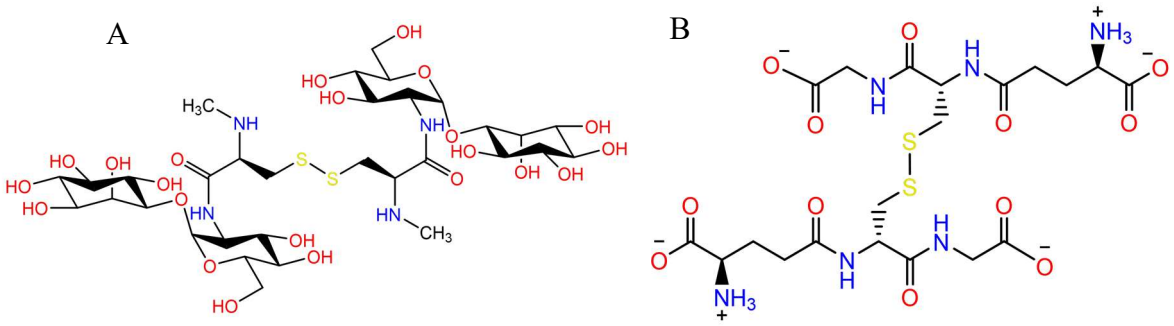

Figure 4.8 Lewis structures of mycothione (**A**) and GSSG (**B**).

To explore this possibility, the structure for Mtr was predicted using the online server Phyre[2] and aligned to GRLMR in Pymol.[56] Previous work has been done on Mtr from *Mycobacterium tuberculosis* which is 65.64% similar.[241–243] *M. tuberculosis* Mtr structural studies recognized 3 different domains similar to GRLMR enzyme and were used to highlight the possible active site for Te-reducing Mtr. While the Pymol cavity size approximations should be considered qualitative, there none the less exists a larger cavity calculated at ~2200 Å^2, at the Mtr active site. This is not unexpected as mycothiol is composed of an acetylated cysteine, a glucosamine, and an

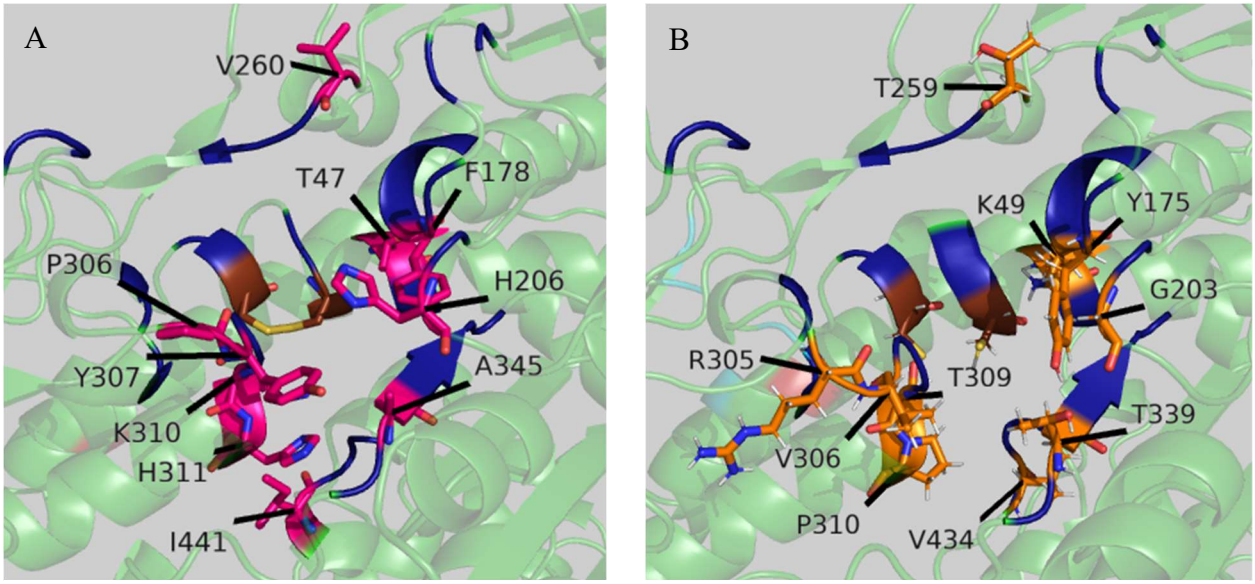

Figure 4.9 Predicted Phyre[2] structures of Mtr (**A**) and GRLMR (**B**) illustrated in Pymol. Brown residues correspond to the redox active cysteines in the active site. The dark blue residues represent identical residues within the active site. Magenta and orange residues represent the differing residues between Mtr and GRLMR.

inositol ring. The presence of the two carbon rings increases the bulkiness of MSSM considerably when compared to GSSG (**Figure 4.8**).[244–246]

When a closer look is taken to the sizes of the oxyanions however this large cavity size can easily fit either. If for simplicity a sphere for tellurite and selenite is assumed, the diameters are 8.54 Å and 7.2 Å, respectively; well within the size of the cavity.[239,247,248] There are also several residues in the predicted active site that differ between GSHR and Mtr. Specifically, Mtr possesses several aromatic rings, H206, Y307, and H311, protruding into the mouth or the cavity of the active site itself. Within the chalcogens, π-interaction potential decreases going towards heavier elements, S > Se > Te.[240] The residues H206 and Y307 are predicted as pointing towards the opening and could be involved in interactions with SeO_3^{2-} that are more energetically favorable for TeO_3^{2-}. Graphical representation of the two predicted active sites highlighting the different residues is shown in **Figure 4.9**.

4.3 Future Considerations

The identification and subsequent activity possessed by Mtr is exciting for several reasons. First, a metal reducing enzyme that reduces Te selectively over Se provides a second candidate for a cNP. GRLMR has been characterized with a specificity to Se.[23] Being able to utilize both of these enzymes simultaneously within a biological system brings the end goal of a GFP-analogue EM tag closer to realization. There are a few caveats pertaining to the usage of Mtr in this regard. (i) Unlike Se, Te is extremely toxic to most organisms. (ii) Mtr does not seem to be able to instill Te-resistance in a species that utilizes glutathione. (iii) Like GRLMR, Mtr is a homodimer and therefore not an *ideal* candidate.

Second, Mtr provides insight into substrate selectivity through active sight residues. It would be interesting to see if point mutations within GRLMR would allow selectivity for Te and therefore Te resistance in glutathione utilizing organisms. It could also be possible, in the case of identification of a monomeric oxidoreductase scaffold, that the Mtr active site could allow for a 'plug and play' construct allowing Te reduction.

Third, Mtr's lack of portability could also be overcome if a fixation protocol could be developed that still allows the function of GRLMR and Mtr. If a protocol is identified that facilitates enzyme function than merely soaking fixed whole cell or sectioned samples in corresponding metal salts and required cofactors would allow the formation of *in situ* nanoparticles.

Lastly, Mtr might be able to form quantum dots (QDs) much like GRLMR (paper submitted, *J. Phys. Chem. C*, June 2019). Being able to produce both Se and Te derived QDs presents avenues towards correlative light electron microscopy (CLEM) as well as unique approaches to inorganic material production.

4.4 Summary and Conclusion

The screening of organisms from the Colorado Mining Belt have already provided several organisms that can survive in a wide range of high concentration metal salts. The further study of organisms that have developed new metal resistance mechanisms could lead to further identification of enzymes capable of bioremediation. Already, the metal screening of cell lysates has already led to identification of a Te-reducing mycothione reductase identified from *R. erythropolis* PR4.

The expansion of the metal reducing enzyme catalogue proves exciting for the development of cNP tags. Specifically, Mtr shows great promise as a cTeNP. Mtr has great selectivity in the presence of both tellurite and selenite, is orthogonal to species that utilize glutathione for redox homeostasis and can be produced in large quantities in *E. coli* lending to its overall stability. Further work needs to be done to identify the vital active site residues within Mtr. If the construct of the Te-reducing active site could be identified, perhaps it could be engineered into a more appropriate cNP construct.

4.5 Experimental Details

4.5.1 *Materials*

PCR and ligation components, restriction enzymes, and T7 Expression *lysY/I*^{q} Competent *E. coli* cells (Cat # C3013I) were purchased from New England Biolabs, Inc. Primers were purchased from Integrated DNA Technologies. The expression vector pD441-CH was originally purchased

from ATUM (Dna Twopointo Inc.). Antibiotics were purchased from GoldBio. Na_2SeO_3, $HNaSeO_3$, and K_2TeO_3 were purchased from Alfa Aesar. NADPH was purchased from BioVision and Coomassie Plus Bradford Reagent from Thermo Scientific. GTP was purchased from Chem-Impex Int'l Inc. GeneJet Plasmid Miniprep Kit (Cat# K0503) and PCR Cleanup Kit (Cat# K0702) were purchased from ThermoFisher Scientific.

4.5.2 *Environmental Bacterial Isolation and Metal Screening*

Water ways around the Colorado Mineral Belt were visited and samples of water and soil were collected. For the soil samples, a small sample of soil was added to PBS and gently agitated. Supernatant was removed and applied to LB-agar or minimal media agar plates of various pH 3, 5, or 7. Samples were applied in dilutions of $10^0 – 10^6$. These various environs were expected to give some of the environmental isolates better chances to grow increasing the number of culturable microbes.

Plates were grown at RT for 2 weeks. After each week colonies were picked and grown in liquid media that corresponded to the plate the colony was picked from. Cultures were also grown at RT. Once grown to concentration a fraction of the cultures were stored in glycerol at -80°C until future studies.

Metal screening were initially performed in culture. First, liquid cultures of the targeted isolates were grown to until dense. A 1/100 fraction of the dense culture was then added to growth tubes that had media supplemented with the metals of interest, Fe(II) (5 mM), Cu(II) (2 mM), AsO_3^{2-} (2 mM), SeO_3^{2-} (2 mM), TeO_3^{2-} (0.1 mM), Cd(II) (1 mM), or Zn(II) (2 mM) and allowed to grow. Aspects of the incubated cultures were recorded; the density of the culture and if there was a color change of the colony indicating presence of metal reductive capabilities.

4.5.3 *Metal Screening of Lysates*

Lysate metal screens were then conducted to try and identify specific enzymes responsible for the reduction of the metals tested. 25 mL cultures of the environmental isolates were grown to density, cells were collected, and lysed using intense agitation with glass beads. Lysate was collected and run in a native-PAGE gel for crude separation of the lysate. The PAGE gel was then

cut into vertical strips and incubated in 50 mM HEPES buffer with 5 mM of a metal salt and either NADPH or NADH as a cofactor. Reactions were run in an inert atmosphere and the next day, gels were observed for possible metal band development, indicating metal salt reduction. Corresponding bands in the gel were then excised and sent for LC-MS/MS.

4.5.4 *LC-MS/MS*

4.5.4.1 *Sample Preparation*

Gel fragments were subjected to in-gel trypsin digestion and LC-MS/MS as previously described.[249] Briefly, the gel pieces were washed with 200 µL of LC-MS Grade Water (Optima LC-MS, Fisher Scientific) for 30 sec and destained with 2 x 200 µL of 50% Acetonitrile (ACN; Optima LC-MS Grade)/50 mM Ammonium bicarbonate at 60°C, with intermittent mixing. The pieces were dehydrated with 100% ACN and allowed to air dry. Proteins were reduced and alkylated, in-gel with 25 mM DTT in 50 mM ammonium bicarbonate (60°C for 20 min) and 55 mM IAA or IAH in 50 mM ammonium bicarbonate at room temperature in the dark for 20 min. Gel pieces were then washed with Optima water and dried. The dried gel pieces were rehydrated in 20 µL 12 ng/µL MS-grade Trypsin (ThermoPierce, San Jose, CA)/0.01% ProteaseMAX surfactant/50 mM ammonium bicarbonate mixture for 10 min at room temperature, overlaid with 30 µL 0.01% ProteaseMAX surfactant/50 mM ammonium bicarbonate and incubated at 50°C for 1 h. Extracted peptides were transferred and the digestion halted by addition of 10% trifluoro-acetic acid to a final concentration of 0.5%. Peptide extracts were dehydrated then resuspended in 5% ACN/0.1% formic acid. Once resolubilized, absorbance at 205 nm was measured on a NanoDrop (ThermoScientific) and total peptide concentration was subsequently calculated using an extinction coefficient of 31[250].

4.5.4.2 *Mass Spectrometry Analysis*

A total of 1µg of peptides were purified and concentrated using an on-line enrichment column (Thermo Scientific 5µm, 100 µm ID x 2cm C18 column). Subsequent chromatographic separation was performed on a reverse phase nanospray column (Thermo Scientific EASYnano-LC, 3 µm, 75 µm ID x 100 mm C-18 column) using a 30 minute linear gradient from 5% – 30% buffer B

(100% ACN, 0.1% formic acid) at a flow rate of 400 nanoliters/min. Peptides were eluted directly into the mass spectrometer (Orbitrap Velos, Thermo Scientific) equipped with a Nanospray Flex ion source (Thermo Scientific) and spectra were collected over a m/z range of 400 – 2000, positive mode ionization, using a dynamic exclusion limit of 2 MS/MS spectra of a given m/z value for 30 s (exclusion duration of 90 s). The instrument was operated in FT mode for MS detection (resolution of 60,000) and ion trap mode for MS/MS detection with a normalized collision energy set to 35%. Compound lists of the resulting spectra were generated using Xcalibur 3.0 software (Thermo Scientific) with a S/N threshold of 1.5 and 1 scan/group.

4.5.4.3 *Data Analysis*

Tandem mass spectra were extracted, charge state deconvoluted and deisotoped by ProteoWizard MsConvert (version 3.0). Spectra from all samples were searched using Mascot (Matrix Science, London, UK; version 2.3.01) against the customized Uniprot_Ecoli_rev_082416 database (unknown version, 8630 entries) assuming the digestion enzyme trypsin. Mascot was searched with a fragment ion mass tolerance of 0.80 Da and a parent ion tolerance of 20 PPM. Oxidation of methionine, carbamidomethyl of cysteine and carboxymethyl of cysteine were specified in Mascot as variable modifications. Search results from all samples were imported and combined using the probabilistic protein identification algorithms implemented in the Scaffold software (version Scaffold_4.5.1, Proteome Software Inc., Portland, OR).[251,252] The peptide threshold (95%) was set such that a peptide FDR of 0.0% was achieved based on hits to the reverse database[253]. Protein identifications were accepted if they could be established at greater than 95.0% probability and contained at least 2 identified peptides. Protein probabilities were assigned by the Protein Prophet algorithm[254]. Proteins that contained similar peptides and could not be differentiated based on MS/MS analysis alone were grouped to satisfy the principles of parsimony.

4.5.5 *MIC Determination*

MIC for *R. erythropolis* PR4 was determined using a broth microdilution protocol.[225] First, a starter culture was begun of *R. erythropolis* in LB media with 5 μM K_2TeO_3 as a selecting agent and grown at RT with agitation. After 2 days, the culture was dense. Culture tubes were filled

with 990 µL LB media and supplemented with 0.1 – 10 mM metal. 10 µL of the dense culture was then added to the culture tube. All inoculated tubes were then allowed to grow at RT for 3 days with gentle agitation to aerate the culture. After 3 days, the tube in which no growth was observed was considered the MIC.

4.5.6 *Plasmid Construction*

Colony PCR (cPCR) was used to amplify the gene for all the NADPH-dependent proteins that resulted from LC-MS/MS. Briefly, gene sequences were identified using an amino acid sequence BLAST against the genome and 3 plasmids of *Rhodococcus erythropolis* PR4. Sequences then directed the design of primers that would be used for gene amplification. PCR reactions were then set up as follows, 100 nM final concentration of each primer, 200 µM dNTPs, 10 µL of Q5 buffer, 10 µL of GC Enhancer, 1U of NEB's Q5 High-Fidelity Polymerase were brought up to 50 µL with milli-Q water. To each PCR reaction tube, an aliquot of *R. erythropolis* was added to provide a genomic template for the reaction. Denaturing of the template occurred at 98°C for 2 min followed by 37 cycles of a 10 sec denaturing at 98°C, 65°C for 20 sec, and extension at 72°C for 2 min and 45 sec. A final 2 min extension at 72°C to finish any incomplete extensions. PCR product was cleaned using the Thermo Gene-jet PCR purification kit and eluted with 50 µL of milli-Q water for future digestion and ligation. 1 µg of PCR product was then digested at 50°C for at least 1 h using 10 U of corresponding restriction enzyme, 5 µL corresponding NEB Buffer, and a final volume of 50 µL using milli-Q water. The restriction digestion was again cleaned using the Thermo purification kit and eluted using 40 µL of milli-Q water. Insertion of the genes into the expression vector pD441-CH with a C-terminal His-tag purchased originally from ATUM were performed using T4 Ligase and resulting plasmids were transformed into BL21(DE3) cells for protein isolation. Gene insertion was confirmed through sequencing. The primers for Mtr amplification and a full plasmid sequence can be found at **Appendix D, D.2**

4.5.7 *Small Batch Protein Isolation*

Small batch protein isolation was performed for each enzyme as follows: 50 mL cultures of BL21(DE3) cells containing the protein gene were grown to an OD600 of 0.4-0.6 and induced

using 1 mM IPTG. Cultures were grown for 6 hours at 37°C for 6 hours in aerobic conditions. Cells were then collected, resuspended in 1.5 mL bacterial lysis buffer (BLS, 0.5% and lysed using glass beads. Lysate was collected and small batch Ni-NTA isolations were performed as follows: 500 µL of Ni-NTA agarose beads were added to 2 mL centrifuge tubes and washed 3 times with 3 x column volume of milliQ water. Beads were then equilibrated with 3 x column volumes of binding buffer (50 mM Tris-HCl pH 8, 5 mM imidazole, 100 mM NaCl). Lysates were then added to the Ni-NTA beads and allowed to bind for ~10 minutes at 4°C with gentle agitation. Remaining lysate was pipetted off the column and Ni-NTA beads were washed 4 x with 3 x column volumes of wash buffer (50 mM Tris-HCl pH 8, 20 mM imidazole, 300 mM NaCl). Finally, bound protein was eluted using elution buffer (50 mM Tris-HCl pH 8, 300 mM imidazole, 50 mM NaCl) and proteins were dialyzed into PBS, pH 7.4 for future study.

Screening of enzyme activity was done utilizing procedures described previously.[23] Proteins were run on a native PAGE gel and soaked in a solution of TeO_3^{2-} and NADPH or Coomassie stain. Development of dark bands indicated enzymes capable of reducing TeO_3^{2-} to its zero-valent form.

4.5.8 *Mycothione Reductase Isolation*

A started culture of BL21(DE3) containing Mtr with a C-terminal His tag was grown overnight at 37°C and 225 RPM. The next day a 1.2 L LB growth flask supplemented with chloramphenicol and kanamycin was inoculated with the starter culture and grown until an OD_{600} ~0.5 at which time the culture was induced using 500 µM IPTG and grown at ~30°C overnight in aerobic conditions. The next day cells were collected, resuspended in 20 mM TEA-HCl, pH 7.6 and lysed on ice using sonication. Insoluble material was removed through centrifugation and the resulting lysate, which was red in color due to the presence of concentrated Mtr. Fast Protein Liquid Chromatography (FPLC) was then used for initial isolation of Mtr using a Ni-NTA column. Briefly, a HisTrap FF column was equilibrated with TEA-HCl, pH 7.6, 2.5 mM imidazole. Lysate was then loaded on the column for 30 minutes at 5 mL/min. Once lysate was loaded onto the column a gradient from 2.5 mM imidazole to 150 mM imidazole over 60 minutes at 5 mL/min.

Fractions were collected every minute and the presence of Mtr was indicated by a bright yellow color. These fractions were then combined and run on a HiTrap DEAE FF column to further isolate Mtr using a gradient from 0 to 500 mM NaCl over 60 min. Mtr, an enzyme with a pI of 5.1 was eluted from the DEAE column above 400 mM NaCl. Protein purification was checked using PAGE gel analysis.

4.5.9 *Kinetics Studies*

Reduction reactions were performed using 15 µg of Mtr in either 20 mM HEPES pH 7, 20 mM TEA-HCl pH 7.6, or PBS pH 7.4. Varying concentrations of K_2TeO_3, $HNaSeO_3$, or GSSG were added to the reaction and final volumes were brought to 1 mL. Reactions were then initiated by the addition of 200 µM NADPH. The degradation of NADPH corresponding with the decrease in absorbance at 340 nm was correlated to the activity of the enzyme ass a reaction velocity.

4.5.10 *Scanning Electron Microscopy*

Samples for SEM were prepared by the following: 15 µg of Mtr, and 1, 3, or 7 mM K_2TeO_3 brought to 1 mL PBS pH 7.4. Reactions initiated with an excess amount of NADPH and run overnight at room temperature. The next day, aliquots (4 µL) were deposited on C-coated Cu TEM grids and imaged using a JEOL JSM-6500-F Scanning Electron Microscope at an accelerating voltage of 15 kV.

4.5.11 *ICP-MS*

Samples for SEM were prepared by the following: 50 µg of Mtr, 500 µM NADPH, 1 mM K_2TeO_3 and either 1, 5, or 10 mM $HNaSeO_3$ brought to 1 mL PBS pH 7.4. Reactions were run overnight at room temperature. The next day, reactions were centrifuged to collect the particulate formed during the reduction. Particulate was washed with 3x1 mL milliQ water before the particulate was dissolved in 70% HNO_3. The solution was then diluted using 2% HNO_3 until concentrations of Te and Se fell within their standardized curves.

REFERENCES

5. Chalfie, M., Tu, Y., Euskirchen, G., Ward, W. W. & Prasher, D. C. Green fluorescent protein as a marker for gene expression. *Science* **263**, 802–805 (1994).
22. Fox, B. & Walsh, C. T. Mercuric reductase. Purification and characterization of a transposon-encoded flavoprotein containing an oxidation-reduction-active disulfide. *J. Biol. Chem.* **257**, 2498–2503 (1982).
23. Ni, T. W. *et al.* Progress toward clonable inorganic nanoparticles. *Nanoscale* **7**, 17320–17327 (2015).
24. Avazéri, C. *et al.* Tellurite reductase activity of nitrate reductase is responsible for the basal resistance of Escherichia coli to tellurite. *Microbiology* **143**, 1181–1189 (1997).
47. Freedman, Z., Zhu, C. & Barkay, T. Mercury Resistance and Mercuric Reductase Activities and Expression among Chemotrophic Thermophilic Aquificae. *Appl Environ Microbiol* **78**, 6568–6575 (2012).
56. Kelley, L. A., Mezulis, S., Yates, C. M., Wass, M. N. & Sternberg, M. J. E. The Phyre2 web portal for protein modeling, prediction and analysis. *Nat Protoc* **10**, 845–858 (2015).
79. Engst, S. & Miller, S. M. Rapid Reduction of Hg(II) by Mercuric Ion Reductase Does Not Require the Conserved C-Terminal Cysteine Pair Using HgBr2 as the Substrate. *Biochemistry* **37**, 11496–11507 (1998).
89. Zhou, S. *et al.* Reducing capacity and enzyme activity of chromate reductase in a ChrT-engineered strain. *Exp Ther Med* **14**, 2361–2366 (2017).
91. Castro, M. E., Molina, R., Díaz, W., Pichuantes, S. E. & Vásquez, C. C. The dihydrolipoamide dehydrogenase of Aeromonas caviae ST exhibits NADH-dependent tellurite reductase activity. *Biochemical and Biophysical Research Communications* **375**, 91–94 (2008).
92. Calderón, I. L. *et al.* Catalases Are NAD(P)H-Dependent Tellurite Reductases. *PLOS ONE* **1**, e70 (2006).
93. Sabaty, M., Avazeri, C., Pignol, D. & Vermeglio, A. Characterization of the Reduction of Selenate and Tellurite by Nitrate Reductases. *Appl. Environ. Microbiol.* **67**, 5122–5126 (2001).
99. Yang, Z., Lu, L., Kiely, C. J., Berger, B. W. & McIntosh, S. Single Enzyme Direct Biomineralization of CdSe and CdSe-CdS Core-Shell Quantum Dots. *ACS Appl. Mater. Interfaces* **9**, 13430–13439 (2017).
195. Nägeli (von), C. W. *Ueber oligodynamische Erscheinungen in lebenden Zellen*. (Druck von Zürcher & Furrer, 1893).
196. Hobman, J. L. & Crossman, L. C. Bacterial antimicrobial metal ion resistance. *Journal of Medical Microbiology* **64**, 471–497 (2015).
197. Seiler, C. & Berendonk, T. U. Heavy metal driven co-selection of antibiotic resistance in soil and water bodies impacted by agriculture and aquaculture. *Front. Microbiol.* **3**, (2012).
198. Zhang, X. *et al.* Acid mine drainage affects the diversity and metal resistance gene profile of sediment bacterial community along a river. *Chemosphere* **217**, 790–799 (2019).
199. Lima de Silva, A. A. *et al.* Heavy metal tolerance (Cr, Ag AND Hg) in bacteria isolated from sewage. *Braz J Microbiol* **43**, 1620–1631 (2012).

200. Puskárová, A. *et al.* Regulation of yodA encoding a novel cadmium-induced protein in Escherichia coli. *Microbiology (Reading, Engl.)* **148**, 3801–3811 (2002).
201. Choudhury, R. & Srivastava, S. Zinc resistance mechanisms in bacteria. *Current Science* **81**, 768–775 (2001).
202. Lal, D., Nayyar, N., Kohli, P. & Lal, R. Cupriavidus metallidurans: A Modern Alchemist. *Indian J Microbiol* **53**, 114–115 (2013).
203. Llorens, I. *et al.* Uranium Interaction with Two Multi-Resistant Environmental Bacteria: Cupriavidus metallidurans CH34 and Rhodopseudomonas palustris. *PLOS ONE* **7**, e51783 (2012).
204. Sarret, G. *et al.* Chemical forms of selenium in the metal-resistant bacterium Ralstonia metallidurans CH34 exposed to selenite and selenate. *Appl. Environ. Microbiol.* **71**, 2331–2337 (2005).
205. Arenas, F. A. *et al.* Isolation, identification and characterization of highly tellurite-resistant, tellurite-reducing bacteria from Antarctica. *Polar Science* **8**, 40–52 (2014).
206. Ollivier, P. R. L. *et al.* Volatilization and Precipitation of Tellurium by Aerobic, Tellurite-Resistant Marine Microbes. *Appl. Environ. Microbiol.* **74**, 7163–7173 (2008).
207. von Rozycki, T. & Nies, D. H. Cupriavidus metallidurans: evolution of a metal-resistant bacterium. *Antonie van Leeuwenhoek* **96**, 115 (2008).
208. Magos, L., Tuffery, A. A. & Clarkson, T. W. Volatilization of Mercury By Bacteria. *Br J Ind Med* **21**, 294–298 (1964).
209. Klaassen, C. D., Liu, J. & Choudhuri, S. Metallothionein: an intracellular protein to protect against cadmium toxicity. *Annu. Rev. Pharmacol. Toxicol.* **39**, 267–294 (1999).
210. Huang, P. C., Morris, S., Dinman, J., Pine, R. & Smith, B. Role of metallothionein in detoxification and tolerance to transition metals. *Experientia Suppl.* **52**, 439–446 (1987).
211. Schor-Fumbarov, T., Goldsbrough, P. B., Adam, Z. & Tel-Or, E. Characterization and expression of a metallothionein gene in the aquatic fern Azolla filiculoides under heavy metal stress. *Planta* **223**, 69–76 (2005).
212. Li, L.-S. *et al.* Type 1 metallothionein (ZjMT) is responsible for heavy metal tolerance in Ziziphus jujuba. *Biochemistry Moscow* **81**, 565–573 (2016).
213. Reddy, M. S., Prasanna, L., Marmeisse, R. & Fraissinet-Tachet, L. Differential expression of metallothioneins in response to heavy metals and their involvement in metal tolerance in the symbiotic basidiomycete Laccaria bicolor. *Microbiology (Reading, Engl.)* **160**, 2235–2242 (2014).
214. Ecker, D. J. *et al.* Yeast metallothionein function in metal ion detoxification. *J. Biol. Chem.* **261**, 16895–16900 (1986).
215. Yang, Z. *et al.* Biomanufacturing of CdS quantum dots. *Green Chemistry* **17**, 3775–3782 (2015).
216. Laczi, K. *et al.* Metabolic responses of Rhodococcus erythropolis PR4 grown on diesel oil and various hydrocarbons. *Appl. Microbiol. Biotechnol.* **99**, 9745–9759 (2015).
217. Singhi, D., Jain, A. & Srivastava, P. Localization of Low Copy Number Plasmid pRC4 in Replicating Rod and Non-Replicating Cocci Cells of Rhodococcus erythropolis PR4. *PLoS ONE* **11**, e0166491 (2016).
218. Bosello, M. *et al.* Structural Characterization of the Heterobactin Siderophores from Rhodococcus erythropolis PR4 and Elucidation of Their Biosynthetic Machinery. *J. Nat. Prod.* **76**, 2282–2290 (2013).

219. van der Geize, R. & Dijkhuizen, L. Harnessing the catabolic diversity of rhodococci for environmental and biotechnological applications. *Current Opinion in Microbiology* **7**, 255–261 (2004).
220. Larkin, M. J., Kulakov, L. A. & Allen, C. C. Biodegradation and Rhodococcus – masters of catabolic versatility. *Current Opinion in Biotechnology* **16**, 282–290 (2005).
221. Sekine, M. *et al.* Sequence analysis of three plasmids harboured in Rhodococcus erythropolis strain PR4. *Environmental Microbiology* **8**, 334–346 (2006).
222. Nies, D. H. Efflux-mediated heavy metal resistance in prokaryotes. *FEMS Microbiol. Rev.* **27**, 313–339 (2003).
223. Crupper, S. S., Worrell, V., Stewart, G. C. & Iandolo, J. J. Cloning and Expression of cadD, a New Cadmium Resistance Gene of Staphylococcus aureus. *Journal of Bacteriology* **181**, 4071–4075 (1999).
224. Arnesano, F., Banci, L., Bertini, I., Mangani, S. & Thompsett, A. R. A redox switch in CopC: An intriguing copper trafficking protein that binds copper(I) and copper(II) at different sites. *PNAS* **100**, 3814–3819 (2003).
225. Broth Microdilution MIC Test. in *Clinical Microbiology Procedures Handbook, 3rd Edition* (ed. Garcia, L. S.) 25–41 (American Society of Microbiology, 2010). doi:10.1128/9781555817435.ch5.2
226. European Committee for Antimicrobial Susceptibility Testing (EUCAST) of the European Society of Clinical Microbiology and Infectious Diseases (ESCMID). Determination of minimum inhibitory concentrations (MICs) of antibacterial agents by broth dilution. *Clinical Microbiology and Infection* **9**, ix–xv (2003).
227. Borghese, R., Borsetti, F., Foladori, P., Ziglio, G. & Zannoni, D. Effects of the Metalloid Oxyanion Tellurite (TeO32−) on Growth Characteristics of the Phototrophic Bacterium Rhodobacter capsulatus. *Appl. Environ. Microbiol.* **70**, 6595–6602 (2004).
228. Moore, M. D. & Kaplan, S. Identification of intrinsic high-level resistance to rare-earth oxides and oxyanions in members of the class Proteobacteria: characterization of tellurite, selenite, and rhodium sesquioxide reduction in Rhodobacter sphaeroides. *Journal of Bacteriology* **174**, 1505–1514 (1992).
229. Rathgeber, C., Yurkova, N., Stackebrandt, E., Beatty, J. T. & Yurkov, V. Isolation of Tellurite- and Selenite-Resistant Bacteria from Hydrothermal Vents of the Juan de Fuca Ridge in the Pacific Ocean. *Appl. Environ. Microbiol.* **68**, 4613–4622 (2002).
230. Green, R. M., Seth, A. & Connell, N. D. A Peptide Permease Mutant of Mycobacterium bovis BCG Resistant to the Toxic Peptides Glutathione and S-Nitrosoglutathione. *Infection and Immunity* **68**, 429–436 (2000).
231. Dayaram, Y. K., Talaue, M. T., Connell, N. D. & Venketaraman, V. Characterization of a Glutathione Metabolic Mutant of Mycobacterium tuberculosis and Its Resistance to Glutathione and Nitrosoglutathione. *J Bacteriol* **188**, 1364–1372 (2006).
232. Temme, K., Hill, R., Segall-Shapiro, T. H., Moser, F. & Voigt, C. A. Modular control of multiple pathways using engineered orthogonal T7 polymerases. *Nucleic Acids Res* **40**, 8773–8781 (2012).
233. Wilks, J. C. & Slonczewski, J. L. pH of the Cytoplasm and Periplasm of Escherichia coli: Rapid Measurement by Green Fluorescent Protein Fluorimetry. *J Bacteriol* **189**, 5601–5607 (2007).
234. Aoi, W. & Marunaka, Y. Importance of pH Homeostasis in Metabolic Health and Diseases: Crucial Role of Membrane Proton Transport. *Biomed Res Int* **2014**, (2014).

235. Fahey, R. C., Brown, W. C., Adams, W. B. & Worsham, M. B. Occurrence of glutathione in bacteria. *Journal of Bacteriology* **133**, 1126–1129 (1978).
236. Jozefczak, M., Remans, T., Vangronsveld, J. & Cuypers, A. Glutathione Is a Key Player in Metal-Induced Oxidative Stress Defenses. *Int J Mol Sci* **13**, 3145–3175 (2012).
237. Ottosson, L.-G. *et al.* Sulfate Assimilation Mediates Tellurite Reduction and Toxicity in Saccharomyces cerevisiae. *Eukaryot Cell* **9**, 1635–1647 (2010).
238. Rankin, D. W. H. CRC handbook of chemistry and physics, 89th edition, edited by David R. Lide. *Crystallography Reviews* **15**, 223–224 (2009).
239. Shannon, R. D. Revised effective ionic radii and systematic studies of interatomic distances in halides and chalcogenides. *Acta Cryst A* **32**, 751–767 (1976).
240. Chivers, T. & S. Laitinen, R. Tellurium: a maverick among the chalcogens. *Chemical Society Reviews* **44**, 1725–1739 (2015).
241. Kumar, A., Nartey, W., Shin, J., Manimekalai, M. S. S. & Grüber, G. Structural and mechanistic insights into Mycothiol Disulphide Reductase and the Mycoredoxin-1-alkylhydroperoxide reductase E assembly of Mycobacterium tuberculosis. *Biochimica et Biophysica Acta (BBA) - General Subjects* **1861**, 2354–2366 (2017).
242. Kumar, A., Manimekalai, M. S. S. & Grüber, G. Substrate-induced structural alterations of Mycobacterial mycothione reductase and critical residues involved. *FEBS Letters* **592**, 568–585 (2018).
243. Patel, M. P. & Blanchard, J. S. Expression, Purification, and Characterization of Mycobacterium tuberculosis Mycothione Reductase. *Biochemistry* **38**, 11827–11833 (1999).
244. Newton, G. L., Buchmeier, N. & Fahey, R. C. Biosynthesis and Functions of Mycothiol, the Unique Protective Thiol of Actinobacteria. *Microbiol. Mol. Biol. Rev.* **72**, 471–494 (2008).
245. Newton, G. L. & Fahey, R. C. Mycothiol biochemistry. *Arch Microbiol* **178**, 388–394 (2002).
246. Sharma, S. V., Van Laer, K., Messens, J. & Hamilton, C. J. Thiol Redox and pKa Properties of Mycothiol, the Predominant Low-Molecular-Weight Thiol Cofactor in the Actinomycetes. *ChemBioChem* **17**, 1689–1692 (2016).
247. Mills, S. J., Dunstan, M. A. & Christy, A. G. YCu(TeO3)2(NO3)(H2O)3: a novel layered tellurite. *Acta Crystallogr E Crystallogr Commun* **72**, 1138–1142 (2016).
248. Wicke, H. & Meleshyn, A. Microhydration of the Selenite Dianion: A Theoretical Study of Structures, Hydration Energies, and Electronic Stabilities of SeO32−(H2O)n (n = 0−6, 9) Clusters. *J. Phys. Chem. A* **114**, 8948–8960 (2010).
249. Saveliev, S. V. *et al.* Mass spectrometry compatible surfactant for optimized in-gel protein digestion. *Anal. Chem.* **85**, 907–914 (2013).
250. Scopes, R. K. Measurement of protein by spectrophotometry at 205 nm. *Analytical Biochemistry* **59**, 277–282 (1974).
251. Keller, A., Nesvizhskii, A. I., Kolker, E. & Aebersold, R. Empirical Statistical Model To Estimate the Accuracy of Peptide Identifications Made by MS/MS and Database Search. *Anal. Chem.* **74**, 5383–5392 (2002).
252. Searle, B. C., Turner, M. & Nesvizhskii, A. I. Improving sensitivity by probabilistically combining results from multiple MS/MS search methodologies. *J. Proteome Res.* **7**, 245–253 (2008).
253. Käll, L., Storey, J. D., MacCoss, M. J. & Noble, W. S. Assigning significance to peptides identified by tandem mass spectrometry using decoy databases. *J. Proteome Res.* **7**, 29–34 (2008).

254. Nesvizhskii, A. I., Keller, A., Kolker, E. & Aebersold, R. A statistical model for identifying proteins by tandem mass spectrometry. *Anal. Chem.* **75**, 4646–4658 (2003).

BIBLIOGRAPHY

1. Gerlach, J. von. *Mikroskopische Studien aus dem Gebeite der menschlichen Morphologie*. (Ferdinand Enke, 1858).
2. Titford, M. Progress in the Development of Microscopical Techniques for Diagnostic Pathology. *Journal of Histotechnology* **32**, 9–19 (2009).
3. Abbe, E. Beiträge zur Theorie des Mikroskops und der mikroskopischen Wahrnehmung. *Archiv f. mikrosk. Anatomie* **9**, 413–418 (1873).
4. Adams, S. R. *et al.* New Biarsenical Ligands and Tetracysteine Motifs for Protein Labeling in Vitro and in Vivo: Synthesis and Biological Applications. *J. Am. Chem. Soc.* **124**, 6063–6076 (2002).
5. Chalfie, M., Tu, Y., Euskirchen, G., Ward, W. W. & Prasher, D. C. Green fluorescent protein as a marker for gene expression. *Science* **263**, 802–805 (1994).
6. Moerner, W. E. & Ambrose, W. P. Finding a single molecule in a haystack: laser spectroscopy of solids from (square root of)N to N=1. in *Optical Methods for Ultrasensitive Detection and Analysis: Techniques and Applications* **1435**, 244–251 (International Society for Optics and Photonics, 1991).
7. Dickson, R. M. *et al.* Single Molecules Solvated in Pores of Polyacrylamide Gels. *Molecular Crystals and Liquid Crystals Science and Technology. Section A. Molecular Crystals and Liquid Crystals* **291**, 31–39 (1996).
8. Dickson, R. M., Norris, D. J., Tzeng, Y.-L. & Moerner, W. E. Three-Dimensional Imaging of Single Molecules Solvated in Pores of Poly(acrylamide) Gels. *Science* **274**, 966–968 (1996).
9. Hänninen, P. E., Lehtelä, L. & Hell, S. W. Two- and multiphoton excitation of conjugate-dyes using a continuous wave laser. *Optics Communications* **130**, 29–33 (1996).
10. Hell, S. & Wijnaendts-van-Resandt, R. W. The Application Of Polarized Confocal Microscopy For The Size Measurement Of Resist Structures. in *Optical Storage and Scanning Technology* **1139**, 92–98 (International Society for Optics and Photonics, 1989).
11. Harootunian, A., Betzig, E., Isaacson, M. & Lewis, A. Super-resolution fluorescence near-field scanning optical microscopy. *Appl. Phys. Lett.* **49**, 674–676 (1986).
12. Betzig, E., Lewis, A., Harootunian, A., Isaacson, M. & Kratschmer, E. Near Field Scanning Optical Microscopy (NSOM): Development and Biophysical Applications. *Biophysical Journal* **49**, 269–279 (1986).
13. Betzig, E., Harootunian, A., Lewis, A. & Isaacson, M. Near-field diffraction by a slit: implications for superresolution microscopy. *Appl. Opt., AO* **25**, 1890–1900 (1986).
14. Freundlich, M. M. Origin of the Electron Microscope. *Science* **142**, 185–188 (1963).
15. Porter, K. R., Claude, A. & Fullam, E. F. A Study of Tissue Culture Cells by Electron Microscopy: Methods and Preliminary Observations. *Journal of Experimental Medicine* **81**, 233–246 (1945).
16. Lysova, I. *et al.* ReAsH/tetracystein-based correlative light-electron microscopy for HIV-1 imaging during the early stages of infection. *Methods Appl. Fluoresc.* **6**, 045001 (2018).
17. Novikoff, P. M. & Novikoff, A. B. Peroxisomes in Absorptive Cells of Mammalian Small Intestine. *The Journal of Cell Biology* **53**, 532–560 (1972).

18. Beard, M. E. Distribution of Peroxisomes (Microbodies) in the Nephron of the Rat: A Cytochemical Study. *The Journal of Cell Biology* **42**, 501–518 (1969).
19. Antoine, J.-C. Plasma Membrane and Internalized Immunoglobulins of Lymph Node Cells Studied with Conjugates of Antibody or its FAB Fragments with Horseradish Peroxidase. *The Journal of Cell Biology* **63**, 12–23 (1974).
20. Shu, X. *et al.* A Genetically Encoded Tag for Correlated Light and Electron Microscopy of Intact Cells, Tissues, and Organisms. *PLOS Biology* **9**, e1001041 (2011).
21. Martell, J. D. *et al.* Engineered ascorbate peroxidase as a genetically-encoded reporter for electron microscopy. *Nat Biotechnol* **30**, 1143–1148 (2012).
22. Fox, B. & Walsh, C. T. Mercuric reductase. Purification and characterization of a transposon-encoded flavoprotein containing an oxidation-reduction-active disulfide. *J. Biol. Chem.* **257**, 2498–2503 (1982).
23. Ni, T. W. *et al.* Progress toward clonable inorganic nanoparticles. *Nanoscale* **7**, 17320–17327 (2015).
24. Avazéri, C. *et al.* Tellurite reductase activity of nitrate reductase is responsible for the basal resistance of Escherichia coli to tellurite. *Microbiology* **143**, 1181–1189 (1997).
25. Yamamura, S. & Amachi, S. Microbiology of inorganic arsenic: From metabolism to bioremediation. *Journal of Bioscience and Bioengineering* **118**, 1–9 (2014).
26. Tapiero, H., Townsend, D. M. & Tew, K. D. The antioxidant role of selenium and seleno-compounds. *Biomed Pharmacother* **57**, 134–144 (2003).
27. Turner, R. J., Weiner, J. H. & Taylor, D. E. Selenium metabolism in Escherichia coli. *Biometals* **11**, 223–227 (1998).
28. Harrison, P. M. The structure and function of ferritin. *Biochemical Education* **14**, 154–162 (1986).
29. Kolinko, I. *et al.* Biosynthesis of magnetic nanostructures in a foreign organism by transfer of bacterial magnetosome gene clusters. *Nature Nanotechnology* **9**, 193–197 (2014).
30. Müller, W. E. G. *et al.* Silicateins, the major biosilica forming enzymes present in demosponges: Protein analysis and phylogenetic relationship. *Gene* **395**, 62–71 (2007).
31. Carter, C. J. *et al.* In vitro selection of RNA sequences capable of mediating the formation of iron oxide nanoparticles. *J. Mater. Chem.* **19**, 8320–8326 (2009).
32. Slocik, J. M., Kuang, Z., Knecht, M. R. & Naik, R. R. Optical Modulation of Azobenzene-Modified Peptide for Gold Surface Binding. *ChemPhysChem* **17**, 3252–3259 (2016).
33. Yeh, H.-C., Sharma, J., Han, J. J., Martinez, J. S. & Werner, J. H. A DNA−Silver Nanocluster Probe That Fluoresces upon Hybridization. *Nano Lett.* **10**, 3106–3110 (2010).
34. Klug, M. T. *et al.* Mediated Growth of Zinc Chalcogen Shells on Gold Nanoparticles by Free-Base Amino Acids. *Chem. Mater.* **29**, 6993–7001 (2017).
35. Wang, Q., Mercogliano, C. P. & Löwe, J. A Ferritin-Based Label for Cellular Electron Cryotomography. *Structure* **19**, 147–154 (2011).
36. Castruita, M. *et al.* Overexpression and Characterization of an Iron Storage and DNA-Binding Dps Protein from Trichodesmium erythraeum. *Appl. Environ. Microbiol.* **72**, 2918–2924 (2006).
37. Reed, J. K. Studies on the kinetic mechanism of lipoamide dehydrogenase from rat liver mitochondria. *J. Biol. Chem.* **248**, 4834–4839 (1973).
38. Staicu, L. C. *et al.* Pseudomonas moraviensis subsp. stanleyae, a bacterial endophyte of hyperaccumulator Stanleya pinnata, is capable of efficient selenite reduction to elemental selenium under aerobic conditions. *J. Appl. Microbiol.* **119**, 400–410 (2015).

39. Fernández-Llamosas, H., Castro, L., Blázquez, M. L., Díaz, E. & Carmona, M. Speeding up bioproduction of selenium nanoparticles by using Vibrio natriegens as microbial factory. *Sci Rep* **7**, 16046 (2017).
40. Fernández-Llamosas, H., Castro, L., Blázquez, M. L., Díaz, E. & Carmona, M. Biosynthesis of selenium nanoparticles by Azoarcus sp. CIB. *Microb. Cell Fact.* **15**, 109 (2016).
41. Wang, Y. *et al.* Selenite Reduction and the Biogenesis of Selenium Nanoparticles by Alcaligenes faecalis Se03 Isolated from the Gut of Monochamus alternatus (Coleoptera: Cerambycidae). *Int J Mol Sci* **19**, (2018).
42. Bebien, M., Chauvin, J.-P., Adriano, J.-M., Grosse, S. & Verméglio, A. Effect of Selenite on Growth and Protein Synthesis in the Phototrophic Bacterium Rhodobacter sphaeroides. *Appl. Environ. Microbiol.* **67**, 4440–4447 (2001).
43. Weiss, K. F., Ayres, J. C. & Kraft, A. A. Inhibitory Action of Selenite on Escherichia coli, Proteus vulgaris, and Salmonella thompson. *Journal of Bacteriology* **90**, 857–862 (1965).
44. Lian, P. *et al.* X-ray Structure of a Hg2+ Complex of Mercuric Reductase (MerA) and Quantum Mechanical/Molecular Mechanical Study of Hg2+ Transfer between the C-Terminal and Buried Catalytic Site Cysteine Pairs. *Biochemistry* **53**, 7211–7222 (2014).
45. Fox, B. S. & Walsh, C. T. Mercuric reductase: homology to glutathione reductase and lipoamide dehydrogenase. Iodoacetamide alkylation and sequence of the active site peptide. *Biochemistry* **22**, 4082–4088 (1983).
46. Li, X. & Krumholz, L. R. Thioredoxin Is Involved in U(VI) and Cr(VI) Reduction in Desulfovibrio desulfuricans G20. *Journal of Bacteriology* **191**, 4924–4933 (2009).
47. Freedman, Z., Zhu, C. & Barkay, T. Mercury Resistance and Mercuric Reductase Activities and Expression among Chemotrophic Thermophilic Aquificae. *Appl Environ Microbiol* **78**, 6568–6575 (2012).
48. Pugin, B. *et al.* Glutathione Reductase-Mediated Synthesis of Tellurium-Containing Nanostructures Exhibiting Antibacterial Properties. *Appl Environ Microbiol* **80**, 7061–7070 (2014).
49. Otwell, A. E. *et al.* Identification of proteins capable of metal reduction from the proteome of the Gram-positive bacterium Desulfotomaculum reducens MI-1 using an NADH-based activity assay. *Environ. Microbiol.* **17**, 1977–1990 (2015).
50. Scott, D., Toney, M. & Muzikár, M. Harnessing the mechanism of glutathione reductase for synthesis of active site bound metallic nanoparticles and electrical connection to electrodes. *J. Am. Chem. Soc.* **130**, 865–874 (2008).
51. Wang, Z. *et al.* De novo assembly and characterization of root transcriptome using Illumina paired-end sequencing and development of cSSR markers in sweet potato (Ipomoea batatas). *BMC Genomics* **11**, 726 (2010).
52. Arscott, L. D., Gromer, S., Schirmer, R. H., Becker, K. & Williams, C. H. The mechanism of thioredoxin reductase from human placenta is similar to the mechanisms of lipoamide dehydrogenase and glutathione reductase and is distinct from the mechanism of thioredoxin reductase from Escherichia coli. *Proc. Natl. Acad. Sci. U.S.A.* **94**, 3621–3626 (1997).
53. Mittl, P. R. & Schulz, G. E. Structure of glutathione reductase from Escherichia coli at 1.86 A resolution: comparison with the enzyme from human erythrocytes. *Protein Sci* **3**, 799–809 (1994).
54. Pai, E. F. & Schulz, G. E. The catalytic mechanism of glutathione reductase as derived from x-ray diffraction analyses of reaction intermediates. *J. Biol. Chem.* **258**, 1752–1757 (1983).

55. Ganther, H. E. Reduction of the selenotrisulfide derivative of glutathione to a persulfide analog by gluthathione reductase. *Biochemistry* **10**, 4089–4098 (1971).
56. Kelley, L. A., Mezulis, S., Yates, C. M., Wass, M. N. & Sternberg, M. J. E. The Phyre2 web portal for protein modeling, prediction and analysis. *Nat Protoc* **10**, 845–858 (2015).
57. Dowd, J. E. & Riggs, D. S. A Comparison of Estimates of Michaelis-Menten Kinetic Constants from Various Linear Transformations. *J. Biol. Chem.* **240**, 863–869 (1965).
58. Choi, B., Rempala, G. A. & Kim, J. K. Beyond the Michaelis-Menten equation: Accurate and efficient estimation of enzyme kinetic parameters. *Sci Rep* **7**, (2017).
59. Carrillo, N., Ceccarelli, E. & Roveri, O. Usefulness of kinetic enzyme parameters in biotechnological practice. *Biotechnol. Genet. Eng. Rev.* **27**, 367–382 (2010).
60. Yu, J. & Zhou, C.-Z. Crystal structure of glutathione reductase Glr1 from the yeast Saccharomyces cerevisiae. *Proteins* **68**, 972–979 (2007).
61. Kice, J. L., Lee, T. W. S. & Pan, S.-T. Mechanism of the reaction of thiols with selenite. *J. Am. Chem. Soc.* **102**, 4448–4455 (1980).
62. Forman, H. J., Zhang, H. & Rinna, A. Glutathione: Overview of its protective roles, measurement, and biosynthesis. *Mol Aspects Med* **30**, 1–12 (2009).
63. Hunter, P. A toxic brew we cannot live without. Micronutrients give insights into the interplay between geochemistry and evolutionary biology. *EMBO Rep.* **9**, 15–18 (2008).
64. Ramamurthy, C. *et al.* Green synthesis and characterization of selenium nanoparticles and its augmented cytotoxicity with doxorubicin on cancer cells. *Bioprocess Biosyst Eng* **36**, 1131–1139 (2013).
65. Nath, S., Ghosh, S. K., Panigahi, S., Thundat, T. & Pal, T. Synthesis of selenium nanoparticle and its photocatalytic application for decolorization of methylene blue under UV irradiation. *Langmuir* **20**, 7880–7883 (2004).
66. Grek, C. L., Zhang, J., Manevich, Y., Townsend, D. M. & Tew, K. D. Causes and consequences of cysteine S-glutathionylation. *J. Biol. Chem.* **288**, 26497–26504 (2013).
67. Sullivan, D. M., Wehr, N. B., Fergusson, M. M., Levine, R. L. & Finkel, T. Identification of oxidant-sensitive proteins: TNF-alpha induces protein glutathiolation. *Biochemistry* **39**, 11121–11128 (2000).
68. Townsend, D. M. *et al.* A glutathione S-transferase pi-activated prodrug causes kinase activation concurrent with S-glutathionylation of proteins. *Mol. Pharmacol.* **69**, 501–508 (2006).
69. Fiaschi, T. *et al.* Redox regulation of beta-actin during integrin-mediated cell adhesion. *J. Biol. Chem.* **281**, 22983–22991 (2006).
70. Hill, B. G. & Bhatnagar, A. Protein S-glutathiolation: redox-sensitive regulation of protein function. *J. Mol. Cell. Cardiol.* **52**, 559–567 (2012).
71. Humphries, K. M., Juliano, C. & Taylor, S. S. Regulation of cAMP-dependent protein kinase activity by glutathionylation. *J. Biol. Chem.* **277**, 43505–43511 (2002).
72. Townsend, D. M. *et al.* Nitrosative stress-induced s-glutathionylation of protein disulfide isomerase leads to activation of the unfolded protein response. *Cancer Res.* **69**, 7626–7634 (2009).
73. Stepovaya, E. A. *et al.* The role of oxidative protein modification and the glutathione system in modulation of the redox status of breast epithelial cells. *Biochem. Moscow Suppl. Ser. B* **10**, 235–239 (2016).
74. Blake, R. C. *et al.* Chemical transformation of toxic metals by a Pseudomonas strain from a toxic waste site. *Environmental Toxicology and Chemistry* **12**, 1365–1376 (1993).

75. Hunter, W. J. & Manter, D. K. Reduction of Selenite to Elemental Red Selenium by Pseudomonas sp. Strain CA5. *Curr Microbiol* **58**, 493–498 (2009).
76. Lortie, L., Gould, W. D., Rajan, S., McCready, R. G. L. & Cheng, K.-J. Reduction of Selenate and Selenite to Elemental Selenium by a Pseudomonas stutzeri Isolate. *Appl. Environ. Microbiol.* **58**, 4042–4044 (1992).
77. Avendaño, R. *et al.* Production of selenium nanoparticles in *Pseudomonas putida* KT2440. *Scientific Reports* **6**, 37155 (2016).
78. Mackenzie, E. L., Iwasaki, K. & Tsuji, Y. Intracellular Iron Transport and Storage: From Molecular Mechanisms to Health Implications. *Antioxid Redox Signal* **10**, 997–1030 (2008).
79. Engst, S. & Miller, S. M. Rapid Reduction of Hg(II) by Mercuric Ion Reductase Does Not Require the Conserved C-Terminal Cysteine Pair Using HgBr2 as the Substrate. *Biochemistry* **37**, 11496–11507 (1998).
80. Holmes, J. D. *et al.* Energy-dispersive X-ray analysis of the extracellular cadmium sulfide crystallites of Klebsiella aerogenes. *Arch. Microbiol.* **163**, 143–147 (1995).
81. Cunningham, D. P. & Lundie, L. L. Precipitation of cadmium by Clostridium thermoaceticum. *Appl. Environ. Microbiol.* **59**, 7–14 (1993).
82. Klaus-Joerger, T., Joerger, R., Olsson, E. & Granqvist, C.-G. Bacteria as workers in the living factory: metal-accumulating bacteria and their potential for materials science. *Trends in Biotechnology* **19**, 15–20 (2001).
83. Reduction of Selenite and Detoxification of Elemental Selenium by the Phototrophic BacteriumRhodospirillum rubrum | Applied and Environmental Microbiology. Available at: https://aem.asm.org/content/65/11/4734.long. (Accessed: 14th December 2018)
84. Yong, P., Rowson, N. A., Farr, J. P. G., Harris, I. R. & Macaskie, L. E. Bioreduction and biocrystallization of palladium by Desulfovibrio desulfuricans NCIMB 8307. *Biotechnology and Bioengineering* **80**, 369–379 (2002).
85. Sweeney, R. Y. *et al.* Bacterial Biosynthesis of Cadmium Sulfide Nanocrystals. *Chemistry & Biology* **11**, 1553–1559 (2004).
86. Bai, H. J., Zhang, Z. M., Guo, Y. & Yang, G. E. Biosynthesis of cadmium sulfide nanoparticles by photosynthetic bacteria Rhodopseudomonas palustris. *Colloids and Surfaces B: Biointerfaces* **70**, 142–146 (2009).
87. Ovais, M. *et al.* Biosynthesis of Metal Nanoparticles via Microbial Enzymes: A Mechanistic Approach. *International Journal of Molecular Sciences* **19**, 4100 (2018).
88. Singh, P. *et al.* Biosynthesis, characterization, and antimicrobial applications of silver nanoparticles. *Int J Nanomedicine* **10**, 2567–2577 (2015).
89. Zhou, S. *et al.* Reducing capacity and enzyme activity of chromate reductase in a ChrT-engineered strain. *Exp Ther Med* **14**, 2361–2366 (2017).
90. Chasteen, T. G., Fuentes, D. E., Tantaleán, J. C. & Vásquez, C. C. Tellurite: history, oxidative stress, and molecular mechanisms of resistance. *FEMS Microbiol Rev* **33**, 820–832 (2009).
91. Castro, M. E., Molina, R., Díaz, W., Pichuantes, S. E. & Vásquez, C. C. The dihydrolipoamide dehydrogenase of Aeromonas caviae ST exhibits NADH-dependent tellurite reductase activity. *Biochemical and Biophysical Research Communications* **375**, 91–94 (2008).
92. Calderón, I. L. *et al.* Catalases Are NAD(P)H-Dependent Tellurite Reductases. *PLOS ONE* **1**, e70 (2006).

93. Sabaty, M., Avazeri, C., Pignol, D. & Vermeglio, A. Characterization of the Reduction of Selenate and Tellurite by Nitrate Reductases. *Appl. Environ. Microbiol.* **67**, 5122–5126 (2001).
94. Curran, C. D. *et al.* Direct Single-Enzyme Biomineralization of Catalytically Active Ceria and Ceria–Zirconia Nanocrystals. *ACS Nano* **11**, 3337–3346 (2017).
95. Chowdhury, T., Sarkar, M., Chaudhuri, B., Chattopadhyay, B. & Halder, U. C. Participatory role of zinc in structural and functional characterization of bioremediase: a unique thermostable microbial silica leaching protein. *J Biol Inorg Chem* **20**, 791–803 (2015).
96. Dunleavy, R., Lu, L., Kiely, C. J., McIntosh, S. & Berger, B. W. Single-enzyme biomineralization of cadmium sulfide nanocrystals with controlled optical properties. *PNAS* **113**, 5275–5280 (2016).
97. Spangler, L. C. *et al.* Enzymatic biomineralization of biocompatible CuInS2, (CuInZn)S2 and CuInS2/ZnS core/shell nanocrystals for bioimaging. *Nanoscale* **9**, 9340–9351 (2017).
98. Spangler, L. C., Lu, L., Kiely, C. J., Berger, B. W. & McIntosh, S. Biomineralization of PbS and PbS–CdS core–shell nanocrystals and their application in quantum dot sensitized solar cells. *J. Mater. Chem. A* **4**, 6107–6115 (2016).
99. Yang, Z., Lu, L., Kiely, C. J., Berger, B. W. & McIntosh, S. Single Enzyme Direct Biomineralization of CdSe and CdSe-CdS Core-Shell Quantum Dots. *ACS Appl. Mater. Interfaces* **9**, 13430–13439 (2017).
100. Nemeth, R., Neubert, M., Butz, Z. J., Ni, T. W. & Ackerson, C. J. Metalloid Reductase of Pseudomonas moravenis Stanleyae Conveys Nanoparticle Mediated Metalloid Tolerance. *ACS Omega* **3**, 14902–14909 (2018).
101. Flynn, C. E. *et al.* Synthesis and organization of nanoscale II–VI semiconductor materials using evolved peptide specificity and viral capsid assembly. *J. Mater. Chem.* **13**, 2414–2421 (2003).
102. Dickerson, M. B. *et al.* Identification and Design of Peptides for the Rapid, High-Yield Formation of Nanoparticulate TiO2 from Aqueous Solutions at Room Temperature. *Chem. Mater.* **20**, 1578–1584 (2008).
103. Dickerson, M. B., Naik, R. R., Stone, M. O., Cai, Y. & Sandhage, K. H. Identification of peptides that promote the rapid precipitation of germania nanoparticle networks via use of a peptide display library. *Chem. Commun.* **0**, 1776–1777 (2004).
104. Reiss, B. D. *et al.* Biological Routes to Metal Alloy Ferromagnetic Nanostructures. *Nano Lett.* **4**, 1127–1132 (2004).
105. Naik, R. R. *et al.* Peptide Templates for Nanoparticle Synthesis Derived from Polymerase Chain Reaction-Driven Phage Display. *Advanced Functional Materials* **14**, 25–30 (2004).
106. Li, C., Botsaris, G. D. & Kaplan, D. L. Selective in Vitro Effect of Peptides on Calcium Carbonate Crystallization. *Crystal Growth & Design* **2**, 387–393 (2002).
107. Lee, S.-W., Mao, C., Flynn, C. E. & Belcher, A. M. Ordering of Quantum Dots Using Genetically Engineered Viruses. *Science* **296**, 892–895 (2002).
108. Oh, D. *et al.* Biologically enhanced cathode design for improved capacity and cycle life for lithium-oxygen batteries. *Nature Communications* **4**, 2756 (2013).
109. Courchesne, N.-M. D. *et al.* Assembly of a bacteriophage-based template for the organization of materials into nanoporous networks. *Adv Mater* **26**, 3398–3404 (2014).
110. Oh, D. *et al.* M13 Virus-Directed Synthesis of Nanostructured Metal Oxides for Lithium–Oxygen Batteries. *Nano Lett.* **14**, 4837–4845 (2014).

111. Ahmad, G. *et al.* Rapid Bioenabled Formation of Ferroelectric BaTiO3 at Room Temperature from an Aqueous Salt Solution at Near Neutral pH. *J. Am. Chem. Soc.* **130**, 4–5 (2008).
112. Bassindale, A. R., Codina-Barrios, A., Frascione, N. & Taylor, P. G. An improved phage display methodology for inorganic nanoparticle fabrication. *Chem. Commun.* **0**, 2956–2958 (2007).
113. Carter, C. J., Ackerson, C. J. & Feldheim, D. L. Unusual Reactivity of a Silver Mineralizing Peptide. *ACS Nano* **4**, 3883–3888 (2010).
114. Birrell, G. B., Hedberg, K. K. & Griffith, O. H. Pitfalls of immunogold labeling: analysis by light microscopy, transmission electron microscopy, and photoelectron microscopy. *J Histochem Cytochem.* **35**, 843–853 (1987).
115. McLellan, T. Electrophoresis buffers for polyacrylamide gels at various pH. *Analytical Biochemistry* **126**, 94–99 (1982).
116. Singh, B. R. *Infrared analysis of peptides and proteins*. (American Chemical Society, 2000).
117. Barth, A. Infrared spectroscopy of proteins. *Biochimica et Biophysica Acta (BBA) - Bioenergetics* **1767**, 1073–1101 (2007).
118. Talari, A. C. S., Movasaghi, Z., Rehman, S. & Rehman, I. ur. Raman Spectroscopy of Biological Tissues. *Applied Spectroscopy Reviews* **50**, 46–111 (2015).
119. DiGuiseppi, D. & Schweitzer-Stenner, R. Probing conformational propensities of histidine in different protonation states of the unblocked glycyl-histidyl-glycine peptide by vibrational and NMR spectroscopy. *Journal of Raman Spectroscopy* **47**, 1063–1072 (2016).
120. Takeuchi, H. Raman structural markers of tryptophan and histidine side chains in proteins. *Biopolymers* **72**, 305–317 (2003).
121. Zhu, G., Zhu, X., Fan, Q. & Wan, X. Raman spectra of amino acids and their aqueous solutions. *Spectrochim Acta A Mol Biomol Spectrosc* **78**, 1187–1195 (2011).
122. Toyama, A., Ono, K., Hashimoto, S. & Takeuchi, H. Raman Spectra and Normal Coordinate Analysis of the N1−H and N3−H Tautomers of 4-Methylimidazole: Vibrational Modes of Histidine Tautomer Markers. *J. Phys. Chem. A* **106**, 3403–3412 (2002).
123. Hasegawa, K., Ono, T. & Noguchi, T. Vibrational Spectra and Ab Initio DFT Calculations of 4-Methylimidazole and Its Different Protonation Forms: Infrared and Raman Markers of the Protonation State of a Histidine Side Chain. *J. Phys. Chem. B* **104**, 4253–4265 (2000).
124. Rust, M. J., Bates, M. & Zhuang, X. Sub-diffraction-limit imaging by stochastic optical reconstruction microscopy (STORM). *Nature Methods* **3**, 793–796 (2006).
125. Sengupta, P., Van Engelenburg, S. B. & Lippincott-Schwartz, J. Superresolution imaging of biological systems using photoactivated localization microscopy. *Chem Rev* **114**, 3189–3202 (2014).
126. de Matos, L. L., Trufelli, D. C., de Matos, M. G. L. & da Silva Pinhal, M. A. Immunohistochemistry as an Important Tool in Biomarkers Detection and Clinical Practice. *Biomark Insights* **5**, 9–20 (2010).
127. Bolognesi, M. M. *et al.* Multiplex Staining by Sequential Immunostaining and Antibody Removal on Routine Tissue Sections. *J Histochem Cytochem* **65**, 431–444 (2017).
128. Kim, S.-W., Roh, J. & Park, C.-S. Immunohistochemistry for Pathologists: Protocols, Pitfalls, and Tips. *J Pathol Transl Med* **50**, 411–418 (2016).
129. Gustafsson, M. G. L. Nonlinear structured-illumination microscopy: Wide-field fluorescence imaging with theoretically unlimited resolution. *PNAS* **102**, 13081–13086 (2005).

130. Litman, R. B. & Barrnett, R. J. The mechanism of the fixation of tissue components by osmium tetroxide via hydrogen bonding. *Journal of Ultrastructure Research* **38**, 63–86 (1972).
131. Scarff, C. A., Fuller, M. J. G., Thompson, R. F. & Iadaza, M. G. Variations on Negative Stain Electron Microscopy Methods: Tools for Tackling Challenging Systems. *J Vis Exp* (2018). doi:10.3791/57199
132. Booth, D. S., Avila-Sakar, A. & Cheng, Y. Visualizing Proteins and Macromolecular Complexes by Negative Stain EM: from Grid Preparation to Image Acquisition. *J Vis Exp* (2011). doi:10.3791/3227
133. Hopwood, D. Fixatives and fixation: a review. *Histochem J* **1**, 323–360 (1969).
134. Mundkur, B. Problems of fixation and staining in microbial cytology. *Trans N Y Acad Sci* **24**, 30–35 (1961).
135. Wolman, M. Problems of Fixation in Cytology, Histology, and Histochemistry. in *International Review of Cytology* (eds. Bourne, G. H. & Danielli, J. F.) **4**, 79–102 (Academic Press, 1955).
136. Bullock, G. R. The current status of fixation for electron microscopy: A review. *Journal of Microscopy* **133**, 1–15 (1984).
137. Boassa, D. *et al.* Split-miniSOG for detecting and localizing intracellular protein-protein interactions: application to correlated light and electron microscopy. *bioRxiv* 423566 (2018). doi:10.1101/423566
138. Han, Y. *et al.* Directed evolution of split APEX peroxidase. *bioRxiv* (2018). doi:10.1101/452888
139. Han, Y. *et al.* Directed Evolution of Split APEX2 Peroxidase. *ACS Chem. Biol.* **14**, 619–635 (2019).
140. Lam, S. S. *et al.* Directed evolution of APEX2 for electron microscopy and proteomics. *Nat Methods* **12**, 51–54 (2015).
141. Thach, R. E. & Thach, S. S. Damage to Biological Samples Caused by the Electron Beam during Electron Microscopy. *Biophysical Journal* **11**, 204–210 (1971).
142. Blaauwen, T. D., Buddelmeijer, N., Aarsman, M. E. G., Hameete, C. M. & Nanninga, N. Timing of FtsZ Assembly in Escherichia coli. *J. Bacteriol.* **181**, 5167–5175 (1999).
143. Ma, X., Ehrhardt, D. W. & Margolin, W. Colocalization of cell division proteins FtsZ and FtsA to cytoskeletal structures in living Escherichia coli cells by using green fluorescent protein. *PNAS* **93**, 12998–13003 (1996).
144. Haydon, D. J. *et al.* An Inhibitor of FtsZ with Potent and Selective Anti-Staphylococcal Activity. *Science* **321**, 1673–1675 (2008).
145. Mathew, B. *et al.* Screening and Development of New Inhibitors of FtsZ from M. Tuberculosis. *PLOS ONE* **11**, e0164100 (2016).
146. Stokes, N. R. *et al.* An Improved Small-Molecule Inhibitor of FtsZ with Superior In Vitro Potency, Drug-Like Properties, and In Vivo Efficacy. *Antimicrobial Agents and Chemotherapy* **57**, 317–325 (2013).
147. Domadia, P., Swarup, S., Bhunia, A., Sivaraman, J. & Dasgupta, D. Inhibition of bacterial cell division protein FtsZ by cinnamaldehyde. *Biochem. Pharmacol.* **74**, 831–840 (2007).
148. Pazos, M. *et al.* FtsZ Placement in Nucleoid-Free Bacteria. *PLOS ONE* **9**, e91984 (2014).
149. Chen, Y., Anderson, D. E., Rajagopalan, M. & Erickson, H. P. Assembly Dynamics of Mycobacterium tuberculosis FtsZ. *J. Biol. Chem.* **282**, 27736–27743 (2007).

150. Srinivasan, R. & Ajitkumar, P. Bacterial cell division protein FtsZ is stable against degradation by AAA family protease FtsH in Escherichia coli cells. *J. Basic Microbiol.* **47**, 251–259 (2007).
151. Moore, D. A., Whatley, Z. N., Joshi, C. P., Osawa, M. & Erickson, H. P. Probing for Binding Regions of the FtsZ Protein Surface through Site-Directed Insertions: Discovery of Fully Functional FtsZ-Fluorescent Proteins. *Journal of Bacteriology* **199**, e00553-16 (2017).
152. Anderson, D. E., Gueiros-Filho, F. J. & Erickson, H. P. Assembly Dynamics of FtsZ Rings in Bacillus subtilis and Escherichia coli and Effects of FtsZ-Regulating Proteins. *J Bacteriol* **186**, 5775–5781 (2004).
153. Sun, Q. & Margolin, W. FtsZ Dynamics during the Division Cycle of Live Escherichia coli Cells. *J Bacteriol* **180**, 2050–2056 (1998).
154. Camberg, J. L., Hoskins, J. R. & Wickner, S. The Interplay of ClpXP with the Cell Division Machinery in Escherichia coli. *Journal of Bacteriology* **193**, 1911–1918 (2011).
155. Camberg, J. L., Viola, M. G., Rea, L., Hoskins, J. R. & Wickner, S. Location of Dual Sites in E. coli FtsZ Important for Degradation by ClpXP; One at the C-Terminus and One in the Disordered Linker. *PLoS One* **9**, (2014).
156. Zupan, J. R., Cameron, T. A., Anderson-Furgeson, J. & Zambryski, P. C. Dynamic FtsA and FtsZ localization and outer membrane alterations during polar growth and cell division in Agrobacterium tumefaciens. *PNAS* **110**, 9060–9065 (2013).
157. Yu, X.-C. & Margolin, W. Ca2+-mediated GTP-dependent dynamic assembly of bacterial cell division protein FtsZ into asters and polymer networks in vitro. *The EMBO Journal* **16**, 5455–5463 (1997).
158. Popp, D., Iwasa, M., Narita, A., Erickson, H. P. & Maéda, Y. FtsZ Condensates: An In Vitro Electron Microscopy Study. *Biopolymers* **91**, 340–350 (2009).
159. Díaz-Espinoza, R. *et al.* Domain folding and flexibility of Escherichia coli FtsZ determined by tryptophan site-directed mutagenesis. *Protein Sci* **16**, 1543–1556 (2007).
160. Lu, C., Stricker, J. & Erickson, H. P. FtsZ from Escherichia coli, Azotobacter vinelandii, and Thermotoga maritima—quantitation, GTP hydrolysis, and assembly. *Cell Motility* **40**, 71–86 (1998).
161. Huecas, S. *et al.* Self-Organization of FtsZ Polymers in Solution Reveals Spacer Role of the Disordered C-Terminal Tail. *Biophys J* **113**, 1831–1844 (2017).
162. Galli, E. & Gerdes, K. FtsZ-ZapA-ZapB Interactome of Escherichia coli. *Journal of Bacteriology* **194**, 292–302 (2012).
163. Mukherjee, A. & Lutkenhaus, J. Analysis of FtsZ Assembly by Light Scattering and Determination of the Role of Divalent Metal Cations. *J. Bacteriol.* **181**, 823–832 (1999).
164. Lu, C. & Erickson, H. P. [25] Purificationa and assembly of FtsZ. in *Methods in Enzymology* **298**, 305–313 (Academic Press, 1998).
165. Mukherjee, A. & Lutkenhaus, J. Dynamic assembly of FtsZ regulated by GTP hydrolysis. *EMBO J* **17**, 462–469 (1998).
166. Pacheco-Gómez, R., Roper, D. I., Dafforn, T. R. & Rodger, A. The pH Dependence of Polymerization and Bundling by the Essential Bacterial Cytoskeltal Protein FtsZ. *PLOS ONE* **6**, e19369 (2011).
167. Monterroso, B., Reija, B., Jiménez, M., Zorrilla, S. & Rivas, G. Charged Molecules Modulate the Volume Exclusion Effects Exerted by Crowders on FtsZ Polymerization. *PLOS ONE* **11**, e0149060 (2016).

168. Leistler, B. & Perham, R. N. Solubilizing Buried Domains of Proteins: A Self-Assembling Interface Domain from Glutathione Reductase. *Biochemistry* **33**, 2773–2781 (1994).
169. Poussu, E., Jäntti, J. & Savilahti, H. A gene truncation strategy generating N- and C-terminal deletion variants of proteins for functional studies: mapping of the Sec1p binding domain in yeast Mso1p by a Mu in vitro transposition-based approach. *Nucleic Acids Res* **33**, e104 (2005).
170. Himanen, J.-P. *et al.* Crystal structure of an Eph receptor–ephrin complex. *Nature* **414**, 933 (2001).
171. Köker, T., Fernandez, A. & Pinaud, F. Characterization of Split Fluorescent Protein Variants and Quantitative Analyses of Their Self-Assembly Process. *Sci Rep* **8**, (2018).
172. Xue, M. *et al.* Optimizing the fragment complementation of APEX2 for detection of specific protein-protein interactions in live cells. *Scientific Reports* **7**, 12039 (2017).
173. Feng, S. *et al.* Improved split fluorescent proteins for endogenous protein labeling. *Nature Communications* **8**, 370 (2017).
174. Nygren, P.-Å., Stefan, S. & Uhlén, M. Engineering proteins to facilitate bioprocessing. *Trends in Biotechnology* **12**, 184–188 (1994).
175. LaVallie, E. R. *et al.* A Thioredoxin Gene Fusion Expression System That Circumvents Inclusion Body Formation in the E. coli Cytoplasm. *Bio/Technology* **11**, 187 (1993).
176. Pryor, K. D. & Leiting, B. High-Level Expression of Soluble Protein inEscherichia coliUsing a His6-Tag and Maltose-Binding-Protein Double-Affinity Fusion System. *Protein Expression and Purification* **10**, 309–319 (1997).
177. Zheng, C.-F., Simcox, T., Xu, L. & Vaillancourt, P. A new expression vector for high level protein production, one step purification and direct isotopic labeling of calmodulin-binding peptide fusion proteins. *Gene* **186**, 55–60 (1997).
178. Samuelsson, E., Moks, T., Uhlen, M. & Nilsson, B. Enhanced in vitro Refolding of Insulin-like Growth Factor I Using a Solubilizing Fusion Partner. *Biochemistry* **33**, 4207–4211 (1994).
179. Collins-Racie, L. A. *et al.* Production of Recombinant Bovine Enterokinase Catalytic Subunit in Escherichia coli Using the Novel Secretory Fusion Partner DsbA. *Bio/Technology* **13**, 982 (1995).
180. Dai, K. & Lutkenhaus, J. The proper ratio of FtsZ to FtsA is required for cell division to occur in Escherichia coli. *Journal of Bacteriology* **174**, 6145–6151 (1992).
181. Dewar, S. J., Begg, K. J. & Donachie, W. D. Inhibition of cell division initiation by an imbalance in the ratio of FtsA to FtsZ. *Journal of Bacteriology* **174**, 6314–6316 (1992).
182. von Stetten, D., Noirclerc-Savoye, M., Goedhart, J., Gadella, T. W. J. & Royant, A. Structure of a fluorescent protein from Aequorea victoria bearing the obligate-monomer mutation A206K. *Acta Crystallogr. Sect. F Struct. Biol. Cryst. Commun.* **68**, 878–882 (2012).
183. Roberts, G. A. *et al.* Mutations of the domain forming the dimeric interface of the ArdA protein affect dimerization and antimodification activity but not antirestriction activity. *FEBS J* **280**, 4903–4914 (2013).
184. Huston, J. S. *et al.* Protein engineering of antibody binding sites: recovery of specific activity in an anti-digoxin single-chain Fv analogue produced in Escherichia coli. *Proc Natl Acad Sci U S A* **85**, 5879–5883 (1988).
185. Arai, R., Ueda, H., Kitayama, A., Kamiya, N. & Nagamune, T. Design of the linkers which effectively separate domains of a bifunctional fusion protein. *Protein Eng Des Sel* **14**, 529–532 (2001).

186. Romberg, L. & Levin, P. A. Assembly Dynamics of the Bacterial Cell Division Protein FtsZ: Poised at the Edge of Stability. *Annu Rev Microbiol* **57**, 125–154 (2003).
187. Monterroso, B. *et al.* Mg2+-Linked Self-Assembly of FtsZ in the Presence of GTP or a GTP Analogue Involves the Concerted Formation of a Narrow Size Distribution of Oligomeric Species. *Biochemistry* **51**, 4541–4550 (2012).
188. Weekley, C. M. & Harris, H. H. Which form is that? The importance of selenium speciation and metabolism in the prevention and treatment of disease. *Chem. Soc. Rev.* **42**, 8870–8894 (2013).
189. Fossum, S., Crooke, E. & Skarstad, K. Organization of sister origins and replisomes during multifork DNA replication in Escherichia coli. *EMBO J* **26**, 4514–4522 (2007).
190. McDonald, K. L. & Auer, M. High-Pressure Freezing, Cellular Tomography, and Structural Cell Biology. *BioTechniques* **41**, 137–143 (2006).
191. Willingham, M. C. & Yamada, S. S. Development of a new primary fixative for electron microscopic immunocytochemical localization of intracellular antigens in cultured cells. *J Histochem Cytochem.* **27**, 947–960 (1979).
192. Rosano, G. L. & Ceccarelli, E. A. Recombinant protein expression in Escherichia coli: advances and challenges. *Front Microbiol* **5**, (2014).
193. Dvorak, P. *et al.* Exacerbation of substrate toxicity by IPTG in Escherichia coli BL21(DE3) carrying a synthetic metabolic pathway. *Microb Cell Fact* **14**, (2015).
194. Król, E. & Scheffers, D.-J. FtsZ Polymerization Assays: Simple Protocols and Considerations. *J Vis Exp* (2013). doi:10.3791/50844
195. Nägeli (von), C. W. *Ueber oligodynamische Erscheinungen in lebenden Zellen*. (Druck von Zürcher & Furrer, 1893).
196. Hobman, J. L. & Crossman, L. C. Bacterial antimicrobial metal ion resistance. *Journal of Medical Microbiology* **64**, 471–497 (2015).
197. Seiler, C. & Berendonk, T. U. Heavy metal driven co-selection of antibiotic resistance in soil and water bodies impacted by agriculture and aquaculture. *Front. Microbiol.* **3**, (2012).
198. Zhang, X. *et al.* Acid mine drainage affects the diversity and metal resistance gene profile of sediment bacterial community along a river. *Chemosphere* **217**, 790–799 (2019).
199. Lima de Silva, A. A. *et al.* Heavy metal tolerance (Cr, Ag AND Hg) in bacteria isolated from sewage. *Braz J Microbiol* **43**, 1620–1631 (2012).
200. Puskárová, A. *et al.* Regulation of yodA encoding a novel cadmium-induced protein in Escherichia coli. *Microbiology (Reading, Engl.)* **148**, 3801–3811 (2002).
201. Choudhury, R. & Srivastava, S. Zinc resistance mechanisms in bacteria. *Current Science* **81**, 768–775 (2001).
202. Lal, D., Nayyar, N., Kohli, P. & Lal, R. Cupriavidus metallidurans: A Modern Alchemist. *Indian J Microbiol* **53**, 114–115 (2013).
203. Llorens, I. *et al.* Uranium Interaction with Two Multi-Resistant Environmental Bacteria: Cupriavidus metallidurans CH34 and Rhodopseudomonas palustris. *PLOS ONE* **7**, e51783 (2012).
204. Sarret, G. *et al.* Chemical forms of selenium in the metal-resistant bacterium Ralstonia metallidurans CH34 exposed to selenite and selenate. *Appl. Environ. Microbiol.* **71**, 2331–2337 (2005).
205. Arenas, F. A. *et al.* Isolation, identification and characterization of highly tellurite-resistant, tellurite-reducing bacteria from Antarctica. *Polar Science* **8**, 40–52 (2014).

206. Ollivier, P. R. L. *et al.* Volatilization and Precipitation of Tellurium by Aerobic, Tellurite-Resistant Marine Microbes. *Appl. Environ. Microbiol.* **74**, 7163–7173 (2008).
207. von Rozycki, T. & Nies, D. H. Cupriavidus metallidurans: evolution of a metal-resistant bacterium. *Antonie van Leeuwenhoek* **96**, 115 (2008).
208. Magos, L., Tuffery, A. A. & Clarkson, T. W. Volatilization of Mercury By Bacteria. *Br J Ind Med* **21**, 294–298 (1964).
209. Klaassen, C. D., Liu, J. & Choudhuri, S. Metallothionein: an intracellular protein to protect against cadmium toxicity. *Annu. Rev. Pharmacol. Toxicol.* **39**, 267–294 (1999).
210. Huang, P. C., Morris, S., Dinman, J., Pine, R. & Smith, B. Role of metallothionein in detoxification and tolerance to transition metals. *Experientia Suppl.* **52**, 439–446 (1987).
211. Schor-Fumbarov, T., Goldsbrough, P. B., Adam, Z. & Tel-Or, E. Characterization and expression of a metallothionein gene in the aquatic fern Azolla filiculoides under heavy metal stress. *Planta* **223**, 69–76 (2005).
212. Li, L.-S. *et al.* Type 1 metallothionein (ZjMT) is responsible for heavy metal tolerance in Ziziphus jujuba. *Biochemistry Moscow* **81**, 565–573 (2016).
213. Reddy, M. S., Prasanna, L., Marmeisse, R. & Fraissinet-Tachet, L. Differential expression of metallothioneins in response to heavy metals and their involvement in metal tolerance in the symbiotic basidiomycete Laccaria bicolor. *Microbiology (Reading, Engl.)* **160**, 2235–2242 (2014).
214. Ecker, D. J. *et al.* Yeast metallothionein function in metal ion detoxification. *J. Biol. Chem.* **261**, 16895–16900 (1986).
215. Yang, Z. *et al.* Biomanufacturing of CdS quantum dots. *Green Chemistry* **17**, 3775–3782 (2015).
216. Laczi, K. *et al.* Metabolic responses of Rhodococcus erythropolis PR4 grown on diesel oil and various hydrocarbons. *Appl. Microbiol. Biotechnol.* **99**, 9745–9759 (2015).
217. Singhi, D., Jain, A. & Srivastava, P. Localization of Low Copy Number Plasmid pRC4 in Replicating Rod and Non-Replicating Cocci Cells of Rhodococcus erythropolis PR4. *PLoS ONE* **11**, e0166491 (2016).
218. Bosello, M. *et al.* Structural Characterization of the Heterobactin Siderophores from Rhodococcus erythropolis PR4 and Elucidation of Their Biosynthetic Machinery. *J. Nat. Prod.* **76**, 2282–2290 (2013).
219. van der Geize, R. & Dijkhuizen, L. Harnessing the catabolic diversity of rhodococci for environmental and biotechnological applications. *Current Opinion in Microbiology* **7**, 255–261 (2004).
220. Larkin, M. J., Kulakov, L. A. & Allen, C. C. Biodegradation and Rhodococcus – masters of catabolic versatility. *Current Opinion in Biotechnology* **16**, 282–290 (2005).
221. Sekine, M. *et al.* Sequence analysis of three plasmids harboured in Rhodococcus erythropolis strain PR4. *Environmental Microbiology* **8**, 334–346 (2006).
222. Nies, D. H. Efflux-mediated heavy metal resistance in prokaryotes. *FEMS Microbiol. Rev.* **27**, 313–339 (2003).
223. Crupper, S. S., Worrell, V., Stewart, G. C. & Iandolo, J. J. Cloning and Expression of cadD, a New Cadmium Resistance Gene of Staphylococcus aureus. *Journal of Bacteriology* **181**, 4071–4075 (1999).
224. Arnesano, F., Banci, L., Bertini, I., Mangani, S. & Thompsett, A. R. A redox switch in CopC: An intriguing copper trafficking protein that binds copper(I) and copper(II) at different sites. *PNAS* **100**, 3814–3819 (2003).

225. Broth Microdilution MIC Test. in *Clinical Microbiology Procedures Handbook, 3rd Edition* (ed. Garcia, L. S.) 25–41 (American Society of Microbiology, 2010). doi:10.1128/9781555817435.ch5.2
226. European Committee for Antimicrobial Susceptibility Testing (EUCAST) of the European Society of Clinical Microbiology and Infectious Diseases (ESCMID). Determination of minimum inhibitory concentrations (MICs) of antibacterial agents by broth dilution. *Clinical Microbiology and Infection* **9**, ix–xv (2003).
227. Borghese, R., Borsetti, F., Foladori, P., Ziglio, G. & Zannoni, D. Effects of the Metalloid Oxyanion Tellurite (TeO32−) on Growth Characteristics of the Phototrophic Bacterium Rhodobacter capsulatus. *Appl. Environ. Microbiol.* **70**, 6595–6602 (2004).
228. Moore, M. D. & Kaplan, S. Identification of intrinsic high-level resistance to rare-earth oxides and oxyanions in members of the class Proteobacteria: characterization of tellurite, selenite, and rhodium sesquioxide reduction in Rhodobacter sphaeroides. *Journal of Bacteriology* **174**, 1505–1514 (1992).
229. Rathgeber, C., Yurkova, N., Stackebrandt, E., Beatty, J. T. & Yurkov, V. Isolation of Tellurite- and Selenite-Resistant Bacteria from Hydrothermal Vents of the Juan de Fuca Ridge in the Pacific Ocean. *Appl. Environ. Microbiol.* **68**, 4613–4622 (2002).
230. Green, R. M., Seth, A. & Connell, N. D. A Peptide Permease Mutant of Mycobacterium bovis BCG Resistant to the Toxic Peptides Glutathione and S-Nitrosoglutathione. *Infection and Immunity* **68**, 429–436 (2000).
231. Dayaram, Y. K., Talaue, M. T., Connell, N. D. & Venketaraman, V. Characterization of a Glutathione Metabolic Mutant of Mycobacterium tuberculosis and Its Resistance to Glutathione and Nitrosoglutathione. *J Bacteriol* **188**, 1364–1372 (2006).
232. Temme, K., Hill, R., Segall-Shapiro, T. H., Moser, F. & Voigt, C. A. Modular control of multiple pathways using engineered orthogonal T7 polymerases. *Nucleic Acids Res* **40**, 8773–8781 (2012).
233. Wilks, J. C. & Slonczewski, J. L. pH of the Cytoplasm and Periplasm of Escherichia coli: Rapid Measurement by Green Fluorescent Protein Fluorimetry. *J Bacteriol* **189**, 5601–5607 (2007).
234. Aoi, W. & Marunaka, Y. Importance of pH Homeostasis in Metabolic Health and Diseases: Crucial Role of Membrane Proton Transport. *Biomed Res Int* **2014**, (2014).
235. Fahey, R. C., Brown, W. C., Adams, W. B. & Worsham, M. B. Occurrence of glutathione in bacteria. *Journal of Bacteriology* **133**, 1126–1129 (1978).
236. Jozefczak, M., Remans, T., Vangronsveld, J. & Cuypers, A. Glutathione Is a Key Player in Metal-Induced Oxidative Stress Defenses. *Int J Mol Sci* **13**, 3145–3175 (2012).
237. Ottosson, L.-G. *et al.* Sulfate Assimilation Mediates Tellurite Reduction and Toxicity in Saccharomyces cerevisiae. *Eukaryot Cell* **9**, 1635–1647 (2010).
238. Rankin, D. W. H. CRC handbook of chemistry and physics, 89th edition, edited by David R. Lide. *Crystallography Reviews* **15**, 223–224 (2009).
239. Shannon, R. D. Revised effective ionic radii and systematic studies of interatomic distances in halides and chalcogenides. *Acta Cryst A* **32**, 751–767 (1976).
240. Chivers, T. & S. Laitinen, R. Tellurium: a maverick among the chalcogens. *Chemical Society Reviews* **44**, 1725–1739 (2015).
241. Kumar, A., Nartey, W., Shin, J., Manimekalai, M. S. S. & Grüber, G. Structural and mechanistic insights into Mycothiol Disulphide Reductase and the Mycoredoxin-1-

alkylhydroperoxide reductase E assembly of Mycobacterium tuberculosis. *Biochimica et Biophysica Acta (BBA) - General Subjects* **1861**, 2354–2366 (2017).
242. Kumar, A., Manimekalai, M. S. S. & Grüber, G. Substrate-induced structural alterations of Mycobacterial mycothione reductase and critical residues involved. *FEBS Letters* **592**, 568–585 (2018).
243. Patel, M. P. & Blanchard, J. S. Expression, Purification, and Characterization of Mycobacterium tuberculosis Mycothione Reductase. *Biochemistry* **38**, 11827–11833 (1999).
244. Newton, G. L., Buchmeier, N. & Fahey, R. C. Biosynthesis and Functions of Mycothiol, the Unique Protective Thiol of Actinobacteria. *Microbiol. Mol. Biol. Rev.* **72**, 471–494 (2008).
245. Newton, G. L. & Fahey, R. C. Mycothiol biochemistry. *Arch Microbiol* **178**, 388–394 (2002).
246. Sharma, S. V., Van Laer, K., Messens, J. & Hamilton, C. J. Thiol Redox and pKa Properties of Mycothiol, the Predominant Low-Molecular-Weight Thiol Cofactor in the Actinomycetes. *ChemBioChem* **17**, 1689–1692 (2016).
247. Mills, S. J., Dunstan, M. A. & Christy, A. G. YCu(TeO3)2(NO3)(H2O)3: a novel layered tellurite. *Acta Crystallogr E Crystallogr Commun* **72**, 1138–1142 (2016).
248. Wicke, H. & Meleshyn, A. Microhydration of the Selenite Dianion: A Theoretical Study of Structures, Hydration Energies, and Electronic Stabilities of SeO32−(H2O)n (n = 0−6, 9) Clusters. *J. Phys. Chem. A* **114**, 8948–8960 (2010).
249. Saveliev, S. V. *et al.* Mass spectrometry compatible surfactant for optimized in-gel protein digestion. *Anal. Chem.* **85**, 907–914 (2013).
250. Scopes, R. K. Measurement of protein by spectrophotometry at 205 nm. *Analytical Biochemistry* **59**, 277–282 (1974).
251. Keller, A., Nesvizhskii, A. I., Kolker, E. & Aebersold, R. Empirical Statistical Model To Estimate the Accuracy of Peptide Identifications Made by MS/MS and Database Search. *Anal. Chem.* **74**, 5383–5392 (2002).
252. Searle, B. C., Turner, M. & Nesvizhskii, A. I. Improving sensitivity by probabilistically combining results from multiple MS/MS search methodologies. *J. Proteome Res.* **7**, 245–253 (2008).
253. Käll, L., Storey, J. D., MacCoss, M. J. & Noble, W. S. Assigning significance to peptides identified by tandem mass spectrometry using decoy databases. *J. Proteome Res.* **7**, 29–34 (2008).
254. Nesvizhskii, A. I., Keller, A., Kolker, E. & Aebersold, R. A statistical model for identifying proteins by tandem mass spectrometry. *Anal. Chem.* **75**, 4646–4658 (2003).

APPENDIX A: SUPPLEMENTAL TO CHAPTER 1

A.1 Templates for GRLMR Model Generation

Table A.1. Templates used for Structure Predictions and Values in **Chapter 1, Table 1.1**

Homology	PDB	Enzyme	Organism
1	4DNA	Putative Glutathione Reductase	*Sinorhizobium meliloti* 1021
2	5V36	Glutathione Reductase	*Streptococcus mutans* UA159
3	2R9Z	Glutathione Amide Reductase	*Chromatium gracile*
4	3O0H	Glutathione Reductase	*Bartonella henselsea*
5	1GEU	Glutathione Reductase (Engineererd NAD Site)	*Escherichia coli*
6	6B4O	Glutathione Reductase	*Enterococcus faecalis*
7	5W1J	Thioredoxin Glutathione Reductase	*Echinococcus granulosus*
8	1TYT	Trypanothione Reductase	*Crithidia fasciculata*
9	1BWC	Glutathione Reductase	*Homo sapiens*
10	2W0H	Trypanothione Reductase	*Leishmania infantum*
11	1EBD	Dihydrolipoamide Dehydrogenase	*Geobacillus stearotherophilus*
12	2EQ8	Lipoamide Dehydrogenase	*Thermus thermophilus*
13	2V6O	Thioredoxin Glutathione Reductase	*Schistosoma mansoni*
14	1NDA	Trypanothione Reductase	*Trypanosoma cruzi*
15	1OJT	Dihydrolipoamide Dehydrogenase	*Neisseria meningitidis*
16	2EQ7	Lipoamide Dehydrogenase	*Thermus thermophilus*
17	2A8X	Lipoamide Dehydrogenase	*Mycobacterium tuberculosis*
18	1XDI	Dihydrolipoyl Dehydrogenase	*Mycobacterium tuberculosis*

A.2 Alignment of GRLMR to various GSHR

```
CLUSTAL O(1.2.4) multiple sequence alignment


PSEPF      ------------------------------------------------------------      0
PMS        ------------------------------------------------------------      0
YEAST      ----------------------------ML-------------SATKQTFRSLQIRTMST      19
HUMAN      MALLPRALSAGAGPSWRRAARAFRGFLLLLPEPAALTRALSRAMACRQEPQPQGPPPAAG      60
ECOLI      ------------------------------------------------------------      0


PSEPF      MAYDFDLYVIGAGSGGVRAARFAAGFGAKVAVAESRYLGGTCVNVGCVPKKLLVYGAHFA      60
PMS        MAYDFDLYVIGAGSGGVRAARFAAGFGAKVAVAESRYLGGTCVNVGCVPKKLLVYGAHFA      60
```

```
YEAST      NTKHYDYLVIGGGSGGVASARRAASYGAKTLLVEAKALGGTCVNVGCVPKKVMWYASDLA     79
HUMAN      AVASYDYLVIGGGSGGLASARRAAELGARAAVVESHKLGGTCVNVGCVPKKVMWNTAVHS     120
ECOLI      MTKHYDYIAIGGGSGGIASINRAAMYGQKCALIEAKELGGTCVNVGCVPKKVMWHAAQIR     60
            .  :*  .**.****: : . **  * :  : *:: **************::   :

PSEPF      EDFE-QSSGFG------WNLGEADFDWATLIANKDREINRLNGIYRNLLVNSGVTLHEAH     113
PMS        EDFE-QASGFG------WNLGEANFDWATLIANKDREINRLNGIYRNLLVNSGVTLHEAH     113
YEAST      TRVS-HANEYGLYQNLPLDKEHLTFNWPEFKQKRDAYVHRLNGIYQKNLEKEKVDVVFGW     138
HUMAN      EFMH-DHADYG------FPSCEGKFNWRVIKEKRDAYVSRLNAIYQNNLTKSHIEIIRGH     173
ECOLI      EAIHMYGPDYG------FDTTINKFNWETLIASRTAYIDRIHTSYENVLGKNNVDVIKGF     114
             .      :*            *:*  :  .:   : *::  *.: * :. : :  .

PSEPF      AKIVGPH--EV---EVNGERYTAKNILIATGGWPQIP---EIPGHEHAISSNQAFFLKEL     165
PMS        AKIVGPH--EV---EVNGERFTAKNILIATGGWPQIP---GIPGHEHAIGSNEAFFLKEL     165
YEAST      ARFNKDGNVEVQKRDNTTEVYSANHILVATGGKAIFPE--NIPGFELGTDSDGFFRLEEQ     196
HUMAN      AAFTSDPKPTIE---VSGKKYTAPHILIATGGMPSTPHESQIPGASLGITSDGFFQLEEL     230
ECOLI      ARFVDA--KTLE---VNGETITADHILIATGGRPSHP---DIPGVEYGIDSDGFFALPAL     166
           * :       :     . :  :* :**:****    *    *** . .  *:  * *

PSEPF      PKRVLVVGGGYIAVEFAGIFHGLGANTTLLYRGDLFLRGFDGSVRNHLKEELTKRGMDLQ     225
PMS        PKRVLVVGGGYIAVEFAGIFHGLGANTTLLYRGDLFLRGFDGSVRKHLQEELTKRGLDLQ     225
YEAST      PKKVVVVGAGYIGIELAGVFHGLGSETHLVIRGETVLRKFDECIQNTITDHYVKEGINVH     256
HUMAN      PGRSVIVGAGYIAVEMAGILSALGSKTSLMIRHDKVLRSFDSMISTNCTEELENAGVEVL     290
ECOLI      PERVAVVGAGYIAVELAGVINGLGAKTHLFVRKHAPLRSFDPMISETLVEVMNAEGPQLH     226
           * :  :**.***.:*:**:: .**::* *. * .  ** **  :     :     * ::

PSEPF      FNADIARIDKQSDGS-LKATL---------KDGRVLEADCVFYATGRRPMLDNLGLENID     275
PMS        FNADIARIDKQADGS-LKATL---------KDGRVLEADCVFYATGRRPMLDNLGLENID     275
YEAST      KLSKIVKVEKNVETDKLKI--------HMNDSKSIDDVDELIWTIGRKSHL-GMGSENVG     307
HUMAN      KFSQVKEVKKTLSG--LEVSMVTAVPGRLPVMTMIPDVDCLLWAIGRVPNTKDLSLNKLG     348
ECOLI      TNAIPKAVVKNTDGS-LTLEL---------EDGRSETVDCLIWAIGREPANDNINLEAAG     276
             :    : *  .   *                   .* :::: **     .:. :  .

PSEPF      VQLDDKGFIKVDEQYQTTEPSILALGDVIGRVQLTPVALAEGMAVARRLFKPEQY--RPV     333
PMS        VQLDDKGFIKVDGEYQTTEPSILALGDVIGRVQLTPVALAEGMAVARRLFKPEQY--RPV     333
YEAST      IKLNSHDQIIADEYQNTNVPNIYSLGDVVGKVELTPVAIAAGRKLSNRLFGPEKFRNDKL     367
HUMAN      IQTDDKGHIIVDEFQNTNVKGIYAVGDVCGKALLTPVAIAAGRKLAHRLFEYK--EDSKL     406
ECOLI      VKTNEKGYIVVDKYQNTNIEGIYAVGDNTGAVELTPVAVAAGRRLSERLFNNK--PDEHL     334
           :: :.:. * .*   :*.  .* ::**  * . *****:* *  ::.***  :      :

PSEPF      DYKMIPTAVFSLPNIGTVGLTEEEAREA--GHDVVIYESRFRPMKLTLTDCQERTLMKLV     391
PMS        DYKMIPTAVFSLPNIGTVGLSEEEAREC--GHEVVIFESRFRPMKLTLTDCQEKTLMKLV     391
YEAST      DYENVPSVIFSHPEAGSIGISEKEAIEKYGKENIKVYNSKFTAMYYAMLSEKSPTRYKIV     427
HUMAN      DYNNIPTVVFSHPPIGTVGLTEDEAIHKYGIENVKTYSTSFTPMYHAVTKRKTKCVMKMV     466
ECOLI      DYSNIPTVVFSHPPIGTVGLTEPQAREQYGDDQVKVYKSSFTAMYTAVTTHRQPCRMKLV     394
           **. :*:.:** *  *::*::* :* .    .::  :.: *  *  ::   :     *:*

PSEPF      VDGKSDKVLGCHMVGPDAGEIVQGLAIALKAGATKRDFDDTIGVHPTAAEEFVTMRTPVG     451
PMS        VDARTDKVLGCHMVGPDAGEIVQGLAIALKAGATKRDFDDTIGVHPTAAEEFVTMRTPVS     451
YEAST      CAGPNEKVVGLHIVGDSSAEILQGFGVAIKMGATKADFDNCVAIHPTSAEELVTMR----     483
HUMAN      CANKEEKVVGIHMQGLGCDEMLQGFAVAVKMGATKADFDNTVAIHPTSSEELVTLR----     522
ECOLI      CVGSEEKIVGIHGIGFGMDEMLQGFAVALKMGATKKDFDNTVAIHPTAAEEFVTMR----     450
                :*::* *  * .  *::**:.:*:* **** ***: :.:***::**:**:*

PSEPF      A     452
PMS        A     452
YEAST      -     483
HUMAN      -     522
ECOLI      -     450
```

PSEPF, *P. fluorescens*
PMS, *P. moraviensis* stanleyae
* Identical, : strongly similar, . weakly similar

A.3 EDS Analysis

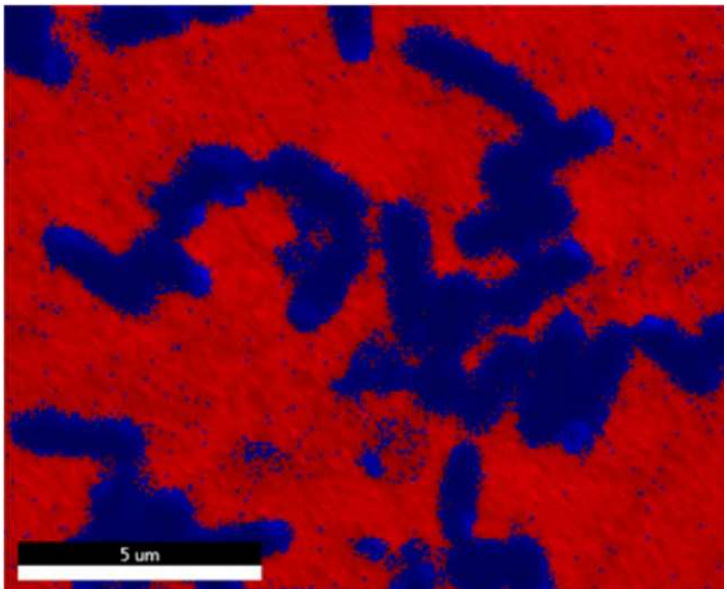

Figure A.1. EDS Map overlay of *E. coli* cells not expressing GRLMR after SeO_3^{2-} incubation. Se is indicated by red and does not overlay with C, N, or O present in the *E. coli* cells (blue).

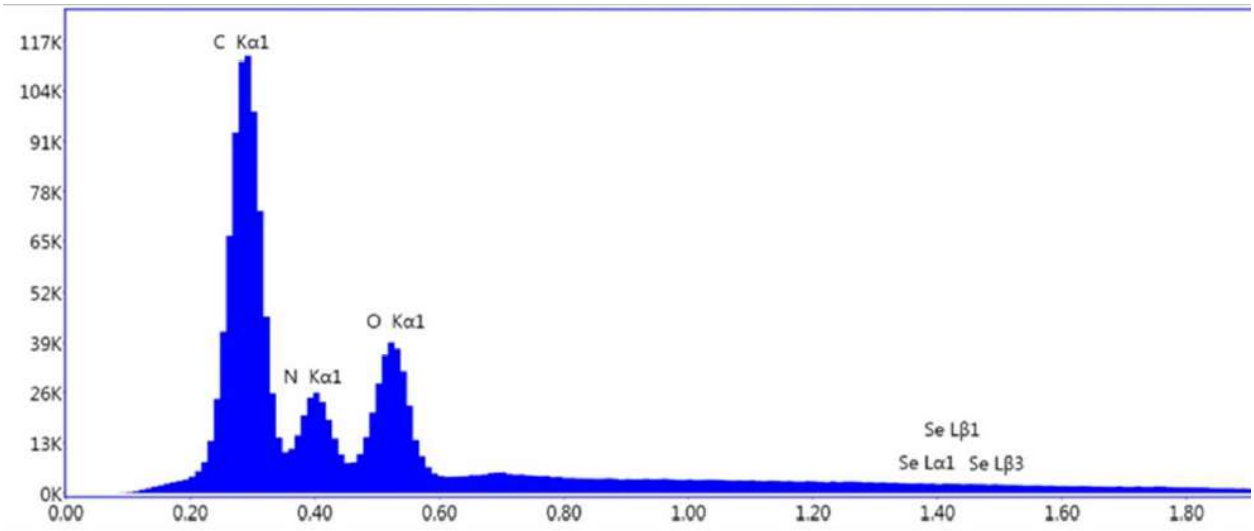

Figure A.2. EDS Spectra of **Figure A.2.**

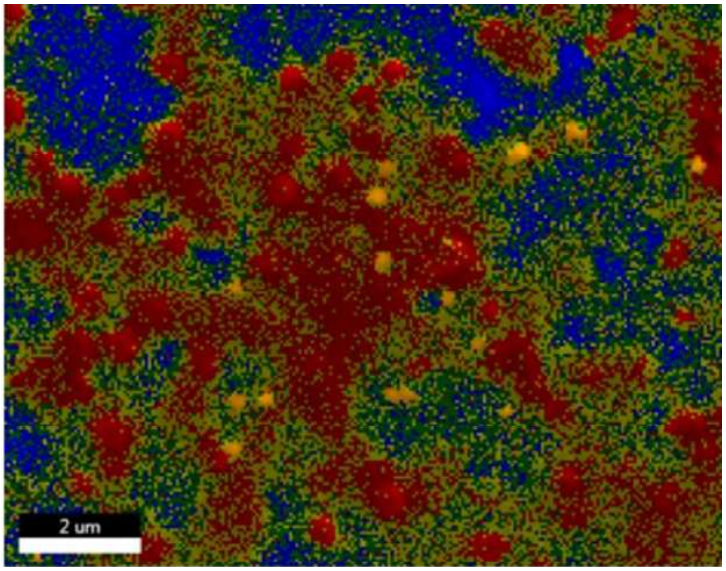

Figure A.3. EDS Map overlay of *E. coli* cells expressing GRLMR after SeO_3^{2-} incubation. SeNPs indicated by orange overlaps C, N, and O indicated by red, green, and yellow.

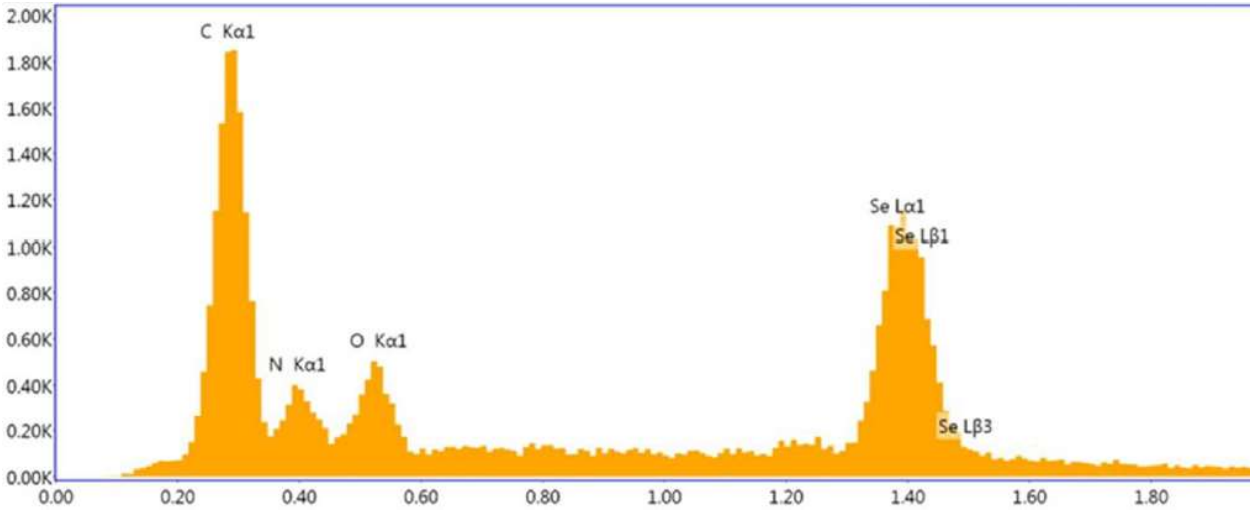

Figure A.4. EDS Spectra of **Figure A.4.**

A.4 Plasmid Sequence of GRLMR

> pD441-CH with GSHR - 5360 bp

TGCAAATGCTGAATGAGGGCATCGTTCCCACTGCGATGCTGGTTGCCAACGATCAGATGGCGCTGGGCGCAATGCGCGCC
ATTACCGAGTCCGGGCTGCGCGTTGGTGCGGATATCTCGGTAGTGGGATACGACGATACCGAAGATAGCTCATGTTATAT
CCCGCCGTTAACCACCATCAAACAGGATTTTCGCCTGCTGGGGCAAACCAGCGTGGACCGCTTGCTGCAACTCTCTCAGG
GCCAGGCGGTGAAGGGCAATCAGCTGTTGCCAGTCTCACTGGTGAAAAGAAAAACCACCCTGGCGCCCAATACGCAAACC
GCCTCTCCCCGCGCGTTGGCCGATTCATTAATGCAGCTGGCACGACAGGTTTCCCGACTGGAAAGCGGGCAGTGACTCAT
GACCAAAATCCCTTAACGTGAGTTACGCGCGCGTCGTTCCACTGAGCGTCAGACCCCGTAGAAAAGATCAAAGGATCTTC
TTGAGATCCTTTTTTTTCTGCGCGTAATCTGCTGCTTGCAAACAAAAAAACCACCGCTACCAGCGGTGGTTTGTTTGCCGG
ATCAAGAGCTACCAACTCTTTTTCCGAAGGTAACTGGCTTCAGCAGAGCGCAGATACCAAATACTGTTCTTCTAGTGTAG
CCGTAGTTAGCCCACCACTTCAAGAACTCTGTAGCACCGCCTACATACCTCGCTCTGCTAATCCTGTTACCAGTGGCTGC
TGCCAGTGGCGATAAGTCGTGTCTTACCGGGTTGGACTCAAGACGATAGTTACCGGATAAGGCGCAGCGGTCGGGCTGAA
CGGGGGGTTCGTGCACACAGCCCAGCTTGGAGCGAACGACCTACACCGAACTGAGATACCTACAGCGTGAGCTATGAGAA
AGCGCCACGCTTCCCGAAGGGAGAAAGGCGGACAGGTATCCGGTAAGCGGCAGGGTCGGAACAGGAGAGCGCACGAGGGA

GCTTCCAGGGGGAAACGCCTGGTATCTTTATAGTCCTGTCGGGTTTCGCCACCTCTGACTTGAGCGTCGATTTTTGTGAT
GCTCGTCAGGGGGGCGGAGCCTATGGAAAAACGCCAGCAACGCGGCCTTTTTACGGTTCCTGGCCTTTTGCTGGCCTTTT
GCTCACATGTTCTTTCCTGCGTTATCCCCTGATTCTGTGGATAACCGTATTACCGCCTTTGAGTGAGCTGATACCGCTCG
CCGCAGCCGAACGACCGAGCGCAGCGAGTCAGTGAGCGAGGAAGCGGAAGGCGAGAGTAGGGAACTGCCAGGCATCAAAC
TAAGCAGAAGGCCCCTGACGGATGGCCTTTTTGCGTTTCTACAAACTCTTTCTGTGTTGTAAAACGACGGCCAGTCTTAA
GCTCGGGCCCCCTGGGCGGTTCTGATAACGAGTAATCGTTAATCCGCAAATAACGTAAAAACCCGCTTCGGCGGGTTTTT
TTATGGGGGGAGTTTAGGGAAAGAGCATTTGTCAGAATATTTAAGGGCGCCTGTCACTTTGCTTGATATATGAGAATTAT
TTAACCTTATAAATGAGAAAAAAGCAACGCACTTTAAATAAGATACGTTGCTTTTTCGATTGATGAACACCTATAATTAA
ACTATTCATCTATTATTTATGATTTTTTGTATATACAATATTTCTAGTTTGTTAAAGAGAATTAAGAAAATAAATCTCGA
AAATAATAAAGGGAAAATCAGTTTTTGATATCAAAATTATACATGTCAACGATAATACAAAATATAATACAAACTATAAG
ATGTTATCAGTATTTATTATGCATTTAGAATAAATTTTGTGTCGCCCTTAATTGTGAGCGGATAACAATTACGAGCTTCA
TGCACAGTGAAATCATGAAAAATTTATTTGCTTTGTGAGCGGATAACAATTATAATATGTGGAATTGTGAGCGCTCACAA
TTCCACAACGGTTTCCCTCTAGAAATAATTTTGTTTAACTTTTCGAGACCTAAGGAGGTAAAAAATGTGGAGCCATCCGC
AGTTTGAAAAAGGCGGCAGCGGCGCCTACGATTTTGACCTTTATGTGATTGGTGCCGGTTCCGGCGGTGTGCGGGCTGCG
CGGTTTGCTGCCGGCTTCGGGGCGAAAGTGGCGGTGGCCGAGAGCCGTTATCTGGGCGGCACCTGCGTCAACGTCGGCTG
CGTGCCGAAAAAGCTTTTGGTCTACGGTGCGCACTTTGCCGAGGACTTCGAGCAAGCGTCCGGTTTCGGCTGGAACCTGG
GCGAAGCCAACTTCGATTGGGCCACGCTGATCGCCAACAAGGATCGCGAGATCAATCGCCTCAACGGCATTTACCGCAAT
CTTCTGGTCAACAGTGGCGTGACCCTGCACGAGGCGCACGCGAAAATTGTCGGGCCGCACGAGGTCGAGGTCAACGGCGA
GCGCTTCACCGCGAAAAACATCCTGATCGCCACCGGCGGCTGGCCGCAGATCCCTGGAATCCCGGGGCATGAACACGCTA
TCGGTTCGAACGAAGCGTTCTTCCTCAAAGAATTGCCCAAGCGCGTGCTGGTGGTCGGCGGCGGTTATATCGCGGTCGAG
TTCGCCGGAATTTTCCATGGTCTCGGCGCCAACACTACACTGCTGTATCGCGGTGATCTGTTCCTGCGTGGTTTCGACGG
GTCTGTGCGCAAGCACCTGCAAGAAGAATTGACCAAGCGCGGCCTCGACCTGCAATTCAATGCCGACATCGCACGCATCG
ACAAACAAGCTGATGGCAGCTTGAAGGCGACGCTCAAGGATGGTCGCGTACTCGAAGCCGATTGCGTGTTCTACGCCACC
GGCCGGCGTCCGATGCTGGACAATCTGGGCCTGGAAAACATCGATGTGCAGCTCGACGACAAGGGCTTCATCAAAGTCGA
CGGCGAGTATCAAACCACCGAACCGTCGATTCTGGCGCTGGGTGACGTCATCGGTCGCGTGCAACTGACCCCTGTCGCGC
TCGCCGAAGGCATGGCCGTGGCGCGGCGCCTGTTCAAGCCAGAGCAATATCGTCCAGTGGATTACAAGATGATCCCGACT
GCCGTGTTCAGTCTGCCGAATATCGGCACGGTTGGTTTAAGCGAGGAAGAAGCGCGCGAATGTGGCCATGAGGTGGTGAT
TTTCGAGAGTCGCTTCCGGCCGATGAAGCTGACCCTGACTGACTGTCAGGAGAAAACCCTGATGAAGCTGGTGGTCGACG
CCAGGACTGACAAGGTGCTTGGCTGTCACATGGTGGGCCCGGACGCTGGCGAGATCGTGCAAGGTCTGGCGATCGCCTTG
AAGGCCGGCGCGACCAAGCGCGACTTCGACGACACCATCGGGGTGCACCCGACGGCCGCCGAAGAGTTTGTGACCATGCG
CACGCCGGTCAGCGCTGGTCATCACCACCACCACCATTGAGGTCTCACCCCAAGGGCGACACCCCCTAATTAGCCCGGGC
GAAAGGCCCAGTCTTTCGACTGAGCCTTTCGTTTTATTTGATGCCTGGCAGTTCCCTACTCTCGCATGGGGAGTCCCCAC
ACTACCATCGGCGCTACGGCGTTTCACTTCTGAGTTCGGCATGGGGTCAGGTGGGACCACCGCGCTACTGCCGCCAGGCA
AACAAGGGGTGTTATGAGCCATATTCAGGTATAAATGGGCTCGCGATAATGTTCAGAATTGGTTAATTGGTTGTAACACT
GACCCCTATTTGTTTATTTTTCTAAATACATTCAAATATGTATCCGCTCATGAGACAATAACCCTGATAAATGCTTCAAT
AATATTGAAAAAGGAAGAATATGAGCCATATTCAACGGGAAACGTCGAGGCCGCGATTAAATTCCAACATGGATGCTGAT
TTATATGGGTATAAATGGGCTCGCGATAATGTCGGGCAATCAGGTGCGACAATCTATCGCTTGTATGGGAAGCCCGATGC
GCCAGAGTTGTTTCTGAAACATGGCAAAGGTAGCGTTGCCAATGATGTTACAGATGAGATGGTCAGACTAAACTGGCTGA
CGGAATTTATGCCACTTCCGACCATCAAGCATTTTATCCGTACTCCTGATGATGCATGGTTACTCACCACTGCGATCCCC
GGAAAAACAGCGTTCCAGGTATTAGAAGAATATCCTGATTCAGGTGAAAATATTGTTGATGCGCTGGCAGTGTTCCTGCG
CCGGTTGCACTCGATTCCTGTTTGTAATTGTCCTTTTAACAGCGATCGCGTATTTCGCCTCGCTCAGGCGCAATCACGAA
TGAATAACGGTTTGGTTGATGCGAGTGATTTTGATGACGAGCGTAATGGCTGGCCTGTTGAACAAGTCTGGAAAGAAATG
CATAAACTTTTGCCATTCTCACCGGATTCAGTCGTCACTCATGGTGATTTCTCACTTGATAACCTTATTTTTGACGAGGG
GAAATTAATAGGTTGTATTGATGTTGGACGAGTCGGAATCGCAGACCGATACCAGGATCTTGCCATCCTATGGAACTGCC
TCGGTGAGTTTTCTCCTTCATTACAGAAACGGCTTTTTCAAAAATATGGTATTGATAATCCTGATATGAATAAATTGCAG
TTTCATTTGATGCTCGATGAGTTTTTCTAAGCGGCGCGCCATCGAATGGCGCAAAACCTTTCGCGGTATGGCATGATAGC
GCCCGGAAGAGAGTCAATTCAGGGTGGTGAATATGAAACCAGTAACGTTATACGATGTCGCAGAGTATGCCGGTGTCTCT
TATCAGACCGTTTCCCGCGTGGTGAACCAGGCCAGCCACGTTTCTGCGAAAACGCGGGAAAAAGTGGAAGCGGCGATGGC
GGAGCTGAATTACATTCCCAACCGCGTGGCACAACAACTGGCGGGCAAACAGTCGTTGCTGATTGGCGTTGCCACCTCCA
GTCTGGCCCTGCACGCGCCGTCGCAAATTGTCGCGGCGATTAAATCTCGCGCCGATCAACTGGGTGCCAGCGTGGTGGTG
TCGATGGTAGAACGAAGCGGCGTCGAAGCCTGTAAAGCGGCGGTGCACAATCTTCTCGCGCAACGCGTCAGTGGGCTGAT
CATTAACTATCCGCTGGATGACCAGGATGCCATTGCTGTGGAAGCTGCCTGCACTAATGTTCCGGCGTTATTTCTTGATG
TCTCTGACCAGACACCCATCAACAGTATTATTTTCTCCCATGAGGACGGTACGCGACTGGGCGTGGAGCATCTGGTCGCA
TTGGGTCACCAGCAAATCGCGCTGTTAGCGGGCCCATTAAGTTCTGTCTCGGCGCGTCTGCGTCTGGCTGGCTGGCATAA
ATATCTCACTCGCAATCAAATTCAGCCGATAGCGGAACGGGAAGGCGACTGGAGTGCCATGTCCGGTTTTCAACAAACCA

*GRLMR gene sequence is underlined

A.5 UV-vis Spectra of Seleno-diglutathione

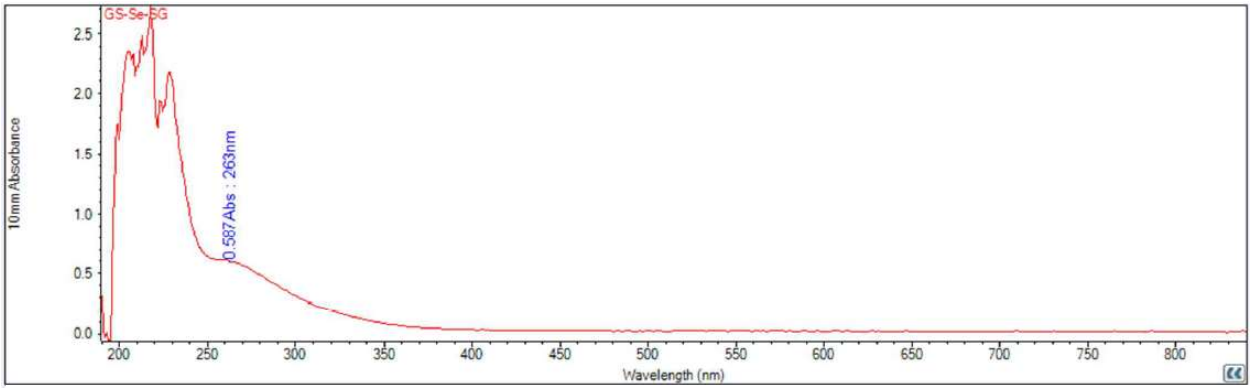

Figure A.5. Full UV-Vis spectra of synthesized GSSeSG.

APPENDIX B: SUPPLEMENTAL TO CHAPTER 2

B.1 Dynamic Light Scattering

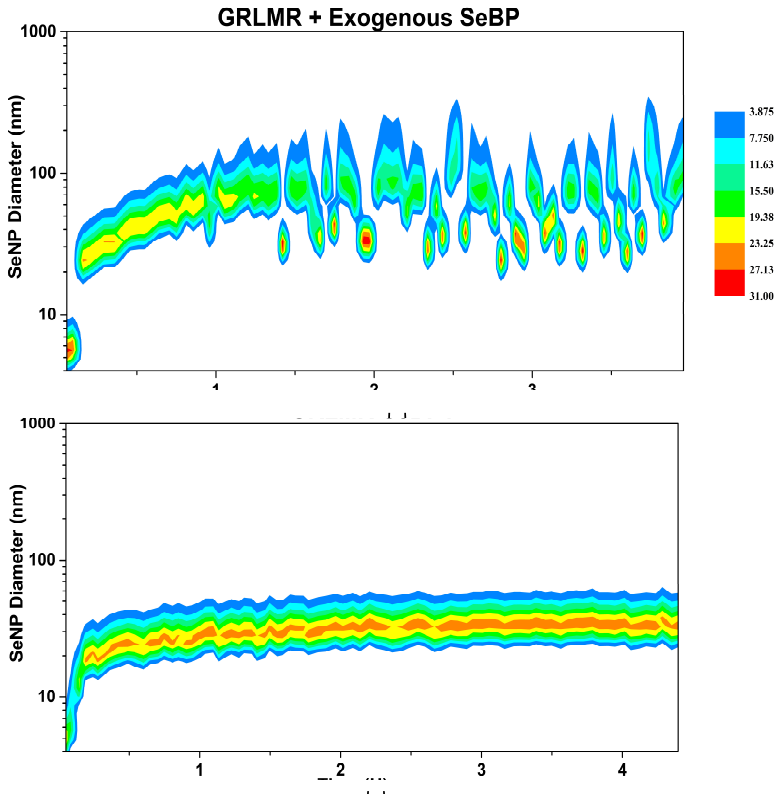

Figure B.1. Contour maps following population size of SeNPs overtime in DLS. The color legend is in population % .

B.2 pH Native-PAGE gel

Native PAGE gels were prepared and run following the preparation established in previous manuscripts.[115] Buffer for the PAGE gel was composed of a final concentration of 25 mM Histidine and 30 mM MOPS instead of the common Tris/Glycine buffer. Gels were prepared and run at 4°C for >4 hours. Gels were then stained using either Coomassie stain or SeO_3^{2-}/NADPH solution. Results indicate a pI for GRLMR-SeBP as being close to pH 6.6 as the migration was minimal.

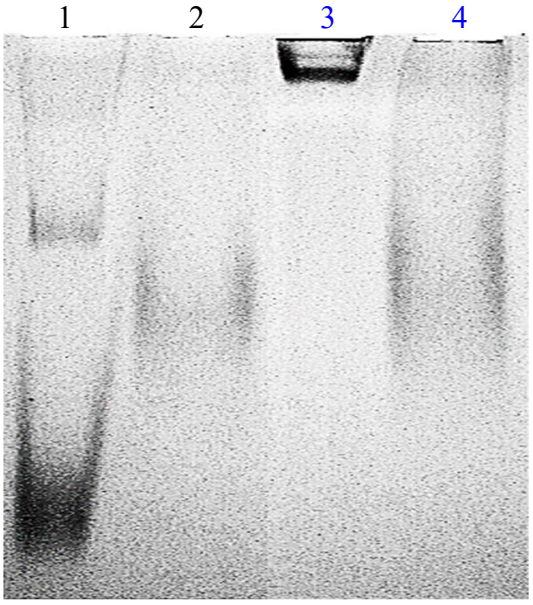

Figure B.2. A pH 6.6 native PAGE gel with unreacted GRLMR (Lane 1), reacted GRLMR (Lane 2), unreacted GRLMR-SeBP (Lane 3), and reacted GRLMR-SeBP (Lane 4).

B.3 Attempts to Characterize Binding Affinity of SeBP to SeNP

Attempts were made to quantify the affinity of SeBP for SeNPs through pull-down and fluorescence quenching assays. Despite multiple attempts, none of the assays produced interpretable data.

Quantification of affinity of SeBP for SeNPs was attempted through several assays relying on pull down assays and fluorescence quenching of a fluorophore labeled SeBP through binding of a 6-FAM labeled exogenous SeBP with a SeNP target. These experiments proved exceedingly difficult giving results that were both inconsistent and sporadic. Initially inorganically produced

SeNPs through reduction of Na_2SeO_3 reduced with $NaBH_4$ in an ice cooled milliQ water solution were titrated into a solution of fluorophore labeled SeBP. However, reduction of fluorescence was convoluted with both the presence of scattering SeNPs and possible quenching of the fluorophore. Next, SeNPs were produced by GRLMR in the presence of varying concentrations of fluorophore labeled SeBP. The expectation of the reaction was to see a decrease in fluorescence as well as a SeNP size arrest under proper concentrations of SeBP. Again, the results were sporadic and lacked reproducibility. Finally, competitive binding assays between both unlabeled and labeled SeBP were attempted. Briefly, SeNPs were produced by GRLMR in the presence of high concentrations (>500 μM) of labeled or unlabeled SeBP. SeNPs were then collected and then incubated with varying concentrations of the SeBP not used in the SeNP synthesis. Again, data could not be interpreted to give a binding isotherm.

B.4 Expected Raman Shifts

Table B.1. Expected Shifts of His Tautomers Before and After Metal Binding

Tautomer Marker	Expected Shift (cm^{-1})	Assignment	Ref
N^{τ}-H, N^{π}	1568 – 1573	$C^4=C^5$ st	120
	1282 – 1287	$N^{\pi}C^4$ st, C^4C^{β} st, C^5N^{τ} st	120, 122
N^{τ}-H, N^{π}-M	1573 – 1590	$C^4=C^5$ st	120, 123
	1272 – 1277	$N^{\pi}C^4$ st, C^4C^{β} st, C^5N^{τ} st	120, 123
N^{π}-H, N^{τ}	1583 – 1588	$C^4=C^5$ st + $N^{\pi}H$ bending	120
	1260 – 1265	C^5H def, C^2H def, $N^{\pi}C^2$ st	120, 122
N^{π}-H, N^{τ}-M	1594 – 1606	$C^4=C^5$ st $N^{\pi}H$ bending	120, 123
	1434 – 1440	Ring st	123
N^{τ}-H, N^{π}-H	1627 – 1634	$C^4=C^5$ st	120, 122
	1264 – 1269	Ring st	120
N^{τ}-M, N^{π}-M	1555 – 1567	$C^4=C^5$ st	120, 123
	1282 – 1292	$C^2N^{\pi}C^4$ st; $N^{\pi}C^4$ st, C^4C^{β} st, C^5N^{τ} st	120, 123

*st = stretch; def = deformation

B.5 Raman Spectra

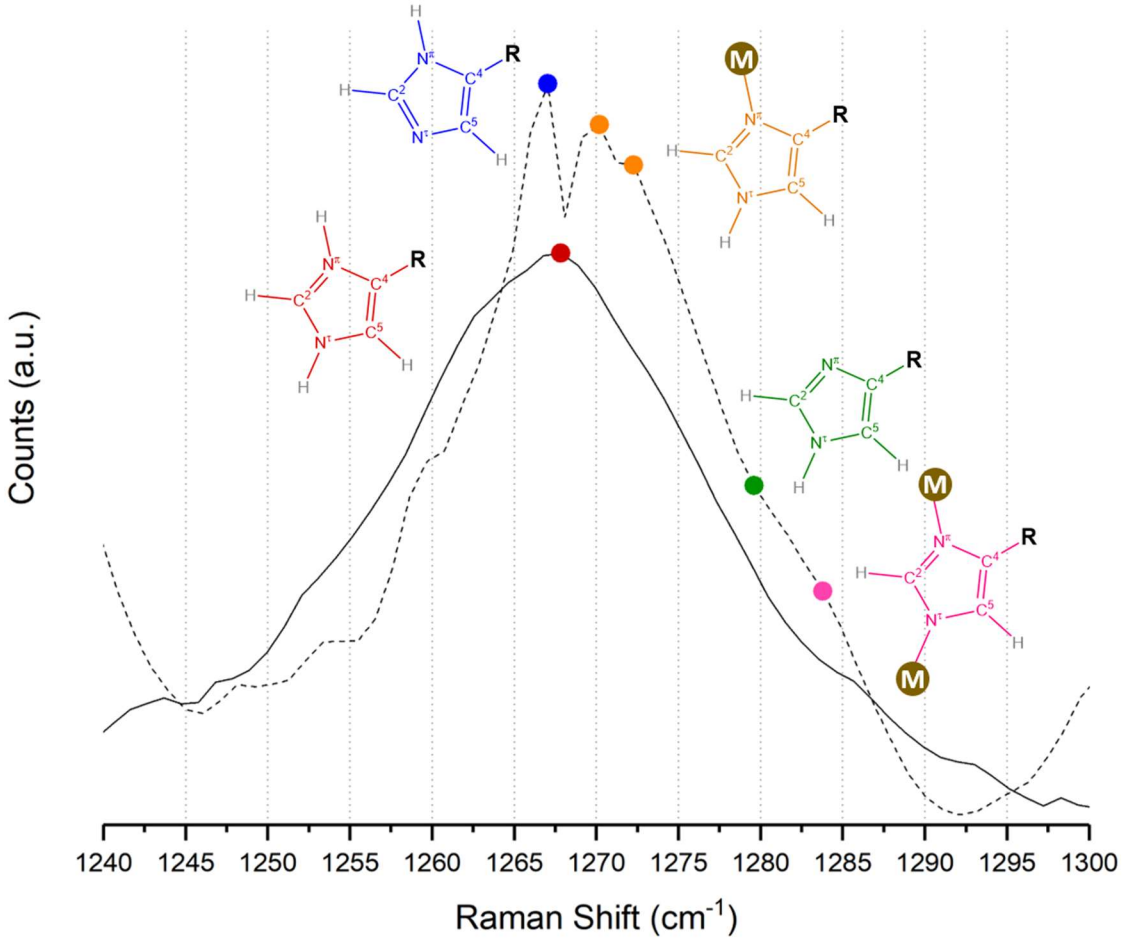

Figure B.3. Traces of SeBP (solid) and SeBP/SeNP (dashed) from **Figure 2.8**, expanded to the 1240 – 1300 cm^{-1} region to show the relevant His modes described. The marks are color coded to the structure that represents each shift shown.

B.6 Primers for SeBP Insertion

Primers used for SeBP insertion are depicted below:

Rev. Primer:
TAGGTACATACTTGATTGACGGCTCTTCTACCAGCGTGCAGATGTTTGTGATGTTTATGTGGTGTCAgaccagcgctgaccg

Frwd Primer:
CTATCTGTCGATCTGGCTCTTctggtcatcaccaccacc

The restriction site is underlined and the annealing sequence is lowercase.

REFERENCES

115. McLellan, T. Electrophoresis buffers for polyacrylamide gels at various pH. *Analytical Biochemistry* **126**, 94–99 (1982).
120. Takeuchi, H. Raman structural markers of tryptophan and histidine side chains in proteins. *Biopolymers* **72**, 305–317 (2003).
122. Toyama, A., Ono, K., Hashimoto, S. & Takeuchi, H. Raman Spectra and Normal Coordinate Analysis of the N1−H and N3−H Tautomers of 4-Methylimidazole: Vibrational Modes of Histidine Tautomer Markers. *J. Phys. Chem. A* **106**, 3403–3412 (2002).
123. Hasegawa, K., Ono, T. & Noguchi, T. Vibrational Spectra and Ab Initio DFT Calculations of 4-Methylimidazole and Its Different Protonation Forms: Infrared and Raman Markers of the Protonation State of a Histidine Side Chain. *J. Phys. Chem. B* **104**, 4253–4265 (2000).
254. Nesvizhskii, A. I., Keller, A., Kolker, E. & Aebersold, R. A statistical model for identifying proteins by tandem mass spectrometry. *Anal. Chem.* **75**, 4646–4658 (2003).

APPENDIX C: SUPPLEMENTAL TO CHAPTER 3

C.1 Sequence of Plasmid Ordered from ATUM.

> pD441-CH with F-cSeNPHis sans linkers - 7928 bp

TGCAAATGCTGAATGAGGGCATCGTTCCCACTGCGATGCTGGTTGCCAACGATCAGATGGCGCTGGGCGCAATGCGCGCC
ATTACCGAGTCCGGGCTGCGCGTTGGTGCGGATATCTCGGTAGTGGGATACGACGATACCGAAGATAGCTCATGTTATAT
CCCGCCGTTAACCACCATCAAACAGGATTTTCGCCTGCTGGGGCAAACCAGCGTGGACCGCTTGCTGCAACTCTCTCAGG
GCCAGGCGGTGAAGGGCAATCAGCTGTTGCCAGTCTCACTGGTGAAAAGAAAAACCACCCTGGCGCCCAATACGCAAACC
GCCTCTCCCCGCGCGTTGGCCGATTCATTAATGCAGCTGGCACGACAGGTTTCCCGACTGGAAAGCGGGCAGTGACTCAT
GACCAAAATCCCTTAACGTGAGTTACGCGCGCGTCGTTCCACTGAGCGTCAGACCCCGTAGAAAAGATCAAAGGATCTTC
TTGAGATCCTTTTTTTCTGCGCGTAATCTGCTGCTTGCAAACAAAAAAACCACCGCTACCAGCGGTGGTTTGTTTGCCGG
ATCAAGAGCTACCAACTCTTTTTCCGAAGGTAACTGGCTTCAGCAGAGCGCAGATACCAAATACTGTTCTTCTAGTGTAG
CCGTAGTTAGCCCACCACTTCAAGAACTCTGTAGCACCGCCTACATACCTCGCTCTGCTAATCCTGTTACCAGTGGCTGC
TGCCAGTGGCGATAAGTCGTGTCTTACCGGGTTGGACTCAAGACGATAGTTACCGGATAAGGCGCAGCGGTCGGGCTGAA
CGGGGGGTTCGTGCACACAGCCCAGCTTGGAGCGAACGACCTACACCGAACTGAGATACCTACAGCGTGAGCTATGAGAA
AGCGCCACGCTTCCCGAAGGGAGAAAGGCGGACAGGTATCCGGTAAGCGGCAGGGTCGGAACAGGAGAGCGCACGAGGGA
GCTTCCAGGGGGAAACGCCTGGTATCTTTATAGTCCTGTCGGGTTTCGCCACCTCTGACTTGAGCGTCGATTTTTGTGAT
GCTCGTCAGGGGGGCGGAGCCTATGGAAAAACGCCAGCAACGCGGCCTTTTTACGGTTCCTGGCCTTTTGCTGGCCTTTT
GCTCACATGTTCTTTCCTGCGTTATCCCCTGATTCTGTGGATAACCGTATTACCGCCTTTGAGTGAGCTGATACCGCTCG
CCGCAGCCGAACGACCGAGCGCAGCGAGTCAGTGAGCGAGGAAGCGGAAGGCGAGAGTAGGGAACTGCCAGGCATCAAAC
TAAGCAGAAGGCCCCTGACGGATGGCCTTTTTGCGTTTCTACAAACTCTTTCTGTGTTGTAAAACGACGGCCAGTCTTAA
GCTCGGGCCCCCTGGGCGGTTCTGATAACGAGTAATCGTTAATCCGCAAATAACGTAAAAACCCGCTTCGGCGGGTTTTT
TTATGGGGGGAGTTTAGGGAAAGAGCATTTGTCAGAATATTTAAGGGCGCCTGTCACTTTGCTTGATATATGAGAATTAT
TTAACCTTATAAATGAGAAAAAAGCAACGCACTTTAAATAAGATACGTTGCTTTTTCGATTGATGAACACCTATAATTAA
ACTATTCATCTATTATTTATGATTTTTTGTATATACAATATTTCTAGTTTGTTAAAGAGAATTAAGAAAATAAATCTCGA
AAATAATAAAGGGAAAATCAGTTTTTGATATCAAAATTATACATGTCAACGATAATACAAAATATAATACAAACTATAAG
ATGTTATCAGTATTTATTATGCATTTAGAATAAATTTTGTGTCGCCCTTAATTGTGAGCGGATAACAATTACGAGCTTCA
TGCACAGTGAAATCATGAAAAATTTATTTGCTTTGTGAGCGGATAACAATTATAATATGTGGAATTGTGAGCGCTCACAA
TTCCACAACGGTTTCCCTCTAGAAATAATTTTGTTTAACTTTTCGAGACCTAAGGAGGTAAAAAATGTTTGAGCCAATGG
AGCTGACCAATGATGCGGTGATCAAAGTGATTGGTGTAGGCGGTGGTGGTGGCAACGCCGTTGAGCACATGGTGCGTGAG
CGTATCGAGGGCGTGGAGTTCTTCGCGGTCAACACGGACGCACAAGCCCTGCGTAAGACCGCAGTGGGCCAAACCATCCA
AATTGGCAGCGGCATTACTAAAGGTCTGGGTGCTGGTGCGAACCCGGAAGTTGGCCGCAACGCAGCAGACGAGGACCGTG
ACGCTTTGCGTGCGGCGCTGGAAGGTGCGGATATGGTTTTCATTGCGGCAGGCATGGGTGGCGGTACCGGTACGGGTGCA
GCGCCGGTTGTCGCGGAAGTGGCGAAAGATCTGGGCATCTTGACCGTTGCAGTTGTTACGAAGCCGTTCAACTTCGAGGG
CAAGAAACGCATGGCGTTCGCGGAACAGGGTATCACCGAGTTGAGCAAACACGTTGATAGCCTGATCACGATTCCGAACG
ACAAACTGCTGAAGGTGCTGGGCCGTGGTATTAGCTTGCTGGACGCATTTGGTGCGGCAAATGACGTTCTGAAAGGTGCC
GTCCAAGGTATTGCCGAGCTGATTACCCGTCCGGGTCTGATGAACGTCGATTTTGCGGACGTGCGCACCGTAATGAGCGA
GATGGGTTATGCGATGATGGGTAGCGGTGTGGCGTCGGGTGAGGACCGCGCTGAAGAAGCCGCAGAGATGGCGATTAGCA
GCCCGCTGTTGGAAGATATCGATCTGAGCGGCGCTCGCGGTGTCCTGGTTAACATCACCGCGGGTTTTGACTTGCGCCTG
GACGAGTTCGAAACCGTTGGCAATACGATTCGTGCCTTCGCGAGCGACAACGCCACCGTGGTCATCGGTACGAGCCTGGA
CCCGGATATGAATGATGAGCTGCGCGTGACGGTCGTTGCGACTGGTATCGGTATGGATAAGCGTCCGGAAATCACCCTGG
TGACCAACAAACAGGTGCAGCAACCGGTGATGGATCGCTATCAACAGCACGGCATGGCACCTCTGACGCAGGAGCAGAAG
CCGGTCGCGAAGGTCGTCAATGATAATGCGCCGCAGACGGCGAAAGAGCCGGATTACCTGGATATCCCGGCGTTTCTGCG
TAAACAAGCAGATAAGTCTTCTTATGTCTATGTTTGCTATATTGAGCGCTACCTATTAAGAAGACATGCGTATGACTTCG
ATCTGTACGTTATCGGCGCGGGCAGCGGTGGCGTTCGTGCGGCCCGTTTCGCAGCGGGTTTTGGCGCCAAGGTTGCCGTT
GCGGAATCTCGCTACTTAGGTGGTACGTGTGTGAATGTGGGTTGTGTTCCAAAGAAATTGCTGGTGTATGGCGCCCATTT
CGCGGAAGATTTTGAACAGGCCAGCGGCTTTGGTTGGAATTTAGGTGAGGCGAATTTTGACTGGGCGACCTTAATTGCGA
ATAAAGACCGTGAAATTAACCGTCTGAATGGTATCTATCGTAACCTGTTAGTGAATTCCGGTGTTACGTTACATGAAGCC
CATGCCAAGATCGTGGGCCCACATGAAGTGGAAGTGAATGGTGAACGTTTTACTGCCAAGAATATTTTAATTGCGACGGG
TGGTTGGCCACAAATTCCGGGCATTCCAGGCCACGAGCATGCGATTGGCAGCAATGAGGCCTTTTTTTTGAAGGAGCTTC
CGAAACGTGTTTTAGTCGTGGGTGGTGGCTACATTGCCGTGGAATTTGCGGGCATCTTTCACGGCCTGGGTGCGAATACC
ACCTTGTTATACCGTGGCGACTTATTTCTTCGCGGCTTTGATGGCAGCGTTCGTAAACATCTTCAGGAGGAGCTTACGAA
ACGTGGTCTGGATTTACAGTTTAACGCGGATATTGCGCGTATTGATAAGCAGGCAGACGGTTCTCTGAAAGCCACCCTGA
AAGACGGCCGTGTGCTGGAGGCGGACTGTGTTTTTTATGCGACGGGTCGTCGCCCAATGTTAGATAACTTAGGTCTTGAG
AATATTGACGTTCAACTGGATGATAAAGGTTTTATTAAGGTGGATGGTGAATACCAGACGACGGAGCCAAGCATCTTAGC
CTTGGGCGATGTGATTGGCCGTGTCCAGTTAACGCCGGTGGCCCTGGCGGAGGGTATGGCGGTTGCCCGCCGTTTATTTA
AACCGGAACAGTACCGCCCGGTCGACTATAAAATGATTCCAACCGCGGTTTTTTCCTTACCAAACATTGGTACCGTGGGC
CTGTCTGAAGAGGAGGCCCGTGAGTGCGGTCACGAAGTTGTCATCTTTGAATCTCGTTTTCGCCCAATGAAATTAACGCT
TACCGATTGCCAAGAAAAGACGTTAATGAAATTAGTTGTGGATGCGCGTACCGATAAAGTCCTGGGTTGCCATATGGTTG

GTCCAGATGCGGGTGAAATTGTCCAGGGCTTAGCCATTGCGCTTAAAGCGGGTGCCACGAAACGTGATTTTGATGATACG
ATTGGCGTCCATCCAACCGCGGCGGAGGAATTCGTCACGATGCGTACCCCCGTGTCTGCGAGAGACGATACATTACGCCG
TATGCGCAAGAGCGTTATATCCGCCGTCTCAGCCTACGATTTTGACCTTTATGTGATTGGTGCCGGTTCCGGCGGTGTGC
GCGCTGCGCGCTTTGCTGCCGGCTTCGGGGCGAAAGTGGCGGTGGCCGAGAGCCGTTATCTGGGCGGCACCTGCGTCAAC
GTCGGCTGCGTGCCGAAAAAACTTTTGGTCTACGGTGCGCACTTTGCCGAGGACTTCGAGCAAGCGTCCGGTTTCGGCTG
GAACCTGGGCGAAGCCAACTTCGATTGGGCCACGCTGATCGCCAACAAGGATCGCGAGATCAATCGCCTCAACGGCATTT
ACCGCAATCTTCTGGTCAACAGTGGCGTGACCCTGCACGAGGCGCACGCGAAAATTGTCGGGCCGCACGAGGTCGAGGTC
AACGGCGAGCGCTTCACCGCGAAAAACATCCTGATCGCCACCGGCGGCTGGCCGCAGATCCCTGGAATCCCGGGGCATGA
ACACGCTATCGGTTCGAACGAAGCGTTCTTCCTCAAAGAATTGCCCAAGCGCGTGCTGGTGGTCGGCGGCGGTTATATCG
CGGTCGAGTTCGCCGGAATTTTCCATGGTCTCGGCGCCAACACTACACTGCTGTATCGCGGTGATCTGTTCCTGCGTGGT
TTCGACGGGTCTGTGCGCAAGCACCTGCAAGAAGAATTGACCAAGCGCGGCCTCGACCTGCAATTCAATGCCGACATCGC
ACGCATCGACAAACAAGCTGATGGCAGCTTGAAGGCGACGCTCAAGGATGGTCGCGTACTCGAAGCCGATTGCGTGTTCT
ACGCCACCGGCCGGCGTCCGATGCTGGACAATCTGGGCCTGGAAAACATCGATGTGCAGCTCGACGACAAGGGCTTCATC
AAAGTCGACGGCGAGTATCAAACCACCGAACCGTCGATTCTGGCGCTGGGTGACGTCATCGGTCGCGTGCAACTGACCCC
TGTCGCGCTCGCCGAAGGCATGGCCGTGGCGCGTCGCCTGTTCAAGCCAGAGCAATATCGTCCAGTGGATTACAAGATGA
TCCCGACTGCCGTGTTCAGTCTGCCGAATATCGGCACGGTTGGTTTAAGCGAGGAAGAAGCGCGCGAATGTGGCCATGAG
GTGGTGATTTTCGAGAGTCGCTTCCGTCCGATGAAGCTGACCCTGACTGACTGTCAGGAGAAAACCCTGATGAAGCTGGT
GGTCGACGCCCGCACTGACAAGGTGCTTGGCTGTCACATGGTGGGCCCGGACGCTGGCGAGATCGTGCAAGGTCTGGCGA
TCGCCTTGAAGGCCGGCGCGACCAAGCGCGACTTCGACGACACCATCGGGGTGCACCCGACGGCCGCCGAAGAGTTTGTG
ACCATGCGCACGCCGGTCAGCGCTGGTCATCACCACCACCACCATTGAGGTCTCACCCCAAGGGCGACACCCCCTAATTA
GCCCGGGCGAAAGGCCCAGTCTTTCGACTGAGCCTTTCGTTTTATTTGATGCCTGGCAGTTCCCTACTCTCGCATGGGGA
GTCCCCACACTACCATCGGCGCTACGGCGTTTCACTTCTGAGTTCGGCATGGGGTCAGGTGGGACCACCGCGCTACTGCC
GCCAGGCAAACAAGGGGTGTTATGAGCCATATTCAGGTATAAATGGGCTCGCGATAATGTTCAGAATTGGTTAATTGGTT
GTAACACTGACCCCTATTTGTTTATTTTTCTAAATACATTCAAATATGTATCCGCTCATGAGACAATAACCCTGATAAAT
GCTTCAATAATATTGAAAAAGGAAGAATATGAGCCATATTCAACGGGAAACGTCGAGGCCGCGATTAAATTCCAACATGG
ATGCTGATTTATATGGGTATAAATGGGCTCGCGATAATGTCGGGCAATCAGGTGCGACAATCTATCGCTTGTATGGGAAG
CCCGATGCGCCAGAGTTGTTTCTGAAACATGGCAAAGGTAGCGTTGCCAATGATGTTACAGATGAGATGGTCAGACTAAA
CTGGCTGACGGAATTTATGCCACTTCCGACCATCAAGCATTTTATCCGTACTCCTGATGATGCATGGTTACTCACCACTG
CGATCCCCGGAAAAACAGCGTTCCAGGTATTAGAAGAATATCCTGATTCAGGTGAAAATATTGTTGATGCGCTGGCAGTG
TTCCTGCGCCGGTTGCACTCGATTCCTGTTTGTAATTGTCCTTTTAACAGCGATCGCGTATTTCGCCTCGCTCAGGCGCA
ATCACGAATGAATAACGGTTTGGTTGATGCGAGTGATTTTGATGACGAGCGTAATGGCTGGCCTGTTGAACAAGTCTGGA
AAGAAATGCATAAACTTTTGCCATTCTCACCGGATTCAGTCGTCACTCATGGTGATTTCTCACTTGATAACCTTATTTTT
GACGAGGGGAAATTAATAGGTTGTATTGATGTTGGACGAGTCGGAATCGCAGACCGATACCAGGATCTTGCCATCCTATG
GAACTGCCTCGGTGAGTTTTCTCCTTCATTACAGAAACGGCTTTTTCAAAAATATGGTATTGATAATCCTGATATGAATA
AATTGCAGTTTCATTTGATGCTCGATGAGTTTTTCTAAGCGGCGCGCCATCGAATGGCGCAAAACCTTTCGCGGTATGGC
ATGATAGCGCCCGGAAGAGAGTCAATTCAGGGTGGTGAATATGAAACCAGTAACGTTATACGATGTCGCAGAGTATGCCG
GTGTCTCTTATCAGACCGTTTCCCGCGTGGTGAACCAGGCCAGCCACGTTTCTGCGAAAACGCGGGAAAAAGTGGAAGCG
GCGATGGCGGAGCTGAATTACATTCCCAACCGCGTGGCACAACAACTGGCGGGCAAACAGTCGTTGCTGATTGGCGTTGC
CACCTCCAGTCTGGCCCTGCACGCGCCGTCGCAAATTGTCGCGGCGATTAAATCTCGCGCCGATCAACTGGGTGCCAGCG
TGGTGGTGTCGATGGTAGAACGAAGCGGCGTCGAAGCCTGTAAAGCGGCGGTGCACAATCTTCTCGCGCAACGCGTCAGT
GGGCTGATCATTAACTATCCGCTGGATGACCAGGATGCCATTGCTGTGGAAGCTGCCTGCACTAATGTTCCGGCGTTATT
TCTTGATGTCTCTGACCAGACACCCATCAACAGTATTATTTTCTCCCATGAGGACGGTACGCGACTGGGCGTGGAGCATC
TGGTCGCATTGGGTCACCAGCAAATCGCGCTGTTAGCGGGCCCATTAAGTTCTGTCTCGGCGCGTCTGCGTCTGGCTGGC
TGGCATAAATATCTCACTCGCAATCAAATTCAGCCGATAGCGGAACGGGAAGGCGACTGGAGTGCCATGTCCGGTTTTCA
ACAAACCA

*Encoded gene is underlined

C.2 Oligonucleotides for Linker Insertion

Linkers for insertion between FtsZ and $GSHR_1$

$(GGGGS)_1$ Forward:

tatatatgtatagaagacaaagatggcggtggcggttctggtggcgcgtaagtcttctctatatagatc

$(GGGGS)_1$ Reverse:

gatctatatagagaagacttacgcgccaccagaaccgccaccgccatctttgtcttctatacatatata

$(GGGGS)_2$ Forward:

tatatatgtatagaagacaaagatggcggtggtggcagcggcggtggcggttctggtggcgcgtaagtcttctctatatagat
c

$(GGGGS)_2$ Reverse:

gatctatatagagaagacttacgcgccaccagaaccgccaccgccgctgccaccaccgccatctttgtcttctatacatatat
a

$(GGGGS)_3$ Forward:
tatatatgtatagaagacaaagatggcggtggtggcagcggcggtggcggttctggcggtggcggtagcggcggtgcgtaagt
cttctctatatagatc
$(GGGGS)_3$ Reverse:
gatctatatagagaagacttacgcaccgccgctaccgccaccgccagaaccgccaccgccgctgccaccaccgccatctttgt
cttctatacatatata
$(EAAAK)_1$ Forward:
tatatatgtatagaagacaaagatgaagcggccgcaaaagcgtaagtcttctctatatagatc
$(EAAAK)_1$ Reverse:
gatctatatagagaagacttacgcttttgcggccgcttcatctttgtcttctatacatatata
$(EAAAK)_2$ Forward:
tatatatgtatagaagacaaagatgaagcggccgcaaaagaagcggccgcaaaagcgtaagtcttctctatatagatc
$(EAAAK)_2$ Reverse:
gatctatatagagaagacttacgcttttgcggccgcttcttttgcggccgcttcatctttgtcttctatacatatata
$(EAAAK)_3$ Forward:
tatatatgtatagaagacaaagatgaagcggccgcaaaagaagcggccgcaaaagaagcggccgcaaaagcgtaagtcttctc
tatatagatc
$(EAAAK)_3$ Reverse:
gatctatatagagaagacttacgcttttgcggccgcttcttttgcggccgcttcttttgcggccgcttcatctttgtcttcta
tacatatata

Linkers for insertion between $GSHR_1$ and $GSHR_2$
$(GGGGS)_1$ Forward:
aaattgtcgatagtcgtctcatgcgggcggtggcggtagcgcctagagacgtttgtgtaatacgta
$(GGGGS)_1$ Reverse:
tacgtattacacaaacgtctctaggcgctaccgccaccgcccgcatgagacgactatcgacaattt
$(GGGGS)_2$ Forward:
aaattgtcgatagtcgtctcatgcgggcggtggcggttctggcggtggcggtagcgcctagagacgtttgtgtaatacgta
$(GGGGS)_2$ Reverse:
tacgtattacacaaacgtctctaggcgctaccgccaccgccagaaccgccaccgcccgcatgagacgactatcgacaattt
$(GGGGS)_3$ Forward:
aaattgtcgatagtcgtctcatgcgggcggcggtggcggtagcggcggtggcggttctggcggtggcggtagcgcctagagac
gtttgtgtaatacgta
$(GGGGS)_3$ Reverse:
tacgtattacacaaacgtctctaggcgctaccgccaccgccagaaccgccaccgccgctaccgccaccgccgcccgcatgaga
cgactatcgacaattt
GGGGSEAAAKGGGGS Forward:
aaattgtcgatagtcgtctcatgcgggcggtggcggtagcgaagcggcagccaaaggcggtggcggtagcgcctagagacgtt
tgtgtaatacgta
GGGGSEAAAKGGGGS Reverse:
tacgtattacacaaacgtctctaggcgctaccgccaccgcctttggctgccgcttcgctaccgccaccgcccgcatgagacga
ctatcgacaattt
EAAAKGGGGSEAAAK Forward:
aaattgtcgatagtcgtctcatgcggaagcggcagccaaaggcggtggcggtagcgaagcggcagccaaagcctagagacgtt
tgtgtaatacgta
EAAAKGGGGSEAAAK Reverse:
tacgtattacacaaacgtctctaggctttggctgccgcttcgctaccgccaccgcctttggctgccgcttccgcatgagacga
ctatcgacaattt

C.3 Primers for SeBP Insertion into cSeNP
Primers for SeBP Insertion After $GSHR_1$ and $GSHR_2$
$GSHR_1$ SeBP Insert Forward:
tctctggatggctcttcacaccataaacacttacatgcaggtggcggcggtagcgaagcg
$GSHR_1$ SeBP Insert Reverse:
ttatatcgcggctcttcagtgcttatgtggggtcaggccagcagacacggggg

GSHR$_2$ SeBP Insert Forward:
acaatgtccaggctcttcacatcacaagcatctgcacgctggtcatcaccaccacc
GSHR$_2$ SeBP Insert Reverse:
tatgggaacagctcttcaatgtttgtgaggtgttaaacccgcgctgaccggc

APPENDIX D: SUPPLEMENTAL TO CHAPTER 4

D.1 LC-MS/MS Data

Below are the amino acid sequences of the protein hits from the LC-MS/MS data. Yellow indicates unique peptides identified during the analysis.

C1A3D2_RHOE4 (100%), 49,317.5 Da
Putrescine oxidase OS=Rhodococcus erythropolis (strain PR4 / NBRC 100887) GN=puo PE=4 SV=1
25 exclusive unique peptides, 34 exclusive unique spectra, 935 total spectra, 271/453 amino acids (60% coverage)

MPTLQRDVAIVGAGPSGLAAATALRKAGLTVAVIEARDRVGGRTWTDTIDGAVLEIGGQWVS
PDQTALISLLDELGLKTFERYREGESVYISSAGERTQYTGDSFPTNDTTKKEMDRLIDEMDD
LAAQIGAEEPWAHPLARDLDTVSFKQWLINQSDDAEARDNIGLFIAGGMLTKPAHSFSALQA
VLMAASAGSFSHLVDEDFILDKRVIGGMQQVSIRMAEALGDDVFLNAPVRTVKWNESGATVL
ADGDVRVEASRVILAVPPNLYSRISYDPPLPRRQHQMHQHQSLGLVIKVHAVYETPFWREAG
LSGTGFGASEVVQEVYDNTNHEDDRGTLVAFVSDEKADAMFELSVEERKATILASLARYLGP
KAEEPVVYYESDWGSEEWTRGAYAASFDLGGLHRYGADSRTPVGPIHFSCSDIAAEGYQHVD
GAVRMGQRTAADIIARSKA

C1A2Z1_RHOE4 (100%), 42,243.8 Da
Putative beta-ketoadipyl-CoA thiolase OS=Rhodococcus erythropolis (strain PR4 / NBRC 100887) GN=RER_42680 PE=3
13 exclusive unique peptides, 18 exclusive unique spectra, 254 total spectra, 200/405 amino acids (49% coverage)

MPEAVIVSAVRSPIGRAMKGSLKDIRPDDLATQMVAAALAKIPELDPTEIDDLMLGCGQPAG
QSGFNIARVVAVQLGYDFLPGVTVNRYCSSSLQTTRMALHAIRAGEGDVFISAGVESVSSFI
TGNADGLPNTKNPLFDAAQARSAKLAEGGVAWTDPREEGLIPDVYLGMGQTAENVASATGIT
REDQDRWAVRSQNRAEEAIARGFFERGITPVTLADGTVVSKDDGPRAGTTYEGISGLKPVFR
PDGTVTAGNACPLNDGAAALVIMSDTKAKALGLTPLARIVSTGVSGLSPEIMGLGPIQAVKN
ALKIAGKSISDIDLFEINEAFAVQVLGSARELGIEEDKLNISGGAIALGHPFGMTGARITNT
LINNLQEQDKTFGVETMCVGGGQGMAMVIERLS

C0ZY75_RHOE4 (100%), 49,323.4 Da
Mycothione reductase OS=Rhodococcus erythropolis (strain PR4 / NBRC 100887) GN=mtr PE=3 SV=1
14 exclusive unique peptides, 17 exclusive unique spectra, 216 total spectra, 179/458 amino acids (39% coverage)

MTHYDLAIIGSGSGNSLPDERFDGKKIAILEEGTFGGTCLNVGCIPTKMFVYAAEVARTITT
AEKYGVDATLDGVRWSDIVKRVFGRIDPISAGGERYRSEDSPNTTVYRGHATFTGDKTIDTG
TGETITADQVVIAAGSRPIIPEEIASSGVKYYTNEDIMRLPELPEHLVIVGSGFIATEFAHV
FSALGSRVSIIGRSQRLLRHLDDEISERFTELAEQKWDVHLGSPLTSVRGDGDNIAVELANG
TVVSGDVLLVAVGRQPNGDLLGLDKAGVELDDKGSVVVDEYQRTTAEGVFALGDVSSPYQLK
HVANHEARVVQHNLLQDAWKDTSGLRSTDHRFVPAAVFTDPQIADVGMTEKQARDAGLDITV
KVQAYGDVAYGWAMEDQEGICKVIAERGTGRILGAHVMGTQAPTVIQPLIQAMSFGLSAQDM
ARGQYWIHPALAEVVENALLGLDI

C1A2K5_RHOE4 (100%), 41,135.4 Da
Malate dehydrogenase OS=Rhodococcus erythropolis (strain PR4 / NBRC 100887) GN=RER_41320 PE=3 SV=1
9 exclusive unique peptides, 10 exclusive unique spectra, 81 total spectra, 134/397 amino acids (34% coverage)

MSLVTEAINVPKVELTDEEIFAAHVGGKLSVETTAPLDTQRALSIAYTPGVAQVSRAIAADE
TLADRYTWTNRLVVVVSDGTAVLGLGDIGPRASLPVMEGKSALFKNFAGLNSIPLVLDTKDP
DEIVETLIRLRPSFGAVNLEDISAPRCFEIEKRVIEALDCPVMHDDQHGTAIVVLAALKGAV
KVQSRDITTLKVVISGAGAAGVACANILLAAGISDVIVLDSKGIISGERSDLNDVKAELAAR
TNPRDLHGGAIEALEGADVFLGVSAGKIPEELIASMAPESIVFALSNPDPEIHPETASKYAA
IVATGRSDFPNQINNVLAFPGVFKGALDAGARRITEGMKLAAAEAILSVVGDELAADKIVPS
PLDPRVAPAVAEAVAAAAHAEGVTS

C1A007_RHOE4 (100%), 90,849.2 Da
Aminopeptidase N OS=Rhodococcus erythropolis (strain PR4 / NBRC 100887) GN=pepN PE=4 SV=1
6 exclusive unique peptides, 7 exclusive unique spectra, 59 total spectra, 90/827 amino acids (11% coverage)

MSTANLNRSEVAERSRTIDVTGYRVELDLRSAADSASKTFSTVTTIDLTSSAESTWLDFIGA
AVDSVDVDGASIPVEYDGSRIVLRGLGGSNVVRVAAHGHYSRSGEGLHRFVDDADDQTYLYT
QYEPADARRVFACFEQPDLKAPFTFEVTAPDGWEVLSNQPATRTLSVDGAQRVTFAPTLPIS
TYITAIAAGPYHRVASSWSRGELTVELGALCRASLAPHLDADNVFDITRQGLDFYAEHFDYP
YPFGKYDQIFVPEYNLGAMENPGLVTFTEAYVFRGTATDEQHQRRANTILHEMAHMWFGDLV
TMVWWDDLWLKESFADFMGSLVSAEATRFTDAWVAFAIKRKAWAYLQDQLPTTHPIVADIVD
LEAAKLNFDGITYAKGASVLKQLVAFVGRDAFFEAARRYFKAHAFGNTTLVDLLDVLAETSG
RDVREWARIWLQTTGVSTLSLDGTDLVQTDPRPHRLAVGIYDYNESGDLVRTERVELDITES
RTSVDLPPGALTLLNDEDLTYAKVRLDAESLSTVEASLDRVSDPLARGVIWSSLWNSVRDAQ
LSVFRYLDMVERFAPAETDLAILSAILTDAQYAVLHYVPKSLRPNVSAGWLETTWKALFEAE
PESGRQLAWARALSAAAAVNDARAGELRSILDGTCPGPVGLALDPDLRWALWIALSATGHAS
VSDFDGELSKDSTSAGRTAYVRAAASIPDGETKAAAWASATTDASLSNDRLDATIAGFRSGT
DPSLIEGYAVEYFSSLGKWWSERSIEIARRLVNGLFPAAEDTSAVDSWIQANAEAPASLRRL
VLERRDHLARDLRAQASNAVI

PCKG_RHOE4 (100%), 67,398.9 Da
Phosphoenolpyruvate carboxykinase [GTP] OS=Rhodococcus erythropolis (strain PR4 / NBRC 100887) GN=pckG PE=3
6 exclusive unique peptides, 6 exclusive unique spectra, 28 total spectra, 60/609 amino acids (10% coverage)

MTSATIPGLNGTDGTPPTQHKELLAWVQEVAELTQPDRVVFADGSDEEWDRLTTKLVEAGTF
TRLNDEKKPNSFLGNSDPSDVARVESRTYICSKEEIDAGPTNNWMDPAEMRTLMGDLYRGCM
RGRTMYVVPFCMGPLDAEDPKLGVELTDSEYVVVSMRVMTRMGSKVLDKLGTDGFFVKALHS
LGAPLADGQEDVAWPCNDTKYITHFPEDREIWSFGSGYGGNALLGKKCYSLRIASAMAHDEG
WLAEHMLILKLISPEDKAYYIAAAFPSACGKTNLAMIQPTIPGWRAETLGDDIAWMRFGEDG
QLYAVNPEFGFFGVAPGTNWSSNPNAMRTIDQGNTVFTNVALTDDGDVWWEGLEGDPQHLID
WKGNEWTPESGTHAAHPNSRYCTPMSQCPIMAPEWDDPKGVPISAILFGGRRKTTVPLVTEA
RDWQHGVFMGATVGSEQTAAAEGQVGTVRRDPMAMLPFLGYNVGDYFQHWIDLGKSADASKL
PKVFYVNWFRRGDDGRFLWPGFGENSRVLKWIVERIEHKAAGIDTPIGVVPTGSALDIDGLD
VSDADITEALAVNIDEWKAEIPLIEEWFDFVGEKLPTGIRDEFEALKQRLA

C0ZLP5_RHOE4 (100%), 22,995.5 Da
Superoxide dismutase OS=Rhodococcus erythropolis (strain PR4 / NBRC 100887) GN=sodA PE=3 SV=1
3 exclusive unique peptides, 3 exclusive unique spectra, 22 total spectra, 50/207 amino acids (24% coverage)

MSVYTLPELPYDYAALEPHISGKIMELHHDKHHAAYVAGANAALEKLAEARENDTIAAQANL
LEKNLAFHLGGHTNHTVFWNNLSADGGDKPEGELAAAIDDNFGSFDLFRAHFSANANAIQGS
GWSILAWDSIGQRLIIVQLYDQQGNISIGLTPLLLLDMWEHAFYLDYQNVKGDYVKAFWNIV
NWNDVSARFDRARTQTAGLIV

C0ZXP4_RHOE4 (100%), 27,116.8 Da
Putative enoyl-CoA hydratase OS=Rhodococcus erythropolis (strain PR4 / NBRC 100887) GN=RER_24210 PE=4 SV=1
4 exclusive unique peptides, 4 exclusive unique spectra, 22 total spectra, 52/264 amino acids (20% coverage)
MTSIDDLSKVTLDEGVLRITISTAANGTSLDDEGLVQGAQALETVGNDIGSILLVGEGANFC
AGGNVRAFAAAPDRGEYVAEVARVFHVFVRALDAATAPVVAGVHGWAAGAGMSLVCLADVAI
GGTGTKLRPAYPSIGFTPDGGMSWTLPRIVGVARAREILLNDSVIGGDEAVRLGILTRLVGD
DEVQEEAARLARALANGPSTSYSGIKALLRSSRTNSLAEQLDAEAASIALAANSPIGREGVD
AFVDKRRPDFTSAKQA
C0ZX51_RHOE4 (100%), 49,507.1 Da
Uncharacterized protein OS=Rhodococcus erythropolis (strain PR4 / NBRC 100887) GN=RER_22280 PE=4 SV=1
4 exclusive unique peptides, 4 exclusive unique spectra, 13 total spectra, 58/466 amino acids (12% coverage)
MSNMPFGFSNSDDDPDRDKNAAGGNPFGGGDTPFGFGAGGEGFDPAQLGQMLTQFGQMLSGM
GSSMGQGGTSGPVNYDIAKKLARQQIGSVTPITEGNVKAIADAAHLAEMWLDAATTLPAGAS
RTLAWTPNDWLDNTIDTWKRLCDPVAEKVAGMWVQGLPAEAQQMAGPMLGMLGQMGGLAFGS
QLGQALGQLSTEVLSSTDIGLPLGPEGTAALLPAAVQAFSEGLEQPHQEVLVFLAAREAAHQ
RLYSHVPWLRQRVLATVEEYARGITMDFSAMEEFAKDLDPSALTDPSKLEALMQQGTFEPQN
TPEQKAALERLETLLALVEGWVETVVTAALGERLPGVAAMSETLRRRRATGGPAEQTFATLV
GLELRPRKVREAAGLWQKLTAEAGMDVRDGVWSHPDLMPDSSDLDAPDGFVARVLGGGEAGN
FDDPIAQLEAVEAKERAAEAAMDKTREDDEEK
Q3L9K9_RHOE4 (100%), 34,909.1 Da
Thioredoxin reductase OS=Rhodococcus erythropolis (strain PR4 / NBRC 100887) GN=trxB PE=3 SV=1
3 exclusive unique peptides, 4 exclusive unique spectra, 19 total spectra, 61/328 amino acids (19% coverage)
MTIPSAVHDVIIVGSGPAGYTAGVYTARAELAPLLFEGTQFGGALMTTTEVENFPGFREGIM
GPDLMEQMREQALRFDTDIRTEDVEEIDLSGPIKTVVANGETYAAHAIILAMGAAARYLGIP
GEERLLGRGVSACATCDGFFFRDQDIVVVGGGDSAMEEATFLTRFARSVTLVHRREEFRASR
IMLERAKANEKIRFLTNAEPVEVLGENSVTGLVVRDTVTGETSTLEITGMFVAIGHDPRSEL
VKDQVDLDDAGYVRVAPGSTATSVDGVFAAGDLVDHTYRQAITAAGTGCSAAIDAERWLADR
GDITANTLDAAGHTVDAV
C0ZZY6_RHOE4 (100%), 48,487.5 Da
Putative hydrolase OS=Rhodococcus erythropolis (strain PR4 / NBRC 100887) GN=RER_32130 PE=4 SV=1
2 exclusive unique peptides, 2 exclusive unique spectra, 16 total spectra, 27/450 amino acids (6% coverage)
MTTTPNNPNPSRAEAEVVELVSSLIRFDTSNTGELETTKGERACAEWVAAQLQEVGYETEYV
ESGAPGRGNVFARLKGAESGRGALMLHGHLDVVPAEPADWSVHPFAGTVQDGYVWGRGAVDM
KDMVGMILALARQFKAEGVVPPRDLVFAFVADEEAGGKYGCQWLVEHRPDLFEGVTEAVGEV
GGFSLTVPRPDGTDRRLYLVETAEKGLGWMRLTAKGRAGHGSFLHDDNAVATLAGAVSRLAA
HQFPIVISDSVAEFLTAVGEETGLDFDPGSPDIDGTLAKLGTIANIIGATFRDTANPTMLKA
GYKANVIPQTAEAVFDCRVLPGRQAEFERTVDQLIGPDVTREWITKLDSYETTFDGHLVDAM
NEAILAHDPEARTVPYMLSGGTDAKAFAKLGIRCFGFAPLQLPPELDFSALFHGVDERVPVD
ALLFGTRVLEHFLLNS
C1A225_RHOE4 (100%), 30,068.0 Da
3-hydroxyisobutyrate dehydrogenase OS=Rhodococcus erythropolis (strain PR4 / NBRC 100887) GN=mmsB PE=3 SV=1
2 exclusive unique peptides, 2 exclusive unique spectra, 7 total spectra, 27/297 amino acids (9% coverage)
MSTIGFIGLGHMGGPMAANLVKAGHKVVGFDLAPAALEQAVKDGASVADSAVDAVRGADVVI
TMLPSGKHVLGLYEELLPVATPGTLFIDCSTIDVADAREAHDKAEAAGHRSVDAPVSGGVVG
ATAGTLAFMVGGSEADFQAASPLLDVMGRKVVHCGDAGVGQAAKICNNMILGISMIAISEAF
VLGEKLGLSNQALFDVASNASGQCWALTTNCPVPGPVPTSPANNDYQPGFAVALMDKDLGLA
ANALRNNGVDAEIGLKAAELYSRFHAAGGGGQDFSAIINDIRDRSTEGQ

C0ZW54_RHOE4 (100%), 37,957.0 Da
DNA-directed RNA polymerase subunit alpha OS=Rhodococcus erythropolis (strain PR4 / NBRC 100887) GN=rpoA PE=3
2 exclusive unique peptides, 2 exclusive unique spectra, 6 total spectra, 24/353 amino acids (7% coverage)

MLISQRPTLTEEVIADNRSKFVIEPLEPGFGYTLGNSLRRTLLSSIPGAAVTSIRIDGVLHE
FTTVPGVKEDVTDIILNLKGLVVNSEEDEPVTMYVRKQGPGAVTAGDIVPPAGVTVNNPDLH
IATLNDKGKLEIELVVERGRGYVPAVQNKASGAEIGRIPVDSIYSPVLKVTYKVEATRVEQR
TDFDRLVLDVETKNSITARDALASAGKTLVELFGLARELNVEAEGIEIGPSPAEADHIASFG
LPIEDLDLTVRSYNCLKREGVHTVGELVGRTESDLLDIRNFGQKSIDEVKVKLHSLGLSLKD
SPASFDPTTVAGYDAATGTWSDTDAGSFGDAEGTEDYAETEQL

D.2. Primers for the Amplification of Mtr and the Full Mtr Plasmid

Mtr Frwd:
CTGCTTCTCAATCAGCTCTTCTATGacgcactacgaccttgc

Mtr Rvs
CGAAGTAAGTCGAGATGCTCTTCAACCgatgtcgaggccgagc

Lowercase letters indicate the annealing portion of the primer

Full Plasmid for Mtr expression:

>pD441-CH with Mtr - 5342 bp

TGCAAATGCTGAATGAGGGCATCGTTCCCACTGCGATGCTGGTTGCCAACGATCAGATGGCGCTGGGCGCAATGCGCGCC
ATTACCGAGTCCGGGCTGCGCGTTGGTGCGGATATCTCGGTAGTGGGATACGACGATACCGAAGATAGCTCATGTTATAT
CCCGCCGTTAACCACCATCAAACAGGATTTTCGCCTGCTGGGGCAAACCAGCGTGGACCGCTTGCTGCAACTCTCTCAGG
GCCAGGCGGTGAAGGGCAATCAGCTGTTGCCAGTCTCACTGGTGAAAAGAAAAACCACCCTGGCGCCCAATACGCAAACC
GCCTCTCCCCGCGCGTTGGCCGATTCATTAATGCAGCTGGCACGACAGGTTTCCCGACTGGAAAGCGGGCAGTGACTCAT
GACCAAAATCCCTTAACGTGAGTTACGCGCGCGTCGTTCCACTGAGCGTCAGACCCCGTAGAAAAGATCAAAGGATCTTC
TTGAGATCCTTTTTTTCTGCGCGTAATCTGCTGCTTGCAAACAAAAAAACCACCGCTACCAGCGGTGGTTTGTTTGCCGG
ATCAAGAGCTACCAACTCTTTTTCCGAAGGTAACTGGCTTCAGCAGAGCGCAGATACCAAATACTGTTCTTCTAGTGTAG
CCGTAGTTAGCCCACCACTTCAAGAACTCTGTAGCACCGCCTACATACCTCGCTCTGCTAATCCTGTTACCAGTGGCTGC
TGCCAGTGGCGATAAGTCGTGTCTTACCGGGTTGGACTCAAGACGATAGTTACCGGATAAGGCGCAGCGGTCGGGCTGAA
CGGGGGGTTCGTGCACACAGCCCAGCTTGGAGCGAACGACCTACACCGAACTGAGATACCTACAGCGTGAGCTATGAGAA
AGCGCCACGCTTCCCGAAGGGAGAAAGGCGGACAGGTATCCGGTAAGCGGCAGGGTCGGAACAGGAGAGCGCACGAGGGA
GCTTCCAGGGGGAAACGCCTGGTATCTTTATAGTCCTGTCGGGTTTCGCCACCTCTGACTTGAGCGTCGATTTTTGTGAT
GCTCGTCAGGGGGGCGGAGCCTATGGAAAAACGCCAGCAACGCGGCCTTTTTACGGTTCCTGGCCTTTTGCTGGCCTTTT
GCTCACATGTTCTTTCCTGCGTTATCCCCTGATTCTGTGGATAACCGTATTACCGCCTTTGAGTGAGCTGATACCGCTCG
CCGCAGCCGAACGACCGAGCGCAGCGAGTCAGTGAGCGAGGAAGCGGAAGGCGAGAGTAGGGAACTGCCAGGCATCAAAC
TAAGCAGAAGGCCCCTGACGGATGGCCTTTTTGCGTTTCTACAAACTCTTTCTGTGTTGTAAAACGACGGCCAGTCTTAA
GCTCGGGCCCCCTGGGCGGTTCTGATAACGAGTAATCGTTAATCCGCAAATAACGTAAAAACCCGCTTCGGCGGGTTTTT
TTATGGGGGGAGTTTAGGGAAAGAGCATTTGTCAGAATATTTAAGGGCGCCTGTCACTTTGCTTGATATATGAGAATTAT
TTAACCTTATAAATGAGAAAAAAGCAACGCACTTTAAATAAGATACGTTGCTTTTTCGATTGATGAACACCTATAATTAA
ACTATTCATCTATTATTTATGATTTTTTGTATATACAATATTTCTAGTTTGTTAAAGAGAATTAAGAAAATAAATCTCGA
AAATAATAAAGGGAAAATCAGTTTTTGATATCAAAATTATACATGTCAACGATAATACAAAATATAATACAAACTATAAG
ATGTTATCAGTATTTATTATGCATTTAGAATAAATTTTGTGTCGCCCTTAATTGTGAGCGGATAACAATTACGAGCTTCA
TGCACAGTGAAATCATGAAAAATTTATTTGCTTTGTGAGCGGATAACAATTATAATATGTGGAATTGTGAGCGCTCACAA
TTCCACAACGGTTTCCCTCTAGAAATAATTTTGTTTAACTTTTCGAGACCTAAGGAGGTAAAAAATGACGCACTACGACC
TTGCAATCATCGGCAGCGGATCCGGAAACTCGCTGCCAGACGAGCGGTTCGACGGCAAGAAGATCGCAATCCTCGAAGAG
GGCACCTTCGGCGGAACGTGCCTCAATGTCGGGTGTATCCCGACCAAGATGTTCGTCTACGCCGCCGAGGTGGCACGCAC
CGTCACCACTGCCGAGAAGTATGGCGTCGACGCCACGCTCGACGGCGTTCGTTGGTCCGACATCGTCAAGCGTGTCTTCG
GCCGCATCGATCCCATTTCTGCAGGTGGTGAGCGGTACCGCAGCGAAGACAGTCCCAACACCACCGTCTACCGCGGCCAC
GCCACGTTCACCGGCGACAAGACGATCGACACCGGAACCGGCGAGACGATCACCGCTGACCAGGTGGTCATCGCAGCCGG
TTCGCGTCCGATCATCCCGGACGAGATCGCGTCGAGCGGTGTGAAGTACTACACCAACGAAGACATCATGCGACTGCCCG
AACTTCCCGAGCACCTCGTGATCGTCGGCTCCGGATTCATCGCCACCGAGTTCGCACACGTGTTCTCCGCGTTGGGTTCT
CGCGTGTCGATCATCGGTCGCAGCCAGCGACTGCTGCGGCACCTCGACGACGAGATCTCCGAGCGCTTCACCGAGTTGGC
CGAACAGAGGTGGGACGTCCATCTGGGCTCCCCCCTCACGTCGGTACGCGGCGATGGCGACAACATCGCCGTCGAACTGG
CAAATGGCACAGTCGTTTCCGGTGACGTTCTCCTCGTCGCGGTGGGTCGTCAGCCGAACGGTGACCTACTCGGTCTCGAC
AAGGCCGGCGTCGAACTCGACGACAAGGGCTCGATCGTGGTCGACGAATACCAACGCACCACCGCCGAGGGCGTCTTCGC
ACTCGGTGACGTCTCCTCGCCGTACCAGCTCAAGCACGTCGCCAACCATGAAGCGCGCGTTGTTCAGCACAACCTGCTCC

AGGACGCGTGGAAGGACACGTCCGGGCTTCGCAGCACCGATCACCGCCTCGTACCGGCAGCCGTGTTCACCGACCCGCAG
ATCGCCGACGTCGGAATGACGGAGAAGCAGGCTCGCGACGCCGGACTCGACATCACCATCAAGGTGCAGGCTTACGGCGA
CGTCGCGTACGGCTGGGCGATGGAGGATCAGGAGGGTATCTGCAAGGTGATCGCCGAGCGCGGCACCGGACGCATCCTCG
GTGCCCACGTCATGGGCACTCAGGCTCCGACCGTCATCCAGCCCCTCATCCAGGCGATGAGCTTCGGTTTGTCAGCTCAG
GACATGGCGCGTGGCCAGTACTGGATCCACCCGGCCCTGGCCGAAGTGGTCGAGAACGCGCTGCTCGGCCTCGACATCGG
TCATCACCACCACCACCATTGAGGTCTCACCCCAAGGGCGACACCCCCTAATTAGCCCGGGCGAAAGGCCCAGTCTTTCG
ACTGAGCCTTTCGTTTTATTTGATGCCTGGCAGTTCCCTACTCTCGCATGGGGAGTCCCCACACTACCATCGGCGCTACG
GCGTTTCACTTCTGAGTTCGGCATGGGGTCAGGTGGGACCACCGCGCTACTGCCGCCAGGCAAACAAGGGGTGTTATGAG
CCATATTCAGGTATAAATGGGCTCGCGATAATGTTCAGAATTGGTTAATTGGTTGTAACACTGACCCCTATTTGTTTATT
TTTCTAAATACATTCAAATATGTATCCGCTCATGAGACAATAACCCTGATAAATGCTTCAATAATATTGAAAAAGGAAGA
ATATGAGCCATATTCAACGGGAAACGTCGAGGCCGCGATTAAATTCCAACATGGATGCTGATTTATATGGGTATAAATGG
GCTCGCGATAATGTCGGGCAATCAGGTGCGACAATCTATCGCTTGTATGGGAAGCCCGATGCGCCAGAGTTGTTTCTGAA
ACATGGCAAAGGTAGCGTTGCCAATGATGTTACAGATGAGATGGTCAGACTAAACTGGCTGACGGAATTTATGCCACTTC
CGACCATCAAGCATTTTATCCGTACTCCTGATGATGCATGGTTACTCACCACTGCGATCCCCGGAAAAACAGCGTTCCAG
GTATTAGAAGAATATCCTGATTCAGGTGAAAATATTGTTGATGCGCTGGCAGTGTTCCTGCGCCGGTTGCACTCGATTCC
TGTTTGTAATTGTCCTTTTAACAGCGATCGCGTATTTCGCCTCGCTCAGGCGCAATCACGAATGAATAACGGTTTGGTTG
ATGCGAGTGATTTTGATGACGAGCGTAATGGCTGGCCTGTTGAACAAGTCTGGAAAGAAATGCATAAACTTTTGCCATTC
TCACCGGATTCAGTCGTCACTCATGGTGATTTCTCACTTGATAACCTTATTTTTGACGAGGGGAAATTAATAGGTTGTAT
TGATGTTGGACGAGTCGGAATCGCAGACCGATACCAGGATCTTGCCATCCTATGGAACTGCCTCGGTGAGTTTTCTCCTT
CATTACAGAAACGGCTTTTTTCAAAAATATGGTATTGATAATCCTGATATGAATAAATTGCAGTTTCATTTGATGCTCGAT
GAGTTTTTCTAAGCGGCGCGCCATCGAATGGCGCAAAACCTTTCGCGGTATGGCATGATAGCGCCCGGAAGAGAGTCAAT
TCAGGGTGGTGAATATGAAACCAGTAACGTTATACGATGTCGCAGAGTATGCCGGTGTCTCTTATCAGACCGTTTCCCGC
GTGGTGAACCAGGCCAGCCACGTTTCTGCGAAAACGCGGGAAAAAGTGGAAGCGGCGATGGCGGAGCTGAATTACATTCC
CAACCGCGTGGCACAACAACTGGCGGGCAAACAGTCGTTGCTGATTGGCGTTGCCACCTCCAGTCTGGCCCTGCACGCGC
CGTCGCAAATTGTCGCGGCGATTAAATCTCGCGCCGATCAACTGGGTGCCAGCGTGGTGGTGTCGATGGTAGAACGAAGC
GGCGTCGAAGCCTGTAAAGCGGCGGTGCACAATCTTCTCGCGCAACGCGTCAGTGGGCTGATCATTAACTATCCGCTGGA
TGACCAGGATGCCATTGCTGTGGAAGCTGCCTGCACTAATGTTCCGGCGTTATTTCTTGATGTCTCTGACCAGACACCCA
TCAACAGTATTATTTTCTCCCATGAGGACGGTACGCGACTGGGCGTGGAGCATCTGGTCGCATTGGGTCACCAGCAAATC
GCGCTGTTAGCGGGCCCATTAAGTTCTGTCTCGGCGCGTCTGCGTCTGGCTGGCTGGCATAAATATCTCACTCGCAATCA
AATTCAGCCGATAGCGGAACGGGAAGGCGACTGGAGTGCCATGTCCGGTTTTCAACAAACCA

*Mtr gene underlined